Development, evaluation and evolution of bacteriophage cocktails active against clinical *Pseudomonas aeruginosa* isolated from Cystic Fibrosis patients.

Victoria Louise Lambert MSc

PhD

University of York

Biology

October 2025

Abstract

Cystic fibrosis (CF) is a genetic disorder where impaired mucociliary clearance predisposes patients to chronic pulmonary infection with *Pseudomonas aeruginosa*, a pathogen increasingly resistant to conventional antibiotic therapy. Bacteriophage therapy offers a promising alternative, yet clinical translation requires systematic evaluation of phage activity, rational cocktail design, and understanding of resistance evolution under therapeutic pressure.

The first study characterised phages with bactericidal activity against clinical *P. aeruginosa* isolates from CF patients, evaluating clearance and resistance interactions relative to antibiotics. Experiments examined clearance kinetics, the effect of infection duration on phage efficacy, whereby strains from patients with longer chronic infections displayed greater phage resistance, and the capacity of phages to prevent or disrupt biofilms, highlighting variable performance across physiological contexts.

Building on these findings, the second study used clearance and biofilm inhibition profiles to design a broad-spectrum phage cocktail targeting genetically diverse clinical isolates. Efficacy was assessed across multiplicities of infection (MOI), simulating early empirical administration prior to personalised matching. Results demonstrated that broad-spectrum cocktails may present a viable first-line treatment, allowing time for a more personalised approach.

The final study examined evolutionary trajectories under single phage and cocktail selection, quantifying the rate, stability, and mechanisms of resistance emergence. Sub-inhibitory polymyxin B treatment revealed synergistic killing and altered resistance dynamics, supporting phage–antibiotic combinations to suppress resistance while maintaining efficacy. These studies demonstrate that host range, biofilm physiology, MOI, and resistance evolution are critical determinants of efficacy, and rational cocktail design with phage–antibiotic synergy offers a promising framework for treating chronic CF infections.

Clinical isolates were sourced from the Danish CF treatment model, which employs centralised patient management and intensive longitudinal microbiological surveillance, providing a uniquely well-characterised framework for studying infection dynamics. This work highlights the need for clinically relevant biofilm models, adaptive cocktail formulation, and integration of phages into combinatorial treatment frameworks.

Declaration

I declare that this thesis is a presentation of original work and I am the sole author. This work has not previously been presented for a degree or other qualification at this University or elsewhere. All sources are acknowledged as references.

Table of Contents

List of Tables

Chapter 1

Chapter 2

Chapter 3

Table 3.6: Linear regression analysis statistical output for the correlation between length of infection and antibiotic resistance (MIC) across eight antibiotics (Figure 3.7).

Table 3.7: Linear regression analysis statistical output for the correlation between antibiotic resistance (MIC) and phage resistance score across eight antibiotics (Figure 3.9).

Chapter 4

Table 4.1: Pairwise Tukey-adjusted comparisons of each cocktail-treated strain at MOI 0.001 versus the positive control, based on estimated marginal means (emmeans) from a linear mixed-effects model.

Table 4.2: Pairwise Tukey-adjusted comparisons of each cocktail-treated strain at MOI 0.1 versus the positive control, based on estimated marginal means (emmeans) from a linear mixed-effects model.

Table 4.3: Pairwise Tukey-adjusted comparisons of each cocktail-treated strain at MOI 10 versus the positive control, based on estimated marginal means (emmeans) from a linear mixed-effects model.

Table 4.4: Wilcoxon rank-sum test results and effect sizes comparing Designed and Random assemblies across MOIs and experimental conditions.

Table 4.5: Wilcoxon rank-sum test results comparing Designed vs Random assemblies for each strain and MOI.

Table 4.6: Wilcoxon rank-sum test results comparing Disrupter and Preventer cocktails at three MOIs (0.001, 0.1, and 10) across 24 h, 48 h, and biofilm assays.

Table 4.7: Wilcoxon rank-sum test results comparing percent reduction between Preventer and Disrupter phage cocktails for each strain and MOI.

Table 4.8: Comparison of treatment effects on bacterial growth (AUC) relative to control for each strain.

Chapter 5

Table 5.1 - 5.7: Statistical comparison of phage treatment conditions to the no-treatment positive control for growth curves recorded during hours 0–48 (Fig. 5.1), 48–96 (Fig. 5.2), 96–144 (Fig. 5.3), 144–192 (Fig. 5.4), 192–240 (Fig. 5.5), 240–288 (Fig. 5.6), and 288–336 (Fig. 5.7).

Table 5.8: Comparison of cumulative bacterial growth, measured as area under the growth curve (AUC), across all 14-day timepoints for each phage treatment condition relative to the no-treatment positive control, pooled across strains 203.1, 342, and 413.

Table 5.9: Condensed results from long read sequencing performed by MicrobesNG with descriptive columns added for whether the gene affects a cellular process or an anti-phage defense system and the general effect.

Table 5.10: Mutations identified in no-treatment evolved clones from long-read sequencing.

Table 5.11 MIC assay results for clones from the evolutionary experiment. OD_{600} values at five antibiotic concentrations (C2–G2) are shown relative to the ancestral (ANC) strain.

List of Figures

Chapter 1

Chapter 2

Chapter 3

Chapter 4

Figure 4.4: Heatmap showing OD reduction relative to the no-phage positive control for 17 clinical *P. aeruginosa* strains exposed to 9 individual cocktail phages at cocktail concentration in liquid SCFM.

Figure 4.5: Optical density measurements (OD_{600}) of bacterial growth for 16 clinical *P. aeruginosa* strains exposed to 12 bacteriophage cocktails at MOI 0.1.

Figure 4.6: Optical density measurements (OD_{600}) of bacterial growth for 16 clinical *P. aeruginosa* strains exposed to 12 bacteriophage cocktails at MOI 10.

Figure 4.7: Box plots comparing percentage reduction in *P. aeruginosa* growth between designed (red) and randomly assembled (teal) phage cocktails across three MOIs (0.001, 0.1, and 10) and three timepoints (24 h, 48 h, and biofilm staining).

Figure 4.8: Box plots comparing percentage reduction in *P. aeruginosa* growth between designed (red) and randomly assembled (teal) phage cocktails across 17 clinical strains at three MOIs (0.001, 0.1, and 10).

Figure 4.9: Box plots comparing percentage reduction in *P. aeruginosa* growth between cocktails containing the Disrupter phage (red) and cocktails containing the Preventer phage (teal) at three MOIs (0.001, 0.1, and 10) across three timepoints (24 h, 48 h, and biofilm staining).

Figure 4.10: Box plots comparing percentage reduction in *P. aeruginosa* growth between cocktails containing the Preventer (teal) and Disrupter (red) phages across 17 clinical strains at three MOIs (0.001, 0.1, and 10).

Figure 4.11: Growth curves showing optical density (OD_{600}) over 24 hours for a subset of 10 clinical *P. aeruginosa* strains treated with selected phage cocktails at MOI 0.1.

Chapter 5

Figure 5.1–5.7: Growth curves for strains 203.1, 413, and 342 under the indicated treatments during hours 0–48 (Fig. 5.1), 48–96 (Fig. 5.2), 96–144 (Fig. 5.3), 144–192 (Fig. 5.4), 192–240 (Fig. 5.5), 240–288 (Fig. 5.6), and 288–336 (Fig. 5.7).

Figure 5.8: Box plot showing the area under the growth curve (AUC) as a measure of cumulative bacterial growth across all 14-day timepoints for each treatment condition, pooled across all three *P. aeruginosa* strains (203.1, 342, and 413).

Figure 5.9: Panels show mean phage density reduction of *P. aeruginosa* strains 342 (a) and 413 (b) following exposure to each phage treatment during the confirmation of resistance (CoR) assay.

Figure 5.10: Heatmaps showing clone-level phage density reduction for *P. aeruginosa* strains 342 (a) and 413 (b) during the confirmation of resistance (CoR) assay.

Figure 5.11: Images of MIC assay plates for 5 antibiotics tested against the ancestral clinical *P. aeruginosa* strain 342.

Figure 5.12: Combined heatmap of percent inhibition and FICI values for *P. aeruginosa* strain 342 exposed to phage cocktail C and polymyxin B.

Acknowledgements

First and foremost, I would like to express my deepest gratitude to my supervisors Dr Paul CM Fogg, Professor Ville Petri-Friman and Professor Jon Pitchford, for their invaluable guidance, support, and patience throughout this PhD journey. Their mentorship has been instrumental in shaping my research, my growth as a scientist and my teaching practice. I also extend my heartfelt thanks to my Thesis Advisory Panel chair Professor Daniela Barilla for her advice, encouragement, and feedback, which has significantly contributed to my work.

I am incredibly grateful to the University of York, in particular the Department of Biology and the York Biomedical Research Institute (YBRI) for providing the resources, facilities, training and academic environment that made this research possible.

A special thank you to the Fogg Lab for welcoming me to their team and offering their support to enhance my research and working environment. Thanks should also go to the Friman Lab, in particular Dr Bryden Fields, Dr Sara Franco Ortega, Dr Ezra Herman, Dr Sophie James and Dr Evelyn Farnham for supporting me at the start of my journey and guiding me through the PhD process. Their camaraderie, training and technical support made even the most challenging moments more manageable. I also extend my thanks to Monica Bandeira for her administrative support throughout the last three and a half years.

I deeply appreciate the contributions of Helle Krogh Johansen from Rigshospitalet, Denmark for providing clinical bacterial strains as well as Jean-Paul Pirnnay, Matti Jalasvuori, Rob Lavigne and Edze Westra for providing various bacteriophages. Without these resources this research would not have been possible. Additionally, I would like to acknowledge Microbes NG for providing a stellar sequencing service for the final chapter of my thesis.

Beyond academia, I owe a great deal to my family, in particular my dad Neil Lambert, mum Julie Turner and grandma Audrey Lambert for their unwavering love and encouragement throughout this process. Their support has kept me grounded during the most challenging times. Special thanks go to my children William and Evie Hudson for their patience and sacrificing their time with mummy. They have truly brightened the darkest of days. I'd like to recognise my good friend Elizabeth Kaye for her encouragement, assistance and providing a supportive ear through arduous times, as well as her company on a long haul voyage to an international conference. A huge thank you also to my emotional support pets, Odin, Sky and Reggie who have been a constant source of comfort and stress relief.

Finally, to all my colleagues, friends, and everyone who has supported me along the way—thank you. This thesis would not have been possible without you.

1. General Introduction

1.1 Cystic Fibrosis

Cystic fibrosis (CF) is an autosomal recessive genetic disorder caused by mutations in the genes encoding the cystic fibrosis transmembrane conductance regulator (CFTR) protein. Formerly known as cystic fibrosis of the pancreas, CF affects multiple systems including disruption of endocrine function in the pancreas, meconium ileus, biliary cirrhosis, high sweat electrolytes, infertility and, most notably, increased viscosity of the airway surface liquid (ASL) in the lungs (Farinha, 2017). This increased viscosity leads to chronic bacterial infection, lung scarring, damage, necessity for organ transplantation and ultimately high rates of morbidity and mortality (Farinha, 2017). CF lung disease alternates between periods of relative clinical stability and acute pulmonary exacerbations, the latter characterised by worsening respiratory symptoms, increased bacterial infection and accelerated lung function decline. Disease progression is commonly monitored using forced expiratory volume in one second (FEV_1) a key spirometric measure of airway obstruction and a strong predictor of morbidity and mortality in CF. Repeated exacerbations are associated with irreversible declines in FEV_1 and contribute substantially to long-term disease progression (Sanders *et al.*, 2011).

With an annual cost to the National Health Service (NHS) (2020-21) of over £70 million (NHS England, 2022), it is clear that CF presents a substantial financial burden. It has been estimated that improving adherence to inhaled antibiotic treatment for *Pseudomonas aeruginosa* in CF patients could generate NHS savings of £49.5 million over five years across the UK patient population alone (Tappenden *et al.*, 2017), underscoring the considerable economic as well as clinical value of effective antimicrobial management in this condition. However, the increasing prevalence of multidrug-resistant (MDR) *P. aeruginosa*, resistant to multiple antibiotic classes including β-lactams, aminoglycosides, and fluoroquinolones, threatens not only the lives of patients but also this potential cost-reducing treatment.

Across Europe, clinical management strategies for CF vary considerably, particularly in approaches to infection control and antibiotic treatment. The Danish CF care model represents a distinctive and extensively characterised system, defined by centralised specialist care, aggressive early eradication protocols targeting *P. aeruginosa*, frequent microbiological surveillance, and long-term longitudinal monitoring within national cohorts. This highly standardised framework has generated one of the most comprehensive datasets on chronic infection dynamics and antibiotic resistance development in CF populations.

Denmark's early adoption of intensive anti-pseudomonal treatment strategies has created a unique clinical environment in which evolutionary pressures from sustained antibiotic exposure can be observed over extended periods, effectively providing a natural experimental model for studying resistance emergence and alternative therapeutic approaches (Høiby *et al.*, 2010; Møller *et al.*, 2022). Consequently, focusing on the Danish system allows investigation of novel treatment strategies within a well-defined and consistently managed patient population, improving interpretability of microbiological and clinical outcomes.

This study aims to address antibiotic resistance using bacteriophage therapy as an alternate treatment method and explore combinatorial treatment options such as bacteriophage cocktails and phage–antibiotic synergy (PAS). Firstly, this chapter will address the epidemiology and aetiology of CF, followed by focus on bacterial infections within the CF lung, current treatments and bacteriophage therapy. Evolution of resistance will be addressed along with how treatment occurs in different countries.

1.1.1 Epidemiology

Historically CF was considered to be a predominantly caucasian condition with 1 in 2500-6000 newborns (approximately 54% male to 46% female (Mirtajani *et al.*, 2017) being affected (Farinha, 2017), however a study by Mirtajani *et al.* (2017) highlighted that this may not be the case. They determined that countries with a greater public health concern such as famine, malaria or civil war, did not have the reporting systems in place to collate accurate data on CF numbers within the population. Primarily an issue in Africa, Asia and parts of the Middle East and South America, this erroneous rhetoric has the potential to be dangerous for non-caucasian populations as current treatments target defects that are less common within this populace (McGarry and McColley, 2021). Consequently the World Health Organisation (WHO) listed CF as an important disease, requesting all countries to accurately report CF occurrences (Mirtajani *et al.*, 2017) . Despite the observed prevalence of CF in countries which have since begun to report CF numbers, there are still 109 countries where no CF data is available, 40 of which are in Africa (Guo, Garratt and Hill, 2022).

Life expectancy for people with cystic fibrosis (pwCF) has dramatically improved over the years in line with scientific advances (Simmonds, 2013). Key discoveries, acknowledgement and improved care of patients, saw an increase in life expectancy from 14 years in 1968 to 20 years in the 1970s. With the improved knowledge of pathophysiology through the discovery of hypertonic sweat in the 1950s and the *CFTR* gene in 1989, this has increased further. With the addition of new drugs and therapies such as antibiotics and CFTR modulators, life expectancy in the UK currently stands at 56 years (Yumi *et al.*, 2023). It is

important to note that the result of this is that there is now a larger proportion of adults with CF and it is predicted that this will increase rapidly into the 60s, particularly with recent advances in modulator therapy (Yumi *et al.*, 2023).

1.1.2 Aetiology

Historical instances of CF have been identified as far back as the mediaeval era with references to salty tasting children who were considered bewitched and expected not to survive (Farinha, 2017). The first medical reports appear in the 17th century with descriptions of symptoms but no cause identified. This continued until 1936 when German scientist Fanconi described the thickened mucus associated with the condition. This was shortly followed in 1938 by Dorothy Anderson presenting the first complete pathology of the condition and the first reference to cystic fibrosis of the pancreas. In the 1950s Paul di Sant'Agnese described the increased salt content of CF patient sweat, resulting in the eventual development of the sweat chloride test for diagnosis. It was not until the 1980s when the cloning of the *CFTR* gene and identification of mutations causing the CF phenotype fully explained the genetic cause of this condition (Farinha, 2017). From this point new research occurred rapidly and there is now much more information surrounding the synthesis, mutations and structure and function of the CFTR protein.

Synthesis

The *CFTR* gene is located on the long (q) arm of chromosome 7 at position 31.2 and consists of 27 axons (Vankeerberghen, Cuppens and Cassiman, 2002). Extracellular signalling promotes transcription of the *CFTR* gene into messenger RNA (mRNA) which is then transported through nuclear pores into the endoplasmic reticulum (ER) (Figure 1.1) (Strub and McCray, 2020). Translation into nascent amino acid chains then occurs in the ER, facilitated by transfer RNA (tRNA), and is assembled into immature CFTR. After further folding and maturation CFTR is transported to the Golgi apparatus where it post-translational modifications occur before the protein is packaged into transport vesicles, transported to the apical membrane of the epithelial cells and inserted into the cell membrane as mature CFTR (Strub and McCray, 2020).

Like any complex processes, synthesis of CFTR is prone to errors, molecular quality control checkpoints are present throughout in order to identify misfolded, damaged or otherwise incorrect CFTR protein and label these incorrect proteins, via ubiquitination, for degradation by proteasomes (Farinha, 2017). Over 2000 mutations have been identified in the gene encoding CFTR (Farinha, 2017), each resulting in different effects on the protein's structure,

synthesis and function with a consequent effect on the phenotype of CF patients. These mutations are placed into different classes based on their effects on protein function.

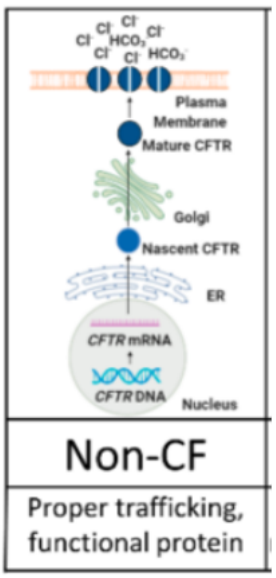

Figure 1.1: Synthesis of wildtype CFTR in human epithelial cells. The *CFTR* gene (located in the nucleus, bottom) is transcribed into CFTR mRNA, which is transported through nuclear pores into the endoplasmic reticulum (ER). Translation produces nascent CFTR protein, which undergoes folding and maturation in the ER before being transported to the Golgi apparatus for post-translational modification. Mature CFTR is then packaged into transport vesicles and trafficked to the apical plasma membrane, where it functions as a Cl^- and HCO_3^- channel. In non-CF cells this process results in proper trafficking and a functional protein. Adapted from Strub and McCray (2020).

Mutation Classes

Initially there were six main classes of CFTR mutation (Welsh and Smith, 1993) with a seventh suggested (Farinha, 2017). Classes one to three and seven result in a severe phenotype while classes four to six are less severe. An overview of these mutations can be seen in Figure 1.2 (Strub and McCray, 2020).

Class I mutations, such as G542X and R553X occur as a result of nonsense mutations or frameshift mutations leading to a premature stop codon. As a result, translation ceases prematurely and a very short amino acid chain is produced. In this case no CFTR is produced (Welsh and Smith, 1993).

Class II mutations include the most commonly observed F508del mutation and occurs in instances of amino acid deletion or, as with S549T, the substitution of an amino acid. This results in defective trafficking, resulting in reduced or no CFTR on the apical membrane (Welsh and Smith, 1993).

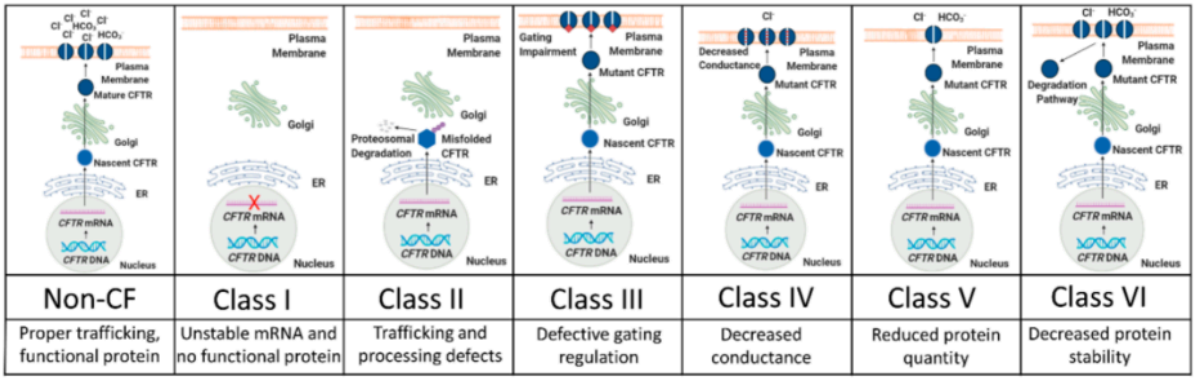

Figure 1.2: Overview of cystic fibrosis classes. Classes I–VI are illustrated, representing the range of molecular defects arising from CFTR mutations. Class I mutations produce unstable mRNA and no functional protein. Class II mutations result in defective protein folding and trafficking, preventing mature CFTR from reaching the apical membrane. Class III mutations produce CFTR that reaches the membrane but has defective gating regulation. Class IV mutations result in CFTR with decreased channel conductance. Class V mutations produce reduced quantities of functional CFTR due to splicing defects. Class VI mutations result in decreased protein stability and a reduced half-life at the membrane. Class VII mutations, in which CFTR mRNA is not produced and the defect is not rescuable by CFTR modulators (Farinha, 2017), are not depicted in this figure. Classes I–III and VII are associated with severe phenotypes; Classes IV–VI are associated with milder disease. Reproduced from Strub and McCray (2020).

Class III mutations such as G551D occur as a result of missense mutations and, while CFTR is present at the cell membrane, results in a defective response to cAMP signalling and does not function (Welsh and Smith, 1993).

Class IV mutations are similar to Class III in that they are caused by missense mutations and CFTR is still present at the membrane. In this case however, conductance across the membrane is reduced, as with mutation R334W (Welsh and Smith, 1993).

Class V mutations, such as 3849-10kbCT, occur where a splicing mutation leads to simultaneous production of wildtype and mutated CFTR. The mutated CFTR is degraded by proteasomes and a reduced amount of CFTR is present at the apical surface (Welsh and Smith, 1993).

Class VI mutations result in reduced stability of the protein thus reduced half-life at the membrane. The protein itself folds, is trafficked and functions almost normally and is therefore missed by the cell's checkpoint mechanisms. This has been found to occur in the F508del mutation once it has been rescued to the cell membrane by CFTR modulators (Welsh and Smith, 1993).

Class VII mutations were previously included with class I defects as they result in an absence of protein production. In this case CFTR mRNA is not produced and there is nothing for the

protein to be translated from. This class arose as these mutations are not rescuable by CFTR modulators (Farinha, 2017).

This is a highly simplistic model and does not encompass the complex interactions and combinatorial effect of these genotypes on patient phenotypes. As such a more comprehensive model was proposed by Veit *et al*. (2016). Which includes the groups discussed above alongside 26 combinations creating a Venn diagram model of CF mutations (Figure 1.3).

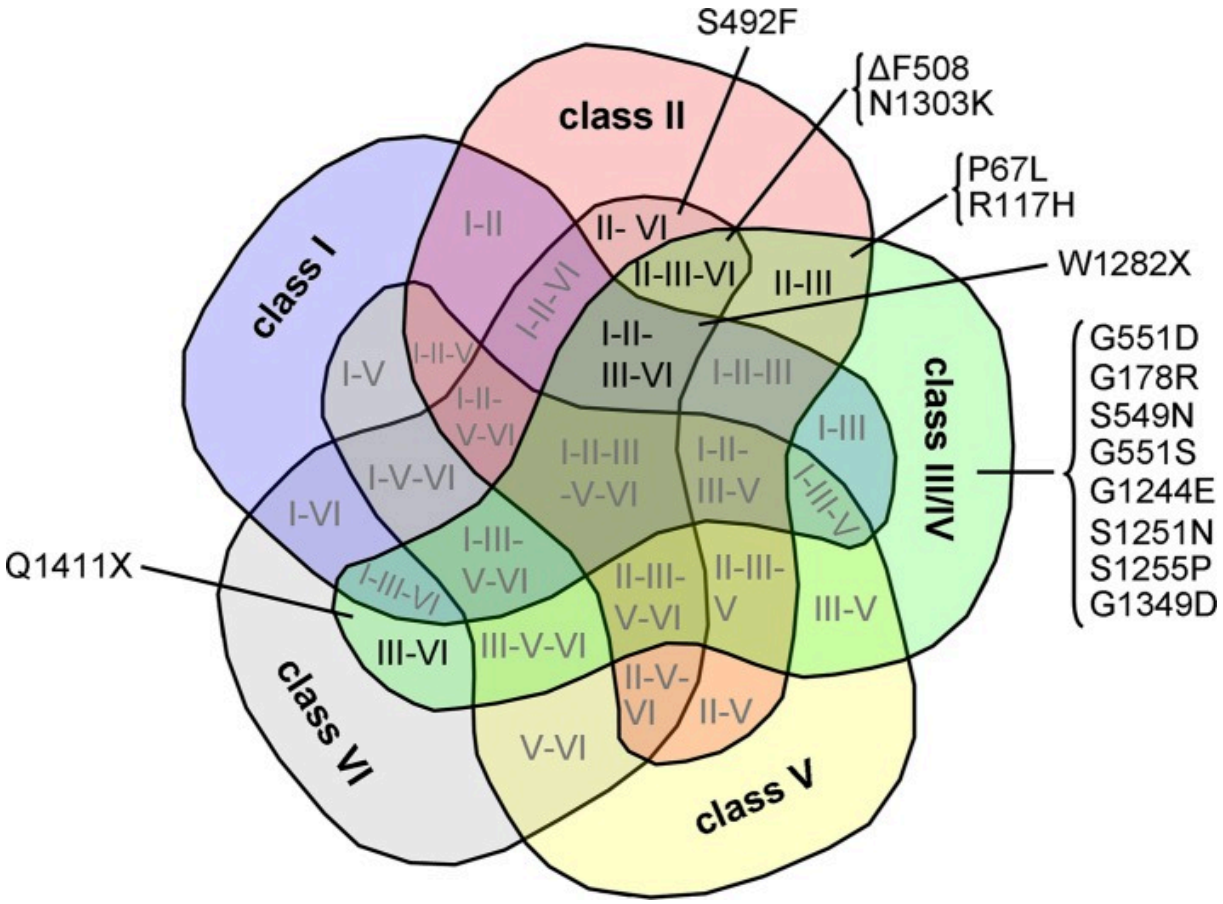

Figure 1.3: Venn diagram classification system of CF mutations as described by Veit *et al.* (2016). The six main mutation classes (I–VI) are represented as overlapping regions, with the intersections indicating mutations that exhibit characteristics of multiple classes simultaneously, producing 26 possible combinations. Selected common mutations and their corresponding class or combination of classes are indicated. The F508del mutation (ΔF508) is shown at the intersection of Classes II–VI, reflecting its complex and multifactorial molecular defects. Reproduced from Veit *et al*. (2016).

It is clear that these mutations are complex and massively affect the normal structure and function of the CFTR protein, resulting in a multitude of phenotypic changes within the body.

Structure and Function

CFTR is an ion channel membrane protein in the ATP-Binding Cassette (ABC) super family (Cant *et al.*, 2014). The protein consists of two transmembrane domains (TMD), each with six membrane spanning regions, two nuclear binding domains (NBD) and one R domain (Figure 1.4). The CFTR protein is unique within the ABC family as it is the only one that acts as an ion channel and as such has unique features such as the R domain and long N- and C-terminal extensions (80 and 30 residues long respectively). It totals 1480 amino acid residues in length and is located on the apical surface of epithelial cell membranes (Cant *et al.*, 2014).

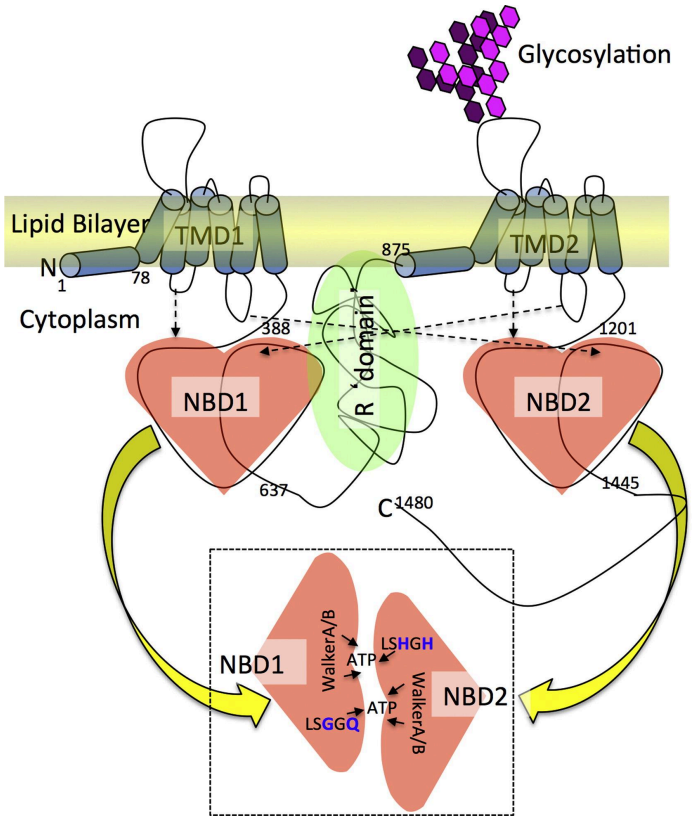

Figure 1.4: Schematic of CFTR protein structure. The extracellular face is shown above the lipid bilayer and the cytoplasmic face below. CFTR consists of two transmembrane domains (TMD1 and TMD2), each comprising six membrane-spanning regions, two nucleotide binding domains (NBD1 and NBD2), and a regulatory R domain (green). Amino acid residue positions are indicated at domain boundaries. Glycosylation (purple) occurs on the extracellular face of TMD2. The lower dashed box illustrates the interaction between NBD1 and NBD2 at the Walker A/B motifs and signature sequences (LSGGQ and LSHGH) during ATP binding, which drives NBD dimerisation and channel gating. Reproduced from Cant *et al.* (2014).

While the primary function of CFTR is transport of bicarbonate (HCO_3^-) and chloride (Cl^-) ions across the cell membrane to the apical surface of the epithelia, it also plays a major role in regulation of additional ion channels, particularly within the lung epithelia (Figure 1.5) (Saint-Criq and Gray, 2017). CFTR inhibits the epithelial sodium channel (EnaC), also on the apical surface, regulating Na^+ absorption into the cell. CFTR positively regulates the

Anoctamin-1 (ANO1) and the solute carrier 26 member 9 (SLC26A9) Cl^- channels as well as the solute carrier 26 member 4 (SLC26A4) anion exchanger (Figure 1.5). This increases both Cl^- and HCO_3^- secretion thus increasing ASL pH and hydration. Coupled with the regulation of EnaC this affects the electrochemical gradient causing the flow of Na+ and water through the paracellular pathway (Figure 1.5). On the basolateral membrane the Na-K-Cl cotransporter (NKCC1) moves Cl^- into the cell, this action is supported by the Na^+/K^+-ATPase channel which moves K^+ into the cell and Na^+ out of the cell. The K^+ is then recycled back out of the cell by the K^+ channel, while sodium is moved back into the cell by the NKCC1 transporter (Figure 1.5). In combination these various channels contribute to a delicate equilibrium which regulates and controls the properties of the airway surface liquid (ASL), a sticky mucus-like substance which coats the airways (Saint-Criq and Gray, 2017).

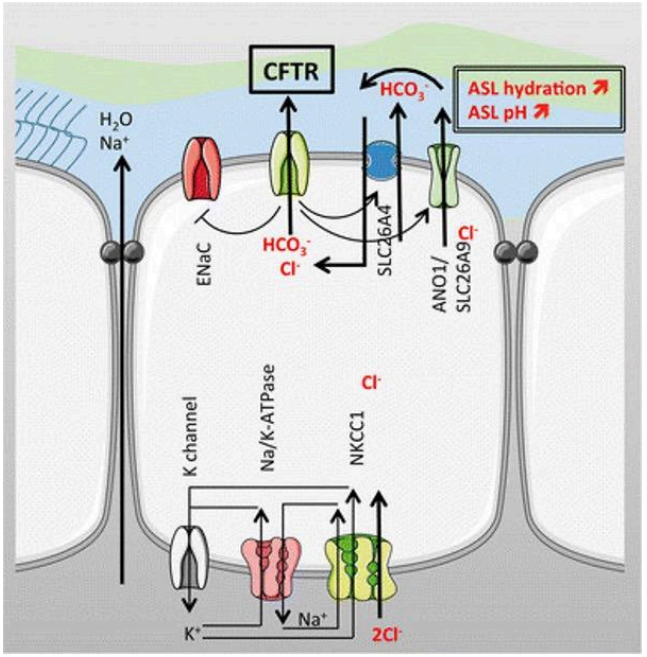

Figure 1.5: Ion transport in lung epithelia. CFTR (apical membrane, centre) mediates secretion of Cl^- and HCO_3^- ions into the airway surface liquid (ASL), and positively regulates the Anoctamin-1 (ANO1) and solute carrier 26 member 9 (SLC26A9) Cl^- channels and the solute carrier 26 member 4 (SLC26A4) anion exchanger, collectively increasing ASL hydration and pH. CFTR simultaneously inhibits the epithelial sodium channel (ENaC), reducing Na^+ absorption. On the basolateral membrane, the Na^+/K^+-ATPase and K^+ channel maintain electrochemical gradients, while the Na-K-Cl cotransporter (NKCC1) moves Cl^- into the cell. Together these channels regulate the composition and hydration of the ASL. Reproduced from Saint-Criq and Gray (2017).

In order to maintain this equilibrium, proper gating of the CFTR channel is essential (Figure 1.6). Prior to receipt of extracellular signals, NBD1 and the R domain interact to maintain the channel in a closed conformation. Phosphorylation of the R domain by PKA disrupts this interaction allowing ATP binding to the NBDs and transitioning the channel to an open-ready state. Dimerisation of the ATP-bound NBDs causes a conformational change in the

transmembrane domains, opening the channel and allowing Cl^- ions to cross the membrane. The channel closes following ATP hydrolysis, with release of inorganic phosphate (Pi) and ADP reverting the NBDs to the closed conformation. ATP may remain bound to one NBD to allow rapid switching between open and closed states, or be released to place the channel in a fully closed state (Cant *et al*., 2014).

Any malfunction in this gating process would result in an inability for Cl^- to cross the channel and would have an impact on delicate equilibrium of ion transport in the lungs, thus affecting the ASL. In these instances the ASL becomes mucus-like and sticky, this prevents cilia from moving the mucus and any trapped debris, such as bacteria, out of the lungs. As the bacteria are not removed from the lungs effectively, they colonise and grow rapidly, causing infection, lung scarring and tissue damage, which in CF patients often leads to lung disease and death.

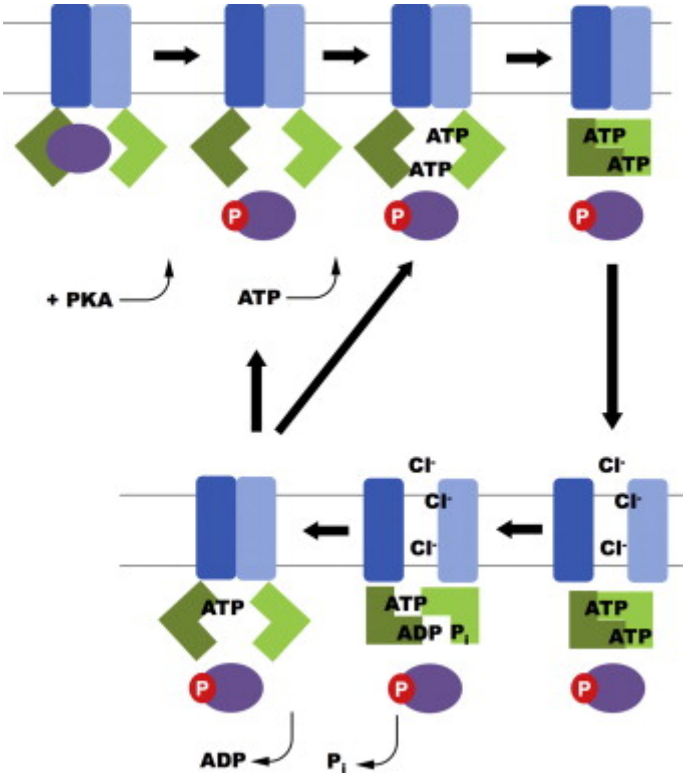

Figure 1.6: CFTR channel gating. NBDs (green) are in the open conformation, with interactions present between NBD1 and the R domain (purple). Phosphorylation (red) of the R domain by PKA disrupts this interaction and allows binding of ATP to the NBDs. This allows the formation of a closed NBD head-to-tail sandwich dimer, resulting in the channel conformation changing to an open-ready transition state, in which the channel is not yet open but is ready to open. Reproduced from Cant *et al.* (2014).

Significance

It is important to note that all of the mutations discussed above result in the thickening of the ASL. This means that in all instances of CF, opportunistic bacteria can thrive in the lungs and cause severe infections and lung damage. While chemotherapeutic solutions are necessary

to correct the defective CFTR it is vital that the issue of bacterial infection is addressed to reduce morbidity and mortality.

1.2 Bacterial Infection in the CF Lung

The most prevalent bacterial infection noted in adult CF patients is *P. aeruginosa*. This is an opportunistic bacteria and is often not the first infection present but rather takes advantage of an already diverse and thriving polymicrobial environment (Filkins and O'Toole, 2015). Understanding the composition and development of this complex community and why the CF lung is an optimal environment is a key consideration when addressing the problem of antibiotic resistance.

1.2.1 CF Lung Environment

The CF lung environment is optimised for increasing microbial colonisation and persistence. Structural defects within the upper respiratory tract, namely the trachea, have been observed in imaging tests on children with CF along with thicker walls and higher dilation of the airway (Meyerholtz *et al.*, 2010; Long *et al.*, 2004). This coupled with the previously discussed increased ASL viscosity and acidity, due to reduction in HCO_3^- and Cl^- transport across the cell membrane via CFTR transporter proteins, contributes to blockage of secretory glands (Inglis *et al.*, 1997). It is thought that this mucus plugging increases the release of cytokines, such as interleukin-1α, even in the absence of bacterial infection, further contributing to respiratory inflammation and airway narrowing (Montgomery *et al.*, 2018). Increased mucin secretion has also been observed with increasing expression of mucin genes *MUC2* and *MUC5AC* and increased glycosyl- production, resulting in altered folding of mucin proteins (Lambin *et al.*, 2001), contributing to viscosity of the mucin. It is thought that this increased mucin production is the prime cause of ASL thickening in the CF airway (Hill *et al.*, 2018) and, along with extracellular DNA, significantly alters the microstructure of the ASL (Lai *et al.*, 2009). Thickened mucus results in anaerobic pockets within the normally aerobic environment resulting in reduced oxygen and consequent persistence of infection due to decreased efficacy of antibiotics, and decreased lung function (Worlitzsch *et al.*, 2002; Borriello *et al.*, 2004). In addition, acidification, in particular through expression of ATP12A, results in reduced host defence and consequently increases microbial activity (Shah *et al.*, 2016).

In summary increased mucin and acidity along with reduced host defence and anaerobic pockets create an environment ideal for microbial growth. While the lungs have their own microbiome, these conditions allow opportunistic pathogens to dominate while reducing the

effectiveness of chemotherapeutics, resulting in lung damage and increased morbidity and mortality within the CF populace.

1.2.2 CF Lung Microbiome

The CF lung is home to a complex and varied microbiome which fluctuates throughout the life of an individual. Given that recurrent infection is a significant issue for those with CF, it is necessary to understand this complex ecosystem and discover how they interact with the host and each other.

Originally considered to be a minor consideration in CF disease progression (Oliver *et al.*, 2003) nontuberculous mycobacteria (NTM), a group of bacteria common in chronic pulmonary disease, are prevalent in the CF lung. While not initially considered to be a pathogen of significant risk there are multiple species within the group making them one of the more abundant in CF patients (Oliver *et al.*, 2003). There is debate within the literature as to whether prevalence in adulthood is greater than in children. It has been observed that the slow growing *Mycobacterium avium* complex (MAC) is more common in mildly symptomatic adult CF patients and the faster growing *M. abscessus* (MABSC) more common in paediatric cases of severe CF (Catherinot *et al.*, 2013). This was refuted by Eikani *et al.* (2018) who found no significant difference between the age of infection for each organism. They also observed significant impact on small airways, contradicting previous minimisation of NTM effect on CF airways. This was based on forced expiratory flow between 25% and 75% of forced vital capacity (FEF25-75), a spirometric measure of small airway function, as FEV1 showed no difference pre or post NTM acquisition, whereas FEF25-75 showed reduced function. It is clear that NTMs are a considerable issue for CF patients despite their recently discovered significance in the CF microbiome.

Staphylococcus aureus is generally the first and most common infective agent in the CF population (Saiman and Siegel, 2004). It is prevalent in children where a single strain can remain in a patient for 1-2 years (Branger *et al.*, 1996). Conversely small colony variants (SCV's) are observed mainly in the adult CF population with phenotypic traits optimised for survival within the CF lung (Kahl *et al.*, 1998; Vergison *et al.*, 2007), though these variants have been found in paediatric patients (Sadowska *et al.,* 2002). It is thought that the damage caused by *S. aureus* to the lung epithelia is a causative pathophysiology of further opportunistic infection such as *P. aeruginosa* which will be discussed in more detail in section 1.2.3 (Lyczak *et al.*, 2002). With recurrent antibiotic treatment and frequent hospital visits, nosocomial Methicillin resistant *S. aureus* (MRSA) is increasingly concerning within the adult CF population (Spicuzza *et al.*, 2009). With the exception of MRSA, *S. aureus* is relatively treatable and the risk of infant mortality has been greatly reduced with the use of prompt

antibiotic therapies (Goerke *et al.*, 2000). Despite this, *S. aureus* is still a major concern due to its prevalence and antecedence to more significant infective agents.

The *Burkholderia cepacia* complex (BCC) is comprised of more than 24 species including, *B. cepacia*, *B. multivorans*, *B. cenocepacia*, *B. stabilis*, *B. vietnamiensis*, *B. dolosa*, *B. ambifaria*, *B. anthina* and *B. pyrrocinia* (Pham *et al.*, 2023; LiPuma *et al.*, 1999). Identification of the specific species within a patient is difficult and as such creates challenges for treatment. Each species is unique from the others with individualistic traits and prognosis though all are highly adaptive and produce enzymes to combat antibiotic therapy (Wallet *et al.*, 2002; Soni *et al.*, 2002; Vermis *et al.*, 2004; Mahenthiralingam *et al.*, 2001). As such the need for rapid identification and treatment are essential to reduce CF patient mortality (Moreno-Flores *et al.*, 2024).

As well as the above major infective agents, there are several more minor pathogens which are still problematic in the CF lung. *Achromobacter xylosoxidans* are increasing in prevalence and result in bacteremia, pneumonia and meningitis (Liu *et al.*, 2002). Relatively little is known about *Inquilinus limosus* though it has been identified almost exclusively in CF patients (McHugh *et al.,* 2016) and contains multiple intrinsic antibiotic resistance mechanisms such as efflux pumps and biofilm formation. Whilst not particularly problematic *Ralstonia sp* have been identified as a chronic infection in CF patients (Coenye *et al.*, 2002). *Pandoraea apista* is often mistaken for BCC or *Ralstonia sp* due to phenotypic similarities. As BCC prevents patients from undergoing lung transplantation it is vital to increase successful identification to avoid unnecessary mortalities (Atkinson *et al.*, 2006). *Streptococcus pneumoniae* is primarily isolated from paediatric patients and is considered to be a transient pathogen in this population (Renders *et al.*, 2001; Del Campo *et al.*, 2005). *Stenotrophomonas maltophilia* is a nosocomial pathogen that is increasingly prevalent in the adult CF population (Bauernfeind *et al.*, 1987). *Haemophilus influenzae* is again mainly observed in paediatric patients though its ability to hypermutate means that this pathogen is a concern for antibiotic resistance (De Baets *et al.*, 2007). *Bordetella bronchiseptica* has been identified in a few cases resulting in CF symptom exacerbations and is considered a zoonotic agent (Magalhães *et al.*, 2004).

Fungi, yeasts and viruses are also key elements of the CF lung microbiome. Increased interactions between yeast and fungi along with reduced fungal biodiversity have been found to contribute to decreased lung function and CF exacerbations (Middleton *et al.*, 2013; Delhaes *et al.*, 2012) . At least 9 fungal species have been identified in the CF airways with *Acrophialophora fusispora* being identified uniquely in CF patients (Bhagirath *et al.*, 2016; Mouhajir *et al.*, 2016). Viruses, in particular bacteriophages which may confer horizontal

transfer of resistance genes, have been isolated in abundance from CF patient sputum (Lim *et al.*, 2013; Willner *et al.*, 2009). While CF patients do not appear to be significantly more susceptible to viral infection, when they do occur they are markedly more severe with an increased recovery time (Ouennane *et al.*, 2015).

Recent studies have highlighted that CF lung disease is associated with shifts in the overall microbial community rather than simply the presence or absence of specific pathogens. Longitudinal microbiome analyses demonstrate that disease progression and declining lung function are linked to reduced microbial diversity and increasing dominance of established CF pathogens, particularly *P. aeruginosa* (Frey *et al.*, 2022). These findings support a model in which CF represents a dynamic polymicrobial ecosystem, where interactions between bacterial, fungal and viral communities contribute to disease progression and exacerbation events (Cuthbertson *et al.*, 2020; Carmody *et al.*, 2015).

1.2.3 *P. aeruginosa*

The most common pathogen in adult CF patients is *P. aeruginosa* (Coutinho *et al.*, 2008), with some patients becoming infected with several different lineages of this bacterium. It can be isolated from a range of different environments, though those with extensive human or animal interaction, such as hospitals, soil, and water systems, are most frequently associated with clinical isolates (Diggle and Whiteley, 2020). *P. aeruginosa* is a Gram-negative, opportunistic, bacterium and as such has an asymmetric outer membrane, creating a permeability barrier, with a lipopolysaccharide (LPS) outer layer and a phospholipid inner face (Chevalier *et al.*, 2017). It is a highly motile species with flagella for swimming, twitching and swarming. This also helps with infection as the flagella has been found to facilitate adherence to mucin, which is in increased abundance in pwCF (Diggle and Whiteley, 2020).

As discussed above, *P. aeruginosa* is part of a complex microbiome within the CF lung, though this diverse collection of organisms do not exist independently of each other and complex relationships occur between them which have not been fully elucidated. NTM's have demonstrated a repressive effect on the species (Olivier *et al.*, 2003) while subsequent development of *P. apista* infection has been associated with prior *P. aeruginosa* infection (Atkinson *et al.*, 2006). Coinfection with *A. xylosoxidans* and *S. maltophilia* has been observed (Tan *et al.*, 2002; Van Daele *et al.*, 2005; Bauernfeind *et al.*, 1987), though further research is needed into the relationships with these minor components of the microbiome. It is generally accepted that paediatric *S. aureus* infection causes considerable lung epithelial damage which allows opportunistic *P. aeruginosa* to infect and thrive (Lyczak *et al.*, 2002), though other studies have demonstrated that this may be a co-infective relationship rather than a causative one (Sagel *et al.*, 2009).

The complex infection profile in pwCF leads to recurrent use of antibiotics which, coupled with generalised misuse of these drug classes, results in widespread antibiotic resistance in *P. aeruginosa*. This organism rapidly develops resistance in response to antibiotic exposure through a range of adaptive mechanisms, compounding its intrinsic resistance features and contributing to its status as the leading cause of morbidity in adult CF patients (Lubamba *et al.*, 2012). While the introduction of highly effective CFTR modulator therapy has reduced *P. aeruginosa* sputum density in eligible patients, chronic infection persists in the majority of those already colonised at the time of treatment initiation, with only 28% of chronically colonised patients becoming repeatedly culture negative within six months of elexacaftor/tezacaftor/ivacaftor initiation (Nichols *et al.*, 2023). Eradication therefore remains rare, and *P. aeruginosa* continues to represent a major clinical challenge particularly in patients with established chronic infection (Armbruster *et al.*, 2024). This bacterial species was therefore selected as the focal pathogen for this study.

1.2.4 Antibiotic Resistance in *P. aeruginosa*

In terms of intrinsic resistance mechanisms, *P. aeruginosa* has embedded within the outer membrane a number of porins which form β-barrel protein channels and allow antibiotics to cross the membrane, modification of these porins through reduced expression, structural modification and mutation to a substrate-specific modality can aid in antibiotic resistance (Delcour, 2009). Outer membrane protein (Opr) F is the main non-specific porin on the membrane. In *P. aeruginosa* the dominant form of this porin channel is the closed conformation leaving just 5% of OprF in the open confirmation. This is much less than in other bacteria and results in reduced access for the aminoglycoside, quinolone and β-lactam antibiotics to cross the membrane, which is necessary for them to reach their target binding sites within the bacteria (Sugawara *et al.*, 2006; Bouffartigues *et al.*, 2015). Some strains lack the outer membrane porin OprD, present in many other bacteria; loss of this channel prevents carbapenem entry into the cell, conferring resistance to this antibiotic class (Li *et al.*, 2012). It has also been demonstrated that overexpression of OprH as a result of Mg^{2+} starvation promotes LPS modification and stabilisation of the outer membrane, resulting in increased resistance to polymyxin B and the aminoglycoside gentamicin (Bell *et al.*, 1991; Macfarlane *et al.*, 1999). Where antibiotics do transverse the outer membrane and enter the bacteria, *P. aeruginosa* is equipped with 12 resistance-nodulation-division (RND) efflux systems, 4 of which are key in the development of antibiotic resistance. MexAB-OprM is responsible for the efflux of β-lactams and quinolones (Dupont *et al.*, 2005; Masuda *et al.*, 2000), MexCD-OprJ also for β-lactams (Okamoto *et al.*, 2002), MexEF-OprN again for quinolones (Llanes *et al.*, 2011) and MexXY-OprM for the efflux of aminoglycosides (Hocquet *et al.*, 2003; Masuda *et al.*, 2000). Overexpression of these efflux systems has been

observed in some clinical strains of *P. aeruginosa*, contributing to increased monotherapy and multidrug resistance (Cabot *et al.*, 2011; Llanes *et al.*, 2004; Shigemura *et al.*, 2015). A summary of the main antibiotics used to treat *P. aeruginosa* infections in CF, together with the corresponding resistance mechanisms which inhibit efficacy, is provided in Table 1.1.

Table 1.1: Main antibiotics used to treat *P. aeruginosa* infections in pwCF in Denmark, and the corresponding resistance mechanisms employed by *P. aeruginosa* that reduce antibiotic efficacy[1].

Antibiotic class	Common CF drugs (Denmark)	Mechanism of action	*P. aeruginosa* resistance mechanisms
β-lactams (penicillins, cephalosporins, monobactams)	Piperacillin, Ceftazidime, Cefepime, Aztreonam	Inhibit cell wall synthesis (bind PBPs)	*AmpC* β-lactamase overexpression[2]; ESBLs[2]; OprD porin loss[3]; Efflux pumps (MexAB-OprM, MexXY-OprM)[4]
Carbapenems	Meropenem, Imipenem	Inhibit cell wall synthesis (bind PBPs)	OprD porin loss[3]; Carbapenemases[2]; Efflux pump overexpression[4]
Aminoglycosides	Tobramycin (inhaled), Gentamicin, Amikacin	Bind 30S ribosome, inhibit protein synthesis	Aminoglycoside-modifying enzymes[5]; Efflux pumps (MexXY-OprM)[4]; Biofilm-mediated tolerance[4]
Fluoroquinolones	Ciprofloxacin, Levofloxacin	Inhibit DNA gyrase / topoisomerase IV	Target site mutations in gyrA/gyrB/parC/parE[5]; Efflux pumps (MexAB-OprM, MexEF-OprN)[4]
Polymyxins	Colistin	Disrupt bacterial outer membrane	LPS modification via arnBCADTEF, PhoPQ/PmrAB regulatory systems[5]; Efflux pumps[4]

[1]Antibiotic usage in Denmark based on CF clinical practice (Møller *et al.*, 2022); resistance mechanisms compiled from mechanistic studies and reviews. [2]β-lactamases: Winstanley *et al.* (2016); Meletis and Karastergiou (2025). [3]Porin loss (OprD): Pai *et al.* (2001). [4]Efflux pumps (MexAB-OprM, MexXY-OprM, MexCD-OprJ, MexEF-OprN): Lorusso *et al*. (2022). [5]Target mutations / modifying enzymes / LPS modification: Meletis and Karastergiou (2025).

As well as the above intrinsic resistance mechanisms, *P. aeruginosa* may also rapidly evolve antibiotic resistance through both mutation and acquisition of resistance genes through horizontal gene transfer. Mutational changes have been found to cause reduced antibiotic uptake, modification of antibiotic targets, and overexpression of both efflux systems and antibiotic inactivating enzymes (Munita *et al.*, 2016). Any remaining antibiotic can be dealt with through the antibiotic inactivating enzymes β-lactamase and aminoglycoside-modifying enzymes (AMEs). β-lactamase breaks down the amide bond of the β-lactam ring, thereby inactivating β-lactam antibiotics (Wright, 2005). Some clinical strains of *P. aeruginosa* have been found to possess extended-spectrum-β-lactamases (ESBLs) which confer a high degree of resistance to most β-lactam antibiotics including penicillins, cephalosporins and aztreonam (Paterson and Bonomo, 2005; Rawat and Nair, 2010). AMEs modify the amino and glycoside groups of the aminoglycoside antibiotics, thus inactivating them (Ratjen *et al.*, 2009). This includes two antibiotics commonly used for the treatment of *P. aeruginosa* in CF patients, namely gentamicin and tobramycin (Jacoby *et al.*, 1990; Subedi *et al.*, 2018). Some clinical isolates have been found to contain mutations in the *ampC* gene, causing

overproduction of β-lactamase, greatly increasing resistance to cephalosporins such as cefalotin which is a common antibiotic used in the treatment of *P. aeruginosa* in pwCF (Berrazeg *et al.*, 2015). Acquisition of resistance genes through horizontal gene transfer occurs via plasmids, integrons, prophages and transposons from either the same or different bacterial species (Breidenstein *et al.*, 2011). For example, integrons and plasmids have been found to carry the genes for metallo-β-lactamases (MBLs) aiding β-lactamase breakdown (Bonomo and Szabo, 2006; Castanheira *et al.*, 2004; Cavalcanti *et al.*, 2015; Khajuria *et al.*, 2013; Yan *et al.*, 2006).

P. aeruginosa is also capable of transient, additive antibiotic resistance in response to environmental stimuli. Two commonly observed adaptations include biofilm formation and the generation of persister cells (Drenkard, 2003; Mulcahy *et al.*, 2010). Biofilms are aggregates of microorganisms adhering to each other on a surface, this adherence often occurs through type IV pili (T4P), which are retractile cell surface filaments involved in initial surface attachment, twitching motility and DNA uptake (Craig *et al.*, 2019). Biofilm consists of exopolysaccharides, proteins, metabolites and extracellular DNA (eDNA), collectively known as extracellular polymeric substances (EPS's) (Das *et al.*, 2013; Donlan, 2002). In pwCF, chronic infection is associated with a mucoid phenotype driven by overproduction of alginate, which increases airway viscosity. Biofilm EPS additionally confers protection against antibiotics through prevention of antibiotic penetration, induction of slow bacterial growth allowing for adaptive stress responses, and the formation of multidrug tolerant persister cells (Stewart, 2002). An eDNA complex with pyocyanin promotes biofilm formation through pyocyanin-mediated cell lysis and eDNA release, which stabilises the biofilm matrix and enhances bacterial aggregation (Das and Manefield, 2012; Das *et al.*, 2013). Pyocyanin has also been implicated as a physiological signal influencing expression of genes involved in efflux pumps and redox homeostasis (Das and Manefield, 2012). Persister cells are not wholly resistant to antibiotics but are tolerant of high concentrations, they do not proliferate in the presence of the drugs but enter a dormant state, resuming growth once the antibiotics have been cleared. It is believed that these members of the bacterial aggregate are responsible for the persistence of chronic infections (Balaban *et al.*, 2013). High levels of persister cells have been observed in pwCF perhaps explaining the persistence of chronic infections in this species, and allowing for the development of adaptive strategies, resulting in higher instances of multidrug-resistant (MDR) strains (Mulcahy *et al.*, 2010; Mlynarcik and Kolar, 2017).

Antibiotics commonly used to treat *P. aeruginosa* infections in pwCF internationally include the polymyxin colistin, aminoglycosides tobramycin and gentamicin, the fluoroquinolone ciprofloxacin, and the β-lactams piperacillin, aztreonam, cefalotin and meropenem; these

antibiotics are also representative of those used in the Danish clinical setting from which the isolates in this study were obtained (Alqasmi, 2024; Møller *et al.*, 2022). However, chronic *P. aeruginosa* lung infections often persist despite repeated antibiotic courses, and high rates of antibiotic resistance have been reported in CF cohorts. For example, many clinical isolates show non-trivial resistance to several major antibiotic classes, including up to ~30% resistance to ciprofloxacin and aminoglycosides and 18–32% resistance to carbapenems (Mustafa *et al.*, 2016). Evolutionary analyses further indicate that *P. aeruginosa* populations adapt during chronic infection, commonly evolving high-level antibiotic resistance, which challenges long-term antibiotic therapy (Winstanley *et al.*, 2016). These observations demonstrate that current antibiotic regimens are frequently insufficient to eradicate infection or prevent repeated exacerbations. Additional strategies, such as quorum sensing inhibition (QSI), antimicrobial peptides (AMPs) and iron chelation, have been suggested (Hurley *et al.*, 2012; Aoki and Ueda, 2013; Chitambar, 2010; Reuter *et al.*, 2016), but perhaps the most promising is that of bacteriophage or phage therapy, which will be discussed in detail in section 1.4.

1.2.5 Evolution of Antimicrobial Resistance

Antimicrobial resistance (AMR), of which antibiotic resistance is a major component, is a major global health concern that undermines the effectiveness of existing antimicrobial agents and poses a substantial threat to the management of bacterial infections, including those associated with CF. The emergence and spread of resistant organisms has been accelerated by widespread antibiotic use in both healthcare and agricultural settings, leading to a selection pressure that favours bacteria capable of surviving chemotherapeutic intervention (Ventola, 2015). Infections caused by resistant microorganisms are associated with prolonged hospital stays, increased medical costs, and higher rates of morbidity and mortality (World Health Organisation, 2025). Within the CF population, where repeated antibiotic exposure is common, AMR represents a particularly acute challenge as it limits the already narrow range of effective therapeutic options (Hurley *et al.*, 2012).

As described above, resistance may occur through intrinsic mechanisms inherent to the bacterial species, or through acquired mechanisms that develop via mutation or horizontal gene transfer (Blair *et al.*, 2015).

In addition to these stable genetic features, many bacteria display transient adaptive resistance, a reversible phenotype that enhances survival under antibiotic stress. These adaptations are typically triggered by environmental conditions such as nutrient limitation, oxidative stress, or antibiotic exposure (Poole, 2012). One of the most clinically significant examples of transient adaptation is biofilm formation, which as described above confers

multifactorial protection against antibiotics and contributes significantly to chronic infection in the CF lung (Mulcahy et al., 2010).

Moreover, biofilm-associated cells exhibit upregulation of stress response pathways and efflux systems, further enhancing their ability to withstand antimicrobial agents (Poole, 2012; Stewart, 2002). The reversible nature of biofilm development and the capacity of bacteria to disperse and recolonise new sites complicates treatment, as eradication of one biofilm community may lead to the establishment of another (Hall-Stoodley *et al.*, 2004). These transient adaptations, combined with intrinsic and acquired resistance mechanisms, highlight the extraordinary capacity of bacteria such as *P. aeruginosa* to persist in hostile environments and evolve under antibiotic selection pressures.

AMR arises through a complex interplay of intrinsic, acquired, and adaptive mechanisms, all of which contribute to the resilience of pathogenic bacteria in the CF lung. Addressing these mechanisms is crucial to developing alternative antimicrobial strategies such as phage therapy, which will be explored in subsequent sections.

1.3 Current Treatments

Management of CF has evolved substantially over the past three decades, shifting from primarily supportive care towards therapies that target the underlying molecular pathology of the disease. Modern CF treatment now employs a multifaceted approach incorporating antibiotic therapy, CFTR modulators, airway-clearance techniques (ACTs), nutritional optimisation and, where appropriate, organ transplantation (Castellani *et al.*, 2018). Despite these advances, chronic pulmonary infection remains the dominant cause of morbidity and mortality, with *P. aeruginosa* representing the most persistent and clinically challenging pathogen in adult CF populations (Greenwald and Wolfgang, 2022).

Current treatment strategies therefore aim to simultaneously manage infection, restore defective ion transport, and mitigate the chronic inflammatory response that characterises CF airway disease. The following sections discuss the principal therapeutic approaches, including antibiotic therapy, CFTR modulators, and emerging and adjunctive treatments, before introducing phage therapy as a potential future modality.

1.3.1 Antibiotics

Antibiotics remain the cornerstone of CF management and are integral to controlling both acute pulmonary exacerbations and chronic bacterial colonisation (Hurley *et al.*, 2012). The thickened mucus characteristic of CF lungs creates an environment conducive to bacterial

persistence and biofilm formation, necessitating aggressive and sustained antimicrobial intervention (Filkins and O'Toole, 2015).

Inhaled Antibiotic Therapy

Inhaled antibiotics have become a mainstay in the long-term management of *P. aeruginosa* infection due to their ability to achieve high local drug concentrations while minimising systemic toxicity. Tobramycin inhalation solution (TOBI®) was the first agent shown to significantly improve lung function and reduce bacterial density in CF airways (Ramsey *et al.*, 1999). The dry-powder formulation later improved ease of use and adherence (Konstan *et al.*, 2011). Colistin (polymyxin E) remains widely used across Europe, including Denmark, for chronic suppression of *P. aeruginosa*, particularly in cases of aminoglycoside intolerance or resistance (Møller *et al.*, 2022). Aztreonam lysine (Cayston®) is also commonly used as part of alternating month regimens to prevent resistance development and maintain microbial suppression (Retsch-Bogart *et al.*, 2009).

The inhaled route provides a pharmacokinetic advantage, allowing local concentrations exceeding the minimal inhibitory concentration (MIC) by several orders of magnitude, even against strains demonstrating systemic resistance (Akkerman-Nijland *et al.*, 2021). However, the thick mucus matrix and bacterial biofilms can restrict diffusion, leading to heterogeneous drug exposure within the lungs, whereby some areas receive therapeutic antibiotic concentrations while others remain sub-therapeutic, potentially selecting for resistance. (Döring *et al.*, 2012). This uneven distribution may fail to eradicate bacteria in poorly penetrated regions, potentially selecting for resistance and contributing to treatment failure.

Intravenous and Oral Antibiotics

Acute pulmonary exacerbations are treated with intravenous (IV) antibiotics, guided by sputum culture results and patient response. Standard regimens often employ a β-lactam (e.g., ceftazidime, piperacillin/tazobactam, meropenem) in combination with an aminoglycoside (e.g., tobramycin or amikacin), a strategy supported by expert consensus given the theoretical advantages of synergistic killing and resistance mitigation (Holland and Jahnke, 2021). Extended or continuous infusion of β-lactams is sometimes used to maintain plasma concentrations above the MIC for time dependent agents (MacVane *et al.*, 2014).

Oral fluoroquinolones, most notably ciprofloxacin, are used for mild exacerbations or as step-down therapy following IV treatment. Their activity against *P. aeruginosa* and ability to penetrate sputum make them suitable for outpatient management (Ratjen *et al.*, 2009).

However, increasing fluoroquinolone resistance, coupled with concerns over long-term side effects, has reduced their utility as chronic suppressive agents (Zhao *et al*., 2020).

Chronic Infection and Resistance Development

The persistence of infection despite repeated antibiotic therapy is largely due to adaptive bacterial mechanisms, including biofilm formation, efflux pump upregulation, and metabolic dormancy (Mulcahy *et al.*, 2010). Within biofilms, *P. aeruginosa* cells are shielded from host defences and antimicrobials, requiring antibiotic concentrations up to 1,000-fold higher to achieve bactericidal effects (Høiby *et al.*, 2010). Additionally, repeated courses of antibiotics exert selective pressure that fosters MDR and promotes the emergence of hypermutator phenotypes — strains with defective DNA repair mechanisms that accumulate mutations at an accelerated rate, rapidly generating resistance to multiple antibiotic classes and significantly limiting treatment options while accelerating disease progression (Oliver and Mena, 2010).

In Denmark, antibiotic protocols are closely standardised under national guidelines coordinated by the Danish CF Centre in Copenhagen. A hallmark of the Danish model is the aggressive early eradication of *P. aeruginosa* upon first detection, typically using a 3 week course of oral ciprofloxacin combined with inhaled colistin (Pressler *et al.*, 2011). Chronic infection is then managed with alternating month inhaled antibiotic therapy and intermittent IV courses during exacerbations. This structured, longitudinal approach has significantly delayed chronic colonisation compared with less standardised international models (Hansen *et al.*, 2008). In contrast, UK guidelines recommend early eradication of *P. aeruginosa* using inhaled tobramycin or colistin, with or without oral ciprofloxacin, though treatment protocols are less rigidly standardised across centres compared to the Danish model (Langton Hewer *et al.*, 2023). This comparative context further illustrates the value of the Danish cohort as a consistently managed reference population for evaluating novel therapeutic strategies.

1.3.2 Modulators

The introduction of CFTR modulators represents a paradigm shift in CF therapy, targeting the root cause of the disease, defective chloride transport due to mutations in the *CFTR* gene. These small molecule compounds act by restoring CFTR protein expression, trafficking, or channel gating, depending on the mutation class (Middleton *et al.*, 2019).

Potentiators

Ivacaftor (VX-770) was the first CFTR potentiator approved for clinical use, designed to increase the open probability (Po) of the CFTR channel at the cell surface. It is particularly effective in patients with gating mutations such as G551D, improving chloride transport,

pulmonary function, and nutritional status (Ramsey *et al.*, 2011). Mechanistically, ivacaftor binds directly to the CFTR protein, stabilising the open conformation of the channel and enhancing ion conductance across the epithelial membrane (Van Goor *et al.*, 2009).

Correctors and Combination Therapies

For patients with the F508del mutation, the most prevalent globally, corrector compounds such as lumacaftor (VX-809) and tezacaftor (VX-661) have been developed to improve CFTR protein folding and trafficking to the cell surface. In combination with ivacaftor, these agents partially restore chloride transport and result in modest improvements in FEV_1, and body mass index (BMI), an indicator of nutritional status (Wainwright *et al.*, 2015). However, lumacaftor/ivacaftor combinations can induce hepatic enzyme changes and drug-drug interactions due to CYP3A modulation which, in pwCF, may reflect hepatic stress or injury and necessitate routine monitoring and potentially dose adjustment or treatment interruption if clinically significant (Elborn *et al.*, 2016).

The triple combination elexacaftor/tezacaftor/ivacaftor (Trikafta® in the U.S.; Kaftrio® in Europe) has shown the most substantial clinical efficacy to date. Elexacaftor acts as an additional corrector with a complementary binding site, improving CFTR protein stability and processing. Clinical trials demonstrated mean FEV_1 improvements of 10–14% and sweat chloride reductions exceeding 40 mmol/L (Middleton *et al.*, 2019). Beyond pulmonary outcomes, patients report enhanced gastrointestinal function, reduced exacerbation frequency, and improved quality of life (Heijerman et al., 2019).

Limitations and Ongoing Challenges

Despite these advances, several limitations remain. Modulator efficacy is mutation-specific, leaving approximately 10% of CF patients without effective molecular therapy (Farinha, 2017). Furthermore, modulators do not directly target chronic infection or inflammation, meaning that antibiotic and anti-inflammatory therapies remain necessary adjuncts (De Boeck and Amaral, 2016). Long-term data suggest that while modulators slow disease progression in CF, they do not completely reverse established lung damage, especially in real-world settings (Muilwijk *et al.*, 2021).

Access to CFTR modulators varies internationally. Denmark and the UK have adopted early national access programmes, while other regions face regulatory and cost-related delays (NICE, 2020). The high annual cost of therapy, estimated at over €250,000 per patient, remains a major barrier to universal access, particularly in lower-income settings (Guo *et al.*, 2022).

1.3.3 Airway Clearance Techniques

There are multiple ACTs used in Denmark CF centres with the primary purpose of clearing mucus from the lungs. These include Positive Expiratory Pressure (PEP) Mask Therapy, Forced Expiration Techniques (FET/Huffing), Physiotherapy, Physical Exercise and Inhalation Therapy. PEP masks allow air to move freely as a patient inhales but creates pressure causing resistance when exhaling (Qvist *et al.*, 2024). This loosens mucus and forces open alveoli that have become collapsed or deflated. This is often paired with FET or Huffing (as are most other ACTs) where a patient breathes out quickly with an open mouth, encouraging the expulsion of loosened mucus. Physiotherapy involves using a cupped or flat hand to create percussive vibrations on the chest, back and sides to loosen mucus which can then be expelled (Qvist *et al.*, 2024). Physical exercise is introduced in early childhood alongside physiotherapy techniques and is guided by physiotherapists to maximise the effect of lung clearance. Inhaled rhDNase begins within the first year of life and is used to reduce the viscosity of the mucus (Qvist *et al.*, 2024). This is often coupled with inhalation of saline solution to increase hydration of the mucus, further reducing the viscosity (Qvist *et al.*, 2024). Bronchodilators can also be used to relax muscles surrounding the airways to make it easier to breathe.

1.3.4 Emerging and Adjunctive Therapies

The rising prevalence of AMR and the incomplete efficacy of CFTR modulators have driven research into novel therapeutic strategies. These approaches aim to reduce bacterial virulence, modulate host immunity, or restore ion transport via alternative mechanisms.

Quorum sensing (QS) is a bacterial communication system that regulates virulence factor expression and biofilm formation in *P. aeruginosa*. Disrupting QS has emerged as a promising antivirulence strategy (Reuter *et al.*, 2016). Compounds such as halogenated furanones and synthetic analogues of acyl-homoserine lactones interfere with QS receptor binding, reducing the production of elastases, which degrade host tissue and evade immune responses, rhamnolipids, which disrupt host cell membranes and inhibit neutrophil function, and pyocyanin, which generates reactive oxygen species causing oxidative damage to host cells and promoting biofilm formation (Hurley *et al.*, 2012). Azithromycin, traditionally used as a macrolide antibiotic, also exhibits QSI properties at sub-inhibitory concentrations, attenuating biofilm formation and improving lung function in pwCF (Southern *et al.*, 2012). Most QSIs remain in preclinical or early translational development, with limited progression into formal human trials (Rémy *et al.*, 2018).

AMPs such as LL-37, defensins, and synthetic analogues represent another class of promising agents. These cationic peptides exert broad-spectrum activity through disruption of bacterial membranes, inhibition of biofilm formation, and immunomodulatory effects (Aoki and Ueda, 2013). Despite promising preclinical results, challenges include peptide stability, potential cytotoxicity, and high manufacturing costs (Drayton *et al.*, 2020). AMPs remain largely preclinical, with only limited early safety evaluations in humans planned (Bugli *et al.*, 2022).

Iron acquisition is essential for bacterial growth and virulence, particularly within the CF lung environment where free iron is limited. Gallium-based therapies exploit this dependency by mimicking ferric iron while being biologically inert. Once incorporated, gallium disrupts bacterial metabolism, inhibiting biofilm development and bacterial proliferation (Chitambar, 2010; Kaneko *et al.*, 2007). Intravenous gallium nitrate has shown efficacy in reducing *P. aeruginosa* load in both animal models and early human studies (Goss *et al.*, 2018) and a Phase 2 clinical trial in adults with CF has been completed, supporting continued investigation (Intravenous Gallium | CFF Clinical Trials Tool, 2026). Gallium has progressed further than QSIs and AMPs by entering early-phase clinical evaluation, although routine clinical use remains investigational (Intravenous Gallium | CFF Clinical Trials Tool, 2026).

Emerging gene-editing technologies and RNA-based therapies, particularly CRISPR-Cas9 and mRNA-based approaches, have demonstrated potential for directly correcting CFTR mutations at the genomic level (Schwank *et al.*, 2013; Rowe *et al.*, 2023). Inhaled mRNA therapies such as MRT5005 and ARCT-032 have progressed through early human clinical trials, demonstrating safety and early trends toward improved FEV_1 in small cohorts, with Phase 2 investigations ongoing (Rowe *et al.*, 2023; Gill *et al.*, 2025). Patient perceptions studies further support broad interest in gene therapy among CF populations (Donnelley *et al.*, 2023).

Collectively, these emerging approaches highlight a shift toward targeted, mechanism-based therapies aimed at reducing infection burden, restoring host function, and overcoming the limitations of conventional antibiotics. While many antivirulence and biologic strategies remain in preclinical or early-phase clinical stages, bacteriophage therapy, supported by ongoing Phase 1b/2 trials (NCT05453578, 2022–2025) and early compassionate use studies showing reductions in bacterial sputum burden and FEV_1 improvements, has progressed further toward clinical translation (Tamma *et al.*, 2022; Chan *et al.*, 2025). The next section will explore bacteriophage therapy in detail, while a summary of the development stages of these emerging and adjunct therapies can be seen in table 1.2.

Table 1.2: Summary of emerging adjunctive therapies for *P. aeruginosa* infection in pwCF, indicating the current stage of clinical or preclinical development for each approach.

Therapy	Example / Notes	Stage of Development	References
Quorum sensing inhibitors (QSIs)	Halogenated furanones, acyl-homoserine lactone analogues, azithromycin (sub-inhibitory)	Preclinical / Early Translational	Reuter *et al.* (2016); Asfour (2018); Hurley *et al*. (2012); Southern *et al.* (2012); Rémy *et al.* (2018)
Antimicrobial peptides (AMPs)	LL-37, defensins, synthetic analogues	Preclinical	Aoki and Ueda (2013); Drayton *et al*. (2020); Bugli *et al.* (2022); Hur *et al.* (2022)
Gallium / metal-based therapies	Gallium nitrate	Early clinical trials (Phase 2 completed)	Chitambar (2010); Kaneko *et al.* (2007); "Intravenous Gallium | CFF Clinical Trials Tool (2026)
Gene / RNA therapies	CRISPR-Cas9, MRT5005, ARCT-032	Early human trials (Phase 1/1b → Phase 2)	Schwank *et al.* (2013); Rowe *et al.* (2023); Gill *et al.* (2025); Donnelley *et al*. (2023)
Bacteriophage therapy	Nebulised/IV phages	Phase 1b/2 clinical evaluation ongoing; compassionate use reports	Tamma *et al*. (2022); NCT05453578 (2022–2025); Chan *et al*. (2025)

1.3.5 Introduction to Phage Therapy

The rise of MDR bacterial pathogens, particularly *P. aeruginosa*, has renewed interest in phage therapy as a potential adjunct or alternative to conventional antibiotics. Phages are viruses that specifically infect bacteria, replicating within and lysing their host cells. Their narrow host range and ability to self-replicate at the site of infection offer distinct advantages over traditional antimicrobials (Abedon *et al.*, 2011; Czaplewski *et al.*, 2016).

Phage therapy has demonstrated encouraging outcomes in experimental and compassionate-use cases involving chronic and antibiotic-resistant infections, including those in CF, and has gained renewed clinical attention through well-documented early-phase clinical studies targeting MDR pathogens (Table 1.3). A landmark example includes the treatment of a pwCF with disseminated *M. abscessus* infection following lung transplantation, where engineered phages achieved sustained clinical improvement after antibiotic failure (Dedrick *et al.*, 2019). Similarly, personalised IV phage therapy was successfully used to treat a life-threatening pan-drug-resistant *Acinetobacter baumannii* infection, demonstrating the feasibility of rapid phage identification and therapeutic deployment in western clinical settings (Schooley *et al.*, 2017). Additional compassionate-use cases, including trauma related bone infections (*Klebsiella pneumoniae*; Nir-Paz *et al.*, 2019) and transplant-associated infections, further demonstrate the feasibility and safety of personalised phage therapy across diverse clinical contexts (Aslam *et al.*, 2020; Leitner *et al.*, 2021). Beyond individual cases, early prospective and controlled clinical studies, such as the PhagoBurn randomised trial for burn wound *P. aeruginosa* infections, have begun to evaluate safety, formulation stability, and

dosing optimisation (Jault *et al.*, 2019). Collectively, these studies illustrate that while phage therapy remains largely investigational, clinical translation has progressed beyond purely experimental models. Moreover, phages can degrade biofilm matrices through depolymerase activity, potentially improving antibiotic penetration and bacterial clearance (Forti *et al.*, 2018).

However, therapeutic implementation remains constrained by regulatory, production, and standardisation challenges, as well as the need for patient-specific matching of phages to target bacterial strains (Rohde *et al.*, 2018). Denmark is among the European countries exploring these challenges through hospital exemption (HE) models and translational research using CF clinical isolates (Møller *et al.*, 2022). HE models are regulatory pathways in the EU and UK whereby Advanced Therapy Medicinal Products (AMTPs) can be prepared and used in hospitals on a non-routine, personalised basis without requiring marketing authorisation (MA) from the European Medicines Agency (EMA) (European Parliament and Council, 2007). This includes therapies such as bacteriophage therapy as well as cell and gene therapies and allows pwCF to access treatments which are not commercially available but are necessary for survival.

Table 1.3: Representative clinical case studies and trials of bacteriophage therapy, summarising study details including country, infection type, cohort size, study design, phages used, and clinical outcome.

Study	Year	Country	Infection type	Cohort size	Study type	Phage(s) used[1]	Outcome
Dedrick *et al.*	2019	UK/USA	Disseminated *M. abscessus* infection (post-lung transplant CF patient)	1	Compassionate-use case	Muddy; engineered derivatives BPsΔ33HTH-HRM10 and ZoeJΔ45	Sustained clinical improvement; reduced bacterial burden
Schooley *et al.*	2017	USA	MDR *A. baumannii* systemic infection	1	Compassionate-use case	AB-Navy1, AB-Navy4, AB-Navy71, AB-Navy97, AB-Navy98	Clinical recovery following antibiotic failure
Jault *et al.* (PhagoBurn trial)	2019	France/ Belgium/ Switzerland	Burn wound infection (*P. aeruginosa*)	27	Randomised clinical trial	PP1131 cocktail (12 lytic phages)	Demonstrated safety; efficacy limited by formulation stability
Nir-Paz *et al.*	2019	Israel	Chronic bone/joint infection (*P. aeruginosa*)	1	Compassionate-use case	Personalised lytic phage preparation (identifiers not disclosed)	Successful infection control alongside antibiotics
Aslam *et al.*	2020	USA	Various MDR infections	13	Case series / clinical experience	Individualised phage preparations (case-dependent; specific identifiers not consistently reported)	Demonstrated feasibility and safety of personalised therapy
Leitner *et al.*	2021	Europe	Severe MDR infection in transplant-associated context	1	Compassionate-use case	Personalised phage cocktail selected via susceptibility testing (specific identifiers not disclosed)	Clinical improvement reported

[1]Phage identifiers are reported where explicitly provided in primary publications. In several compassionate-use cases and clinical feasibility studies, specific phage strain names were not disclosed or were variably reported due to personalised therapy design, regulatory considerations, or emphasis on clinical workflow rather than phage characterisation.

Given the potential of phage therapy to address persistent *P. aeruginosa* infection and AMR in CF, this approach will be explored in greater detail in section 1.4.

1.3.6 International Treatment Strategies

Management of CF varies internationally, reflecting differences in healthcare infrastructure, therapeutic access, and national guidelines. Although the principles of early intervention, infection prevention, and multidisciplinary care are universal, their implementation differs significantly between countries (Elborn, 2016).

Denmark: A Model of Centralised and Standardised Care

Denmark remains an international leader in CF management, underpinned by a centralised model based at the Copenhagen CF Centre. This integrated approach combines medical, microbiological, and physiotherapeutic care, ensuring consistent monitoring and treatment (Høiby, 2011). A cornerstone of the Danish strategy is strict segregation of patients based on microbial colonisation, which has been shown to significantly reduce acquisition of chronic *P. aeruginosa* infection in CF centres (e.g., HR: 0.43 for patients < 15 yrs) (Van Mansfeld *et al.*, 2016). Here the Hazard Ratio (HR) represents the relative risk of acquiring chronic infection over time, with values below 1 indicating a protective effect.

The Danish regimen prioritises early eradication of *P. aeruginosa* upon initial detection, typically employing oral ciprofloxacin and inhaled colistin for three weeks, followed by close microbiological surveillance (Hansen *et al.*, 2008). The CF centre policy of inhaled antibiotics, such as colistin and tobramycin, often in alternating cycles, forms a core part of infection-suppression strategy and contributes to relatively low rates of chronic *P. aeruginosa* infection (Møller *et al.*, 2022).

Furthermore, Denmark ensures universal access to CFTR modulators, including Kaftrio® (elexacaftor/tezacaftor/ivacaftor), and actively contributes to international trials investigating emerging treatments such as phage therapy (Møller *et al*., 2022).

United Kingdom and Ireland

The UK and Ireland operate comprehensive CF care networks guided by national standards (NICE, 2020). Patients are managed through regional centres offering multidisciplinary care, with long-term inhaled antibiotics, tobramycin, colistin, or aztreonam, and chronic azithromycin forming the foundation of infection control (Southern *et al.*, 2012). Home-based IV antibiotic therapy is common, reducing hospitalisation and supporting quality of life. Extensive registry data support outcome monitoring and pharmacovigilance for CFTR modulators.

United States

In the U.S., CF management is coordinated through the Cystic Fibrosis Foundation (CFF) Care Centre Network, ensuring adherence to standardised protocols. The early introduction of CFTR modulators, particularly Trikafta®, has significantly improved life expectancy and reduced the prevalence of *P. aeruginosa* infection (CFF, 2022). Nonetheless, access disparities remain a concern.

Low- and Middle-Income Countries

In low- and middle-income countries (LMICs), diagnostic and therapeutic limitations often result in delayed diagnosis and poorer outcomes. Limited access to inhaled antibiotics and CFTR modulators restricts effective management, and infection control is frequently suboptimal (Guo *et al.*, 2022). In these contexts, the relative affordability and specificity of phage therapy may offer future potential once regulatory and production systems mature.

Denmark's integrated and proactive system continues to represent the international benchmark, demonstrating how standardisation and early intervention can significantly improve infection control and patient outcomes.

1.3.7 Summary

The management of CF has advanced substantially through improved antibiotic protocols, ACTs, and, most recently, CFTR modulators. Nevertheless, chronic infection with *P. aeruginosa* and the persistence of AMR remain major therapeutic challenges, particularly in advanced disease.

Denmark's nationalised and standardised care model exemplifies how coordinated infection management, microbiological surveillance, and antibiotic stewardship can sustain superior outcomes. Yet, as AMR continues to rise, there is an urgent need for complementary approaches that can target biofilm-associated and MDR infections.

Phage therapy has re-emerged as a promising adjunct to antibiotic treatment. Its mechanisms, applications, and translational potential will be explored in depth in the following section.

1.4 Phage Therapy

Phage therapy represents a targeted antimicrobial approach that utilises viruses capable of infecting and lysing specific bacteria. With the rise of MDR pathogens, particularly *P. aeruginosa* in CF, phage therapy has emerged as a potential adjunct or alternative to

conventional antibiotics (Abedon *et al.*, 2011; Chan *et al.*, 2018). Its specificity for bacterial hosts, ability to penetrate biofilms, and potential for synergy with existing antibiotics make it an attractive therapeutic strategy. While historical use of phages dates back to the early 20th century, renewed scientific interest has driven extensive research into phage biology, defence mechanisms, and therapeutic applications, with particular relevance to chronic respiratory infections observed in Danish CF centres.

1.4.1 History and General Profile

Phages are the most abundant biological entities on Earth, with an estimated 10^{31} particles globally, outnumbering bacteria by approximately ten to one (Clokie *et al.*, 2011). Found ubiquitously in environments such as soil, freshwater, marine systems, and within the human microbiome, phages play a critical role in microbial ecology and evolution, mediating horizontal gene transfer and influencing bacterial population dynamics (Breitbart *et al.*, 2018). Structurally, phages are highly diverse; most consist of a nucleic acid core, either DNA or RNA, enclosed within a protein capsid that may be attached to a contractile or non-contractile tail apparatus responsible for host recognition and genome injection (Ackermann, 2009). Their genomic architecture ranges from small single-stranded RNA phages of around 3–4 kb to complex double-stranded DNA tailed phages exceeding 500 kb (Hatfull, 2015).

The discovery of phages occurred independently by Frederick Twort in 1915 and Félix d'Herelle in 1917, who first described an agent capable of lysing bacterial cultures of *Shigella dysenteriae* (d'Herelle, 1917). D'Herelle coined the term "bacteriophage" (bacteria-eater) and recognised its potential as a therapeutic agent against bacterial infections. Early in the twentieth century, phage therapy was trialled for a variety of infections including dysentery, cholera, and staphylococcal abscesses, with variable success (Lin *et al.*, 2017). However, enthusiasm for phage therapy in Western medicine waned following the discovery of penicillin and other antibiotics, which were easier to mass-produce, standardise, and regulate (Sulakvelidze *et al.*, 2001).

In contrast, research continued extensively in Eastern Europe and the former Soviet Union, particularly at the Eliava Institute of Bacteriophage, Microbiology and Virology in Tbilisi, Georgia, and the Hirszfeld Institute in Wrocław, Poland (Kutateladze and Adamia, 2010). These centres developed large libraries of therapeutic phages and produced standardised phage cocktails for clinical use long after antibiotics became mainstream elsewhere. This continuity has been instrumental in sustaining knowledge and infrastructure for modern phage therapy research.

The resurgence of interest in phage therapy in the Western world over the past two decades has been driven primarily by the global escalation of AMR. With MDR pathogens increasingly rendering conventional antibiotics ineffective, phages have re-emerged as an alternative or adjunct therapeutic option (Lin *et al.*, 2017). Phages offer several advantages: extreme host specificity, the ability to self-replicate at the site of infection, minimal disruption to commensal microbiota, and a safety record supported by over a century of use in Eastern Europe (Gordillo Altamirano and Barr, 2019). Furthermore, the capacity to isolate and adapt phages against emerging resistant strains offers a dynamic and renewable antimicrobial platform.

Phages follow two principal life cycles: the lytic and lysogenic (temperate) pathways. Lytic phages attach to specific receptors on the bacterial surface, inject their genetic material, hijack the bacterial replication machinery, and ultimately lyse the host cell to release progeny virions (Young, 2014). This process, occurring within minutes to hours, underpins their use in therapy. Lysogenic, or temperate, phages, by contrast, integrate their genomes into the bacterial chromosome as prophages, replicating passively with the host. While this relationship can enhance bacterial fitness or contribute to horizontal gene transfer of virulence factors, temperate phages are generally avoided in therapeutic applications due to the risk of transducing resistance or virulence genes (Howard-Varona *et al.*, 2017). Modern phage therapy thus focuses primarily on strictly lytic phages, characterised through genomic sequencing to confirm the absence of lysogeny-associated genes.

Within the context of *P. aeruginosa* infection in CF, phages present a particularly appealing option. The CF lung provides an environment that fosters biofilm formation, antibiotic resistance, and chronic infection, all scenarios where phages can exhibit unique advantages. Phages can penetrate biofilms via enzymatic depolymerases, self-amplify within the bacterial population, and evolve alongside bacterial resistance mechanisms (Danis-Wlodarczyk *et al.*, 2016). These features position phages as potentially transformative tools in managing chronic *P. aeruginosa* infections that are refractory to standard therapies.

In Denmark, the increasing prevalence of MDR *P. aeruginosa* in pwCF has renewed clinical interest in phage therapy. The country's highly centralised model of CF care, centred in Copenhagen, has provided a robust framework for integrating phage research into clinical microbiology (Høiby, 2025). Isolation and characterisation of *P. aeruginosa* specific phages from clinical and environmental sources has enabled the development of targeted therapeutic cocktails intended for local infection control (Vaitekenas *et al*., 2021). The present thesis builds on this foundation, exploring the efficacy of these phage cocktails and their combinatorial use with antibiotics in clinical isolates derived from the Danish CF population.

Overall, phage therapy represents a re-emerging but scientifically grounded approach to combating bacterial infection, particularly where conventional antibiotics fail. Modern research, supported by genomic and molecular tools, has transformed what was once an empirical treatment into a precision antimicrobial platform. The following sections will detail the intricate evolutionary arms race between bacteria and their phages, the development and application of phage therapy for clinical infection, and the growing evidence supporting combined phage, antibiotic strategies.

1.4.2 Phage Defence Mechanisms

The widespread application of phages as therapeutic agents is tempered by the remarkable capacity of bacteria to resist phage predation. In the natural environment, bacteria and phages exist in a dynamic coevolutionary arms race, with selective pressures continually shaping microbial communities. Within the CF lung, *P. aeruginosa* exhibits a range of innate and adaptive mechanisms to evade phage attack, which are central considerations in the design and implementation of effective phage therapies (Egido *et al.*, 2022).

One of the most fundamental bacterial defence strategies involves modification of surface receptors. Phages initiate infection through highly specific interactions with bacterial surface components, including lipopolysaccharides (LPS), outer membrane proteins, and T4P (Hyman and Abedon, 2010). Mutational changes in these structures, either through point mutations, phase variation, or the production of protective exopolysaccharides, can prevent phage adsorption and entry (Teklemariam *et al.*, 2023). Within the CF lung, *P. aeruginosa* often exists as mucoid biofilm forming variants that overproduce alginate, which not only impedes antibiotic penetration but also physically shields phage receptor sites, reducing infection efficiency (Drenkard, 2003; Egido *et al.*, 2022). Phenotypic heterogeneity in receptor expression across bacterial populations further enhances survival, creating subpopulations resistant to specific phages while remaining susceptible to others (Chapman-McQuiston and Wu, 2008).

Bacteria also employ active molecular defence systems to counter phage infection. Restriction-modification (R-M) systems constitute one of the earliest discovered mechanisms, whereby host DNA is methylated to prevent cleavage, while unmethylated foreign DNA introduced by phages is degraded by endonucleases (Vasu and Nagaraja, 2013). Beyond these traditional systems, clustered regularly interspaced short palindromic repeats (CRISPR) and their associated Cas proteins provide adaptive immunity, enabling bacteria to acquire short sequences from invading phages and subsequently target them for degradation upon reinfection (Barrangou *et al.*, 2007; Marraffini and Sontheimer, 2010). In *P. aeruginosa*,

both type I and type I-F CRISPR-Cas systems have been identified and shown to confer resistance to lytic phages *in vitro*, although their *in vivo* significance within the CF lung remains under active investigation (Cady *et al.*, 2012; van Belkum *et al.*, 2015). More recently, additional anti-phage defence systems have been characterised in *P. aeruginosa*, including CBASS, Gabija, Wadjet, and Juk, with at least 31 distinct systems identified in this species to date (Johnson *et al*., 2023). The total number of prokaryotic anti-phage defence systems continues to grow rapidly, with over 150 now identified across bacteria (Niault *et al.*, 2025).

Abortive infection (Abi) systems offer a population-level defence, wherein infected bacterial cells trigger programmed cell death upon phage entry to prevent propagation of the viral particle. These altruistic systems are widespread in Gram-negative bacteria, including *P. aeruginosa*, and can significantly limit phage amplification within dense microbial communities such as CF biofilms (Dy *et al.*, 2014). Similarly, toxin–antitoxin modules, frequently encoded on mobile genetic elements, can be activated in response to phage infection, halting cellular processes and effectively preventing successful viral replication (Dy *et al.*, 2014). These mechanisms collectively underscore the multifactorial nature of bacterial resistance to phages and illustrate the challenges in achieving sustained therapeutic efficacy.

Phages themselves are subject to evolutionary pressures that counter bacterial defences. In response to receptor modification, phages may acquire mutations in tail fibers or receptor-binding proteins, restoring infectivity against previously resistant strains (Stern and Sorek, 2011). Similarly, some phages produce depolymerase enzymes capable of degrading extracellular polysaccharides and biofilm matrices, facilitating access to the bacterial surface (Hughes *et al*., 1998; Pires *et al*., 2016). The clinical implication is that phage therapy must consider both the inherent defence capacity of the bacterial target and the potential for adaptive phage evolution, highlighting the rationale for using diverse phage cocktails to overcome resistance (Chan *et al.*, 2013).

Within the Danish CF context, surveillance of chronic *P. aeruginosa* isolates has revealed variable susceptibility patterns to candidate therapeutic phages, reflecting both historical antibiotic exposure and endogenous phage bacteria interactions (Martin *et al.*, 2021; Burgener *et al.*, 2019). This variability underscores the importance of preclinical characterisation of both the bacterial population and the candidate phages, ensuring that therapeutic cocktails incorporate phages capable of targeting the spectrum of receptor variants and resistance phenotypes present in the patient cohort. Strategies such as rotating or combining phages with distinct receptor targets and enzymatic capabilities are increasingly

recognised as essential to mitigating the emergence of phage resistant bacterial subpopulations (Chan *et al.*, 2018; Gordillo Altamirano and Barr, 2019).

In addition to intrinsic and adaptive bacterial defences, environmental factors within the CF lung further influence phage efficacy. The heterogeneous architecture of mucus, the presence of anaerobic pockets, and fluctuating pH levels can all impede phage diffusion and adsorption, creating microenvironments in which phage-bacteria interactions are suboptimal (Labrie et al., 2010; Høiby *et al.*, 2011). Moreover, chronic infections often harbour hypermutable strains with elevated mutation rates, accelerating the development of phage resistance (Oliver *et al.*, 2004). These factors necessitate careful phage selection, dosing strategies, and consideration of combination therapies, including phage–antibiotic synergy (PAS), to maximise clinical benefit.

Collectively, the breadth of bacterial phage defence mechanisms, coupled with the environmental complexity of the CF lung, highlights the necessity of sophisticated therapeutic design. A deep understanding of receptor variability, molecular defence systems, and biofilm mediated protection informs the rationale for phage cocktails and adaptive treatment strategies. The subsequent sections will explore how these insights have been translated into clinical phage applications, with a particular emphasis on *P. aeruginosa*, phage cocktail development, and combinatorial strategies such as PAS.

1.4.3 Phages to Treat Infection

Bacteriophage therapy represents a targeted antimicrobial strategy that has gained renewed attention in the context of increasing antibiotic resistance, particularly in chronic *P. aeruginosa* infections in pwCF. Unlike conventional antibiotics, phages exhibit species or strain specific predation, infecting only their cognate bacterial hosts while leaving commensal microbiota largely intact (Abedon *et al.*, 2011; Sulakvelidze *et al.*, 2001). This precision is especially advantageous in CF, where the lung microbiome is complex and recurrent antibiotic use has led to extensive MDR populations (Høiby, 2011).

The principle of phage therapy involves the administration of lytic bacteriophages that attach to specific bacterial receptors, inject their genetic material, and commandeer host machinery to produce progeny phages, culminating in host lysis (Hyman and Abedon, 2010). *In vitro* studies using CF-derived *P. aeruginosa* isolates have demonstrated that lytic phages can reduce bacterial density by several orders of magnitude, including strains resistant to multiple classes of antibiotics (Kutter *et al.*, 2010; Chan *et al.*, 2013). Clinical case reports and compassionate use applications further highlight the potential of phages to resolve recalcitrant infections. For example, Dedrick *et al*. (2019) described a CF patient with a

disseminated, MDR *M. abscessus* infection who achieved clinical improvement following intravenous and nebulised phage administration. While *P. aeruginosa* infections in CF are the primary target for therapeutic development, these studies illustrate the feasibility of phage therapy against chronic, highly resistant pathogens.

A critical determinant of phage efficacy is the selection of phages with appropriate host range and lytic activity. Isolates from Danish CF patients have been shown to exhibit substantial heterogeneity in receptor expression and biofilm phenotypes, necessitating the use of phage libraries to identify candidates capable of infecting multiple strains (Lee *et al.*, 2005; Burgener *et al.*, 2019). Experimental workflows typically involve initial screening of phage panels against patient derived isolates to identify active phages, followed by *in vitro* and *ex vivo* testing of bactericidal activity under conditions simulating the CF airway environment, including viscous mucus, anaerobic microenvironments, and high bacterial density (Garbe *et al.*, 2010; Fiscarelli *et al.*, 2021; Almeida *et al.*, 2024). The ability of phages to penetrate biofilms is particularly relevant for CF, as *P. aeruginosa* predominantly exists as a biofilm in the lower airways, conferring tolerance to antibiotics and immune clearance (Drenkard, 2003; Mulcahy *et al.*, 2010). Certain phages encode depolymerases capable of degrading exopolysaccharides, enhancing penetration into biofilms and facilitating bacterial lysis; for example, phage-associated depolymerases targeting alginate and Psl, two key structural polysaccharides of *P. aeruginosa* biofilms, have been shown to significantly reduce biofilm biomass and increase bacterial susceptibility to both phage infection and antibiotic treatment (Hughes *et al.*, 1998; Pires *et al.*, 2016; Olszak *et al.,* 2017). Preclinical and clinical studies have confirmed that phage treatment can reduce bacterial load and attenuate inflammatory responses; a recent personalised inhaled phage therapy trial in nine CF patients with MDR *P. aeruginosa* refractory to standard antibiotics reported a median reduction of 10^4 CFU/mL in sputum bacterial density, alongside improved lung function, though complete eradication was not achieved, suggesting phage therapy currently functions as an adjunct to rather than a replacement for antibiotic therapy (Cafora *et al.*, 2019; Waters *et al.*, 2017; Chan *et al.*, 2025).

Route of administration is a critical consideration in clinical translation. Inhalation allows direct delivery of high phage titres to the lower airways, maximising local concentrations while minimising systemic exposure (Wang *et al.*, 2021). Nebulised or dry-powder phage formulations have been optimised for pwCF, accounting for mucus viscosity, airway surface liquid composition, and patient inhalation capacity. IV administration may be required for systemic or disseminated infections but is limited by rapid clearance by the reticuloendothelial system and potential neutralisation by circulating antibodies (Speck and

Smithyman 2016). In Denmark, studies of *Pseudomonas* infecting phages, including those associated with chronic CF lung infections, have highlighted the potential for phage-based interventions informed by local bacterial isolates. While clinical applications remain limited, case reports and cohort studies suggest that phage therapy could complement standard antibiotic regimens in CF patients (Chan *et al.*, 2025;).

The clinical application of phage therapy is also informed by considerations of resistance evolution. Bacterial escape from single phage treatment can occur rapidly through receptor modification, CRISPR-Cas-mediated immunity, or biofilm-mediated protection (Hampton *et al.*, 2020; Chan *et al.*, 2013). To mitigate this, treatment strategies increasingly employ phage cocktails, combinations of multiple, complementary phages targeting different receptors or bacterial phenotypes, which can suppress resistance emergence, broaden host range, and enhance bactericidal activity (Oechslin, 2018; Gordillo *et al.*, 2019). *In vitro* studies have shown that phage cocktails can reduce *P. aeruginosa* biofilm biomass and viability more effectively than single-phage treatments, demonstrating the advantage of multi-phage strategies in controlling established biofilms (Alves *et al.*, 2016). Clinical experience similarly supports the need for customised cocktails tailored to patient-specific isolates, particularly in chronic infections where bacterial populations are heterogeneous and spatially structured (Dedrick *et al.*, 2019; Wright *et al.*, 2009).

Phage therapy is further complemented by the potential for synergistic interactions with antibiotics. PAS can arise when phage mediated lysis enhances antibiotic penetration or when sub-lethal antibiotic stress increases bacterial susceptibility to phages (Comeau *et al.*, 2007; Uchiyama *et al.*, 2018). Experimental models have demonstrated that combining lytic phages with aminoglycosides, fluoroquinolones, or β-lactams results in greater reductions in *P. aeruginosa* density than either agent alone, including strains resistant to both therapeutic modalities (Oechslin *et al.*, 2017). PAS is particularly relevant in CF, where dense biofilms, anaerobic microenvironments, and thick mucus reduce antibiotic efficacy (Döring et al., 2012; Mulcahy *et al.*, 2010). By integrating phage cocktails with tailored antibiotic regimens, clinicians can potentially achieve sustained microbial suppression and limit the emergence of MDR phenotypes (Chan *et al.*, 2018; Gordillo *et al.*, 2019).

Regulatory and translational challenges remain significant. In Europe, phage therapy is typically administered under compassionate use frameworks, with ongoing efforts to establish standardised production, quality control, and clinical trial protocols (Verbeken *et al.*, 2014). In Denmark, the centrally organised adult and paediatric CF services at the Copenhagen CF Centre and partner centres have established a strong research infrastructure, enabling specialised pathogen surveillance, patient-safety protocols and

longitudinal monitoring of chronic infections. This embedded research framework offers a foundation suitable for complex interventions such as tailored phage therapies (Qvist *et al.*, 2024; Høiby, 2025). Such frameworks provide a blueprint for broader implementation, combining personalised phage selection with standardised clinical oversight.

In summary, the application of phage therapy to treat CF infections is grounded in detailed knowledge of phage biology, bacterial defence mechanisms, and the complex lung microenvironment. Effective treatment requires careful selection of lytic phages, often in the form of personalised or pre-formulated cocktails, delivered via optimised routes and potentially in combination with antibiotics. The Danish CF experience underscores the feasibility of this approach, demonstrating how integrated care models can support clinical translation while addressing the challenges of bacterial heterogeneity and chronic infection. Subsequent sections will explore the design and optimisation of phage cocktails (Section 1.4.4) and the mechanistic basis and clinical evidence for PAS (Section 1.4.5).

1.4.4 Phage Cocktail Therapies

Phage cocktail therapy has emerged as a cornerstone of modern phage application in chronic *P. aeruginosa* infections, particularly in pwCF, where bacterial populations are highly heterogeneous and multidrug-resistant. Unlike monophage therapy, which relies on a single phage strain targeting a specific bacterial receptor, cocktails combine multiple phages with complementary host ranges and mechanistic profiles. This strategy enhances the breadth of coverage against genetically diverse isolates, mitigates the rapid emergence of phage-resistant mutants, and increases the probability of successful biofilm penetration (Oechslin, 2018; Gordillo Altamirano and Barr, 2019).

The development of an effective phage cocktail begins with the isolation and characterisation of candidate phages. *In vitro* studies of *P. aeruginosa* isolates from pwCF demonstrate substantial phenotypic heterogeneity, including mucoidy, SCVs and variable phage susceptibility, which underpins the need for screening panels of lytic phages across multiple clinical strains (Olszak *et al.*, 2015). Genomic characterisation is equally critical, allowing the exclusion of temperate phages, or those encoding undesirable genes such as toxins or antibiotic resistance determinants (Kutter *et al.*, 2010; Hyman and Abedon, 2010). Generally, only strictly lytic phages with well-characterised genomes are considered suitable for clinical or preclinical application as temperate phages, which are generally excluded, can integrate into the host genome (Chan *et al.*, 2013). However, in compassionate use cases, such as *M. abscessus* infection, temperate phages have been genetically engineered to be obligately lytic where naturally occurring lytic phages are sparse (Dedrick *et al.*, 2019).

Cocktail optimisation involves several interdependent parameters. The phage–host interaction dynamics, multiplicity of infection (MOI), and potential antagonistic interactions among phages must all be evaluated. For example, when multiple phages compete for the same receptor or interfere with each other's replication cycles, overall bactericidal efficacy can be reduced (Bull *et al.*, 2002; Gu *et al.*, 2012). Conversely, complementary phages that target different receptors or exhibit distinct adsorption kinetics can provide synergistic effects, reducing bacterial density more effectively than any single phage (Chan *et al.*, 2013; Oechslin, 2018). Empirical testing under conditions mimicking the CF lung, including viscous mucus and biofilm structures, is necessary to predict *in vivo* performance (Mulcahy *et al.*, 2010; Pires *et al.*, 2017).

Biofilm disruption is a critical rationale for cocktail therapy in CF. Chronic *P. aeruginosa* infections are dominated by dense biofilms that confer high-level tolerance to antibiotics and immune clearance. Individual phages may exhibit limited penetration into biofilms due to EPS matrices, slow bacterial growth, or physiological heterogeneity (Drenkard, 2003; Stewart, 2002). By employing phages with enzymatic depolymerases or complementary biofilm-targeting profiles, cocktails can synergistically degrade EPS, facilitating access to deeper bacterial layers and promoting lysis (Hughes *et al.*, 1998; Pires *et al.*, 2016). *In vitro* studies demonstrate that phage cocktails can dramatically reduce *P. aeruginosa* biofilm biomass compared with single-phage treatments, for example, reductions exceeding 90% have been observed in static models of *P. aeruginosa* biofilms (Alves *et al.*, 2016). Moreover, phages targeting different receptors reduce the likelihood of resistance emergence. Experimental evolution studies indicate that *P. aeruginosa* exposed to monophage treatment frequently generates receptor-modified escape mutants within hours to days, whereas cocktails dramatically delay or prevent this adaptation (Oechslin, 2018; Chan *et al.*, 2013; Bull *et al.*, 2002).

A key consideration in the Danish CF context is the high degree of clonal heterogeneity within patient populations. The Copenhagen CF Centre routinely monitors chronic *P. aeruginosa* lineages, including epidemic clones such as DK1 and DK2, which exhibit differential biofilm phenotypes, mucoidy, and intrinsic resistance to antibiotics (Marvig *et al.*, 2015). Cocktail design is informed by these local epidemiological data, ensuring that administered phages collectively target the prevalent strains within the patient cohort. Danish CF centres monitor chronic *P. aeruginosa* lineages, including epidemic clones such as DK1 and DK2, to inform the selection of phages for therapeutic applications, ensuring that treatments target locally prevalent strains and account for clonal heterogeneity (Marvig *et al.*, 2015)

Pharmacokinetics and administration routes are also pivotal. Aerosolised or nebulised cocktails are preferred in CF due to the direct deposition in the lower airways, allowing phages to reach mucosal surfaces and biofilms while limiting systemic exposure (Ben Porat *et al.*, 2021; Dedrick *et al.*, 2019). Factors such as phage stability in airway surface liquid, tolerance to local pH, and interactions with host immune components are actively investigated to optimise dosing strategies (Flint *et al.*, 2023; Pezzulo *et al.*, 2012). Cocktail formulations often aim to maintain a high ratio of active phages relative to bacterial density (MOI ≥ 10), which has been shown to improve bacterial clearance and reduce the emergence of resistant subpopulations (Oechslin *et al.*, 2016; Alves *et al.*, 2016).

Synergy with antibiotics further enhances the utility of cocktails. PAS can manifest through multiple mechanisms, including phage induced modulation of bacterial physiology, enhanced antibiotic penetration into biofilms, or exploitation of sub-lethal antibiotic stress to increase phage susceptibility (Comeau *et al.*, 2007; Uchiyama *et al.*, 2018). *In vitro* and *ex vivo* studies combining phage cocktails with aminoglycosides, β-lactams, or fluoroquinolones have demonstrated substantial reductions in CF derived *P. aeruginosa* populations, even when both agents individually showed limited efficacy (Chang *et al.*, 2019; Oechslin *et al.*, 2016; Martin *et al.*, 2023). These findings underscore the potential for integrated phage–antibiotic regimens, particularly in chronic infections characterised by MDR and biofilm persistence (Gordillo Altamirano and Barr, 2019; Ryan *et al.*, 2012).

Beyond bactericidal activity, cocktail therapy offers additional benefits in limiting the evolution of hypermutator phenotypes. Chronic *P. aeruginosa* infections often harbour hypermutable subpopulations, which accelerate resistance acquisition to antibiotics (Oliver *et al.*, 2004; Oliver and Mena, 2010). Phage cocktails, by targeting multiple receptors and exploiting diverse lytic mechanisms, reduce selective pressure on any single bacterial pathway, slowing the emergence of resistance and maintaining long-term efficacy (Chan *et al.*, 2013; Bull *et al.*, 2002).

Clinical translation of cocktail therapy remains in its infancy but is progressing rapidly. Compassionate use cases in Europe and the United States, often involving pwCF and recalcitrant *P. aeruginosa* infections, demonstrate safety, tolerability, and encouraging efficacy signals (Dedrick *et al.*, 2019; Wright *et al.*, 2009). Denmark's centralised CF care system provides extensive pathogen surveillance and research infrastructure, offering a strong foundation for the future development of coordinated phage-cocktail trials tailored to local *P. aeruginosa* isolates, while maintaining rigorous clinical oversight (Qvist *et al.*, 2024; Pedersen *et al.*, 1986). Regulatory considerations, including Good Manufacturing Practice (GMP) production, standardised quality control, and clear pharmacovigilance protocols, are

critical for widespread adoption and are actively addressed in ongoing European initiatives (Verbeken *et al.*, 2014; Kutter *et al.*, 2010).

In conclusion, phage cocktail therapy offers a potent, adaptable, and clinically promising strategy for the treatment of chronic *P. aeruginosa* infections in CF. By combining multiple phages with complementary activity, personalised selection for patient-specific isolates, and integration with PAS approaches, cocktails can overcome key barriers associated with monophage therapy, including resistance emergence, biofilm tolerance, and host heterogeneity. The Danish experience demonstrates the feasibility of this approach in a centralised care setting, providing a robust foundation for future clinical trials and translational development. Subsequent sections will examine the mechanistic basis, preclinical evidence, and clinical applications of PAS (Section 1.4.5), which further enhances the therapeutic potential of cocktail based strategies.

1.4.5 Phage–Antibiotic Synergy (PAS)

PAS describes the phenomenon whereby phages and antibiotics interact to produce a greater bactericidal effect than either agent alone, often enabling sub-inhibitory antibiotic concentrations to become clinically effective (Comeau *et al.*, 2007; Chan *et al.*, 2018). The mechanistic basis of PAS is multifactorial. Phage infection can alter bacterial physiology, increasing susceptibility to antibiotics through changes in cell wall integrity, metabolic stress, or modulation of efflux systems (Ryan *et al.*, 2012; Torres-Barceló *et al.*, 2018). Conversely, sub-lethal antibiotic exposure can enhance phage adsorption and replication by inducing SOS responses, cell filamentation, or the expression of surface receptors, creating a mutually reinforcing cycle of bacterial eradication (Comeau *et al.*, 2007; Uchiyama *et al.*, 2019). In CF *P. aeruginosa* isolates, which frequently display biofilm-associated phenotypic heterogeneity, PAS has been shown to accelerate biofilm disruption, increase lysis of persister cells, and reduce overall bacterial load more effectively than monotherapy (Oechslin *et al.*, 2016; Chan *et al.*, 2018).

Studies using *P. aeruginosa* isolates from pwCF patients have shown that combining lytic phage cocktails with conventional antibiotics, such as tobramycin, ceftazidime, or ciprofloxacin, can significantly enhance biofilm disruption and reduce bacterial load compared with monotherapy. This has been demonstrated both *in vitro* and in CF relevant infection models, highlighting the potential of combination regimens to overcome antibiotic resistance and biofilm persistence (Oechslin *et al.*, 2016; Chang *et al.*, 2019; Martin *et al.*, 2023). Some epidemic clones of *P. aeruginosa* in Denmark, such as DK1 and DK2, have been sequenced and characterised as mucoid isolates with adaptation signatures in CF

patient lineages (Marvig *et al.*, 2015; Norman *et al.*, 2016). These clones are understood to have evolved persistent biofilm-forming capacity under chronic infection.

PAS also mitigates the emergence of resistance. Chronic CF infections are often dominated by hypermutator lineages, which rapidly acquire resistance to antibiotics during prolonged treatment (Oliver *et al.*, 2004; Oliver and Mena, 2010). Phage exposure in isolation can select for receptor modified escape mutants, while antibiotics applied alone drive conventional resistance mechanisms. By simultaneously exerting dual selective pressures, PAS reduces the likelihood of single pathway adaptation, delaying the development of both phage and antibiotic resistance (Chan *et al.*, 2013; Bull *et al.*, 2002). Experimental evolution studies further support this concept, demonstrating that co-administration of phages and β-lactams maintains bacterial susceptibility over prolonged passages, whereas monotherapies rapidly select resistant subpopulations (Oechslin *et al.*, 2016; Torres-Barceló, 2018).

Biofilm penetration is another key area where PAS demonstrates clear advantages. The EPS matrix of CF *P. aeruginosa* biofilms limits antibiotic diffusion and creates oxygen and nutrient gradients that sustain dormant, tolerant cells (Stewart, 2002; Mulcahy *et al.*, 2010). Phages, particularly those encoding depolymerases, can degrade EPS, creating microchannels that facilitate antibiotic access (Hughes *et al.*, 1998; Pires *et al.*, 2016). In combination with aminoglycosides, β-lactams, or fluoroquinolones, PAS enhances drug penetration, leading to increased killing of both metabolically active and dormant biofilm bacteria (Oechslin *et al.*, 2016; Chan *et al.*, 2018). This effect is critical in CF, where biofilm-associated tolerance underlies persistent infection and repeated exacerbations.

Timing, dosing, and sequence of administration are important determinants of PAS efficacy. Preclinical studies indicate that simultaneous application of phages and antibiotics often yields the strongest synergy, whereas staggered treatment can result in antagonism depending on phage-host dynamics and antibiotic mechanism of action (Comeau *et al.*, 2007; Uchiyama *et al.*, 2019). For instance, bacteriostatic antibiotics can delay phage replication by slowing bacterial growth, whereas bactericidal agents may enhance lytic phage efficacy through complementary killing mechanisms rather than direct enhancement of phage replication; additionally, fluoroquinolones can induce the SOS response, triggering prophage induction in lysogenic bacteria and converting them to the lytic cycle, which may contribute to observed synergy in mixed bacterial populations. Optimisation of PAS regimens therefore requires careful consideration of pharmacokinetics, pharmacodynamics, and the microenvironment of chronic infection, particularly the thick mucus characteristic of CF lungs (Stewart, 2002; Döring *et al.*, 2012).

Emerging evidence also suggests that PAS can synergise with CFTR modulators, indirectly improving infection control. By partially restoring airway surface liquid hydration and mucociliary clearance, modulators reduce bacterial density and biofilm establishment, potentially enhancing the accessibility and efficacy of phage–antibiotic combinations (Middleton *et al.*, 2019; Heijerman *et al.*, 2019). This interplay highlights the potential for integrative therapeutic strategies that combine pathogen-targeted and host-modulating interventions.

In clinical translation, several case reports and compassionate-use studies illustrate PAS efficacy. Dedrick *et al*. (2019) describe a patient with chronic MDR *P. aeruginosa* who exhibited sustained bacterial clearance and clinical improvement following combined phage and antibiotic therapy. Similarly, Wright *et al*. (2009) report synergistic reductions in bacterial load in CF patients receiving nebulised phage cocktails in conjunction with inhaled tobramycin. Although large controlled clinical trials remain limited, *in vitro* and CF-relevant studies have demonstrated that PAS can significantly enhance bacterial eradication when using phage cocktails together with routine antibiotics such as tobramycin or ceftazidime. Such findings are especially relevant for care systems with strong surveillance infrastructure, like the Copenhagen CF Centre, that have access to patient derived *P. aeruginosa* isolates, and could in future support personalised phage cocktail regimens tailored to local strain epidemiology (Henriksen *et al.*, 2019; Burgener *et al.*, 2019; Martin *et al*., 2021; Knudsen *et al.*, 2009).

Regulatory and practical considerations for PAS are evolving. Production under GMP standards, careful assessment of pharmacological interactions, and standardised efficacy testing are prerequisites for broader implementation (Verbeken *et al.*, 2014; Kutter *et al.*, 2010). Importantly, the integration of PAS into existing CF care pathways requires close coordination between microbiology, clinical pharmacology, and CF specialists to ensure safety, reproducibility, and maximal therapeutic benefit.

In summary, phage therapy offers a uniquely adaptable and precision-targeted strategy for treating chronic *P. aeruginosa* infections in CF, with particular promise when incorporated into phage cocktails or combined with antibiotics through PAS. PAS enhances bacterial clearance, disrupts biofilms, and reduces resistance emergence, representing a mechanistically rational and empirically supported adjunct to conventional therapy. The Danish CF model, with its centralised care and detailed microbial surveillance, provides an ideal framework for the development and clinical application of personalised phage-based strategies. While regulatory, manufacturing, and standardisation challenges remain, the growing body of preclinical and early clinical evidence supports the capacity of phage therapy

to improve outcomes in patients with limited treatment options, laying the foundation for future clinical trials and routine adoption in CF infection management.

1.5 Objectives

1. To determine clearance the killing activity of 49 phages against 92 clinical *P. aeruginosa* isolates from pwCF, and to characterise the capacity of individual phages to prevent and disrupt *P. aeruginosa* PAO1 biofilms.

2. To use clearance and biofilm profiles to develop a broad spectrum phage cocktail against clinical *P. aeruginosa* pathogens from pwCF and assess the efficacy of the cocktail at different MOI.

3. Investigate how rapidly resistance evolution occurs to previously designed broad spectrum cocktails versus monophage therapy and determine whether a resensitization or synergistic effect can be observed between phage cocktail treatment and the antibiotics commonly used in clinical pwCF.

1.6 Thesis Chapter Overview

1.6.1 Data Chapter 1: Characterisation of phage efficacy against clinical strains of *P. aeruginosa* isolated from pwCF.

This study evaluated the clearance and biofilm disruption capabilities of a collection of 49 bacteriophages against clinical *P. aeruginosa* isolates from pwCF, providing comprehensive insights into the potential application of phage therapy for chronic infections. A principal finding was that length of infection, defined as the number of years since first *P. aeruginosa* culture, did not influence phage susceptibility, suggesting that the timing of bacterial colonisation does not impact the effectiveness of phage therapy *in vitro*. In contrast, greater length of infection was associated with higher levels of antibiotic resistance, consistent with evolutionary adaptation over prolonged infection, with the exception of colistin, where isolates from patients with greater length of infection displayed lower MICs, reflecting a fitness cost associated with maintaining LPS modifications that confer resistance to other antibiotics, which may inadvertently restore susceptibility to polymyxin-class antibiotics by altering outer membrane charge and permeability. These observations underscore the necessity for alternative treatments to conventional antibiotics, particularly in CF populations with chronic, MDR infections.

Importantly, all 92 strains tested were susceptible to at least one phage in the collection, and all phages demonstrated activity against at least one clinical isolate, highlighting the broad

infectivity spectrum and therapeutic potential of phages. Phage titre was not a determinant of bacterial clearance, indicating that efficacy may depend more on phage-host dynamics than concentration alone. Geographic origin also influenced efficacy, with Finnish phages outperforming Belgian counterparts, suggesting potential lineage dependent variations in infectivity. The targeting mechanism of phages, whether LPS or T4P, did not significantly affect clearance, although the use of multiple phages targeting different receptors could enhance treatment robustness and reduce resistance development.

Patterns of antibiotic resistance were found to correlate with genetic lineage groups of *P. aeruginosa*, consistent with previous studies, yet no correlation between antibiotic and phage resistance was observed, supporting the feasibility of combined PAS strategies. Several phages demonstrated capacity to prevent and disrupt biofilms, a key factor in persistent CF infections. Notably, phages were generally more effective at preventing biofilm formation than eradicating established biofilms, with some instances of increased biofilm biomass observed following phage treatment, likely reflecting adaptive bacterial responses and phage-mediated lysis releasing extracellular DNA that may act as a structural scaffold, paradoxically enhancing biofilm matrix stability. These results reinforce the importance of selecting phages with robust biofilm targeting properties for therapeutic applications.

The use of clinical isolates, rather than laboratory adapted strains, enhances the clinical relevance of the findings, providing a realistic assessment of phage efficacy against genetically diverse, antibiotic resistant populations. While the study employed *in vitro* assays that offer efficient screening methods, limitations include the absence of dynamic host factors present *in vivo*, potential long-term coevolution of bacteria and phages, and incomplete mechanistic understanding of phage biofilm interactions. Future studies could address these limitations by incorporating liquid media assays, determining phage surface receptor specificity, sequencing phage lineages and clinical strains, and investigating molecular mechanisms underlying biofilm modulation.

Overall, this chapter provides strong evidence supporting the broad-spectrum activity of phages against clinical *P. aeruginosa* strains, their potential utility in overcoming MDR, and their ability to target biofilm mediated persistence. These findings lay a robust foundation for the development of phage based therapeutic strategies in CF, highlighting the importance of phage selection, strain-specific interactions, and consideration of clinical infection history in optimising treatment outcomes.

1.6.2 Data Chapter 2: Validation of phage cocktails against clinical *P. aeruginosa* with both known and unknown monomicrobial susceptibility.

This chapter focused on the development and evaluation of broad-spectrum phage cocktails targeting clinical *P. aeruginosa* isolates from pwCF. The primary aim was to establish an empirical 'first-line' cocktail capable of providing immediate therapeutic coverage while personalised phage therapies are prepared. This approach mirrors the rationale for broad-spectrum antibiotic use in acute infections, addressing the need for rapid initiation of treatment in clinical settings (Kortright *et al.*, 2019; Hernández & Koskella, 2024).

Computationally designed cocktails were generated using the PhageCocktail R package, identifying minimal two-phage combinations, typically one LPS-binding and one T4P-binding phage, predicted to lyse all 92 isolates. This design strategy capitalised on receptor diversity to maximise host-range breadth and limit bacterial escape, reflecting principles of functional diversity and complementarity in phage targeting (Chan *et al.*, 2013; Torres-Barceló *et al.*, 2014; Rosanna *et al.*, 2022). However, despite broad host-range predictions, many computationally designed cocktails exhibited limited biofilm disrupting activity, necessitating the addition of empirically selected biofilm active phages. This finding highlights the well documented disconnect between planktonic infectivity and biofilm control, emphasising that theoretical cocktail design must be complemented with empirical validation to ensure clinical efficacy (Harper *et al.*, 2014; Melo *et al.*, 2023; Hernández and Koskella, 2024).

Evaluation of cocktail efficacy across different MOI revealed strong concentration-dependent effects. At nominal MOI 0.001 (~10^{-6} effective), minimal clearance was observed, with paradoxical increases in bacterial growth and biofilm biomass in some assays, likely reflecting stress-induced biofilm responses under sublethal phage exposure (Høiby *et al.*, 2010; Darch *et al.*, 2012). Low MOI underperformance was attributed primarily to insufficient phage concentration rather than intrinsic cocktail design flaws, with full-titre individual phages retaining infectivity. This outcome suggests that antagonistic interactions or receptor competition may occur in multi-phage cocktails at low titres, reinforcing the necessity for empirically optimised dosing strategies (Oechslin *et al.*, 2021; Matsuzaki *et al.*, 2020).

At MOI 0.1, cocktails achieved improved planktonic inhibition, though transient paradoxical increases in optical density persisted, consistent with selection for phage-tolerant subpopulations and stress-induced adaptation (Wright *et al.*, 2009; Torres-Barceló *et al.*, 2018). Biofilm clearance remained limited, reflecting the inherent resilience and structural complexity of CF-associated *P. aeruginosa* biofilms. While many phages likely encoded depolymerases or enzymatic adjuncts (Cornelissen *et al.*, 2021; Melo *et al.*, 2023), enzymatic activity may have been insufficient or impeded by dense biofilm architecture, underscoring

the need to include highly efficient biofilm-targeting phages or adjunctive EPS-targeting treatments in empirical first-line cocktails (Bull *et al.*, 2002; Matsuzaki *et al.*, 2020).

At high MOI (10), cocktails achieved substantial reductions in planktonic growth, demonstrating that phage concentration is a critical determinant of empirical efficacy (Payne *et al.*, 2000; Abedon, 2012). Despite improved planktonic control, biofilm clearance remained minimal, reinforcing the challenges of treating established CF biofilms *in vitro* and highlighting that even high-MOI cocktails require validated enzymatic activity and strategic cocktail composition for consistent biofilm disruption (Rahman *et al.*, 2023; Hernández and Koskella, 2024).

Comparison between computationally designed and randomly assembled cocktails revealed no consistent superiority of designed combinations. Effect sizes were uniformly small, suggesting that empirical outcomes are influenced more by MOI, strain variability, and biofilm phenotypes than by theoretical receptor diversity (Oechslin *et al.*, 2021; Zhang *et al.*, 2025). Similarly, categorisation of phages into Disrupter and Preventer groups did not predict cocktail performance across the heterogeneous CF isolates, highlighting that biofilm phenotyping alone is insufficient for guiding first-line cocktail design (Harper *et al.*, 2014; Azeredo *et al.*, 2022). Subset analyses of strain-specific responses further revealed significant heterogeneity, including paradoxical growth stimulation in certain isolates, reflecting diverse bacterial defence strategies such as receptor mutation, CRISPR-Cas immunity, and phenotypic tolerance (Torres-Barceló *et al.*, 2018; Hernández and Koskella, 2024).

The study underscores the importance of integrating broad-spectrum empirical coverage with biofilm targeting strategies to achieve clinically relevant outcomes. While first-line cocktails can provide immediate therapeutic intervention against diverse *P. aeruginosa* populations, their efficacy is highly context dependent, necessitating iterative empirical validation and optimisation. Future work should focus on refining dosing strategies, incorporating phages with potent depolymerase activity, evaluating phage-phage interactions, and assessing performance *in vivo* using CF infection models. Ultimately, a dual strategy combining broad-spectrum empirical initiation with rapid personalised phage selection offers the most robust framework for therapeutic application in CF-associated infections.

1.6.3 Data Chapter 3: Evolutionary investigation of PAS in clinical *P. aeruginosa* samples with known AMR.

This chapter examined the adaptive responses of *P. aeruginosa* to multi-phage cocktail treatment under conditions designed to reflect clinically relevant isolates. By integrating

evolutionary growth assays, clonal resistance confirmation, whole genome sequencing (WGS), and PAS testing, the study dissected both the evolutionary trajectories of bacterial populations and the mechanistic basis of resistance emergence. These findings provide critical insight into the dual nature of phage therapy: while multi-phage cocktails can robustly suppress bacterial growth, they simultaneously impose selective pressures that drive adaptation, including receptor modification, envelope remodeling, activation of stress-response pathways, and engagement of intrinsic defense systems.

Multi-phage cocktail suppression dynamics revealed that combinations targeting distinct bacterial receptors, such as Cocktail C (comprising phages 14/1, PA5P2, and DMS3virAcrFI, targeting LPS and T4P respectively), effectively reduced growth in strain 342 over repeated 48 hour experimental windows, significantly outperforming individual phage treatments and untreated controls. This prolonged suppression aligns with prior studies demonstrating that multi-phage therapies delay resistance emergence and enhance bacterial clearance compared to single-phage interventions (Feng *et al.*, 2025; Lourenço *et al.*, 2020; Liang *et al.*, 2023). However, suppression was strain-dependent: certain isolates exhibited variable growth patterns under cocktail treatment, underscoring the challenge of achieving universal efficacy and highlighting the potential need for adaptive or strain-tailored approaches (Castledine *et al.*, 2022; Majkowska-Skrobek *et al.*, 2021).

Clonal resistance assays revealed distinct patterns of adaptation. Single-phage evolved clones developed resistance primarily to the selecting phage, whereas cocktail-exposed clones often exhibited broader cross-resistance. Whole-genome sequencing identified recurrent mutations in key genes related to LPS and outer-membrane biosynthesis (*galU, rfbB, rfaB*), T4P assembly (*pilB, pilT, pilQ, pilY1*), stress-response pathways (*lon, rtcB, gcvR*), and defense systems including prophage tail assembly components. Mutations in envelope biosynthesis genes likely reduce phage adsorption and simultaneously modulate antibiotic susceptibility, consistent with literature describing pleiotropic effects of LPS modification (Burmeister *et al.*, 2020; Nagy *et al.*, 2022). T4P mutations conferred resistance to pilus-targeting phages but are predicted to incur trade-offs in motility and biofilm formation based on the known functions of the mutated genes, highlighting predictable evolutionary costs of receptor-mediated escape mechanisms (Tan *et al.*, 2014; Hendrix *et al.*, 2024). Mutations in stress-response and defense-system genes likely synergise with structural modifications to stabilise resistant phenotypes and protect against superinfection (Chertkova *et al.*, 2023; Patel *et al.*, 2024).

Optical density analyses occasionally revealed paradoxical increases in growth under phage exposure, likely reflecting lysis-mediated debris, optical scattering, or ecological release of

resistant subpopulations. This emphasises the limitations of OD_{600} as a sole metric and supports the use of complementary methods such as colony forming unit (CFU) enumeration or plaque forming unit (PFU) assays for accurate population assessment.

PAS testing combining Cocktail C with polymyxin B demonstrated strong inhibition at intermediate antibiotic concentrations and low to moderate MOI, with fractional inhibitory concentration index (FICI) analyses indicating additive or synergistic interactions. Mechanistically, phage-induced envelope remodeling may enhance antibiotic permeability, exemplifying a therapeutically exploitable evolutionary trade-off. However, the long-term consequences of dual selective pressures remain uncertain, emphasizing the need for adaptive dosing and dynamic phage cocktail updating to mitigate the emergence of dual-resistant mutants (Torres-Barceló and Hochberg, 2016; Xuan *et al.*, 2022; Tagliaferri *et al.*, 2019).

The study highlights predictable evolutionary trajectories under phage cocktail pressure, where adaptation is predicted to incur trade-offs such as impaired motility, altered virulence, or increased antibiotic sensitivity, based on the known functions of the genes found to be mutated. Exploiting these trade-offs may enhance therapeutic strategies, for example by coupling phage therapy with sub-inhibitory antibiotic doses to exploit evolutionary trade-offs and steer bacterial adaptation toward increased phage susceptibility, rather than simply maximising bacterial killing which may accelerate resistance emergence. The results underscore the importance of adaptive, evolutionarily informed approaches, including sequential or alternating phage–antibiotic regimens, periodic cocktail redesign, and real-time genomic monitoring. Phage training, co-evolving phages with resistant populations prior to therapeutic use, emerges as a promising strategy to improve long-term efficacy and counteract resistance evolution (Borin *et al.*, 2021).

Despite the insights gained, limitations remain. The study was conducted in planktonic cultures, which do not fully recapitulate the spatial heterogeneity, nutrient gradients, or phage penetration barriers characteristic of biofilm-associated CF lung infections. Translational studies incorporating structured growth models or biofilm reactors are essential to validate the clinical relevance of observed resistance trajectories (Testa *et al.*, 2019; Chang *et al.*, 2022). Moreover, expanding PAS testing across additional clinical isolates, antibiotic classes, and MOI ranges is necessary to generalise findings and optimise therapeutic regimens. Functional validation of candidate mutations via targeted genetic manipulation (e.g., CRISPR-Cas) could clarify the causal links between specific genomic changes and phage susceptibility, fitness, and antibiotic responses. Population-level genomic approaches could

further resolve the dynamics of clonal interference, selective sweeps, and coexisting adaptive strategies, informing predictive models for clinical application.

Collectively, these findings demonstrate that while multi-phage cocktails can effectively suppress *P. aeruginosa*, evolutionary adaptation is inevitable, predictable, and exploitable. Therapeutic strategies that integrate PAS, adaptive cocktail updating, and consideration of trade-offs offer the most promising path toward durable, clinically relevant phage interventions in CF-associated infections.

2. Materials and Methods.

2.1 Bacterial Culture Preparation

A total of 141 *P. aeruginosa* isolates collected from pwCF and supplied by Helle Krogh Johansen from Rigshospitalet (Copenhagen, Denmark) were used for this study. Samples were taken primarily from the lungs of patients (Table 2.1) a total of 24 different lineages (genotypes) were isolated from 9 patients (Patient ID: Table 2.1). While the exact course of antibiotic treatment for these patients is unknown, there are standard treatment guidelines for Danish pwCF. At first detection of *P. aeruginosa*, oral ciprofloxacin was administered alongside nebulized colistin. This continued for 3 months for treatments pre 2008 and 3 weeks for treatment starting post 2008. If *P. aeruginosa* infection persisted after this treatment, IV piperacillin or tazobactam was administered in combination with either IV or inhaled tobramycin. Where resistance to piperacillin or tazobactam was observed, meropenem, ceftazidime or aztreonam were administered in combination with tobramycin or colistin (Marvig, *et al.*, 2015). Of the total of 141 isolates, 93 were selected for infectivity assay as a representative spread of the Danish pwCF and *P. aeruginosa* lineages and length of infection (number of years between the first ever *P. aeruginosa* culture, Infection Age, and chronic infection), leaving sufficient isolates for subsequent blind phage cocktail assay testing which was also representative of all lineages. Lineage was determined according to Marvig *et al.* (2015), in which 474 isolate genomes were sequenced and compared. From this dataset, genomes were grouped into 53 genetically distinct clone types. Isolates within the same clone type differed by an average of 122 single nucleotide polymorphisms (SNPs), whereas genomes belonging to different clone types differed by more than 10,000 SNPs

Scrapings from frozen stocks were inoculated in 20 ml Luria-Bertani (LB) broth (Miller formulation; Formedium, Norfolk, UK) and incubated at 37℃, shaking at 180 rpm, for 24 h. 600 µl was then combined with 400 µl 50% glycerol and cryopreserved at -80℃ until required.

2.2 Phage Strain Preparation

59 phages from various sources were considered for inclusion in this study (Table 2.2); for some of these, bacterial receptor information (LPS or T4P) was provided alongside the samples. Source of isolation and known host bacteria was also included with samples. 49 were selected for inclusion in the study based on lifestyle and/or receptor information. Phage strains were inoculated from frozen stocks into 20 mL of LB broth using *P. aeruginosa* PAO1 as the host, except for QAT4 and QAT6 (cultured with *P. aeruginosa* Debi) and DMS3vir and

DMS3vir AcrFI (cultured with PA14). These were incubated in a 37°C shaking (180 rpm) incubator for 24 hours. After 600 µl was cryopreserved as described above, the remaining sample was centrifuged at 400 rpm for 10 minutes, the supernatants were filtered using 0.22 µl filters into glass bottles and the resulting phages stored at 4℃.

Table 2.1: *P. aeruginosa* sample origin information. Infection Age indicates the patient's age when the *P. aeruginosa* genotype was first detected. Length of infection indicates the number of years between the first ever *P. aeruginosa* culture, Infection Age, and chronic infection age.

Strain ID	Patient ID	Date Sample Obtained	Origin	Sinus/Lung	Genotype (Denmark/assigned genome number)	Infection Age	Length of infection
427	CF236	2006-08-29	Expectorate	Lung	DK15	0	27.05
428	CF236	2006-08-29	Expectorate	Lung	DK53	1.169444444	27.06944444
436	CF236	2007-01-30	Expectorate	Lung	DK15	0.419444444	27.46666667
423	CF236	2011-02-24	Expectorate	Lung	DK15	4.486111111	31.53888889
434	CF236	2005-06-28	Expectorate	Lung	DK53	0	25.89166667
422	CF236	2012-05-30	Expectorate	Lung	DK53	6.922222222	32.83333333
431	CF236	2007-12-06	Expectorate	Lung	DK53	1.955555556	27.85
435	CF236	2008-10-20	Expectorate	Lung	DK01	2.469444444	29.16388889
420	CF236	2009-03-26	Expectorate	Lung	DK01	2.902777778	29.61666667
429	CF236	2010-01-11	Expectorate	Lung	DK01	4.5	31.20277778
419	CF236	2010-02-06	Expectorate	Lung	DK01	4.086111111	30.80277778
224	CF382	2007-02-19	Tracheal Secretion	Lung	DK32	0	4.397222222
247	CF382	2012-08-17	Expectorate	Lung	DK32	5.494444444	9.891666667
237	CF382	2010-01-02	Laryngeal Suction	Lung	DK32	2.95	7.347222222
226	CF382	2010-01-02	Laryngeal Suction	Lung	DK32	1.480555556	5.877777778
227	CF382	2009-07-09	Expectorate	Lung	DK32	2.55	6.947222222
228	CF382	2009-07-09	Expectorate	Lung	DK32	2.55	6.947222222
241	CF382	2011-01-06	Grafting/Jaw Cavity	Sinus	DK32	4.283333333	8.680555556

Table 2.1 Continued

Strain ID	Patient ID	Date Sample Obtained	Origin	Sinus/Lung	Genotype (Denmark/assigned genome number)	Infection Age	Length of infection
243	CF382	2011-08-17	Expectorate	Lung	DK32	4.494444444	8.891666667
242	CF382	2011-01-06	Grafting/Jaw Cavity	Sinus	DK32	4.283333333	8.680555556
239	CF382	2010-01-06	Secretion/Jaw Cavity	Sinus	DK32	3.283333333	7.680555556
244	CF382	2011-08-17	Expectorate	Lung	DK32	4.494444444	8.891666667
246	CF382	2012-08-17	Expectorate	Lung	DK32	5.494444444	9.891666667
122	CF405	2008-03-04	Laryngeal Suction	Lung	DK13	0	0.161111111
119	CF405	2008-03-04	Secretion/Sinus	Sinus	DK13	2.397222222	2.558333333
114	CF405	2010-09-16	Expectorate	Lung	DK13	4.85	5.011111111
121	CF405	2007-10-22	Expectorate	Lung	DK13	1.95	2.111111111
112	CF405	2008-03-04	Secretion/Sinus	Sinus	DK13	2.397222222	2.558333333
118	CF405	2008-03-04	Secretion/Sinus	Sinus	DK13	2.397222222	2.558333333
110	CF405	2010-06-10	Grafting/Forehead Cavity	Sinus	DK13	4.905555556	5.066666667
448	CF405	2012-05-12	Laryngeal Suction	Lung	DK13		
116	CF405	2012-05-16	Laryngeal Suction	Lung	DK13	6.516666667	6.677777778
77	CF408	2006-08-05	Laryngeal Suction	Lung	DK09	0	0
84	CF408	2008-12-08	Tracheal Secretion	Lung	DK09	2.261111111	2.261111111
90	CF408	2010-01-07	Grafting/Sinus	Sinus	DK09	4.147222222	4.147222222
89	CF408	2010-01-07	Grafting/Sinus	Sinus	DK09	4.147222222	4.147222222
82.1	CF408	2008-09-18	Secretion/Sinus	Sinus	DK09	2.361111111	2.361111111

Table 2.1 Continued

Strain ID	Patient ID	Date Sample Obtained	Origin	Sinus/Lung	Genotype (Denmark/assigned genome number)	Infection Age	Length of infection
83	CF408	2008-12-15	Tracheal Secretion	Lung	DK09	2.602777778	2.602777778
78	CF408	2007-06-11	Laryngeal Suction	Lung	DK09	1.494444444	1.494444444
80	CF408	2008-05-03	Laryngeal Suction	Lung	DK09	1.825	1.825
81.1	CF408	2008-09-18	Secretion/Sinus	Sinus	DK09	2.361111111	2.361111111
91	CF408	2009-06-22	Secretion/Sinus	Sinus	DK09	3.122222222	3.122222222
182	CF422	2005-05-23	Expectorate	Lung	DK21	0	1.363888889
178	CF422	2009-12-01	Expectorate	Lung	DK22	0	5
177	CF422	2010-02-03	Expectorate	Lung	DK23	0	6.138888889
173	CF422	2012-08-08	Expectorate	Lung	DK24	0	8.572222222
179	CF422	2006-07-26	Expectorate	Lung	DK21	1.175	2.538888889
180.1	CF422	2006-06-13	Expectorate	Lung	DK21	1.055555556	2.419444444
176	CF422	2012-11-19	Expectorate	Lung	DK24	0.280555556	8.852777778
184	CF422	2012-08-10	Expectorate	Lung	DK24	0.166666667	8.738888889
174	CF422	2012-08-08	Expectorate	Lung	DK24	0	8.572222222
181	CF422	2005-08-11	Expectorate	Lung	DK21	0.458333333	1.822222222
414	CF455	2011-12-07	Expectorate	Lung	DK18	0	3.927777778
417	CF455	2007-12-17	Laryngeal Suction	Lung	DK19	0	0.358333333
411	CF455	2012-06-11	Expectorate	Lung	DK18	1.316666667	5.244444444
440	CF455	2012-04-26	Bronchoalveolar Lavage	Lung	DK18	0.788888889	4.716666667

Table 2.1 Continued

Strain ID	Patient ID	Date Sample Obtained	Origin	Sinus/Lung	Genotype (Denmark/assigned genome number)	Infection Age	Length of infection
416	CF455	2008-10-11	Expectorate	Lung	DK19	0.897222222	1.255555556
415	CF455	2009-01-12	Secretion/Sinus	Sinus	DK19	1.955555556	2.313888889
412	CF455	2012-04-26	Bronchoalveolar Lavage	Lung	DK18	0.788888889	4.716666667
413.1	CF455	2011-12-09	Expectorate	Lung	DK18		
349	CF472	2007-01-16	Laryngeal Suction	Lung	DK38	0	1.661111111
339	CF472	2005-05-18	Laryngeal Suction	Lung	DK47	0	0
340	CF472	2010-08-24	Expectorate	Lung	DK48	0	5.266666667
341	CF472	2011-07-02	Laryngeal Suction	Lung	DK49	0	5.719444444
345	CF472	2012-02-11	Bronchoalveolar Lavage	Lung	DK19	3.4	7.455555556
347	CF472	2009-12-16	Laryngeal Suction	Lung	DK19	0.522222222	4.577777778
344	CF472	2012-02-11	Bronchoalveolar Lavage	Lung	DK19	3.4	7.455555556
205	CF496	2004-11-24	Laryngeal Suction	Lung	DK27	0	0
202	CF496	2006-03-21	Laryngeal Suction	Lung	DK28	0	1.325
199	CF496	2007-05-29	Laryngeal Suction	Lung	DK29	0	2.513888889
200	CF496	2007-05-29	Laryngeal Suction	Lung	DK30	0	2.513888889
223	CF496	2012-07-03	Expectorate	Lung	DK27	7.286111111	7.286111111
214	CF496	2009-07-27	Laryngeal Suction	Lung	DK27	4.675	4.675
206	CF496	2012-07-03	Expectorate	Lung	DK29	4.772222222	7.286111111
213	CF496	2010-06-30	Grafting/Jaw Cavity	Sinus	DK29	3.086111111	5.6

Table 2.1 Continued

Strain ID	Patient ID	Date Sample Obtained	Origin	Sinus/Lung	Genotype (Denmark/assigned genome number)	Infection Age	Length of infection
204	CF496	2005-02-05	Laryngeal Suction	Lung	DK27	0.438888889	0.438888889
203	CF496	2005-07-11	Laryngeal Suction	Lung	DK27	0.952777778	0.952777778
201.1	CF496	2006-12-21	Laryngeal Suction	Lung	DK27		
198	CF496	2008-01-12	Tracheal Secretion	Lung	DK29	1.505555556	4.019444444
196	CF496	2008-03-06	Tracheal Secretion	Lung	DK29	0.769444444	3.283333333
210	CF496	2010-03-23	Secretion/Jaw Cavity	Sinus	DK29		
211	CF496	2010-03-23	Secretion/Jaw Cavity	Sinus	DK29	2.816666667	5.330555556
208	CF496	2011-06-20	Laryngeal Suction	Lung	DK29	4.058333333	6.572222222
207	CF496	2011-10-28	Bronchoalveolar Lavage	Lung	DK29	4.413888889	6.927777778
390	CF499	2006-03-15	Expectorate	Lung	DK06	0	0
382	CF499	2012-11-20	Expectorate	Lung	DK26	0	6.680555556
386	CF499	2009-08-07	Expectorate	Lung	DK50	0	3.313888889
388	CF499	2007-07-24	Expectorate	Lung	DK51	0	1.358333333
389	CF499	2006-03-10	Expectorate	Lung	DK06	0.55	0.55
391	CF499	2006-03-24	Expectorate	Lung	DK06	0.025	0.025
383	CF499	2012-07-12	Bronchoalveolar Lavage	Lung	DK26	0.047222222	6.727777778
385	CF499	2012-07-12	Bronchoalveolar Lavage	Lung	DK26	0.047222222	6.727777778
387	CF499	2009-08-31	Expectorate	Lung	DK50	0.147222222	3.461111111

Table 2.2: Origin information for the 59 phages considered for inclusion in this study, including host bacteria, known bacterial receptor targeted (LPS or T4P, where available), source of isolation, and relevant references..

Phage Number	Phage	Host Bacteria	Receptor	Source of Isolation	Source	Reference
1	PhiKZ	*P. aeruginosa PAO1*	T4P	Sewage water, Kazakhstan	Jean-Paul Pirnay	Friman *et al.* (2016)
2	PNM	*P. aeruginosa PAO1*	T4P	Mtkvari River, Tbilisi, Georgia	Jean-Paul Pirnay	Friman *et al.* (2016)
3	PT7	*P. aeruginosa PAO1*	T4P	Lake Ku, Tibilisi, Georgia	Jean-Paul Pirnay	Friman *et al.* (2016)
4	14/01	*P. aeruginosa PAO1*	LPS	Sewage water, Regensburg, Germany	Jean-Paul Pirnay	Friman *et al.* (2016)
5	PA1P1	*P. aeruginosa 61841*	LPS	Sewage water, Jyväskylä, Finland	Matti Jalasvuori	Mattila *et al*. (2015)
6	PA1P2	*P. aeruginosa 61841*	LPS	Sewage water, Jyväskylä, Finland	Matti Jalasvuori	Mattila *et al*. (2015)
7	PA1P3	*P. aeruginosa 61841*	LPS	Sewage water, Jyväskylä, Finland	Matti Jalasvuori	Mattila *et al*. (2015)
8	PA1P4	*P. aeruginosa 61841*	LPS	Sewage water, Jyväskylä, Finland	Matti Jalasvuori	Mattila *et al*. (2015)
9	PA1P5	*P. aeruginosa 61841*	LPS	Sewage water, Jyväskylä, Finland	Matti Jalasvuori	Mattila *et al*. (2015)
10	PA2P1	*P. aeruginosa 61823*	LPS	Sewage water, Jyväskylä, Finland	Matti Jalasvuori	Mattila *et al*. (2015)
11	PA4P2	*P. aeruginosa 61432*	LPS	Sewage water, Jyväskylä, Finland	Matti Jalasvuori	Mattila *et al*. (2015)
12	PA5P1	*P. aeruginosa 11AN03663*	LPS	Sewage water, Jyväskylä, Finland	Matti Jalasvuori	Mattila *et al*. (2015)
13	PA5P2	*P. aeruginosa 11AN03663*	T4P	Sewage water, Jyväskylä, Finland	Matti Jalasvuori	Mattila *et al*. (2015)
14	PA7P1	*P. aeruginosa 62314*	LPS	Sewage water, Jyväskylä, Finland	Matti Jalasvuori	Mattila *et al*. (2015)
15	PA7P2	*P. aeruginosa 62314*	LPS	Sewage water, Jyväskylä, Finland	Matti Jalasvuori	Mattila *et al*. (2015)
16	PA8P1	*P. aeruginosa 62263*	LPS	Sewage water, Jyväskylä, Finland	Matti Jalasvuori	Mattila *et al*. (2015)
17	PA8P2	*P. aeruginosa 62263*	LPS	Sewage water, Jyväskylä, Finland	Matti Jalasvuori	Mattila *et al*. (2015)
18	PA10P1	*P. aeruginosa 62206*	LPS	Sewage water, Jyväskylä, Finland	Matti Jalasvuori	Mattila *et al*. (2015)
19	PA10P2	*P. aeruginosa 62206*	LPS	Sewage water, Jyväskylä, Finland	Matti Jalasvuori	Mattila *et al*. (2015)
20	PA10P3	*P. aeruginosa 62206*	LPS	Sewage water, Jyväskylä, Finland	Matti Jalasvuori	Mattila *et al*. (2015)

Table 2.2 Continued

Phage Number	Phage	Host Bacteria	Receptor	Source of Isolation	Source	Reference
21	PA11P1	*P. aeruginosa 62180*	LPS	Sewage water, Jyväskylä, Finland	Matti Jalasvuori	Mattila *et al*. (2015)
22	PA11P2	*P. aeruginosa 62180*	LPS	Sewage water, Jyväskylä, Finland	Matti Jalasvuori	Mattila *et al*. (2015)
23	PA12P1	*P. aeruginosa 62181*	LPS	Sewage water, Jyväskylä, Finland	Matti Jalasvuori	Mattila *et al*. (2015)
24	PA12P2	*P. aeruginosa 62181*	LPS	Sewage water, Jyväskylä, Finland	Matti Jalasvuori	Mattila *et al*. (2015)
25	PA13P1	*P. aeruginosa 62172*	LPS	Sewage water, Jyväskylä, Finland	Matti Jalasvuori	Mattila *et al*. (2015)
26	PA13P2	*P. aeruginosa 62172*	LPS	Sewage water, Jyväskylä, Finland	Matti Jalasvuori	Mattila *et al*. (2015)
27	PA14P2	*P. aeruginosa 62109*	LPS	Sewage water, Jyväskylä, Finland	Matti Jalasvuori	Mattila *et al*. (2015)
-	LUZ7		TonB (LPS?)		Rob Lavigne (via Craig Maclean)	Betts *et al.* (2016)
28	LUZ19		T4P		Rob Lavigne (via Craig Maclean)	Betts *et al.* (2016)
29	QAT1	*P. aeruginosa 573*		Clinique André Renard (Herstal)	Jean-Paul Pirnay	Unpublished
30	QAT3a	*P. aeruginosa CN573*		CHU (Le Centre hospitalier universitaire de Liège)	Jean-Paul Pirnay	Unpublished
31	QAT3	*P. aeruginosa CN573*		CHU (Le Centre hospitalier universitaire de Liège)	Jean-Paul Pirnay	Unpublished
32	QAT4	*P. aeruginosa Debi*		CHU (Le Centre hospitalier universitaire de Liège)	Jean-Paul Pirnay	Unpublished
33	QAT5	*P. aeruginosa Debi*		Embourg (a province de Liège); Station Epuration	Jean-Paul Pirnay	Unpublished
34	QAT6	*P. aeruginosa Debi*		UZ Gent sewage water	Jean-Paul Pirnay	Unpublished
35	QAT7	*P. aeruginosa PAO1K*		UZ Gent sewage water	Jean-Paul Pirnay	Unpublished
36	QAT8	*P. aeruginosa Debi*		QAMH sewage water	Jean-Paul Pirnay	Unpublished
37	QAT9	*P. aeruginosa Debi*		QAMH sewage water	Jean-Paul Pirnay	Unpublished

Table 2.2 Continued

Phage Number	Phage	Host Bacteria	Receptor	Source of Isolation	Source	Reference
38	QAT10	*P. aeruginosa CN573*		QAMH sewage water	Jean-Paul Pirnay	Unpublished
39	QAT20	*P. aeruginosa CN573*		Tervuren water	Jean-Paul Pirnay	Unpublished
40	QAT21	*P. aeruginosa CN573*		Tervuren water	Jean-Paul Pirnay	Unpublished
41	QAT22	*P. aeruginosa CN573*		Vilvoorde water	Jean-Paul Pirnay	Unpublished
42	QAT23	*P. aeruginosa CN573*		UZ Gent sewage water	Jean-Paul Pirnay	Unpublished
43	QAT24	*P. aeruginosa CN573*		Zaventem water	Jean-Paul Pirnay	Unpublished
44	QAT25	*P. aeruginosa CN573*		Anderlecht water	Jean-Paul Pirnay	Unpublished
45	QAT26	*P. aeruginosa CN573*		Lede water	Jean-Paul Pirnay	Unpublished
46	QAT27	*P. aeruginosa CN573*		Antwerp water	Jean-Paul Pirnay	Unpublished
47	QAT28	*P. aeruginosa CN573*		QAMH sewage water	Jean-Paul Pirnay	Unpublished
48	DMS3vir		T4P		Edze Westra	Broniewski *et al.* (2021)
49	DMS3vir ACrFI		T4P		Edze Westra	Broniewski *et al.* (2021)

2.3 Phage Titre Determination

The concentration (titre) of each phage stock was determined to quantify viable phage particles for subsequent experimental use. Two overnight cultures of *P. aeruginosa* PAO1 were prepared by inoculating 10 mL of LB broth (Miller formulation; Formedium, Norfolk, UK) in 50 mL Falcon tubes and incubating at 37 °C with shaking at 200 RPM.

Each overnight culture was diluted six times at a 1:10 ratio in 9 mL of LB and incubated for approximately three hours at 37 °C and 200 RPM to obtain exponentially growing host cells. During this time, frozen phage stocks were allowed to equilibrate to room temperature to promote disaggregation of phage particles.

Following incubation, 30 mL of the diluted PAO1 culture was introduced into 500 mL of 0.7% LB soft agar, prepared using LB broth powder (Miller formulation; Formedium, Norfolk, UK) supplemented with 0.7% (w/v) bacteriological agar (Formedium, Norfolk, UK), that had been equilibrated in a 48 °C water bath for one hour. This process was repeated to prepare a total of 60 mL of overlay agar. The mixture was poured as an overlay onto pre-prepared LB broth plates (Miller formulation; Formedium, Norfolk, UK) supplemented with 1.5% (w/v) bacteriological agar (Formedium, Norfolk, UK) and allowed to solidify at room temperature.

Serial dilutions of each phage stock were then prepared by labeling seven 1.5 mL microcentrifuge tubes 10^{-1} to 10^{-6} and adding 180 µL of LB to each tube. Serial tenfold dilutions were performed by transferring 20 µL of phage suspension sequentially between tubes, discarding 20 µL from the final 10^{-6} dilution.

Phage plaque assays were conducted by spotting 10 µL of each dilution onto the prepared overlay plates and incubated overnight at 37 °C.

Plaques were counted the following day for each phage and dilution, and phage titres were calculated using the formula:

$$\text{PFU/mL} = \frac{\text{number of plaques x dilution factor}}{\text{Volume plated (mL)}}$$

In cases where plaques were too numerous to count, additional dilutions were prepared and plated up to 10^{-9} to obtain countable spots. All assays were performed in triplicate, and individual titres were determined for each phage strain to ensure consistency across experiments.

2.4 Infectivity Assay

A subset of 93 clinical *P. aeruginosa* isolates was selected from the full Danish CF collection to represent the genetic diversity of the collection, with one isolate selected from each phylogenetic lineage group as classified in the lineage data provided by Rigshospitalet, Copenhagen. Each isolate was cultured in 20 mL of LB broth (Miller formulation; Formedium, Norfolk, UK) and incubated at 37 °C with shaking at 180 RPM. The optical density at 600 nm (OD_{600}) was measured to estimate bacterial cell density prior to plating.

For phage screening, a 120 mm square LB broth plates (Miller formulation; Formedium, Norfolk, UK) supplemented with 1.5% (w/v) bacteriological agar (Formedium, Norfolk, UK) agar plate was divided into a grid pattern, and the phage number previously set (Table 2.2) was used to identify the position of each phage spot. Each clinical isolate was assigned two plates, allowing a total of 49 phages to be tested, 25 spots on the first plate and 24 on the second.

Phage suspensions were not normalized to the same titre prior to spotting. This approach minimized the number of preparatory steps and therefore increased the throughput of screening across the large panel of isolates. Although titres varied between phages, this was acceptable for qualitative screening aimed at identifying susceptible hosts rather than performing comparative infectivity assays.

For each strain, 40 mL of 0.7% LB soft agar, prepared using Luria–Bertani (LB) broth powder (Miller formulation; Formedium, Norfolk, UK) supplemented with 0.7% (w/v) bacteriological agar (Formedium, Norfolk, UK), was inoculated with 400 µL of the corresponding bacterial culture and mixed thoroughly before being poured onto the two pre-labelled plates. Once the agar had solidified, 5 µL of each phage preparation was spotted onto its designated position on the grid. Plates were allowed to air-dry completely and then incubated upside down at 37 °C for 24 hours.

The following day, plates were examined visually and scored for bacterial lysis. Zones of lysis were categorised as strong, moderate, limited, or none, based on the clarity and extent of bacterial clearing. Strong lysis was defined as a uniformly clear area with no residual growth; moderate lysis showed a distinct but slightly turbid clearing; limited lysis displayed faint or partial clearing; and no lysis indicated the absence of any visible clearing or plaques. Representative examples of each lysis category are shown in Figure 2.1.

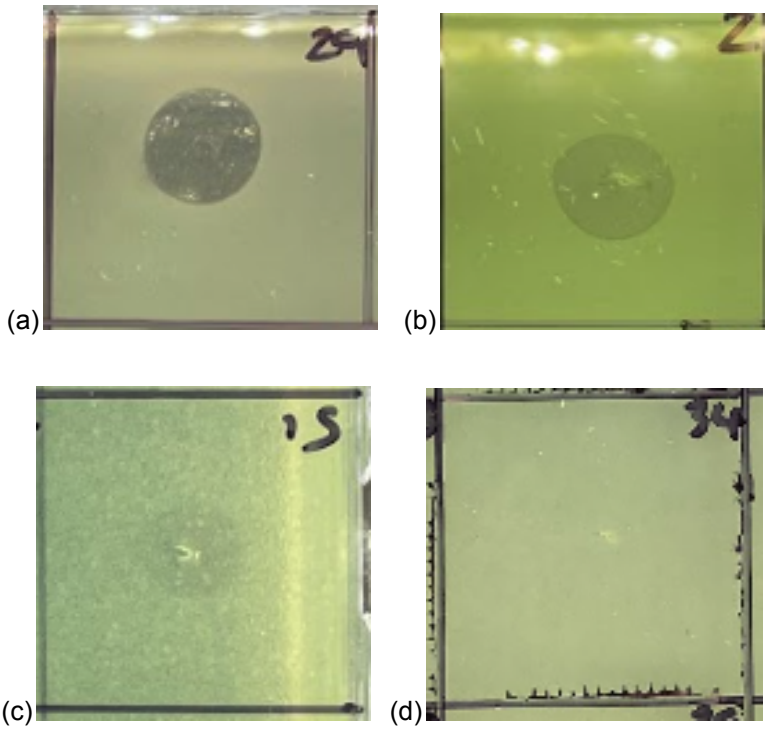

Figure 2.1: Representative examples of bacteriophage lysis categories on *P. aeruginosa* double-layer agar assay plates. Zones of lysis were categorised based on the clarity and extent of bacterial clearing. (a) Strong clearance: a uniformly clear area with no residual bacterial growth, shown here for phage QAT1 on *P. aeruginosa* strain 199. (b) Moderate clearance: a distinct but slightly turbid clearing zone, shown here for phage PNM on *P. aeruginosa* strain 173. (c) Limited clearance: faint or partial clearing, shown here for phage PA7P2 on *P. aeruginosa* strain 244. (d) No clearance: absence of any visible clearing or plaques, shown here for phage QAT6 on *P. aeruginosa* strain 77.

2.5 Biofilm Assay

To assess both the preventive and disruptive effects of phage treatments on *P. aeruginosa* biofilms, 96-well plate assays were conducted under two conditions: prevention of biofilm formation (PB) and disruption of established biofilms (DB). Phage QAT6 (phage 34) was excluded from these assays because its titre from the frozen stock was substantially lower than that of the other phages (approximately 10^3 PFU/mL, compared with 10^7–10^{11} PFU/mL for the remaining phages), which would have required excessive dilution to achieve comparable assay conditions. Whilst titre could theoretically have been increased through additional rounds of propagation on a permissive host strain followed by concentration via ultracentrifugation or polyethylene glycol (PEG) precipitation, this was not pursued as multiple other phages in the collection demonstrated comparable or broader infectivity, rendering inclusion of QAT6 unnecessary for the objectives of this study. All remaining phages were diluted to the same titre prior to use (10^7 PFU/mL) to ensure consistency across treatments. Wells containing no phage were included as negative controls to account for baseline biofilm formation during the staining process. Assays were performed in synthetic

cystic fibrosis medium (SCFM) to mimic the nutritional environment of the CF lung. SCFM was prepared according to lab protocols based on the original recipe from Palmer *et al*. (2007). This specific formulation was chosen because it is widely used and validated in CF biofilm studies, and it closely replicates key aspects of CF sputum, including physiologically relevant salts (sodium, potassium, ammonium, phosphate), ions (calcium, magnesium), amino acids (e.g., serine, glutamic acid, proline, glycine, alanine, valine, methionine, isoleucine, leucine, ornithine, lysine, arginine, aspartic acid, tryptophan, tyrosine, threonine, cysteine, phenylalanine, histidine), carbon sources (glucose, lactic acid), and vitamins (thiamine, niacin, pantothenic acid, biotin) that support bacterial growth and biofilm formation under conditions reflective of the CF lung. While polymers such as mucins, which can influence biofilm architecture and potentially phage binding, were omitted due to technical challenges, the remaining components provide a representative environment for studying *P. aeruginosa* biofilm development. Compared with alternative formulations, this recipe is compatible with phage infection assays and reproducible across multiple experimental replicates (see Appendix 1 for full formulation). Although multiple clinical isolates were used in other experimental components of this study, biofilm prevention and disruption assays were conducted using *P. aeruginosa* PAO1 as a representative strain. PAO1 was selected because it was shown to be a successful host for all remaining phages in the titre assay. This decision balanced experimental depth and feasibility, given the resource- and time-intensive nature of the crystal violet biofilm assay. The methodology was adapted from O'Toole (2011), Müsken *et al.* (2010), and Burton *et al.* (2006).

Bacterial Culture Preparation

P. aeruginosa PAO1 was revived from frozen stock and cultured overnight in 20 mL SCFM at 37 °C with shaking at 200 rpm. The overnight culture was then diluted 1:100 by transferring 200 µL into 19.8 mL of fresh SCFM for use in both PB and DB assays.

Biofilm Prevention Assay (PB)

To assess the efficacy of each phage, in isolation, at preventing biofilm formation, 180 µL of SCFM was added to each well of a 96-well microtiter plate. Wells designated for phage treatment received 10 µL of diluted bacterial culture and 10 µL of the relevant phage solution, while control wells received 10 µL of bacterial culture and 10 µL of sterile SCFM. Where necessary, phage stocks were diluted in SCFM to achieve the desired titre. Plates were incubated for 24 hours at 37 °C in a humidified environment, created by sealing the plates in a plastic bag with a wet paper towel to reduce evaporation and maintain moisture.

Phage-only wells were not included in this assay, as no bacterial growth is expected in the absence of cells, and SCFM alone does not produce a background signal in the crystal violet

staining. It is acknowledged that phage-only wells would additionally have served as contamination controls to confirm the absence of bacterial contamination in phage stocks; however, all phage stocks were filtered through a 0.22 µm membrane filter during preparation to remove bacterial contamination, and stocks were re-filtered or re-plated onto LB agar where anomalous results in any assay raised suspicion of contamination, providing sufficient quality control throughout the experimental period. This approach allowed the efficacy of each phage to be assessed directly, relative to bacterial-only controls.

Biofilm Disruption Assay (DB)

To examine the efficacy of individual phages in disrupting pre-formed biofilms, bacterial cultures were allowed to establish biofilms prior to phage treatment. In 96-well plates, 190 µL of SCFM and 10 µL of diluted bacterial culture were added to each well. Plates were incubated at 37 °C in a humidified environment, created by sealing the plates in a plastic bag with a wet paper towel, for 24 hours to permit biofilm formation.

After biofilm establishment, 10 µL of planktonic culture was carefully removed from each well. It is noted that this approach measures phage activity against residual planktonic cells in addition to established biofilm, rather than biofilm alone. Designated wells then received 10 µL of the relevant phage solution, while control wells received 10 µL of SCFM. Plates were incubated for a further 24 hours at 37 °C under the same humidified conditions.

A schematic of the plate layout is shown in Figure 2.2. Phage-treated wells are indicated in pink, bacterial growth controls (without phage) are shown in blue, and media-only negative controls are included. Numbers correspond to identifiers used in an experimental assay tracker.

Biofilm Staining

Following incubation, planktonic contents were carefully discarded into a Virkon disinfectant container. Wells were gently rinsed with deionised water to remove unattached cells and air dried for 15 minutes. This step minimised background staining from non-adherent bacteria.

To stain the remaining biofilm, 200 µL of 0.1% crystal violet solution (Alfa Aesar, Thermo Fisher Scientific, UK) was added to each well, including an additional, empty, 96-well plate used as a staining control. Plates were incubated at room temperature for 15-20 minutes. The dye was then discarded into Virkon, and the wells were rinsed again with deionised water before being air dried for 15 minutes.

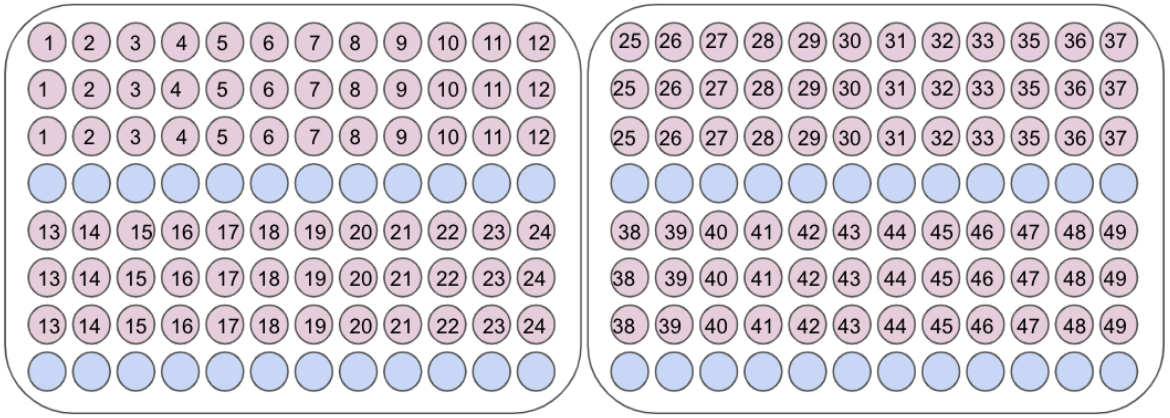

Figure 2.2: Layout of 96 well plates used for biofilm disruption assays. Each plate contains two sections. Pink wells indicate phage-treated wells, with numbers corresponding to individual phage identifiers as listed in Table 2.2. The first row of blue wells in each section contains *P. aeruginosa* PAO1 in the absence of phage, serving as a bacterial growth control. The second row of blue wells contains growth media only, serving as a negative control. Unnumbered pink wells indicate additional phage replicates. Two plates are shown, accommodating phages 1–24 (left) and 25–49 (right).

Biofilm Quantification

To quantify the biomass of stained biofilms, 220 µL of 70% ethanol was added to each well to solubilise the crystal violet. Plates were incubated at room temperature for 15 minutes. OD was then measured at 590 nm using a microtiter plate reader. A crystal violet–treated blank plate (without bacteria) was used as a negative control to normalise the absorbance readings. In subsequent assays, media control wells within the same plate were used as blanks for normalisation, replacing the separate blank plate approach.

2.6 Phage Cocktail Design Using the PhageCocktail R Package

To identify optimal phage combinations for broad-spectrum efficacy, binary infectivity data (presence or absence of lysis for each phage–strain pair) was analysed using the PhageCocktail R package (Díaz-Galián, Vega-Rodríguez, & Molina, 2022). PhageCocktail uses a combinatorial algorithm to rank phage combinations according to their ability to lyse the largest number of bacterial strains while minimizing redundancy among phages.

The software generated 3 two-phage combinations predicted to maximize host coverage. To expand these into three-phage cocktails, each two-phage combination was supplemented first with one of the two phages previously shown to be effective against biofilms, and then separately with the second biofilm-active phage, resulting in a total of six three-phage cocktails for experimental testing. The selection of three-phage cocktails was informed by clinical precedent, as cocktails used in published phage therapy cases and trials have commonly comprised two to four phages, balancing breadth of host coverage with practical

considerations of formulation, regulatory approval, and the risk of phage-phage interactions at higher multiplicities (Gordillo Altamirano and Barr, 2019; Schooley *et al.*, 2017).

Each phage cocktail was prepared at multiple multiplicities of infection (MOI): 0.001, 0.1, and 10. MOI was calculated as the ratio of plaque-forming units (PFU) to colony-forming units (CFU), determined immediately prior to infection. Bacterial density (CFU/mL) was quantified by serial dilution and plating; cultures were serially diluted in sterile media/PBS and appropriate dilutions were spread onto LB agar plates in duplicate. Plates were incubated at 37°C for 24 hours, after which colonies were counted from plates containing 30–300 colonies. CFU/mL was calculated by multiplying colony counts by the dilution factor and plating volume. Phage titres were quantified by plaque assay to determine PFU/mL.

Phage stocks were diluted to achieve the desired PFU concentrations relative to the measured bacterial density. For example, an MOI of 0.001 corresponds to 10^5 PFU per 10^8 CFU. Phages were combined in equal volumes to generate the final cocktail prior to inoculation.

During data verification, it was noted that the initially stated ratio of 100 phage particles per 10^8 bacterial cells corresponds to an MOI of 10^{-6} rather than 0.001. This discrepancy has been corrected in subsequent analyses and is considered when interpreting the limited antimicrobial effect observed at low MOI conditions, as reduced effective phage-to-host ratios may have limited infection dynamics.

To generate random control cocktails, a number between 1 and 49 (corresponding to assigned phage identifiers) was selected using a random number generator (random.org) to assemble three-phage mixtures. This allowed comparison of the efficacy of algorithmically designed cocktails versus randomly assembled combinations.

Cocktail Combinations:

- *Designed cocktails:*
  (a) PNM, PA10P2, DMS3vir AcrFI
  (b) PT7, PA5P1, DMS3vir AcrFI
  (c) 14/01, PA5P2, DMS3vir AcrFI
  (d) PNM, PA10P2, PA7P1
  (e) PT7, PA5P1, PA7P1
  (f) 14/01, PA5P2, PA7P1

- *Random cocktails (generated using random.org):*
  (g) QAT8, PA12P1, PA1P5
  (h) PA1P2, PA10P3, QAT3a
  (i) PT7, PA1P5, PA8P2
  (j) 14/01, DMS3vir AcrFI, PA5P1
  (k) PA12P1, PA5P2, DMS3vir
  (l) PA4P2, PA1P5, PA10P1

2.7 Phage Cocktail Validation Assay

The remaining untested clinical isolates of *P. aeruginosa* (Table 2.3) were not included in the previous assays to allow a subset to be preserved for this assay where the interaction between the strain and phage was unknown. This more closely represents a clinical setting where a first line of defence phage cocktail could be administered. . These isolates had been cryopreserved at –80 °C in 40% glycerol stocks until required. Upon revival, each strain was inoculated into 20 mL of LB broth and incubated at 37 °C with shaking at 180 rpm for 24 hours.

All revived isolates were spot-assayed using 10-fold serial dilutions to 10^{-6} to confirm viable growth and determine which strains produced clearly countable colonies. Based on this assessment, strains meeting the exclusion criteria, those yielding no growth, confluent lawns, or colonies too faint or sparse to reliably enumerate, were removed from further analysis. Exclusion of strains that failed to produce reliably countable colonies was necessary to ensure accurate and reproducible quantification of bacterial growth; repeated subculturing to optimise growth conditions was deliberately avoided to minimise the risk of introducing adaptive mutations that could alter phage susceptibility or antibiotic resistance profiles, thereby maintaining strains as close to their clinically relevant state as possible. 17 strains (indicated in bold in Table 2.3) remained, representing a broad distribution of genetic lineages within the clinical collection.

Each selected strain was inoculated into 20 mL of SCFM and incubated at 37 °C with shaking at 180 rpm for 24 hours. The resulting cultures were then prepared for use in the assay where 180 µL of SCFM was added to 42 wells of a 96-well plate, followed by 10 µL of the prepared bacterial culture. Each of the twelve phage cocktails (six designed and six random) was added to three replicate wells (10 µL per well), leaving six wells containing bacteria only as untreated controls. Each plate also included twelve negative-control wells containing 200 µL of SCFM only. The experiment was repeated for each of the 17 clinical strains, with 2 strains assayed per 96-well plate.

Table 2.3: Sample origin information for the subset of *P. aeruginosa* strains used in subsequent assay testing beyond the initial infectivity assay. Strains in bold indicate the 17 strains selected based on reliable growth and colony formation in the spot assay revival screen for further experimental testing..

Strain ID	Patient ID	Origin	Sinus/Lung	Genotype (Denmark/assigned genome number)	Infection Age (Genotype)	Length of infection from 1st *P.a* colonisation
427.1	CF236	Expectorate	Lung	DK01	0.327777778	27.03333333
437	CF236	Expectorate	Lung	DK53	-	-
432	CF236	Expectorate	Lung	DK01	1.113888889	27.81388889
430	**CF236**	**Expectorate**	**Lung**	**DK53**	**5.341666667**	**31.23888889**
423.1	**CF236**	**Expectorate**	**Lung**	**DK53**	**5.655555556**	**31.56388889**
421	CF236	Expectorate	Lung	DK01	6.080555556	32.79166667
225	**CF382**	**Tracheal Secretion**	**Lung**	**DK32**	**1.191666667**	**5.588888889**
229	CF382	Laryngeal Suction	Lung	DK32	2.419444444	6.816666667
235	CF382	Secretion/maxillary sinus	Sinus	DK32	3.283333333	7.680555556
240	**CF382**	**Grafting/maxillary sinus**	**Sinus**	**DK32**	**4.283333333**	**8.680555556**
241.1	CF382	Grafting/maxillary sinus	Sinus	DK32	4.283333333	8.680555556
245	CF382	Expectorate	Lung	DK32	5.494444444	9.891666667
120	CF405	Expectorate	Lung	DK13	1.95	2.111111111
111	CF405	Laryngeal Suction	Lung	DK13	2.183333333	2.344444444
117	CF405	Secretion/sinus	Sinus	DK13	2.397222222	2.558333333
115	**CF405**	**Expectorate**	**Lung**	**DK13**	**4.177777778**	**4.338888889**
113	CF405	Grafting/frontal sinus	Sinus	DK13	4.905555556	5.066666667
447	CF405	Laryngeal Suction	Lung	DK13	-	-
76	**CF408**	**Laryngeal Suction**	**Lung**	**DK09**	**0.308333333**	**0.308333333**
79	CF408	Laryngeal Suction	Lung	DK09	1.494444444	1.494444444
81	CF408	Secretion/sinus	Sinus	DK09	2.361111111	2.361111111
82	CF408	Secretion/sinus	Sinus	DK09	2.361111111	2.361111111

Table 2.3 Continued

Strain ID	Patient ID	Origin	Sinus/Lung	Genotype (Denmark/assigned genome number)	Infection Age (Genotype)	Length of infection from 1st *P.a* colonisation
85	CF408	Tracheal Secretion	Lung	DK09	-	-
87	CF408	Secretion/sinus	Sinus	DK09	3.122222222	3.122222222
88	**CF408**	**Laryngeal Suction**	**Lung**	**DK09**	**3.294444444**	**3.294444444**
86	CF408	Laryngeal Suction	Lung	DK09	3.975	3.975
180	CF422	Expectorate	Lung	DK21	1.055555556	2.419444444
183	**CF422**	**Expectorate**	**Lung**	**DK24**	**0.166666667**	**8.738888889**
175	**CF422**	**Expectorate**	**Lung**	**DK24**	**0.280555556**	**8.852777778**
413	**CF455**	**Expectorate**	**Lung**	**DK18**	**0.166666667**	**4.094444444**
412.1	**CF455**	**Laryngeal Suction**	**Lung**	**DK18**	**0.788888889**	**4.716666667**
346	**CF472**	**Laryngeal Suction**	**Lung**	**DK19**	**0**	**4.055555556**
348	CF472	Laryngeal Suction	Lung	DK19	0.522222222	4.577777778
343	CF472	Bronchoalveolar Lavage	Lung	DK19	3.4	7.455555556
342	**CF472**	**Laryngeal Suction**	**Lung**	**DK19**	**3.375**	**7.430555556**
203.1	**CF496**	**Laryngeal Suction**	**Lung**	**DK27**	**0.952777778**	**0.952777778**
201	**CF496**	**Laryngeal Suction**	**Lung**	**DK27**	**2.075**	**2.075**
197	CF496	Tracheal Secretion	Lung	DK29	1.505555556	4.019444444
215	CF496	Laryngeal Suction	Lung	DK29	2.161111111	4.675
212	CF496	Grafting/maxillary sinus	Sinus	DK29	3.086111111	5.6
209	**CF496**	**Bronchoalveolar Lavage**	**Lung**	**DK29**	**3.491666667**	**6.005555556**
223	CF496	Expectorate	Lung	DK27	7.286111111	7.286111111
392	**CF499**	**Expectorate**	**Lung**	**DK06**	**0.025**	**0.025**
384	CF499	Bronchoalveolar Lavage	Lung	DK26	0.047222222	6.727777778

Plates were incubated for 48 hours at 37 °C in a humidified environment, and OD_{600} was recorded at 0, 24, and 48 hours. Following incubation, plates were processed for biofilm quantification as described in Section 2.5. The experiment was conducted at three MOI: 0.001, 0.1, and 10.

2.8 Phage Cocktail Spot Assay

Each of the 12 cocktails was spotted in duplicate as per the previous infectivity assay, initially at MOI 0.1 though this was expanded to MOI 10 and MOI 0.001 (see chapter 4). On a separate plate, the 18 phages used in the cocktails were spotted at their original titre. This was done for each of the 17 clinical strains used in the phage cocktail validation assay.

2.9 Calibration Curve

To quantify the relationship between OD_{600} and viable cell count, a dilution and plating assay was conducted. Samples were kept on ice throughout the preparation stages to minimise unintended bacterial growth. *P. aeruginosa* PAO1, along with clinical strains 224, 90, 210, and 201.1, each selected to represent distinct genotype groups as defined in the Marvig *et al.* (2015) study, were revived from frozen glycerol stocks and cultured overnight in SCFM at 37 °C with shaking at 180 rpm.

Following overnight incubation, 1.0 mL of fresh SCFM was added to 6 sterile Falcon tubes per strain. A 1.0 mL aliquot of the overnight culture was added to the first tube, and a 50% serial dilution was performed through the remaining tubes. From each dilution, 200 µL was transferred to designated wells (1–6 or 7–12) of a 96-well microtiter plate. To determine OD_{600} at known bacterial concentrations, a further 1/10 serial dilution was carried out in the vertical direction (rows A–H), by combining 180 µL SCFM and 20 µL of sample per well (Figure 2.3).

To determine viable counts, 10 µL of each diluted sample was spotted onto square SCFM agar plates. A separate plate was used for each strain, and samples were applied in rows corresponding to the layout of the 96-well plate. Plates were incubated at 37 °C for 24 hours. CFU were counted the following day, and values were extrapolated to CFU/mL, taking into account the plated volume and dilution factor. Each strain was tested in triplicate for the entire workflow.

A calibration curve was then constructed by plotting OD_{600} values against corresponding CFU/mL counts, enabling estimation of viable cell numbers based on spectrophotometric readings in subsequent experiments.

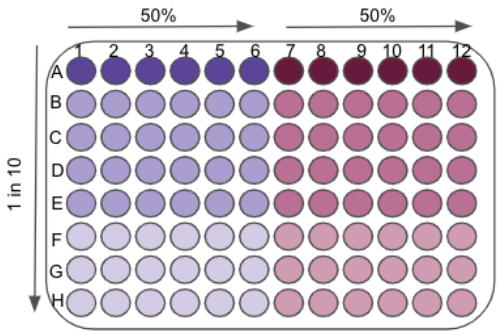

Figure 2.3: 96-well plate layout for OD_{600} calibration data. Wells are arranged in two blocks of six columns, each representing a separate bacterial strain or replicate (columns 1–6 and 7–12). Within each block, a 50% serial dilution is performed horizontally across columns (indicated by arrows, left to right), with each column representing a 50% reduction in bacterial concentration relative to the previous. A further 1-in-10 serial dilution is performed vertically down each column (rows A–H), as indicated by the downward arrow. Decreasing colour intensity from top to bottom and left to right reflects decreasing bacterial concentration. Wells were measured at OD_{600} to generate a calibration curve relating optical density to known bacterial concentrations.

2.10 Confirmation of Optical Density

In order to confirm that OD readings were proportional to CFU, 15 wells from the 0.1 MOI cocktail assay, alongside their positive control (Table 2.4) were selected for a spot assay. These were selected based on samples having the highest percentage change either way when compared to the positive control. 10µL of each sample or control was pipetted onto SCFM agar plates and incubated at 37°C for 24 hours.

Table 2.4: Selected wells from the 0.1 MOI phage cocktail assay and their corresponding positive controls were used to confirm that optical density (OD_{600}) measurements reflected viable bacterial growth. Wells were chosen based on showing the largest percentage deviations relative to the positive control. For each well, 10 µL of culture was spot-plated onto SCFM agar and incubated at 37 °C for 24 hours to assess colony formation.

Bacteria	Cocktail	Well	+ve Control Well	Bacteria	Cocktail	Well	+ve Control Well
183	a	1	11	203.1	b	3	11
225	l	3	5	392	a	3	4
115	b	3	7	88	c	1	11
413	i	3	6	240	j	2	2
175	g	1	10	412.1	j	3	5
430	c	1	4	423.1	f	3	8
209	f	2	8	201	k	3	4
346	a	2	6				

2.11 Growth Curve

From the MOI 0.1 data results were grouped into 8 different groupings dependent on whether each measurement (24Hr OD_{600}, 48Hr OD_{600} and Biofilm) increased or decreased compared to the corresponding positive control (Table 2.5). From these groups, three combinations of bacteria and phage cocktail were selected for a growth curve to more closely assess the growth over the first 24 hours. Groups with an increase at 24Hr OD_{600}, decrease at 48Hr OD_{600} and Biofilm only contained one strain. This was done using BMG Labtech SPECTROstar Nano microplate reader at 37℃ with OD_{600} readings taken every 10 minutes.

Table 2.5: Strain and cocktail groupings selected for growth curve analysis at MOI 0.1. In the grouping column, the three symbols indicate results at 24 h OD_{600}, 48 h OD_{600}, and biofilm timepoints respectively. + indicates an increase in growth compared to the no-treatment positive control and − indicates a decrease in growth compared to the no-treatment positive control.

Grouping	Bacteria	Cocktail	Bacteria	Cocktail	Bacteria	Cocktail
+ - -	412.1	k				
- + -	225	c	175	h	88	f
- + +	225	h	346	j	88	k
+ + -	346	a	203.1	b	412.1	j
+ - +	76	d	412.1	e	88	l
- - -	342	f	115	j	209	d
+ + +	175	e	225	g	88	j
- - +	76	c	115	f	209	i

2.12 Phage Coevolution Assay

The serial transfer coevolution assay design was adapted from established experimental evolution protocols in which bacterial populations are passaged under phage pressure across multiple consecutive growth cycles, allowing observation of resistance emergence and evolutionary trade-offs over time (Castledine *et al.*, 2022; Betts *et al.*, 2013). Clinical *P. aeruginos*a strains 203.1, 413 and 342 were selected based on their diverse responses to phage cocktail treatment observed in the cocktail validation assays (Section 4.3), and Cocktail C was selected based on its biofilm activity and overall performance across MOIs in the same assays (Section 4.3). All 3 strains were incubated overnight from frozen stock in SCFM liquid media. Incubation was at 37 ℃ shaking at 180 rpm. Using previously determined CFU/ml calculations, strains were diluted to MOI 0.1. Bacterial density was determined by OD_{600} measurement prior to dilution, with strain-specific OD values used to calculate CFU/mL and achieve the desired MOI of 0.1; exact OD values varied between strains and experimental runs. A 96 well microtiter plate was set up as in Figure 2.4. Positive

control wells contained 196 µL SCFM and 4 µL *Pseudomonas* strain; Phage cocktail wells contained 192 µL SCFM, 4 µL *Pseudomonas* strain and 4 µL cocktail C at MOI 0.1; individual phage wells contained 192 µL SCFM, 4 µL *Pseudomonas* strain and 4 µL phage at MOI 0.1; negative control wells contained 200 µL SCFM only. The plate was placed in a BMG Labtech SPECTROstar Nano microplate reader and set to take readings every 15 minutes for 48 hours (193 cycles). After completion of the cycle 2 µL of each sample well were added to 198 µL fresh SCFM in a new plate and the spectrophotometer programme was repeated, 120 µL of the original plate was cryopreserved at -80 with 60 µL of 50 % glycerol. No additional phage was added in subsequent plates; phage were carried over solely through the 2 µL transfer of sample from the preceding plate. This approach was deliberately chosen to reflect a clinically realistic scenario in which a fixed initial empirical dose of phage therapy is administered while personalised phage therapy is developed, consistent with current clinical practice in which empirical phage treatment is initiated as a bridge to personalised therapy (Djebara *et al.*, 2025). Whilst phage titre was not measured at each timepoint, this mirrors the practical constraints of a clinical setting where real-time phage quantification is not feasible. This was repeated until a total of 7 plates were run over 14 days.

Figure 2.4: Layout of 96 well plates for phage efficacy assays. Each colour block represents a different *P. aeruginosa* strain: light purple indicates strain 203.1, light green indicates strain 413, and light pink indicates strain 342. Within each colour block, wells are designated as follows: c = phage cocktail treatment (192 µL SCFM, 4 µL bacterial culture, 4 µL cocktail at MOI 0.1); 1, 2, 3 = individual phage treatments (192 µL SCFM, 4 µL bacterial culture, 4 µL individual phage at MOI 0.1); + = bacteria-only positive control (196 µL SCFM, 4 µL bacterial culture); − = media-only negative control (200 µL SCFM). Each condition is performed in triplicate across rows. All bacterial cultures were diluted to MOI 0.1 prior to plating.

Colony Isolation

Using the day 14 plates each well was streaked onto LB broth agar plates and incubated at 37°C for 24 hours. This time duration was too long to isolate individual colonies and was therefore reduced to 18 hours. From each well streak 12 colonies were selected, re streaked

onto further agar plates and incubated under the same conditions. A single colony was taken from these streaks and inoculated in 120 µl SCFM and incubated overnight at 37 ℃, 60 µl of 50 % glycerol was added to each well and the samples were cryopreserved at -80°C; representative clones were subsequently selected for WGS.

A schematic of section 2.12 to 2.14 can be seen in Figure 2.5.

2.13 Confirmation of Phage Resistance

The 30 clones for strain 203.1 from the final resistance assay plate were set up as shown in Figure 2.6. Phage treated wells contained 196 µL LB broth and 4 µL phage at MOI 0.1 while untreated positive control wells and blank media control wells contained 200 µL LB only. Whilst keeping the cryopreserved plate on ice a scraping of each of the frozen sample wells was taken using a multichannel pipette and added to the corresponding wells on the new plate. The plates were then placed in BMG Labtech SPECTROstar Nano microplate reader and set a programme to take readings every 15 minutes for 72 hours (288 cycles). This was then repeated for strains 413 and 342.

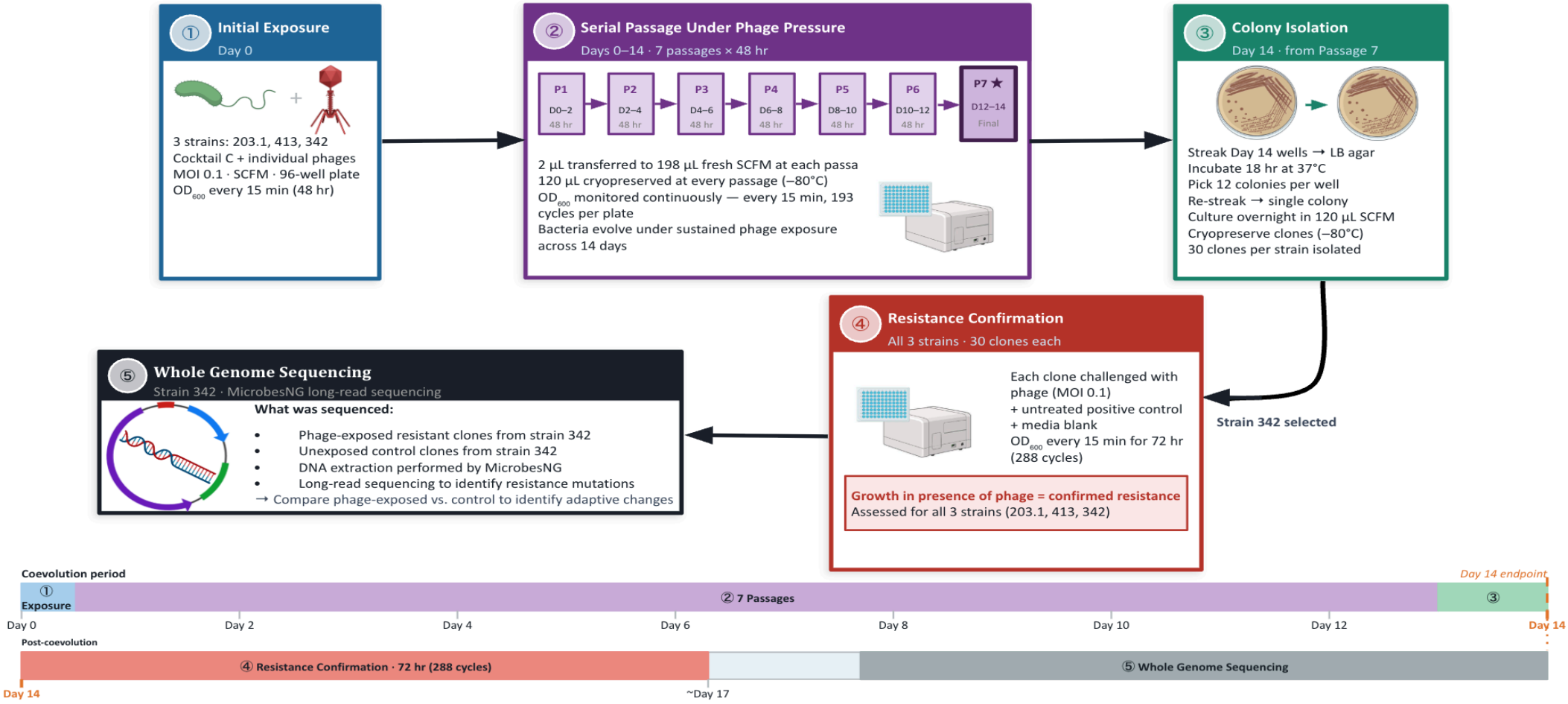

Figure 2.5: Schematic overview of the phage coevolution assay. Three *P. aeruginosa* clinical strains (203.1, 413, 342) were exposed to phage cocktail C and individual phages at MOI 0.1 in SCFM (①). Cultures were serially passaged every 48 hours over 14 days (7 passages total), with OD_{600} monitored continuously and 120 µL cryopreserved at each passage (②). At Day 14, single colonies were isolated and cryopreserved, yielding 30 clones per strain (③). Clones were confirmed as phage-resistant by OD_{600} monitoring over 72 hours in the presence of phage (④). Phage-exposed and control clones from strain 342 were selected for WGS to identify resistance-associated mutations (⑤). ★ denotes the final passage plate used for colony isolation. Created with images from BioRender.com

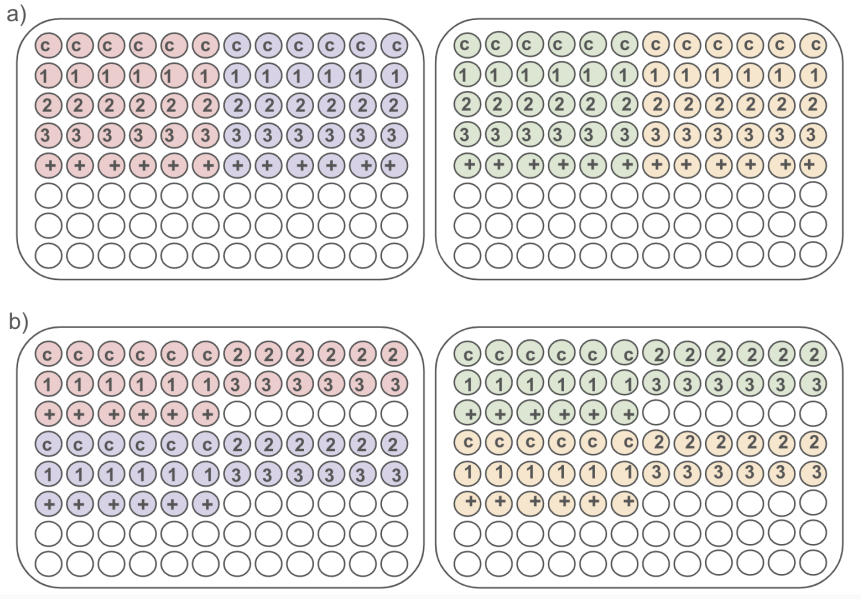

Figure 2.6: Layout of 96 well plates for evolutionary resistance assays**.** Four treatment conditions are indicated by well colour: pink = phage 14/01 (MOI 0.1); purple = phage PA5P2 (MOI 0.1); green = phage DMS3vir AcrFI (MOI 0.1); orange = bacteria-only positive control (no phage treatment). Blank wells contain media only and serve as negative controls. Each phage-treated and control well contained 196 µL LB broth and 4 µL phage, while positive control and media control wells contained 200 µL LB broth only. Bacterial clones were inoculated directly from cryopreserved stocks. (a) Plate layout for strains 203.1 (left) and 413 (right), each accommodating 30 clones across the four treatment conditions. (b) Plate layout for strain 342, with the same treatment structure across two plates.

2.14 Preparation for Sequencing

After selecting strain 342 for WGS by MicrobesNG, the submission protocol (Appendix 2) was followed and samples submitted. Long read sequencing was performed with DNA extraction completed by MicrobesNG prior to sequencing.

2.15 Minimum Inhibitory Concentration

To determine the MICs of clinically relevant antibiotics against the ancestral *P. aeruginosa* strain 342, a broth microdilution assay was performed using SCFM (recipe as described in Section 2.5 / Appendix 1) in 96-well microtiter plates (Figure 2.7).

Bacterial Culture Preparation

P. aeruginosa 342 was revived from frozen glycerol stock and cultured overnight in SCFM at 37 °C with shaking at 180 rpm. The overnight culture was then normalised to OD_{600} reading of approximately 0.2 prior to inoculation into assay plates.

Antibiotic Preparation

Five antibiotics were tested:

- Colistin (polymyxin class, clinically used in CF, Apollo Scientific, UK): 75 mg/mL.
- Polymyxin B (polymyxin class, included for comparison, Sigma-Aldrich, UK): 50 mg/mL.
- Tobramycin (aminoglycoside, clinically used in CF, Sigma-Aldrich, UK): 40 mg/mL.
- Meropenem (carbapenem, β-lactam, clinically used in CF, Fluorochem, UK): 50 mg/mL.
- Ampicillin (penicillin, β-lactam, not used in CF due to known resistance in *P. aeruginosa,* Melford, UK): 100 mg/mL.

All stock solutions were prepared in sterile deionised water.

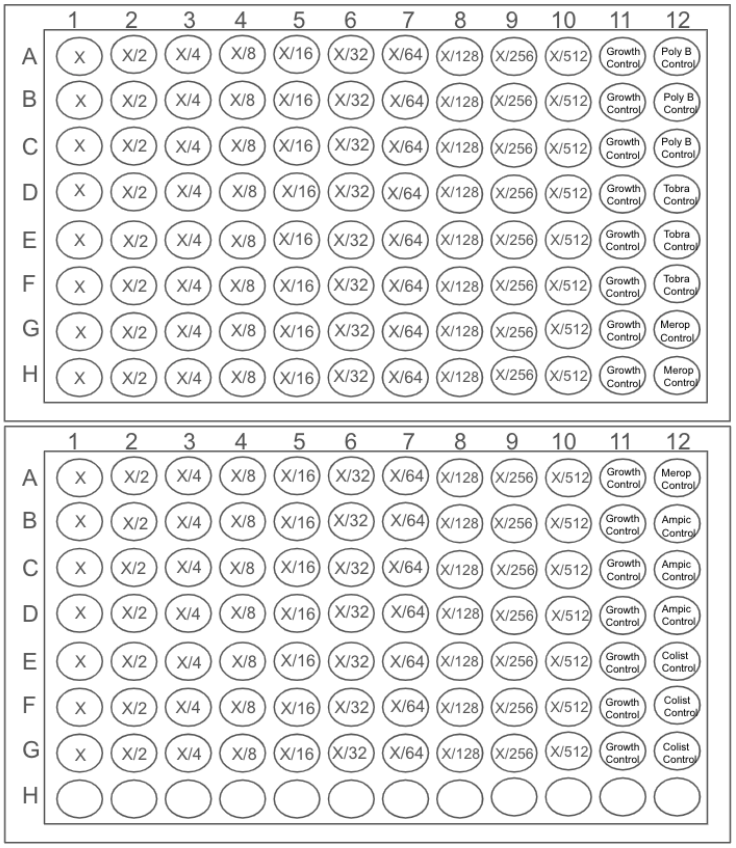

Figure 2.7: Layout of 96 well plates for Minimum Inhibitory Concentration (MIC) determination of 5 clinically relevant antibiotics against *P. aeruginosa* clinical strain 342. Each antibiotic was tested across a two-fold serial dilution series from the starting concentration (X) through to X/512 (columns 1–10), performed in triplicate (rows). Starting concentrations were: Colistin 75 mg/mL; Polymyxin B 50 mg/mL; Tobramycin 40 mg/mL; Meropenem 50 mg/mL; Ampicillin 100 mg/mL. Column 11 contains bacterial growth-only positive controls (no antibiotic). Column 12 contains antibiotic-only negative controls (no bacteria). Two plates are shown, accommodating all five antibiotics across rows A–H. Colistin, Tobramycin and Meropenem are clinically used in CF treatment; Polymyxin B was included for comparison; Ampicillin was included as a resistance control, as *P. aeruginosa* is known to be resistant to penicillin-class antibiotics.

MIC Assay Setup

Antibiotics were tested in triplicate across two 96-well plates. For each antibiotic, 20 µL of stock solution was added to wells in columns 1 and 12. Columns 2–10 were prefilled with 10 µL of sterile deionised water. A two-fold serial dilution was performed across columns 1–10 by transferring 10 µL sequentially, mixing thoroughly at each step, and discarding the final 10 µL to maintain a constant volume.

Each well in columns 1–10 then received 190 µL of the normalised bacterial culture, while wells in column 11 received 200 µL of culture as a no-antibiotic growth control. Plates were incubated at 37 °C overnight.

MIC Determination

Following incubation, wells were visually inspected for turbidity. The MIC was recorded as the lowest antibiotic concentration that completely inhibited visible bacterial growth. The assay was repeated to confirm reproducibility of MIC values.

2.16 Phage–Antibiotic Synergy

A protocol adapted from Nikolić *et al.* (2022) chequerboard method was used to assess the combined effects of phage and antibiotic treatment against *P. aeruginosa* strain 342. Polymyxin B was selected based on its performance in the MIC assay described in section 2.15, and due to its mechanistic relationship to colistin. Whilst colistin is the clinically used agent, it is a prodrug that is converted to polymyxin B *in vivo*, making polymyxin B the active moiety and a more suitable agent for *in vitro* chequerboard assays due to its greater stability and more consistent activity under microtitre plate conditions (Velkov *et al.*, 2010). The phage was applied in a two-fold serial dilution along the vertical axis of a 96-well microtitre plate, starting from a MOI of 10. Antibiotic concentrations were similarly serially diluted two-fold along the horizontal axis of the plate, beginning with a neat concentration from the second column onward. Plate layout can be seen in Figure 2.8.

Control wells were included to enable assessment of treatment effects and background signal. Column 11 contained phage-only treatments, while row H included antibiotic-only treatments. Column 12 served as a no-treatment control and also incorporated several negative controls: antibiotic only (no bacteria), phage only (no bacteria), and media-only wells containing LB broth and sterile water.

Strain 342 was grown overnight in LB broth at 37 °C with shaking at 180 rpm. Phage dilutions were performed directly in the plate, while antibiotic dilutions were prepared separately in

sterile Eppendorf tubes prior to transfer. Each well received 170 µL LB, 10 µL phage solution, and 10 µL antibiotic solution. Wells containing only phage or antibiotic received 180 µL LB and 10 µL of the respective treatment. No-treatment control wells received 190 µL LB.

The overnight bacterial culture was diluted to an OD_{600} of 0.223, and 10 µL of this suspension was added to each treatment well, excluding the sterile negative controls. All wells had a final volume of 200 µL. Plates were incubated at 37 °C in a BMG Labtech SPECTROstar Nano microplate reader for 48 hours. OD_{600} was recorded every 15 minutes to generate growth curves and assess treatment efficacy over time.

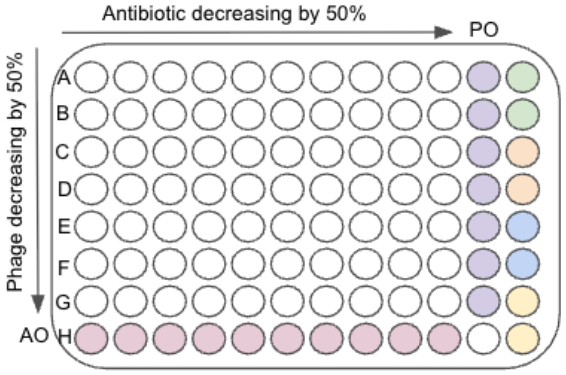

Figure 2.8: Layout of 96 well plate for the phage–antibiotic synergy (PAS) assay. Phage (applied at a starting MOI of 10) decreases in two-fold serial dilutions vertically down the plate (rows A–G), as indicated by the downward arrow. Polymyxin B antibiotic decreases in two-fold serial dilutions horizontally across the plate (columns 1–10), as indicated by the rightward arrow. Control wells are located in the final row (AO, antibiotic only) and final column (PO, phage only). Coloured control wells are as follows: green = no treatment positive control; orange = phage-only negative control; blue = antibiotic-only negative control; yellow = LB only and sterile water negative controls. The chequerboard design allows assessment of all possible phage and antibiotic concentration combinations simultaneously to identify synergistic, additive or antagonistic interactions.

2.17 Data Processing and Statistics

All experimental results were initially tabulated in Google Sheets before transfer to R Studio (R Version 2024.12.0+467) for analysis and visualization. Antibiotic resistance data, provided by the team at Rigshospitalet, Copenhagen, for the clinical isolates, were also compiled in Excel and imported into R. Graphs and figures were generated using the ggplot2 package, ensuring consistent formatting across experiments. Statistical analyses were performed using base R functions and relevant packages, including dplyr and tidyr, for data manipulation. Analyses included calculation of means, standard deviations, and percentages, as well as hypothesis testing where appropriate. Specific statistical models and tests, including ANOVA or Kruskal–Wallis for multi-group comparisons and post hoc tests such as

Tukey’s HSD or Dunn’s test, were applied as required. Significance thresholds and full details of statistical models are presented alongside results in each data chapter.

Whole-genome sequencing data from 30 evolved bacterial clones were analysed using Snippy (Version 4.6.0+galaxy0) on the Galaxy platform to identify variants relative to the ancestral reference strain. Each clone was processed using 14 CPU cores and 12 GB RAM. Snippy was run with the ancestral genome as the reference, with a minimum mapping quality of 1, minimum coverage per site of 1, a minimum fraction of reads supporting a variant of 0.9, and a minimum base quality of 1.0. Contigs from each clone were provided as input for variant calling.

The output from Snippy included tables of single nucleotide polymorphisms (SNPs), insertions, and deletions for each clone. These variant tables were exported for downstream analysis, including mapping mutations to coding sequences and predicting potential functional impacts. Summary statistics and variant counts were compiled in Excel, and the data were visualized in R using ggplot2 to compare mutation profiles across clones.

3. Characterisation of bacteriophage efficacy against clinical strains of *P. aeruginosa* isolated from pwCF.

3.1 Abstract

CF patients are prone to chronic lung infections due to the thickened airway surface liquid (ASL), with *P. aeruginosa* being the dominant pathogen in adults. Repeated antibiotic treatments often lead to AMR, making infections difficult to treat. Phage therapy offers a potential alternative; however, optimization is challenging due to phage specificity, limited host range, and variable efficacy against biofilms.

In this study, we evaluated 49 phages against 92 clinical *P. aeruginosa* strains collected from a Danish CF hospital, representing the majority of genetic lineages in this population. Phages were assessed for infectivity and biofilm disruption, followed by statistical analysis to identify susceptibility patterns.

Our results showed that while some phages exhibited broad infectivity across multiple lineages, others were highly strain-specific. Biofilm-targeting efficacy varied significantly, with only a subset of phages effectively disrupting established biofilms. Phage combinations improved coverage, suggesting that tailored cocktails are necessary for optimal treatment.

These findings highlight the complexity of phage-host interactions in CF *P. aeruginosa* and provide a framework for designing phage therapy strategies. Personalised or cocktail-based approaches are likely required to maximize therapeutic efficacy against AMR infections in this patient population.

3.2 Introduction

As described in Chapter 1, chronic *P. aeruginosa* infection in CF is characterised by progressive antibiotic resistance, biofilm formation, and strain adaptation that together render it resistant to conventional treatment and an important target for bacteriophage based therapeutic strategies.

P. aeruginosa is the most common pathogen in adult pwCF and is particularly difficult to treat due to its intrinsic resistance mechanisms, including efflux pumps, low membrane permeability and biofilm formation, combined with the frequent antibiotic exposure in pwCF (Coutinho *et al.*, 2017; Lubamba *et al.*, 2012). Some patients harbour multiple co-infecting lineages simultaneously (Table 2.1), adding a further layer of complexity to treatment and phage selection. *P. aeruginosa* establishes biofilm communities in the CF airway that confer

substantial antibiotic tolerance and restrict phage diffusion, as the extracellular matrix limits access to bacterial surface receptors (Drenkard, 2003; Mulcahy *et al*., 2010; Stewart, 2002). Persister cells within biofilms survive antibiotic treatment and resuming growth after cessation, contributing to the chronic, relapsing nature of CF lung infections (Balaban *et al.*, 2013).

As described in Chapter 1 (section 1.3.1), Danish CF patients are treated with a range of antibiotics including aminoglycosides, fluoroquinolones, β-lactams, and polymyxins (Møller et al., 2022). Despite this range, increasing MDR in this patient population provides the clinical rationale for exploring phage therapy as an alternative or adjunct treatment approach. A key feature of the bacterial panel used in this study is its longitudinal structure: strains were selected to represent not only the range of genetic lineages circulating in the Danish CF population (Marvig *et al.*, 2015), but also multiple infection timepoints from within individual patients (Table 2.1). This within patient sampling enables analysis of whether phage susceptibility shifts as infection duration increases, a question that cross-sectional collections cannot address and that has direct implications for the timing of phage therapy interventions.

The phage panel comprised 49 phages selected from a larger collection on the basis of clearance, confirmed or predicted receptor specificity, and confirmed lytic lifecycle. Phages in this collection target either LPS or T4P (Hyman and Abedon, 2010), the two major receptor classes in *P. aeruginosa* infecting phages. As will be described in Chapter 4, *in silico* cocktail optimisation using the PhageCocktail R package (Díaz-Galián *et al.*, 2022) consistently identified phage pairs spanning both receptor classes as providing the broadest theoretical coverage, suggesting that receptor diversity is a key determinant of host range across the clinical strain panel. This is mechanistically coherent: resistance to one receptor class does not confer cross-resistance to the other, as mutations conferring escape from T4P-binding phages, typically disrupting pilus assembly, leave LPS intact and therefore susceptible to LPS-binding phages, and vice versa (Tan *et al.*, 2014; Hendrix *et al.*, 2024). Several phages in this panel have been previously characterised against *P. aeruginosa*. PhiKZ, PNM, PT7, and 14/1 have documented infectivity against *P. aeruginosa* PAO1 (Friman *et al.*, 2016), as do the PA phages against their respective isolation hosts (Mattila *et al.*, 2015). LUZ7 and LUZ19 have previously characterised host ranges against *P. aeruginosa* (Betts *et al.*, 2016). DMS3vir and DMS3virAcrFI have previously demonstrated infectivity against *P. aeruginosa* and have been characterised in the context of phage-bacteria coevolution and CRISPR-phage interactions; DMS3virAcrFI specifically carries an anti-CRISPR gene (AcrIF1) that inhibits type I-F CRISPR-Cas immunity in *P. aeruginosa*, distinguishing it from DMS3vir (Broniewski *et al.*, 2021).

Clearance of planktonic bacteria and activity against established biofilm were assessed as independent metrics in this study, rather than assuming the former predicts the latter. A phage that produces strong clearance in a spot assay may perform very differently against a structured biofilm (Harper *et al.*, 2014; Melo *et al.*, 2023; Hernández and Koskella, 2024), where matrix penetration and receptor accessibility are constrained (Drenkard, 2003; Stewart, 2002). In CF, where *P. aeruginosa* exists predominantly in the biofilm state in the lower airways (Drenkard, 2003; Mulcahy *et al.*, 2010), both dimensions of efficacy must be characterised separately to identify therapeutically useful phages.

To determine whether phage susceptibility is predictable from clinical data, variation in phage efficacy was analysed relative to three strain metadata variables: genetic lineage, antibiotic resistance profile, and length of infection. If susceptibility clusters by lineage it would suggest receptor conservation within clonal lineages and support lineage-informed phage selection; if it correlates with antibiotic resistance profiles it would have implications for whether phage therapy offers greatest benefit early in infection or in strains that have failed conventional treatment; and if it shifts with length of infection it would suggest a therapeutic window for intervention.

Chapter Aims

This chapter aimed to characterise and evaluate bactericidal phages against clinical *P. aeruginosa* strains from CF patients. Phage infectivity and biofilm-disrupting activity were assessed, and variation in efficacy analysed relative to strain metadata including lineage, antibiotic resistance profiles, and length of infection, to inform rational phage therapy design.

3.3 Results

3.3.1 Bacteria and Phage Preparation (Methods Chapter 2.1 - 2.3)

Clinical strains of *P. aeruginosa* and associated metadata, including lineage (Table 2.1), were provided by Helle Krogh Johansen from pwCF treated at Rigshospitalet in Copenhagen, Denmark (DK). Samples were collected from either the sinus or lung using multiple techniques (Table 2.1: Origin). Metadata include length of infection and infection age (Genotype), as defined in Section 2.1 (Table 2.1). Blank cells in the table indicate that data were not provided. Samples were retrieved from frozen stock, prepared, and cryopreserved as described in Section 2.1 to ensure the integrity of the original stocks.

Phages and associated metadata (Table 2.2) were provided by multiple sources, from Matti Jalasvuori (all PA phages), Jean-Paul Pirnay (PhiKZ, PNM, PT7, 14/01, and all QAT phages), Rob Lavigne (LUZ7 and LUZ19), and Edze Westra (DMS3vir and DMS3vir AcrFl). Most

phages originated from sewage water and have a range of host bacteria. All PA phages originated in Finland, whereas QAT phages originated in Belgium. Receptor information is indicated where available.

Initially, phages PhiKZ, PNM, PT7, 14/01, and all PA phages were propagated on PAO1, cryopreserved, and prepared in glass vials as described in Section 2.2. Phage titres were then determined using PAO1 as described in Section 2.3. This was first done with dilutions to 10^{-5}, but many phages remained uncountable, so titres were repeated using dilutions to 10^{-8}.

Subsequently, LUZ and QAT phages (LUZ7, LUZ19, QAT7, QAT8, QAT27, QAT28) were prepared and titres determined in the same way on PAO1, with dilutions immediately to 10^{-8}. LUZ7 produced no plaques on PAO1, QAT7 produced merged plaques indicating strong lysis, and the other phages produced faint plaques. Due to QAT7's strong lysis, additional QAT phages were included and further dilutions performed to allow individual plaques to be observed.

Phages QAT1–QAT6, QAT8–QAT10, and QAT20–QAT26 were processed similarly using dilutions to 10^{-9}. LUZ7 and QAT7 titres were repeated, with QAT7 read early to avoid complete lysis merging. LUZ7, QAT2, QAT4, and QAT6 did not produce plaques. PA14 and PAdebi were indicated as potential hosts for phages that failed on PAO1, so isolation was repeated using these hosts (LUZ7 on PA14; QAT2, QAT4, QAT6 on PAdebi; DMS3vir and DMS3vir AcrFI on PA14). LUZ7 and QAT2 remained unsuccessful and were excluded. DMS3vir and DMS3vir AcrFI produced uncountable lysis, so titres were repeated and read early. QAT4 and QAT6 produced clear lysis and were included.

Following isolation and preparation, 49 phages were included in the infectivity assay: PhiKZ, PNM, PT7, 14/01, all PA phages, LUZ19, QAT1, QAT3a–QAT10, QAT20–QAT28, DMS3vir, and DMS3vir AcrFI.

3.3.2 Infectivity Assay (Methods Chapter 2.4)

Initially, 16 clinical *P. aeruginosa* strains were selected for the infectivity assay. These were chosen from strains with the earliest points of infection (i.e., closest to the patient's first colonisation) to evaluate phage efficacy at early stages of infection (with the exception of strain 428). The strains were arranged in batches (Table 3.1).

Batch 1 was exposed to the 49 phages as described in Section 2.4. Complete zones of clearance were recorded as strong clearance. Large zones with plaques inside, or faint zones, were recorded as weak clearance. No clearance was recorded when no lysis or

plaques were observed. Plates were incubated using the existing phage titres without normalising bacterial density, as this was a qualitative screening assay intended to identify phages capable of producing visible clearance across clearance categories rather than to quantitatively compare infectivity across strains. Whilst normalisation of bacterial density would be required for precise quantitative comparisons, the categorical nature of the clearance scoring used here renders this less critical for the purpose of initial phage screening and selection.

The assay for strain 427 was repeated alongside Batch 3 due to unclear plates (indicated in Table 3.1 with “r”). Batches 2 and 3 were then completed; strain 340 showed contamination and was reisolated for a repeat assay.

Table 3.1: Batch information for clinical *P. aeruginosa* strains tested in the infectivity assay. Strains were arranged into sequential batches for practical management of the assay. (r) indicates a repeat from a previous batch.

Batch 1	Batch 2	Batch 3
390	417	339
77	182	340
122	178	341
427	177	386
414	173	388
		428
		427 (r)

The initial three clearance categories were insufficient to capture observed differences, so a refined scheme was adopted:

- **Strong:** clear zone with no plaques in the centre
- **Moderate:** strong zone with plaques or slightly dull lysis
- **Weak:** very faint lysis or faint plaques
- **No clearance:** no lysis or plaques

Images of these lysis morphologies are included in the Methods section for reference. It is acknowledged that without normalisation of phage titre, differences in clearance category may partially reflect variation in starting phage concentration rather than intrinsic differences in infectivity. However, as the primary aim of this assay was qualitative screening to identify phages capable of producing visible clearance against the clinical collection, rather than precise quantitative comparison, this approach was considered sufficient for the purpose of phage selection. Normalisation of phage titre was applied in subsequent quantitative assays.

Further clinical strains were then selected from the mid and end point of infection to ensure that all lengths of infection were included and to determine if this had an effect on clearance.

Samples were selected from the same patient and lineage as the previous 16 strains, though this was not available for lineage DK50. These were isolated and cryopreserved from frozen stock as described in section 2.1 and above. Samples were again split into batches (Table 3.2) with only strain 223 requiring a repeat due to insufficient bacterial growth. This repeat still yielded no growth and was eliminated from the assay.

Table 3.2: Batch information for clinical *P. aeruginosa* strains tested in the infectivity assay. Strains were arranged into sequential batches for practical management of the assay. (r) indicates a repeat from a previous batch.

Batch 4	Batch 5	Batch 6	Batch 7
389	411	176	213
391	440	184	247
84	416	383	237
90	415	385	387
119	179	223	434
114	180.1	214	422
436	340	206	431
423			

To increase sample size, additional strains were selected from a range of infection timepoints and lineages. Samples were cultured in LB from original stocks and cryopreserved to maintain the integrity of the stock samples. This was again done in batches (Table 3.3). Initially, batch 8 strains 433, 438, 425, 424, 419, 439, 420, and 429 showed no obvious growth after 24 hours of incubation. This batch was recultured from original frozen stocks, but still no growth was observed. LB media was remade to eliminate media quality as a factor, but this had no effect, and several strains in this batch continued to fail to thrive. Upon further repetition, strains 419, 420, and 429 cultured successfully, while the remaining strains from this batch were eliminated from the assay. In batch 9, strain 242 showed potential contamination with dual morphologies visible in the bacterial lawn; it was recultured from frozen stock and assayed alongside batch 9. Batches 10–12 were successful with no repeats necessary. After these quality control steps, a total of 88 bacterial strains were successfully cultured and taken forward for further analysis with an additional 6 added at a later stage.

Table 3.3: Batch information for the clinical *P. aeruginosa* strains tested in the infectivity assay. Strains were arranged into sequential batches for practical management of the assay. (r) indicates a repeat from a previous batch. ~~strikethrough~~ denotes sample eventually eliminated from the assay.

Batch 8	Batch 9	Batch 10	Batch 11	Batch 12
~~433~~	243	435	110	91
~~438~~	228	239	448	89
~~425~~	242	242 (r)	116	181
~~424~~	227	244	78	174
419	241	246	80	413.1
420	226	121	81.1	412
429	239	112	82.1	347
~~439~~		118	83	344
		345	420 (r)	208
		204	429 (r)	207
		203		239
		201.1		242
		198		419
		196		
		210		
		211		

As phage titres were not normalised prior to the infectivity assay, phage titre was plotted against infectivity score to determine whether titre variation had confounded the results (Figure 3.1, Table 3.4). No statistically significant correlation was found, suggesting that the range of titres used did not systematically influence clearance outcomes.

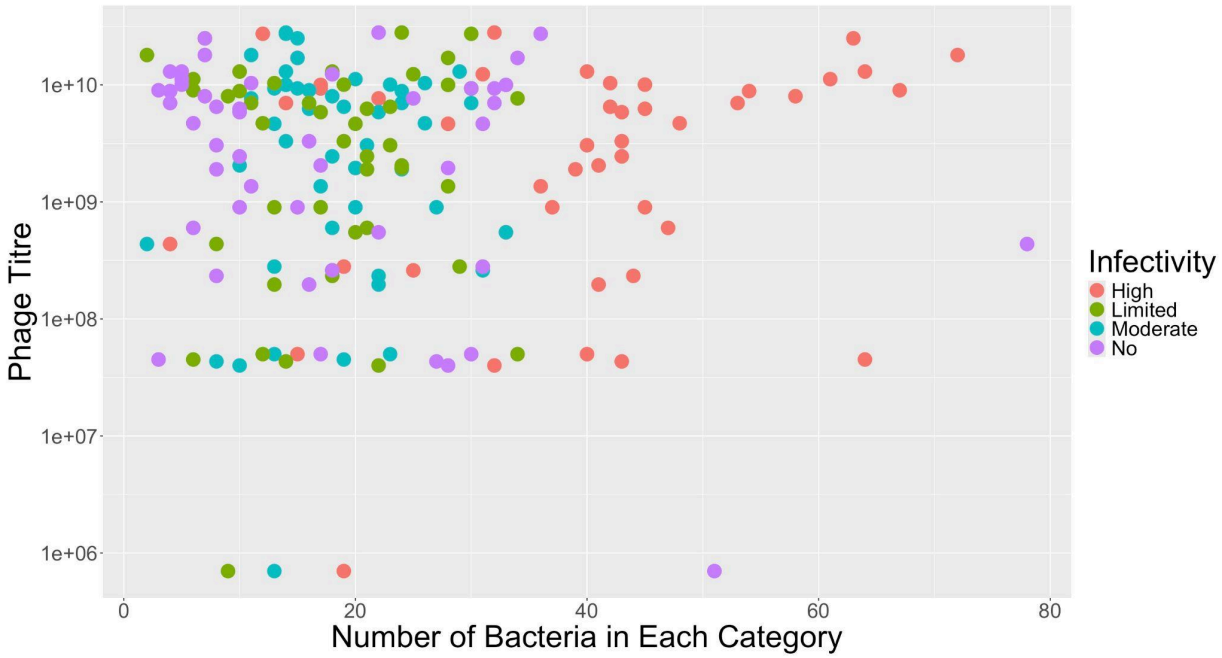

Figure 3.1: Correlation plot showing the relationship between initial phage titre and infectivity category (n = 188). Phage titre (PFU/mL, $\log_{10}$ scale) is plotted on the y-axis against the number of bacteria in each infectivity category on the x-axis. Infectivity categories are indicated by colour: high (pink), moderate (teal), limited (green), and no clearance (purple). Titres ranged from 7×10^{5} to 2.8×10^{10} PFU/mL. No statistically significant correlation was found between phage titre and infectivity (Table 3.4), indicating that variation in initial phage titre did not affect spot assay results. Linear regression was performed in R using the lm() function.

Table 3.4: Linear regression analysis statistical output for the correlation between phage titre and infectivity score (Figure 3.1). Outputs include the regression coefficient (R^2), F-statistic, degrees of freedom, and p-value. A non-significant p-value ($p > 0.05$) indicates no statistically significant linear relationship between phage titre and infectivity score.

Clearance	Estimate	Std. Error	t-value	p-value	Residual SE	R2	Adjusted R2	F-statistic
High	4.613×10^{7}	6.522×10^{7}	0.707	0.4831	7.268×10^{9}	0.01099	-0.01098	0.5002
Moderate	$-1.42876834 \times 10^{8}$	1.65555422×10^{8}	-0.863	0.3927	7.248×10^{9}	0.01628	-0.005579	0.7448
Limited	6.84×10^{6}	1.324×10^{8}	0.052	0.959	7.308×10^{9}	5.927×10^{-5}	-0.02216	0.002667
No	-4.2312593×10^{7}	7.3392306×10^{7}	-0.577	0.5671	7.281×10^{9}	0.007332	-0.01473	0.3324

To explore the effect of length of infection on phage clearance of the clinical *P. aeruginosa* strains, a correlation graph of the two variables was created in ggplot2 in R studio (Figure 3.2). This showed a significant positive correlation between the length of infection and the susceptibility to phages (estimate = 0.0179, t-value 2.226, p = 0.02866, n = 88).

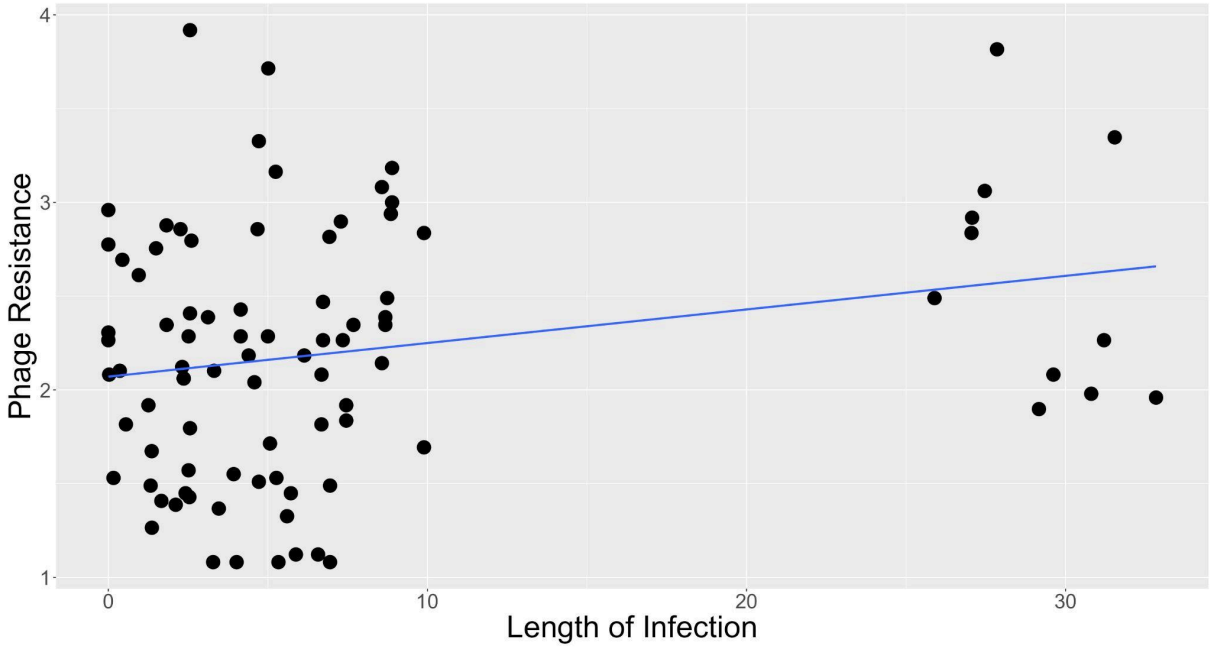

Figure 3.2: Correlation plot showing the relationship between length of infection (years) and phage resistance (n = 88). Each data point represents an individual *P. aeruginosa* strain. Phage resistance was quantified as the mean infectivity score across 49 phages, where clearance categories were scored as follows: strong = 1, moderate = 2, limited = 3, and no clearance = 4. A higher mean score therefore reflects greater overall resistance to phage infection. The blue line shows the linear regression fit, indicating a statistically significant positive association between length of infection and phage resistance (estimate = 0.0179, t = 2.226, p = 0.029), suggesting that strains from patients with longer infections tend to be more resistant to phage. Length of infection data were provided by Rigshospitalet, Copenhagen, Denmark. Strains 413.1, 201.1, 210 and 448 were excluded due to unavailable length of infection data. Linear regression was performed in R using the lm() function; full statistical outputs are presented in Table 3.5.

Table 3.5: Linear regression analysis statistical output for the correlation between length of infection and phage resistance score (Figure 3.2). Outputs include the regression coefficient (R^2), F-statistic, degrees of freedom, and p-value. A non-significant p-value ($p > 0.05$) indicates no statistically significant linear relationship between length of infection and phage resistance.

Estimate	Std. Error	t-value	p-value	Residual SE	R2	Adjusted R2	F-statistic
0.04578	0.03766	1.216	0.2274	0.6658	0.01689	0.005462	1.478

In order to determine how effectively the phage collection infected the clinical strains of *P. aeruginosa*, a matrix was created in ggplot2 in R Studio. For this matrix, the original clearance categories were simplified to indicate whether a phage was able to infect a bacterial strain or not. Infection was considered to have occurred if any lytic activity was observed, that is, if the reaction fell into the ‘strong’, ‘moderate’, or ‘weak’ infectivity categories. Of the 93 bacterial strains included in the initial infectivity assay, none were completely resistant to all phages, and all were strongly infected by at least one phage (Figure 3.3). Similarly, all phages were able to infect at least one *P. aeruginosa* strain (Figure

3.3). In general, similar patterns of resistance were observed within CF lineage groups, though some anomalies were noted. For example, strain 431 in lineage DK53 appeared more resistant to phage infection than other strains within the same lineage. Although genomic data were not available to confirm this, such variation could potentially be explained by differences in bacterial defence mechanisms or LPS modifications. Likewise, while phage QAT6 displayed a notably narrow host range, no specific factor has been identified to explain its reduced clearance compared with other phages in the collection. The most susceptible strains were 122 and 349, each infected by all 49 phages, while strains 110, 208, and 211 were infected by 48 of 49. In contrast, strain 118 showed the lowest susceptibility, infected by only 4 phages, followed by strain 114 (7 phages) and strain 431 (9 phages). Among phages, PA5P2 and PNM demonstrated the broadest host range, each infecting 89 of 92 strains, followed closely by PT7, 14/1, and PA5P1 (88 strains each). QAT6 had the narrowest host range, infecting only 14 strains, consistent with the generally lower clearance of the Belgian-derived QAT phages compared with the Finnish PA phages.

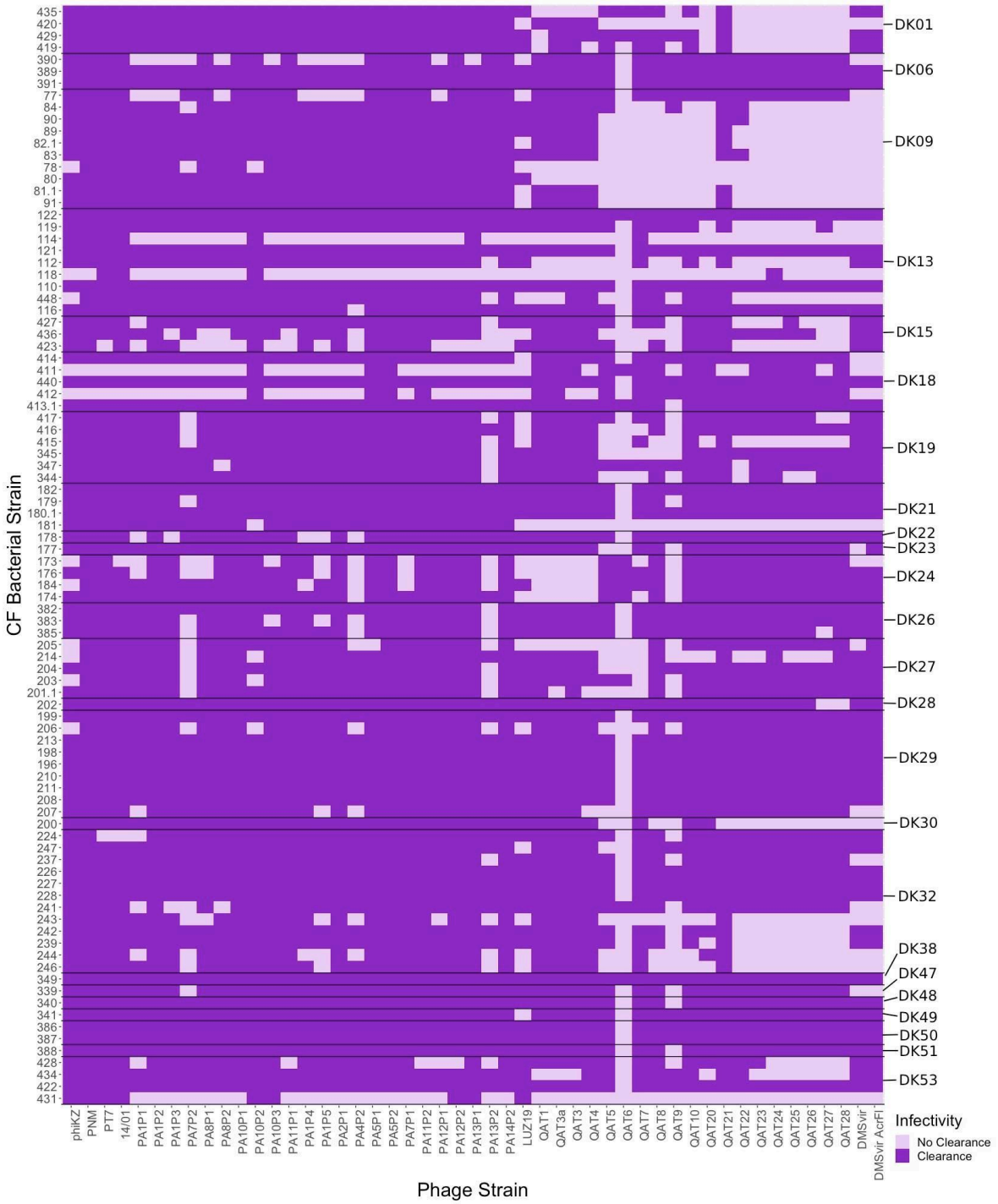

Figure 3.3: Infectivity matrix for 92 clinical strains of *P. aeruginosa* against 49 bacteriophages representing 4508 unique phage-host combinations. Infectivity spot assays were performed in triplicate (n = 3 biological replicates per phage-host pair) and repeated a total of 3 times. For this matrix, clearance categories were simplified to binary: any observable lytic activity (strong, moderate, or limited clearance) is indicated by dark purple; no observable lytic activity is indicated by light purple. Bacterial strains (y-axis) are grouped by CF lineage, indicated by Denmark number (DK) on the right. Phage strains are shown on the x-axis. No bacterial strain was completely resistant to all phages, and all phages infected at least one strain. The most susceptible strains were 122 and 349 (infected by all 49 phages); the most resistant was strain 118 (infected by only 4 phages). PA5P2 and PNM demonstrated the broadest host range (89 of 92 strains); QAT6 demonstrated the narrowest (14 of 92 strains).

A box plot comparison (Figure 3.4) demonstrated that phages from Finland (PA) were significantly better at clearing the Danish clinical strains than the Belgium (QAT) phages (Wilcox rank sum test = 397.5, p-value = 6.260445 × 10-6, n = 42).

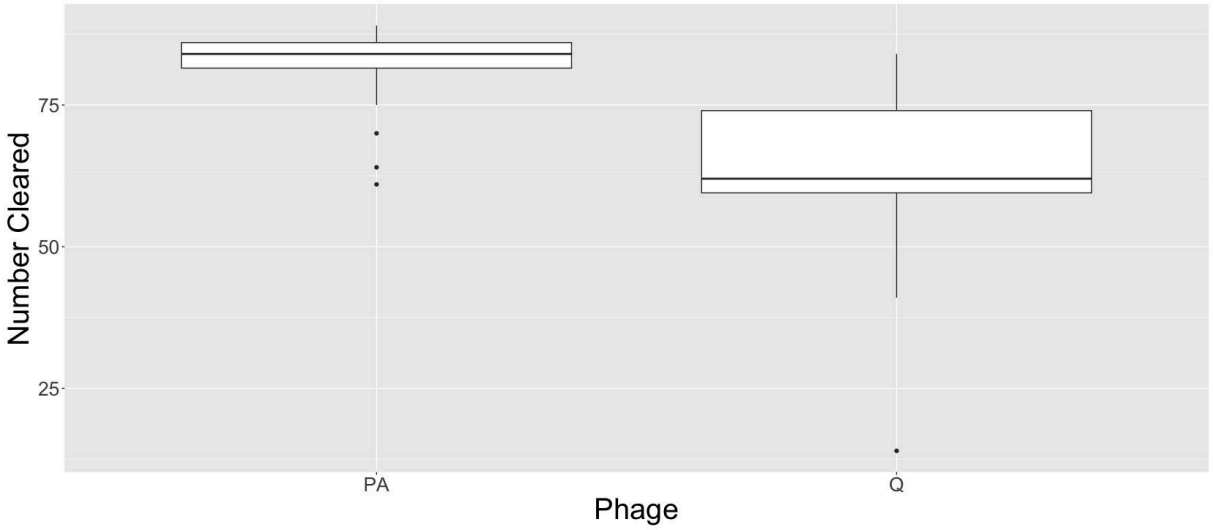

Figure 3.4: **Box plot demonstrating the difference between PA phages (Finland) and QAT phages (Belgium) against 92 clinical *P. aeruginosa* strains.** The y-axis shows the number of bacterial strains cleared by each phage. Box boundaries represent the interquartile range (IQR), the central line represents the median, and whiskers extend to 1.5× IQR. Individual points beyond the whiskers represent outliers. PA phages cleared significantly more strains than QAT phages (Wilcoxon rank-sum test statistic = 397.5, $p = 6.26 \times 10^{-6}$, n = 42), indicating that the Finnish PA phages have a broader host range against these Danish clinical isolates than the Belgian QAT phages.

Data provided with the phages indicated that the receptor target was known for 30 of the 49 phages. A comparison between LPS- and T4P-targeting phages (Figure 3.5) showed no statistically significant difference in infectivity against the clinical strains (Wilcoxon rank-sum test = 70, p = 0.6239). However, this result should be interpreted with caution as the dataset was highly unbalanced, with only 7 T4P-targeting phages compared to 23 LPS-targeting phages, likely reducing the statistical power of the analysis. Effect size analysis confirmed the difference between groups was negligible (rank-biserial correlation r = 0.094), suggesting the non-significant result reflects a genuine absence of meaningful difference in clearance between receptor types rather than insufficient statistical power.

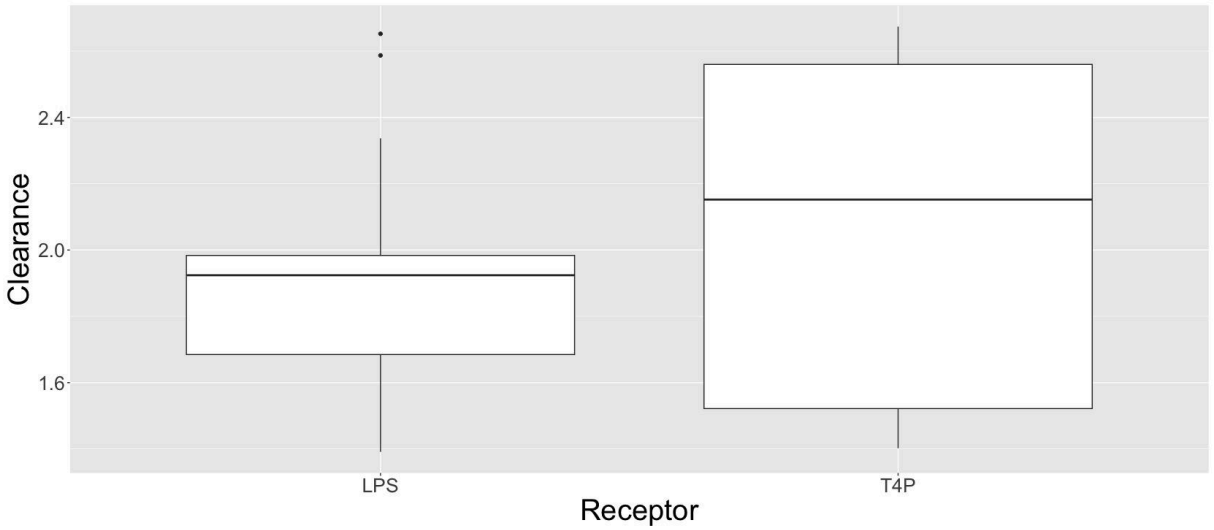

Figure 3.5: **Box plot comparing the infectivity of phages targeting LPS versus type IV pilus (T4P) receptors against 92 clinical *P. aeruginosa* strains (n = 30 phages with known receptor targets: 23 LPS-targeting, 7 T4P-targeting).** The y-axis shows mean infectivity score per phage, where lower scores indicate greater clearance. Box boundaries represent the IQR, the central line represents the median, and whiskers extend to 1.5× IQR. Individual points beyond the whiskers represent outliers. No statistically significant difference in infectivity was found between receptor groups (Wilcoxon rank-sum test = 70, p = 0.624). Effect size analysis confirmed the difference was negligible (rank-biserial correlation r = 0.094, magnitude = small), indicating that the non-significant result is not solely attributable to the unbalanced group sizes.

Using minimum inhibitory concentration (MIC) values provided alongside the clinical strains, Figure 3.6 was produced to visualise the effectiveness of the current antibiotic treatments against them. It was noted that clinical *P. aeruginosa* strains appear to have high MIC values and therefore reduced susceptibility to the β-lactams, piperacillin, aztreonam, cefalotin and meropenem, along with the aminoglycosides gentamicin and tobramycin, with the highest MIC values being observed with these drugs (Figure 3.6). The fluoroquinolone ciprofloxacin and the polymyxin colistin generally displayed lower MICs across the clinical *P. aeruginosa* collection, though it should be noted that the EUCAST resistance breakpoint for ciprofloxacin is >0.5 µg/mL, meaning that many isolates with apparently low MICs may still be classified as resistant (Figure 3.6). On the whole MIC patterns for a particular antibiotic show a similar trend across all lineages within the collection, though there are some exceptions such as strains in lineage DK01 which have a much higher MIC for β-lactams than any other lineage (Figure 3.6). Interestingly a comparison to Figure 3.3 indicates that even where MIC values are very high, phages can successfully infect these strains. This suggests that phages have the potential to control strains of *P. aeruginosa* with reduced antibiotic susceptibility and may offer a complementary approach to antibiotic treatment.

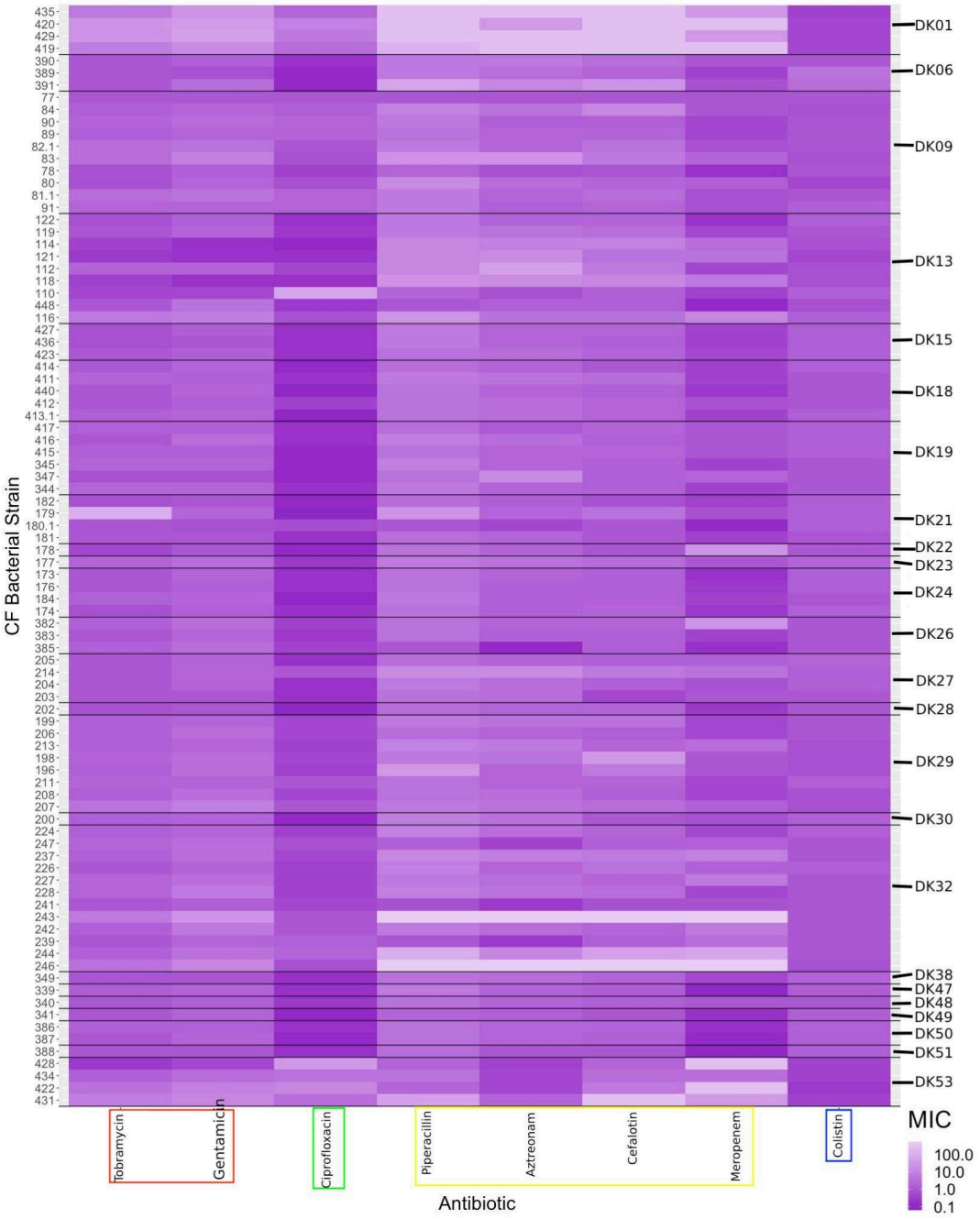

Figure 3.6: **Antibiotic susceptibility heatmap for 92 clinical *P. aeruginosa* strains against 8 antibiotics commonly used in the treatment of CF, representing 720 strain-antibiotic measurements.** Bacterial strains (y-axis) are grouped by CF lineage, indicated by Denmark number (DK) on the right. Antibiotics (x-axis) are grouped by class, indicated by coloured boxes: red = aminoglycosides (tobramycin, gentamicin); green = fluoroquinolone (ciprofloxacin); yellow = β-lactams (piperacillin, aztreonam, cefalotin, meropenem); blue = polymyxin (colistin). Colour intensity indicates MIC value (μg/mL, logarithmic scale); lighter purple indicates higher MIC and therefore reduced antibiotic susceptibility. MIC data were provided by Rigshospitalet, Copenhagen, Denmark, a specialist CF centre. As a clinical microbiology laboratory, standard EUCAST-compliant methods are expected to have been used in MIC determination. Values should be interpreted with this caveat in mind. Clinical *P. aeruginosa* strains showed generally elevated MIC values for β-lactams and aminoglycosides, with lineage DK01 showing notably higher β-lactam MIC values than other lineages. Ciprofloxacin and colistin were associated with lower MIC values across the collection.

In the case of antibiotics, length of infection (Figure 3.7 and Table 3.6) appears to have a significant effect on antibiotic resistance for most antibiotics tested. Aztreonam (estimate = 2.94, $t = 2.814$, $p = 6.06 \times 10^{-3}$, $n = 88$), cefalotin (estimate = 4.56, $t = 4.284$, $p = 4.77 \times 10^{-5}$, $n = 88$), ciprofloxacin (estimate = 0.19, $t = 2.079$, $p = 4.06 \times 10^{-2}$, $n = 88$), gentamicin (estimate = 0.45, $t = 6.235$, $p = 1.63 \times 10^{-8}$, $n = 88$), meropenem (estimate = 4.13, $t = 3.943$, $p = 1.63 \times 10^{-4}$, $n = 88$) and piperacillin (estimate = 3.30, $t = 3.182$, $p = 2.04 \times 10^{-3}$, $n = 88$) all demonstrate a significant positive correlation with length of infection (Figure 3.7), indicating that the longer the infection, the more resistant clinical *P. aeruginosa* isolates were to these antibiotics.

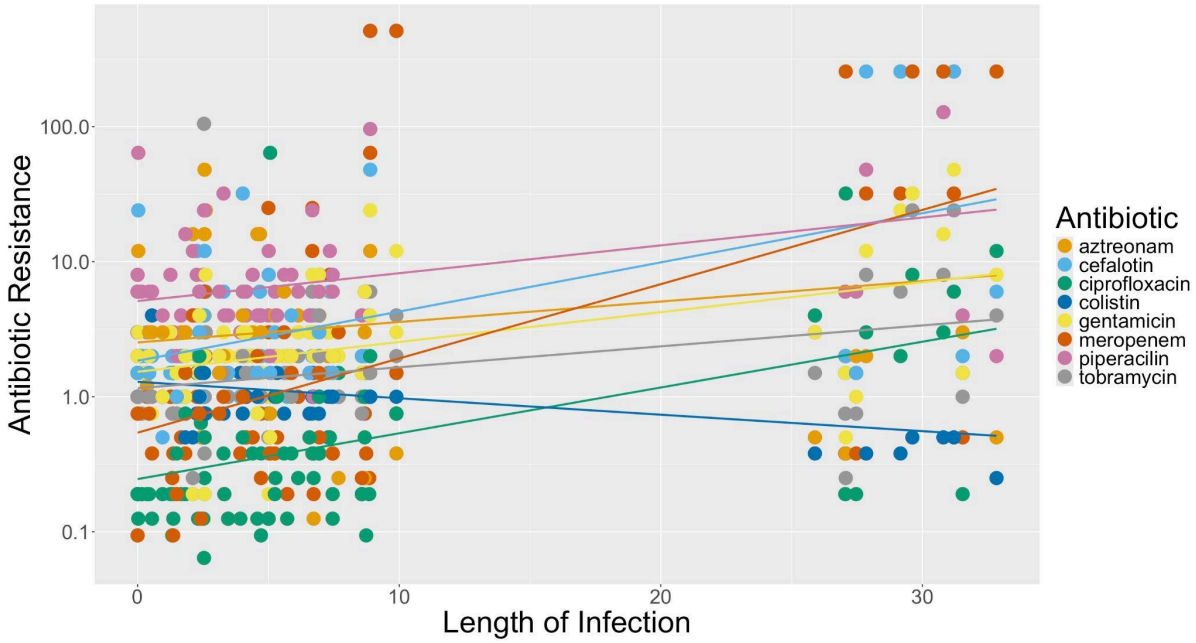

Figure 3.7: **Correlation plot showing the relationship between length of infection (years) and antibiotic resistance, measured as MIC (µg/mL), for 8 antibiotics tested against 92 clinical *P. aeruginosa* strains (n = 88 strains with available length of infection data)**. Each data point represents an individual strain-antibiotic measurement, coloured by antibiotic as indicated in the legend. A semi-logarithmic scale was used on the y-axis to account for large variation in MIC values between strains. Linear regression lines are shown for each antibiotic. Seven of eight antibiotics showed a statistically significant positive correlation between length of infection and MIC, indicating increasing antibiotic resistance over the course of chronic infection; colistin was the exception, showing a significant negative correlation (see Table 3.6 for full statistical outputs). Strains 413.1, 201.1, 210 and 448 were excluded due to unavailable length of infection data. MIC data and length of infection data were provided by Rigshospitalet, Copenhagen, Denmark, a specialist CF centre; standard EUCAST-compliant methods are expected to have been used in MIC determination. Linear regression was performed in R using the lm() function.

Colistin (estimate = −0.024, $t = -3.848$, $p = 2.28 \times 10^{-4}$, $n = 88$), however, demonstrated a significant negative correlation, indicating that the longer the infection, the more susceptible clinical *P. aeruginosa* isolates were to this antibiotic. Tobramycin appeared to follow the

positive correlation observed for several other antibiotics; however, this relationship was not statistically significant (estimate = 0.15, t = 1.039, p = 0.302, n = 88).

Table 3.6: Linear regression analysis statistical output for the correlation between length of infection and antibiotic resistance (MIC) across eight antibiotics (Figure 3.7). Outputs include the regression coefficient (R^2), F-statistic, degrees of freedom, and p-value for each antibiotic. A non-significant p-value ($p > 0.05$) indicates no statistically significant linear relationship between length of infection and antibiotic resistance.

Antibiotic	Estimate	Std Error	t-value	p-value	Residual SE	R2	Adjusted R2	F-statistic
Aztreonam	2.938	1.044	2.814	6.06x10-3	84.68	0.08433	0.07368	7.92
Cefalotin	4.564	1.065	4.284	4.77x10-5	86.41	0.1759	0.1663	18.35
Ciprofloxacin	0.19271	0.09268	2.079	4.06x10-2	7.517	0.04786	0.03679	4.323
Colistin	-0.023608	0.006135	-3.848	2.28x10-4	0.4976	0.1469	0.137	14.81
Gentamicin	0.44839	0.07192	6.235	1.63x10-8	5.833	0.3113	0.3033	38.87
Meropenem	4.128	1.047	3.943	1.63x10-4	84.91	0.1531	0.1433	15.55
Piperacillin	3.297	1.036	3.182	2.04x10-3	84.05	0.1053	0.09492	10.12
Tobramycin	0.1479	0.1423	1.039	3.02x10-1	11.54	0.0124	0.0009131	1.08

Similar patterns of MIC can be seen across the different lineages within the 93 clinical strains (Figure 3.8). Across all lineages, piperacillin exhibited higher MIC (6 µg/mL), with the highest MIC in 13 lineages. In contrast, ciprofloxacin generally displayed the lowest median MIC across the collection (0.38 µg/mL). Meropenem typically showed lower MICs (median 0.75 µg/mL), though had the highest MICs in 4 specific lineages, namely DK26, DK47, DK49 and DK51.

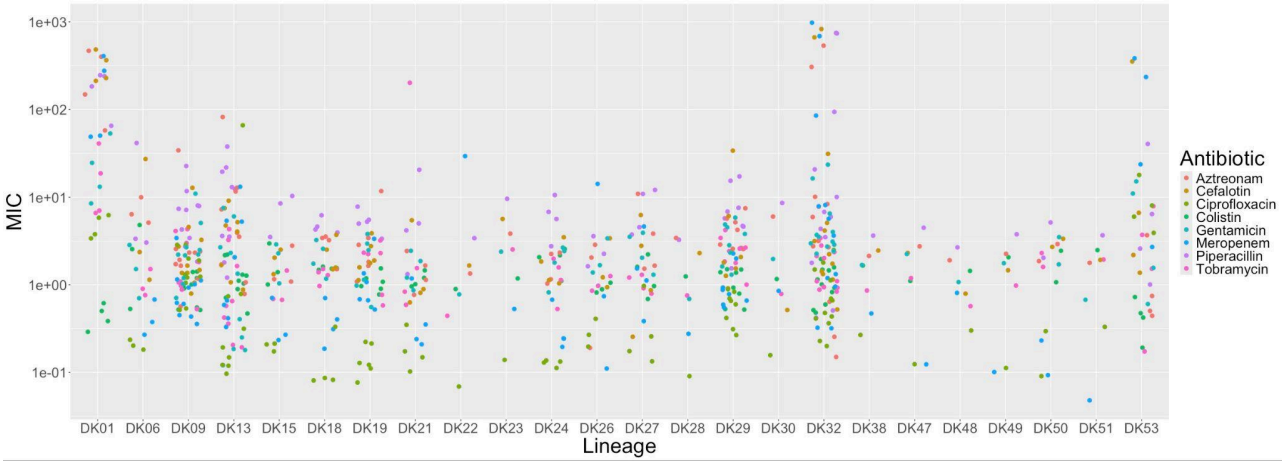

Figure 3.8: **Scatter plot showing MIC values (µg/mL) across 24 *P. aeruginosa* CF lineages for 8 clinically relevant antibiotics (n = 712 strain-antibiotic measurements).** Each data point represents an individual strain, coloured by antibiotic as indicated in the legend. A semi-logarithmic scale is used on the y-axis to account for large variation in MIC values between strains. Data are derived from Figure 3.6. Lineage DK01 shows notably elevated MIC values across multiple antibiotics compared to other lineages. MIC data were provided by Rigshospitalet, Copenhagen, Denmark.

No statistically significant relationship was observed between antibiotic resistance and phage resistance (Figure 3.9) suggesting that antibiotic resistant isolates were equally susceptible to phages as antibiotic susceptible *P. aeruginosa* strains. Trends in the MIC for antibiotic resistance (Figure 3.6) are reflected in this graph with similarities clearly visible.

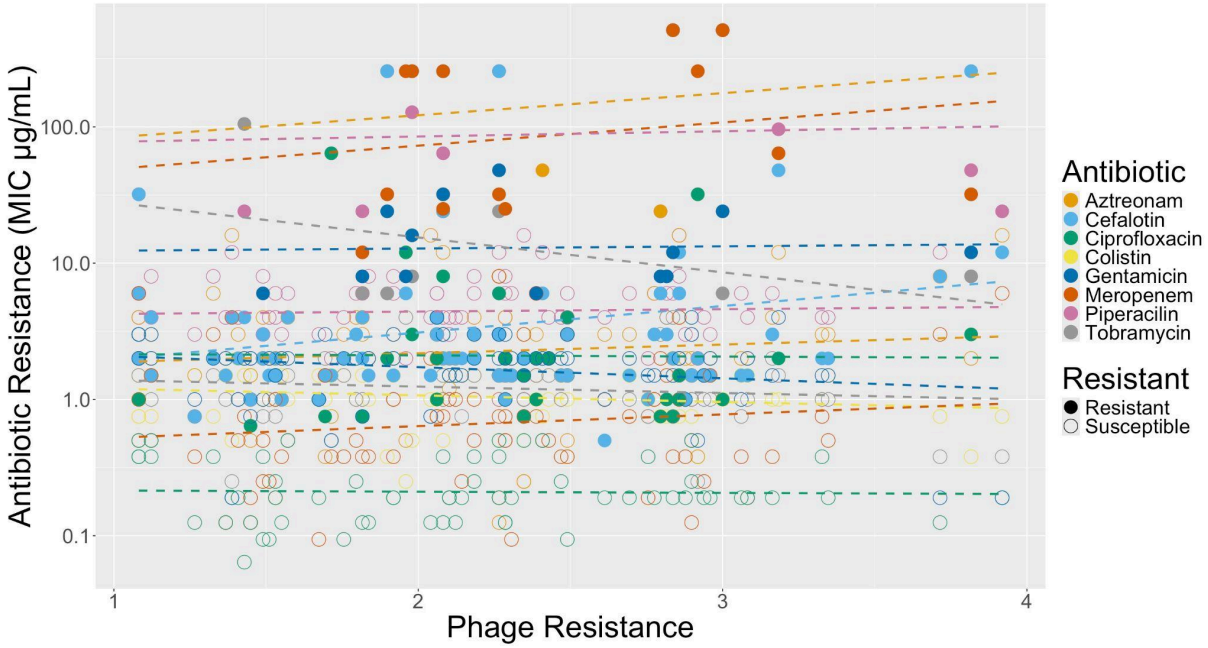

Figure 3.9: **Correlation plot of antibiotic resistance (MIC, µg/mL) against phage resistance (n = 720) for 8 clinically relevant antibiotics.** Each data point represents an individual strain-antibiotic measurement, coloured by antibiotic as indicated. Filled circles indicate strains classified as resistant and open circles indicate strains classified as susceptible, based on EUCAST clinical breakpoints for *P. aeruginosa*: aztreonam >16 µg/mL; ciprofloxacin >0.5 µg/mL; colistin >4 µg/mL; gentamicin >4 µg/mL; meropenem >8 µg/mL; piperacillin >16 µg/mL; tobramycin >4 µg/mL. Cefalotin is not listed in EUCAST guidelines for *P. aeruginosa* as this species is intrinsically resistant; all cefalotin data points are therefore classified as resistant. Phage resistance is scored on a scale of 1–4, where 1 = high infectivity and 4 = no infectivity. A semi-logarithmic scale is used on the y-axis. Dashed lines show linear regression fits per antibiotic. No statistically significant correlation was observed between antibiotic resistance and phage resistance for any antibiotic (Table 3.7), indicating that antibiotic resistance does not predict phage susceptibility. MIC data were provided by Rigshospitalet, Copenhagen, Denmark.

Table 3.7: Linear regression analysis statistical output for the correlation between antibiotic resistance (MIC) and phage resistance score across eight antibiotics (Figure 3.9). Outputs include the regression coefficient (R^2), F-statistic, degrees of freedom, and p-value for each antibiotic. A non-significant p-value ($p > 0.05$) indicates no statistically significant linear relationship between antibiotic resistance and phage resistance.

Antibiotic	Estimate	Std. Error	t-value	p-value	Residual SE	R2	Adjusted R2	F-statistic
Aztreonam	16.64	13.82	1.204	0.2318	86.84	0.01621	0.005026	1.45
Cefalotin	25.8	14.74	1.75	0.08356	92.59	0.03364	0.02266	3.063
Ciprofloxacin	-0.1169	1.2131	-0.096	0.9235	7.62	0.0001055	-0.01126	0.009282
Colistin	-0.12795	0.08416	-1.52	0.132	0.5287	0.02559	0.01452	2.311
Gentamicin	0.6159	1.1048	0.557	0.5786	6.94	0.003519	-0.007805	0.3108
Meropenem	21.87	14.35	1.524	0.131	90.11	0.02573	0.01466	2.324
Piperacillin	19.08	13.85	1.378	0.1718	87.01	0.02111	0.009985	1.898
Tobramycin	-1.894	1.817	-1.042	0.3003	11.42	0.01219	0.0009602	1.086

3.3.3 Biofilm Assay (Methods Chapter 2.5)

Given the importance of biofilm formation to antibiotic resistance and general survival of *P. aeruginosa* strains, it was important to consider whether disruption and/or prevention of biofilm was achievable with any of the phages in the collection. Prior to commencement of the assay, bacterial contamination was observed in some phage vials and confirmed on streak plates. As a result, phages were recultured from frozen stock, and the titres of the new isolates were calculated. Phage QAT6 was not included in the biofilm assay due to an extremely low titre upon reisolation. Although additional attempts to increase the titre could have been made, this was not pursued, as multiple other phages in the collection demonstrated comparable or broader infectivity in the spot assays, and inclusion of QAT6 was therefore considered unnecessary. If a higher titre of QAT6 had been required, titre could be increased by performing additional rounds of propagation on a permissive host strain, followed by ultracentrifugation or polyethylene glycol (PEG) precipitation to concentrate the phage stock (Bonilla *et al.*, 2016).

The biofilm assay was performed in liquid SCFM to mimic the conditions in the human lung. Biofilm prevention, where phage and bacteria were added concurrently, and biofilm disruption, where phage were added 24 hours post bacterial inoculation, were performed and stained using crystal violet (Figure 3.10). Samples were tested in triplicate with an in-time repeat also performed.

Generally, phages were better at preventing than disrupting biofilm formation, with DMS3virAcrFI being particularly competent at both, this could indicate that this phage would be effective at controlling biofilm in both new and well established infections if included in

treatment. PA7P1 demonstrated a contrasting profile, showing increased biofilm biomass compared to the uninfected control in the prevention assay, yet achieving substantial reduction of pre-established biofilm in the disruption assay. This suggests PA7P1 would not be suitable for prophylactic use in new infections but may have utility in treating established biofilm-associated infections.

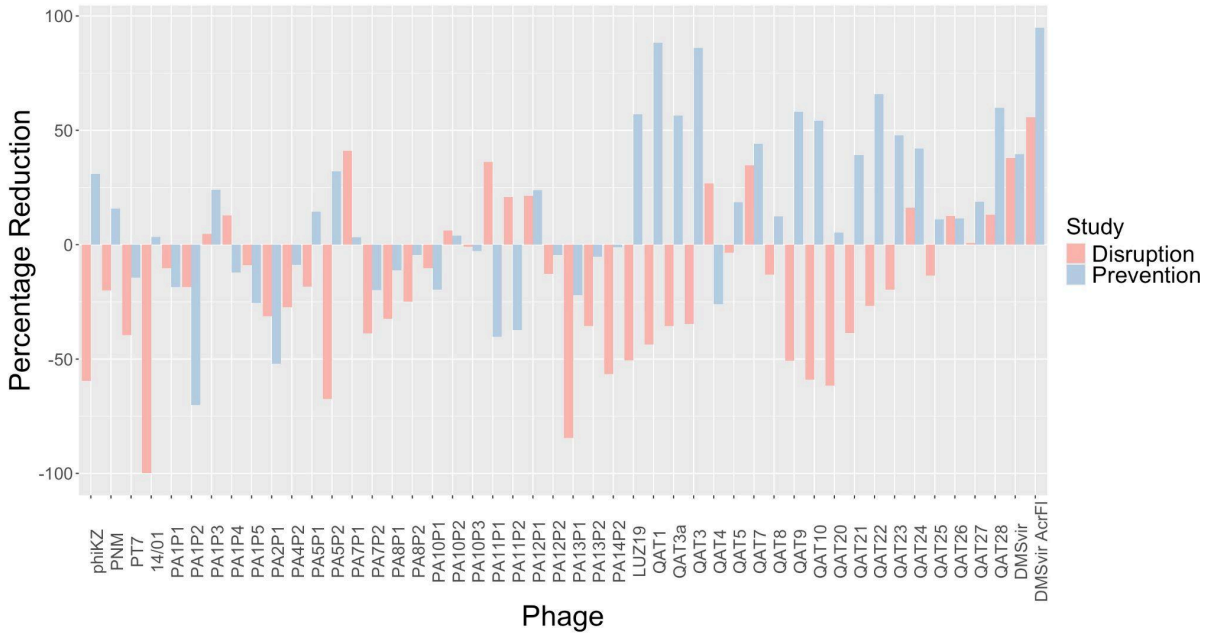

Figure 3.10: Bar chart showing the percentage reduction in *P. aeruginosa* PAO1 biofilm by 48 phages in the collection (QAT6 excluded due to low titre upon reisolation). Data were obtained from a biofilm assay performed in three biological replicates (n = 96). Blue bars indicate biofilm prevention, where phages were added concurrently with bacterial inoculation. Pink bars indicate biofilm disruption, where phages were added after 24 hours of biofilm formation and incubated for a further 24 hours. Percentage reduction was calculated relative to the no-phage positive control using the formula: ((OD_{590} control − OD_{590} phage treated) / OD_{590} control) × 100. Positive values indicate reduction in biofilm biomass relative to the control; negative values indicate an increase in biofilm biomass compared to the control. Biofilm was quantified by crystal violet staining and measured at OD_{590}.

In summary, all clinical *P. aeruginosa* strains were susceptible to infection by at least one phage strain with similarities within same lineage strains, even where antibiotic resistance to the strain was high. Two interesting biofilm disruptors were identified, one efficient at both prevention and disruption and the other a strong preventer but ineffective disruptor: DMS3virAcrFI and PA7P1 respectively.

3.4 Discussion

3.4.1 Introduction

This study examined 49 phages against 93 clinical *P. aeruginosa* strains isolated from pwCF, assessing phage clearance, antibiotic resistance, receptor specificity, geographic origin of phages, and biofilm interactions. Phage therapy offers a promising alternative or adjunct to antibiotics, but factors influencing its efficacy, such as length of infection, strain lineage, phage titre, receptor use, and biofilm status, remain poorly understood. In the following sections we interpret our findings in light of these factors, the wider literature, and their implications for designing phage therapies in CF.

3.4.2 Phage Efficacy and Infection Length

In the dataset, phage clearance (infectivity) showed a weak but statistically significant association with the length of infection, while antibiotic resistance increased with longer infection durations. The latter is consistent with the classic model of *P. aeruginosa* adaptation in chronic CF lungs: repeated antimicrobial exposure, inflammation and selective pressure lead to accumulation of resistance mutations and gene acquisition (Winstanley *et al.*, 2016). The negative correlation observed for colistin is notable and warrants consideration. During chronic CF infection, *P. aeruginosa* undergoes progressive LPS remodelling, including structural changes to lipid A that may inadvertently reduce colistin resistance, as some adaptive modifications to the outer membrane that reduce immunogenicity may also increase membrane permeability to polymyxins (Winstanley *et al.*, 2016). Additionally, colistin resistance mechanisms, such as modification of lipid A with 4-amino-4-deoxy-L-arabinose, carry a significant metabolic cost and may be lost over time in the absence of consistent colistin selection pressure (Lee and Ko, 2014). In the Danish CF cohort, colistin is administered primarily via inhalation rather than systemically, and its clinical use has declined following the introduction of CFTR modulators, meaning that many strains may not have been under sustained colistin selection pressure throughout the infection period. The relatively modest effect size observed for phage susceptibility, suggests that, despite prolonged infection and adaptation, many phage receptors (such as LPS or T4P) are relatively conserved, or that loss/modification of these receptors carries high fitness cost (Wright *et al.*, 2019; Levin *et al.*, 1977). Additionally, recent genomics work indicated that CF isolates often carry fewer canonical phage-defence systems (e.g., CRISPR-Cas, restriction modification) compared to environmental/clinical non-CF isolates, which may explain why phages retained infectivity over time in this patient population (van den Berg *et al.*, 2025).

Experimental evolution supports this interpretation: host–phage arms race dynamics often involve receptor alteration or loss, but these changes can impose costs such as reduced growth or virulence, limiting rapid accumulation of phage resistance (Brockhurst & Koskella, 2013; Lucca *et al.*, 2018). The observed association between length of infection and phage infectivity *in vitro* may reflect gradual evolutionary pressures acting on receptor conservation, alongside limited accumulation of effective phage resistance over the measured period. *In vivo* studies suggest infection timing can matter: for example, Watanabe *et al.* (2007) found that phage administered simultaneously with *P. aeruginosa* infection in mice resulted in much higher survival (~92 %) than delayed phage (~41 %), whereas Waters *et al*. (2017) showed bacterial clearance was still possible up to 7 days post-infection. Differences likely arise from host-immune dynamics, mucus and lung architecture, phage delivery and pharmacokinetics. Our *in vitro* findings therefore emphasise that while length of infection shows a statistically significant relationship with phage susceptibility in an isolated model, additional factors such as delivery timing, host environment and co-therapies will influence translation to clinical settings.

3.4.3 Phage Efficacy Across Strains and Geographic Origin

One of our strongest findings is that each bacterial strain was infectable by at least one phage, and each phage infected at least one strain. This broad spectrum infectivity underlines the therapeutic potential of a well characterised phage library. Phage titre (as assessed via spot assay) did not correlate significantly with clearance; however, this must be interpreted with caution. Spot assays typically show visible lysis zones once a certain infection threshold (~10^3-10^4 infection events) is surpassed, creating a plateau effect beyond which higher titre yields limited additional observable benefit (Mirzaei & Nilsson, 2015; Ács *et al.*, 2020). In practice, this means that once the MOI is sufficient to produce a lysis zone on agar, differences in titre may not show up in the assay but may still matter in *in vivo* settings.

Interestingly, the origin of phages showed a geographic effect: those derived from Finland consistently cleared more clinical strains than Belgian-derived phages. This may reflect local adaptation of phages to sympatric bacterial populations, phages often perform better on hosts from the same region due to prior co-evolution, receptor match-up and host range expansion (Vos *et al.*, 2009; Van Cauwenberghe *et al.*, 2021). Additional contributing factors may include differences in source material (sewage, animal waste, hospital effluent), propagation histories (passage numbers, host strains used for isolation), or small genomic differences affecting adsorption, burst size or latency (Holtappels *et al.*, 2023). Although local adaptation has been extensively documented in environmental systems, its demonstration in

clinical *P. aeruginosa*, phage pairs remains limited and merits next-step genomic pairing of phages and hosts to establish adaptation and host range patterns.

3.4.4 Receptor Specificity: LPS vs Type IV Pili

The comparison between phages targeting LPS versus T4P revealed no statistically significant difference in efficacy, though interpretation is constrained by the small number of T4P-targeting phages in our panel. Mechanistically, both receptor types are common and relatively conserved across *P. aeruginosa* isolates, yet bacteria can still evade via modifications of pilus glycosylation or LPS structure (Harvey *et al.*, 2017; Vaitekenas *et al.*, 2021). Literature suggests that including phages with different receptor specificities may reduce resistance evolution and broaden host-range (Wright *et al*., 2021). Our data are consistent with this view: although receptor class did not significantly influence clearance, the heterogeneity of clearance across phages supports the use of multi-receptor cocktails. Future work should include balanced numbers of phages per receptor class, measure adsorption rates and match receptor presence/absence in the clinical strains to phage performance.

It is well established that during chronic CF infection, *P. aeruginosa* undergoes phenotypic adaptation, including the progressive loss of T4P as the bacterium transitions toward a sessile, biofilm-associated lifestyle (Klausen *et al*., 2003; Burrows, 2012). In contrast, LPS is generally retained due to its essential role in outer membrane integrity, although structural modifications such as loss of O-antigen are frequently observed (Winstanley *et al.*, 2016). This raises the question of whether T4P-targeting phages may become less effective against strains from patients with longer infection histories, as their primary receptor may be progressively downregulated. Within the current dataset, this could be partially assessed by correlating the infectivity of T4P-targeting phages against length of infection data, as explored in Section 3.3. However, the small number of T4P-targeting phages in the collection (n = 7) limits the power of such an analysis. Future work could employ twitching motility assays to assess T4P functionality across strains, or utilise WGS data to identify mutations in key T4P biogenesis genes such as *pilB, pilT, pilQ* and *pilY1* across strains from patients at different infection stages.

3.4.5 Antibiotic Resistance and Phage Susceptibility

Within specific genetic lineages, we found similar antibiotic-resistance profiles, suggesting shared genomic determinants of resistance (Kiyaga *et al.*, 2022). Crucially, even highly antibiotic resistant strains remained susceptible to at least one phage, reinforcing the potential of phage therapy in MDR *P. aeruginosa*. No significant correlation emerged

between antibiotic resistance and phage susceptibility, indicating distinct mechanisms underlie each, consistent with other reports that antibiotic and phage resistance mechanisms seldom overlap (Gupta & Prasad, 2011).

3.4.6 Biofilm Interactions

Biofilms represent a core survival strategy for *P. aeruginosa*, markedly reducing antibiotic susceptibility, promoting persistence and complicating clearance (Fong *et al.*, 2017; Singh *et al.*, 2023). In our assay, several phages disrupted or prevented biofilm formation, but performance was generally stronger in prevention (phage added concurrently with bacteria) than in disruption (phage added to established biofilm). This aligns with prior work: Darch *et al.* (2017) reported that phage addition at inoculation prevented biofilm aggregate formation, whereas later addition achieved partial effect but rarely complete eradication.

Unexpectedly, in some cases phage addition to established biofilms increased biofilm biomass. For example, phage 14/1 induced ~100 % increased biofilm during prevention assays. Similar phenomena have been observed and attributed to bacterial stress responses, such as increased EPS production, or refuge formation within biofilm structure (Hosseinidoust *et al.*, 2013). These findings raise caution: phage therapy, especially in biofilm contexts, may have unintended consequences such as promoting biofilm production under certain conditions. Among the phages tested, DMS3virAcrFl was the most effective at both prevention and disruption, whereas PA7P1 was more effective at prevention than disruption, underscoring the variation between phages and the need for bespoke selection based on target infection/phase. Considering the wider biofilm literature, phage–antibiotic cocktails and enzymes that degrade EPS (e.g., depolymerases) may improve efficacy (Ács *et al.*, 2020; Knecht *et al.*, 2020; Chaudhry *et al.*, 2017).

The observation that some phages increased biofilm biomass compared to the uninfected control warrants consideration. One possible explanation is that phage-mediated lysis of planktonic bacteria releases eDNA, which can act as a structural scaffold within the biofilm matrix, paradoxically enhancing biofilm formation rather than reducing it (Whitchurch *et al.*, 2002; Turnbull *et al.*, 2016). This phenomenon has been reported previously in *P. aeruginosa* and highlights the importance of carefully characterising phage-biofilm interactions prior to therapeutic application.

3.4.7 Antibiotic Resistance Trends by Length of Infection

In longer infections, resistance increased significantly for aztreonam, cefalotin, ciprofloxacin, gentamicin, meropenem and piperacillin, while tobramycin showed a non-significant trend

and colistin curiously showed a negative correlation. The increased resistance with ilength of infection is expected, given chronic exposure and adaptive changes in the lung environment (Cabot *et al.*, 2016). The colistin trend may reflect clinical treatment patterns: early use of colistin followed by withdrawal may allow resensitisation, or may reflect the fitness cost of colistin resistance mechanisms, which can reduce competitiveness when selection pressure is removed (Falagas *et al*., 2010; Andersson & Hughes, 2010). Although our data reflect *in vitro* MICs rather than patient clearance, the trend emphasises the pressing need for alternatives like phage therapy in CF populations where infections are long standing.

3.4.8 Limitations and Future Directions

This study had several limitations. First, we used spot assays, which primarily measure visible lysis (often 'lysis from without') and may not reliably reflect true infection kinetics, burst size or *in vivo* efficacy (Mirzaei & Nilsson, 2015). Observed plateau effects further limit detection of titre clearance relationships once a threshold MOI is achieved. Secondly, the *in vitro* model does not capture host immunity, mucus barriers, pharmacokinetics, lung micro-environment or polymicrobial interactions common in CF lungs. Thirdly, long-term co-evolution of phage and bacteria was not assessed; thus, the durability of observed infectivity remains unknown. Fourthly, mechanistic analyses of phage biofilm interactions were beyond the scope of this work. Whilst comprehensive transcriptomic or proteomic approaches to determine whether effects derive from depolymerase activity or induced bacterial stress responses were not feasible, simpler phenotypic assays such as measurement of EPS breakdown products or turbidity reduction in biofilm matrix following phage treatment could have provided preliminary mechanistic insight and would be a worthwhile addition in future work. Fifthly, the biofilm disruption assay removed only a small volume of planktonic culture rather than fully washing wells prior to phage addition, meaning that phage activity was assessed against a combination of residual planktonic cells and established biofilm rather than biofilm alone. A more stringent approach would have involved complete removal of planktonic culture, washing with fresh SCFM, and replacement with phage in fresh media; this represents a limitation that should be considered when interpreting disruption results. Finally, the geographic origin effect (Finnish vs Belgian phages) remains descriptive without genomic backing.

Future research should therefore incorporate liquid media (e.g., synthetic CF sputum medium) to better replicate lung conditions, employ assays such as time-kill curves and efficiency-of-plating (EOP) to better represent phage dynamics, sequence both phage genomes and clinical strain genomes to explore adaptation and receptor mechanisms, and test phage–antibiotic combinations (PAS) under biofilm contexts. Controlled *in vivo* or *ex vivo*

lung-model studies will be essential to translate these *in vitro* insights into therapeutic strategies.

3.5 Conclusion

The primary objective of this study was to determine the clearance and biofilm profiles for 49 phages against clinical *P. aeruginosa* pathogens isolated from pwCF. Through a comprehensive assessment of phage clearance, biofilm disruption, and related analysis, this research has demonstrated the potential of phage therapy as a viable treatment strategy for *P. aeruginosa* infections, particularly in the context of increasing antibiotic resistance. The study highlighted the broad infectivity of the phages tested and their ability to interfere with biofilm formation, a key feature in chronic infections. Additionally, regional variations in phage efficacy, as seen between Finnish and Belgian phages, point to the importance of geographical factors in the selection of therapeutic phages. While *in vitro* findings suggest promise, further *in vivo* studies are essential to fully understand the therapeutic potential and to optimise treatment strategies for chronic infections. Ultimately, this study provides a foundational characterisation of phage host range and biofilm activity against a clinically representative collection of CF-associated *P. aeruginosa* isolates, informing the rational selection of phages for cocktail design and contributing to the evidence base for phage therapy in chronic CF infections.

4. Validation of phage cocktails against clinical *P. aeruginosa* with both known and unknown monomicrobial susceptibility.

4.1 Abstract

The rise of antibiotic resistance in *P aeruginosa* poses a major therapeutic challenge in CF, where chronic biofilm-associated infections drive progressive morbidity. This chapter aimed to develop broad-spectrum phage cocktails that could function as first-line interventions while personalised therapies are established. Host-range and biofilm-disruption assays across 93 clinical CF isolates were used to identify minimal phage combinations using the PhageCocktail R package. Three two-phage cocktails, each pairing a T4P and an LPS binding phage, achieved complete theoretical coverage of the strain panel. However, validation assays revealed that efficacy was highly dependent on MOI. At the nominal MOI 0.001 (effective ~10^{-6}), cocktails failed to consistently reduce bacterial growth and in some cases stimulated biofilm production, whereas higher doses (MOI 0.1 and 10) improved planktonic inhibition but achieved only modest biofilm disruption.

Comparisons of designed cocktails with randomly assembled cocktails showed no statistically significant differences in efficacy, and classification of phages as preventers or disrupters of biofilm did not predict cocktail performance. Strain-level analysis highlighted considerable heterogeneity, with some isolates exhibiting marked reductions in growth while others displayed paradoxical increases. These findings underscore the complexity of designing universally effective phage cocktails and suggest that MOI optimisation and integration with antibiotics may be required to achieve consistent therapeutic outcomes.

In summary, clearance and biofilm profiling enabled the rational design of phage cocktails with broad theoretical host coverage, but empirical results demonstrated that dosage, strain variability, and biofilm resilience remain major barriers. Broad-spectrum cocktails may nonetheless provide a pragmatic interim therapy in CF infections while personalised phage selection is underway, provided they are carefully optimised for concentration and composition.

4.2 Introduction

As described in Chapter 1 the high rates of AMR in *P. aeruginosa* isolated from pwCF, driven by repeated antibiotic exposure and biofilm-associated tolerance, represent a major and growing therapeutic challenge for which phage therapy has emerged as a promising alternative (Naghavi *et al.*, 2024).

Chapter 3 characterised the clearance and biofilm activity of 49 bacteriophages against 93 clinical *P. aeruginosa* isolates from Danish CF patients, revealing substantial variation in both host range and biofilm prevention/disruption capacity. Two phages showed particularly notable biofilm activity: DMS3virAcrFI demonstrated efficacy at both preventing and disrupting established biofilms, while PA7P1 was a highly effective disruptor of established biofilm. These profiles provided the empirical basis for phage selection in the cocktail design approach described in this chapter.

Because phages are highly specific to bacterial surface receptors, this specificity is advantageous in reducing off-target effects compared with antibiotics. However, it also poses challenges: the number of available therapeutic phages is limited, and effective treatment depends on knowledge of the exact bacterial strain. This requirement for personalisation makes large-scale, standardized phage production difficult.

Bacteria can evolve resistance to phages through several mechanisms. Mutations in phage receptor proteins can alter conformation or expression, preventing attachment and infection. For instance, Li *et al.* (2018) demonstrated that a mutation in the *PA1S_08510* gene encoding Wzy polymerase modified the O-antigen of LPS, preventing binding of phage PaP1. Similarly, mutations in T4P receptors (Xuan *et al.*, 2023) and loss or modification of the MexXY-OprM efflux pump (Koderi Valappil *et al.*, 2021) have been reported. The latter confers phage resistance but also increases antibiotic sensitivity, an example of a potential evolutionary trade-off and PAS.

Because resistance mutations affecting one receptor type do not confer cross-resistance to phages targeting a distinct receptor, combining phages with complementary receptor specificities reduces the probability of complete resistance emerging within a single bacterial population (Wright *et al.*, 2021). Pairing T4P-binding phages, which are rendered ineffective by pili loss, with LPS-binding phages, which are unaffected by T4P modification, provides a mechanistic basis for broader and more durable coverage (Tan *et al.*, 2014; Hendrix *et al.*, 2024). This receptor-diversity principle formed the central design rationale for the cocktails evaluated in this chapter.

The clinical evidence base for phage cocktail therapy, including trials in respiratory infection, is reviewed in Chapter 1 (section 1.4.3–1.4.4).

Because personalisation takes time, a critical factor in compassionate use cases, rapid, broad-spectrum options could improve patient outcomes (Gómez-Ochoa *et al.,* 2022); a key untested assumption, however, is whether rational cocktail design outperforms random

assembly. To address this, randomly compiled cocktails' were included as comparators, enabling the empirical benefit of rational design to be quantified.

Cocktail composition was informed by the PhageCocktail R package (Díaz-Galián *et al.*, 2022), which uses exhaustive combinatorial search to identify the minimum set of phages predicted to infect all strains in a panel, guaranteeing optimal theoretical coverage rather than approximating it via heuristic methods.

Chapter Aims

The aim of this study was to use clearance and biofilm profiling to develop a broad-spectrum phage cocktail against clinical *P. aeruginosa* isolates from CF patients and to assess its efficacy at different MOIs. The ultimate goal was to create a first-line therapeutic option that could be administered while personalised phage selection is underway.

Designed cocktails were compared to randomly compiled cocktails over a 24 to 48-hour period to determine whether rational design significantly outperformed random assembly. Clearance assay data were imported into the R package PhageCocktail (Díaz-Galián *et al.*, 2022) to identify phage combinations predicted to infect all 93 strains. The best theoretical cocktails contained two phages, none of which strongly disrupted biofilms, so the two most broadly infective phages were combined with one of two biofilm-reducing phages, yielding six empirically designed cocktails. Liquid culture infectivity and biofilm assays were then performed using these six cocktails and six randomly assembled cocktails against 17 *P. aeruginosa* CF strains not previously tested.

4.3 Results

4.3.1 Cocktail design

To determine the most effective phage combinations against *P. aeruginosa* clinical isolates, phage cocktail design was carried out using the PhageCocktail R package (Díaz-Galián *et al.*, 2022). An exhaustive search approach was employed, in which all possible combinations of phages (up to a user-defined maximum size) were systematically evaluated to identify the smallest set capable of lysing all target bacterial strains. Unlike heuristic or clustering-based methods, which estimate suitable combinations by grouping phages with similar host ranges, exhaustive search directly tests every possible phage combination within the dataset. This approach identifies the minimal cocktail that provides complete theoretical coverage, although it requires greater computational time.

Infectivity data were converted into a binary format, where any observable lysis was recorded as “1” and absence of lysis as “0”. This simplified matrix was used as the input for cocktail determination. The package identified three two-phage cocktails capable of infecting all 93 clinical strains used for empirical host range determination:

(a) PNM and PA10P2,
(b) PT7 and PA5P1, and
(c) 14/1 and PA5P2.

Following these two-phage cocktails, the next optimal combinations contained three phages and were excluded to maintain consistency in cocktail size. Each of the two-phage cocktails included one LPS-targeting and one T4P-targeting phage, none of which were strong biofilm preventers or disruptors.

To compile the final six cocktails, each two-phage combination was paired independently with either an efficient biofilm preventer/disruptor, DMS3virAcrFI, or a biofilm disruptor, PA7P1, resulting in the following combinations:

(a) PNM, PA10P2, DMS3virAcrFI;
(b) PT7, PA5P1, DMS3virAcrFI;
(c) 14/01, PA5P2, DMS3virAcrFI;
(d) PNM, PA10P2, PA7P1;
(e) PT7, PA5P1, PA7P1;
(f) 14/1, PA5P2, PA7P1.

Alongside these six designed cocktails, six randomly assembled cocktails were generated as baseline comparators to assess whether random combinations could perform comparably to designed cocktails. These were assembled using a random number generator and consisted of the following:

(g) QAT8, PA12P1, PA1P5;
(h) PA1P2, PA10P3, QAT3a;
(i) PT7, PA1P5, PA8P2;
(j) 14/01, DMS3virAcrFI, PA5P1;
(k) PA12P1, PA5P2, DMS3vir;
(l) PA4P2, PA1P5, PA10P1.

Some overlap occurred between designed and random cocktails (e.g., PT7, 14/01, DMS3virAcrFI, and PA5P1 appeared in both groups). The presence of shared phages allowed comparison of performance where identical components were arranged differently.

These overlaps were noted for interpretation of subsequent infectivity and biofilm assay results.

4.3.2 Cocktail Validation at MOI 0.001

With cocktail compositions established, validation experiments were performed using 17 untested clinical *P. aeruginosa* strains from pwCF. All cocktails were initially prepared at an MOI of 0.001. It should be noted that this nominal MOI was miscalculated and corresponds to an effective phage-to-bacteria ratio of ~10^{-6}, due to an earlier error in PFU/CFU calculation. When tested against these strains, very few significant reductions in bacterial growth were observed at either 24 or 48 hours (Figure 4.1). Biofilm reduction was also minimal, with some strains demonstrating increased biofilm production. The observation that OD values in some phage-treated wells exceeded those of the no-phage positive control is noted and may reflect phage-induced bacterial stress responses or aggregation at this very low effective MOI.

Pairwise comparisons between each phage cocktail and the positive control (bacterial growth in the absence of phage) were conducted to determine whether individual cocktails significantly reduced OD_{600} at each time point (Table 4.1). At 24 hours, only cocktail j demonstrated a significant difference relative to the control (estimate = 0.155, p = 0.023). This is consistent with the composition of cocktail j, which contains two phages present in cocktail c and one from cocktail b. All other cocktails were not significantly different ($p > 0.05$). By 48 hours, several cocktails showed significantly reduced OD relative to the control, including cocktails b (estimate = 0.148, p = 0.0019), c (estimate = 0.121, p = 0.034), e (estimate = 0.127, p = 0.018), and j (estimate = 0.177, $p < 0.001$), whereas other cocktails did not differ significantly.

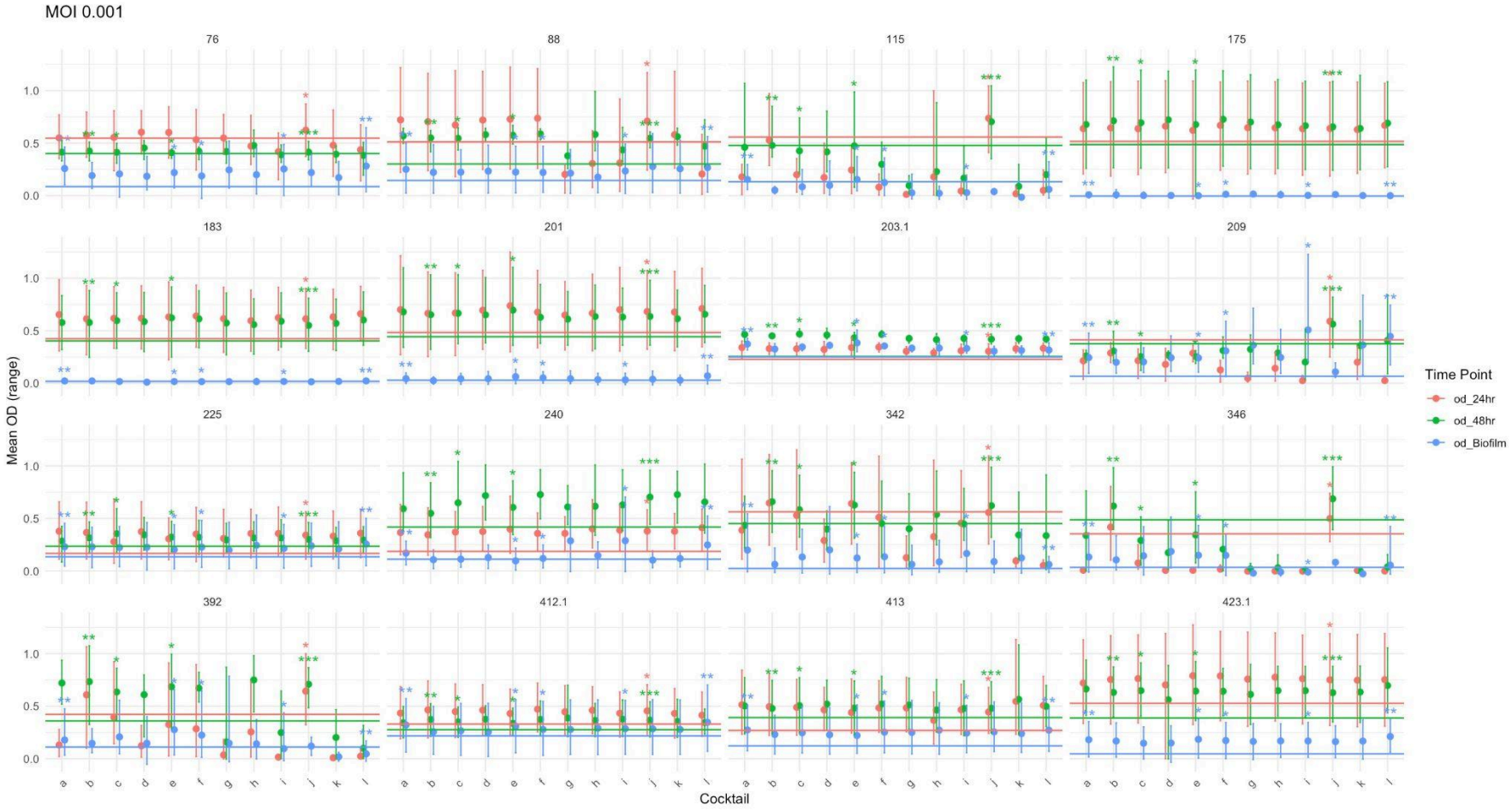

Figure 4.1: **Optical density measurements (OD_{600}) of bacterial growth for 16 clinical *Pseudomonas aeruginosa* strains exposed to 12 bacteriophage cocktails at (nominal) MOI 0.001.** Measurements were recorded at 24 h, 48 h, and following biofilm staining. Horizontal lines indicate the strain-specific positive control (no phage treatment), with red representing 24 h, green representing 48 h, and blue representing post-biofilm staining measurements. Data represent mean values from six biological replicates (n = 6), with error bars indicating the full data range (minimum to maximum OD_{600}). Statistical significance relative to the positive control was assessed using mixed-effects modelling followed by Tukey-adjusted pairwise comparisons; significance is indicated by asterisks (* $p < 0.05$, ** $p < 0.01$, *** $p < 0.001$). Strain 430 was excluded due to lack of growth in the positive control. Note: the nominal MOI of 0.001 corresponds to an effective phage-to-bacteria ratio of ~10^{-6}.

Table 4.1: Pairwise Tukey-adjusted comparisons of each cocktail-treated strain at MOI 0.001 versus the positive control, based on estimated marginal means (emmeans) from a linear mixed-effects model. 'Estimate' values show the mean difference in OD_{600} (24 h and 48 h growth) or OD_{590} (biofilm) relative to the control, reported to three decimal places. Note: the nominal MOI of 0.001 corresponds to an effective phage-to-bacteria ratio of ~10^{-6}.

Comparison	24hr Growth	24hr p-value	48hr Growth	48hr p-value	Biofilm	Biofilm p-value
a	0.03	1	0.11	0.059	0.1	0.001
b	0.12	0.2	0.15	0.002	0.05	0.48
c	0.05	0.998	0.12	0.034	0.07	0.106
d	0.02	1	0.11	0.119	0.07	0.056
e	0.06	0.959	0.13	0.018	0.08	0.01
f	0.04	1	0.11	0.063	0.08	0.014
g	-0.06	0.978	0.02	1	0.07	0.093
h	-0.02	1	0.09	0.336	0.05	0.437
i	-0.03	1	0.03	1	0.08	0.01
j	0.15	0.023	0.18	<0.001	0.05	0.49
k	-0.03	1	0.04	0.997	0.05	0.665
l	-0.06	0.989	0.04	0.995	0.09	0.004

In biofilm assays, multiple cocktails exhibited significant reductions in OD compared with the control. Significant effects were observed for cocktails a (estimate = 0.095, p = 0.0014), e (estimate = 0.084, p = 0.010), f (estimate = 0.082, p = 0.014), i (estimate = 0.084, p = 0.010), and l (estimate = 0.090, p = 0.0036), while the remaining cocktails did not significantly differ from the control under biofilm conditions. The “estimate” values reported correspond to the modeled mean difference in OD between the treated cocktail and the positive control as calculated by the linear mixed-effects model.

4.3.2 Investigation of Low Efficacy

To explore why so few cocktails exhibited significant growth reduction at MOI 0.001, additional experiments were conducted to assess whether low efficacy resulted from phage combinations, strain-specific resistance, or the low MOI. As noted, the nominal MOI 0.001 resulted in an effective phage-to-bacteria ratio of ~10^{-6}, which was insufficient for reliable infection in most strains. Spot tests and growth assays in liquid media with biofilm assessment were performed. Six test strains (76, 225, 115, 430, 203.1, and 392) and six original training strains (435, 78, 243, 206, 214, and 341) representing diverse lineages were selected for spot testing at cocktail concentrations (Methods 2.4). With the exception of strain 115 (Figure 4.2) and strain 435, which produced no bacterial lawn, no infection was observed for any strain, supporting that the low effective MOI (~10^{-6}) was insufficient to allow adequate infection in most lineages.

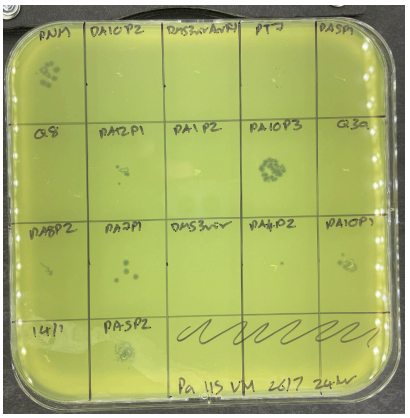

Figure 4.2: **Spot assay plate showing *P. aeruginosa* strain 115 exposed to individual phages at cocktail concentration.** Each spot represents a different phage from the collection, labelled by phage name. Visible zones of clearing indicate successful phage infection. Strain 115 was one of only two strains (alongside strain 435) to show observable infection at this concentration, with 5 phages producing visible clearance zones. The absence of a bacterial lawn in some areas of the plate reflects the extent of phage-mediated lysis. This result confirmed that the low effective MOI (~10^{-6}) was insufficient to produce reliable infection across most strains tested, and that poor cocktail performance at MOI 0.001 was attributable to concentration-dependent failure rather than strain-specific resistance or phage antagonism.

Further spot assays comparing individual phages at their original titre to cocktails showed that individual phages infected strongly (Figure 4.3 a and c), whereas cocktail infections were weak or absent (Figure 4.3 b and d). Liquid media experiments confirmed these results: testing all 17 test strains against individual phages at cocktail MOI demonstrated that while some strains were susceptible to individual phages, the majority exhibited increased growth in the presence of phage (Figure 4.4). These findings prompted reassembly of the cocktails at higher MOIs of 0.1 and 10 to determine whether increased concentrations improved efficacy.

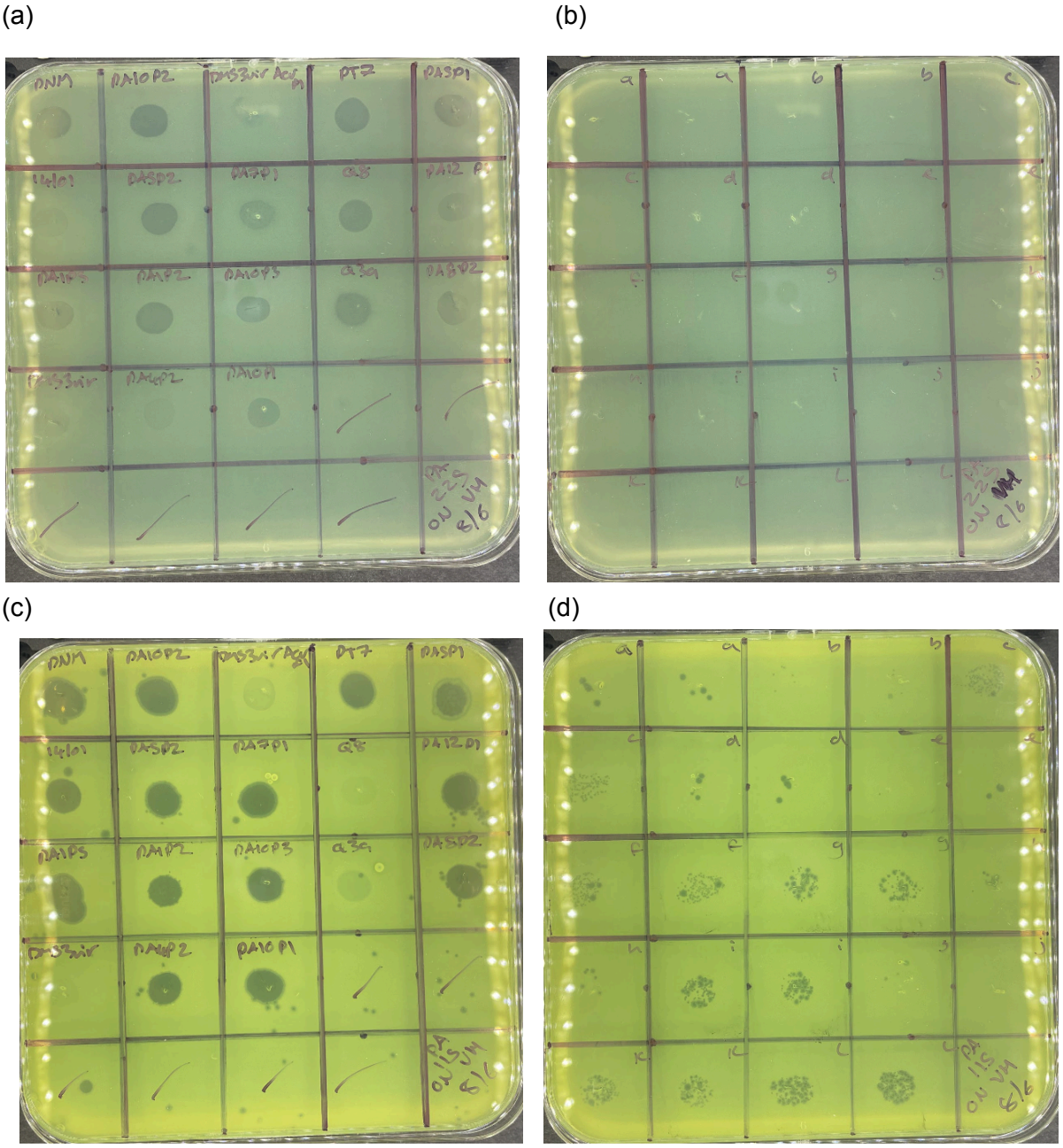

Figure 4.3: **Spot assay plates comparing the infectivity of individual phages at original titre versus phage cocktails against two clinical *P. aeruginosa* strains.** (a) Individual phages spotted onto strain 225, showing strong and widespread zones of clearance for the majority of phages tested. (b) Phage cocktails (labelled a–c) spotted onto strain 225, showing absent or very faint clearance zones, indicating poor infectivity at cocktail concentration. (c) Individual phages spotted onto strain 115, showing strong zones of clearance comparable to those observed for strain 225 in panel (a). (d) Phage cocktails spotted onto strain 115, showing weak or absent clearance for most cocktails, with only isolated small plaques visible for some. Comparison of panels (a) and (c) with panels (b) and (d) demonstrates that individual phages at their original titre were capable of infecting both strains effectively, whereas the same phages combined into cocktails at the nominal MOI of 0.001 (effective ratio ~10^{-6}) failed to produce reliable infection, confirming that poor cocktail performance was attributable to the low effective MOI rather than strain-specific resistance.

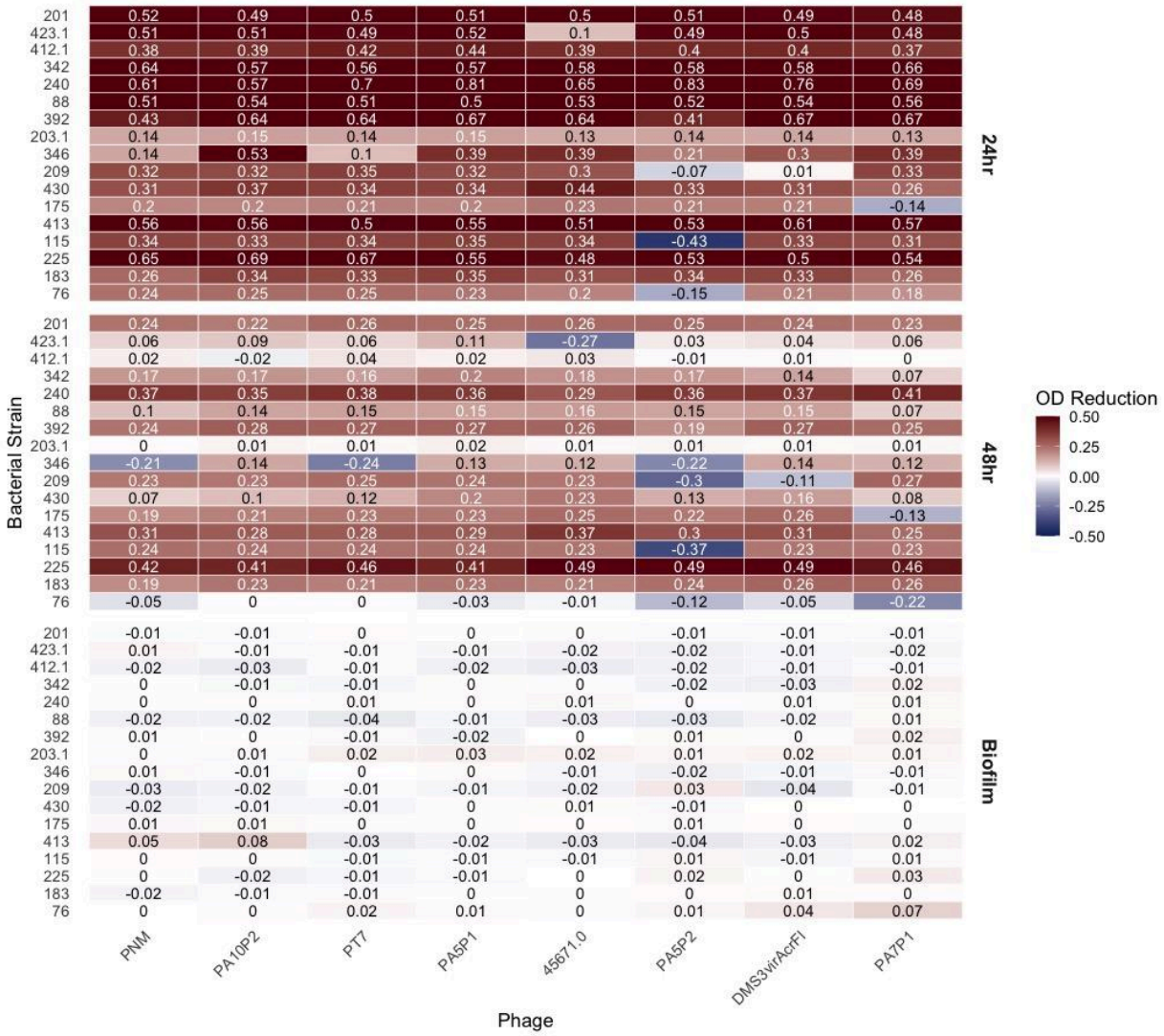

Figure 4.4: **Heatmap showing OD reduction relative to the no-phage positive control for 17 clinical *P. aeruginosa* strains exposed to 9 individual cocktail phages at cocktail concentration in liquid SCFM.** Measurements were taken at three timepoints: 24 hours (top), 48 hours (middle), and following crystal violet biofilm staining (bottom). Colour indicates direction and magnitude of OD change relative to the positive control: red indicates increased OD (increased growth or aggregation compared to control); white indicates no change; blue indicates reduced OD (reduced growth compared to control). The colour scale ranges from −0.50 to +0.50 OD units. No statistical testing was performed; this heatmap is descriptive and intended to confirm and visualise trends observed in the preceding spot assays. The predominance of red and white values, particularly at the biofilm timepoint, is consistent with the low effective MOI (~10^{-6}) being insufficient to suppress bacterial growth reliably across most strains.

4.3.3 MOI 0.1 Results

At MOI 0.1, improved growth control was observed relative to the low effective MOI 0.001 (~10^{-6}) used previously (Figure 4.5). Pairwise Tukey-adjusted comparisons between each cocktail and the positive control were performed at 24 and 48 hours, as well as under biofilm conditions (Table 4.2). The “estimate” values reported correspond to the Tukey-adjusted

mean difference in OD_{600} between each cocktail-treated sample and the positive control, accounting for multiple comparisons.

At 24 hours, several cocktails exhibited significantly higher OD than the positive control, with the largest increases observed for cocktails b (estimate = 0.25, $p < 0.001$), j (estimate = 0.20, $p < 0.001$), and e (estimate = 0.19, $p < 0.001$). Additional significant increases were detected for cocktails d (estimate = 0.16, $p < 0.001$), a (estimate = 0.15, $p < 0.001$), g (estimate = 0.12, $p = 0.003$), i (estimate = 0.12, $p = 0.003$), and h (estimate = 0.11, $p = 0.009$). Cocktails c, f, k, and l did not differ significantly at this time point.

By 48 hours, none of the cocktails differed significantly from the positive control after adjustment for multiple testing (all $p > 0.05$). In biofilm assays, significant increases were observed for cocktail l (estimate = 0.063, $p < 0.001$), a (estimate = 0.030, $p = 0.001$), and j (estimate = 0.025, $p = 0.015$), while other cocktails were not significantly different from the control.

Table 4.2: Pairwise Tukey-adjusted comparisons of each cocktail-treated strain at MOI 0.1 versus the positive control, based on estimated marginal means (emmeans) from a linear mixed-effects model. 'Estimate' values show the mean difference in OD_{600} (24 h and 48 h growth) or OD_{590} (biofilm) relative to the control, reported to three decimal places.

Comp.	24hr Growth	24hr p-value	48hr Growth	48hr p-value	Biofilm	Biofilm p-value
a	0.15	<0.001	-0.04	0.996	0.03	0.001
b	0.25	0	0.09	0.163	0.02	0.225
c	0.05	0.861	-0.03	0.999	0.01	0.91
d	0.16	<0.001	0.03	1	0.01	0.991
e	0.19	<0.001	0.06	0.862	0.01	0.77
f	0.08	0.276	0	1	0.02	0.462
g	0.12	0.003	-0.01	1	0.01	0.883
h	0.11	0.009	0.06	0.848	0.01	0.773
i	0.12	0.003	-0.01	1	0.02	0.241
j	0.2	<0.001	0.09	0.256	0.03	0.015
k	0.06	0.677	0	1	0.02	0.087
l	0.06	0.708	-0.07	0.513	0.06	0

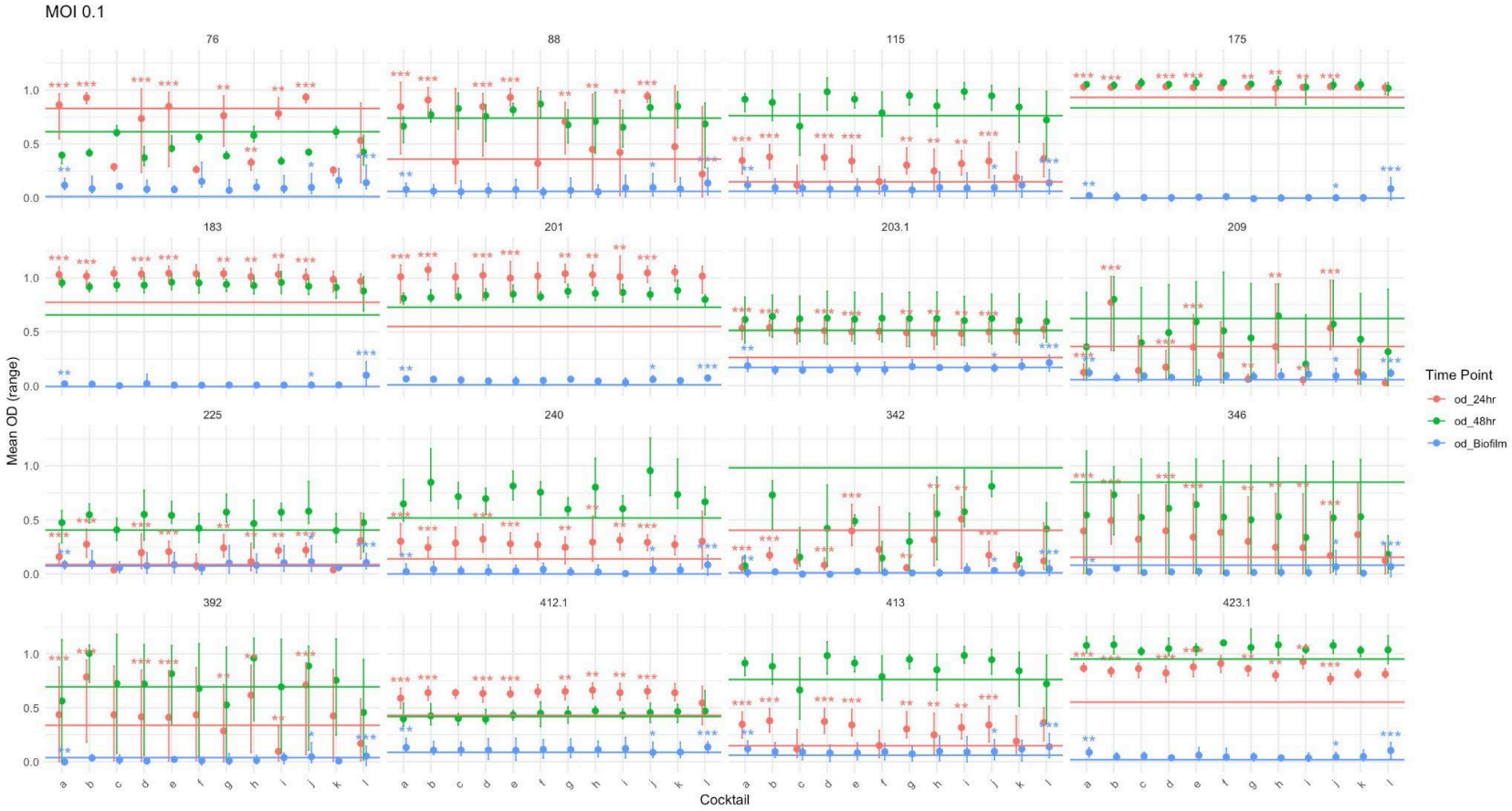

Figure 4.5: Optical density measurements (OD_{600}) of bacterial growth for 16 clinical *Pseudomonas aeruginosa* strains exposed to 12 bacteriophage cocktails at MOI 0.1. Measurements were recorded at 24 h, 48 h, and following biofilm staining. Horizontal lines indicate the strain-specific positive control (no phage treatment), with red representing 24 h, green representing 48 h, and blue representing post-biofilm staining measurements. Data represent mean values from six biological replicates (n = 6), with error bars indicating the full data range (minimum to maximum OD_{600}). Statistical significance relative to the positive control was assessed using mixed-effects modelling followed by Tukey-adjusted pairwise comparisons; significance is indicated by asterisks (* $p < 0.05$, ** $p < 0.01$, *** $p < 0.001$). Strain 430 was excluded due to lack of growth in the positive control. MOI 0.1 represents a 100-fold increase in effective phage concentration compared to the previously tested MOI 0.001 (~10^{-6} effective ratio); however, significant reductions in OD relative to the positive control were not consistently observed, with several cocktails producing significantly higher OD than the control at 24 hours.

4.3.4 MOI 10 Results

At MOI 10, the results were analyzed using Tukey-adjusted pairwise comparisons of estimated marginal means (emmeans) derived from a linear mixed-effects model, comparing each cocktail-treated sample to the positive control. The ‘estimate’ values reported represent the Tukey-adjusted mean difference in OD_{600} between the cocktail and the positive control, with negative values indicating a reduction in growth relative to the control. P-values indicate whether these differences are statistically significant after adjustment for multiple comparisons.

At 24 hours, only cocktails h (estimate = –0.140, $p < 0.001$) and d (estimate = –0.109, $p = 0.002$) differed significantly from the positive control; all other cocktails showed no significant difference. By 48 hours, nearly all cocktails demonstrated significantly lower OD than the positive control, with the largest reductions observed for cocktails d (estimate = –0.287, $p < 0.001$), a (estimate = –0.266, $p < 0.001$), and f (estimate = –0.255, $p < 0.001$), and significant reductions also noted for h, k, c, l, i, g, e, j, and b. These findings indicate that at 48 hours, nearly all cocktails significantly reduced bacterial growth relative to the positive control. No significant differences were observed under biofilm conditions ($p > 0.05$).

Table 4.3: Pairwise Tukey-adjusted comparisons of each cocktail-treated strain at MOI 10 versus the positive control, based on estimated marginal means (emmeans) from a linear mixed-effects model. 'Estimate' values show the mean difference in OD_{600} (24 h and 48 h growth) or OD_{590} (biofilm) relative to the control, reported to three decimal places.

Comparison	24hr Growth	24hr p-value	48hr Growth	48hr p-value	Biofilm	Biofilm p-value
a	-0.07	0.179	-0.27	0	0.01	0.999
b	0.03	0.9989	-0.1	0.006	0.01	0.96
c	-0.06	0.403	-0.22	0	-0.01	0.997
d	-0.11	0.002	-0.29	0	0	1
e	-0.02	0.901	-0.14	<0.001	0.01	0.966
f	-0.07	0.243	-0.25	0	-0.01	0.984
g	-0.04	0.901	-0.15	<0.001	0.01	0.995
h	-0.14	<0.001	-0.24	0	0	1
i	-0.05	0.817	-0.16	<0.001	0	1
j	0.01	1	-0.14	<0.001	0	1
k	-0.07	0.232	-0.23	0	-0.01	0.3841
l	-0.06	0.64	-0.19	0	0.01	1

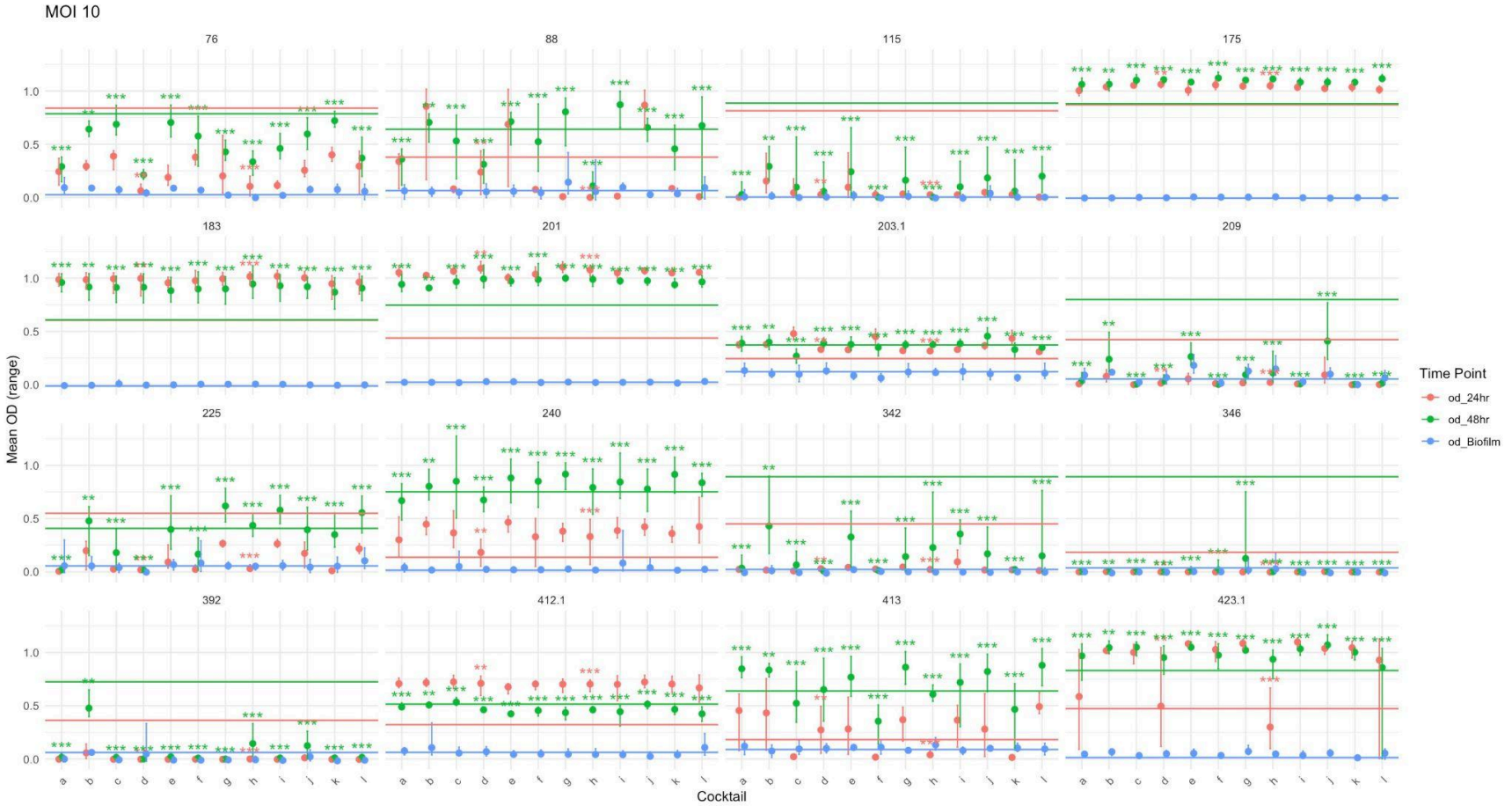

Figure 4.6: **Optical density measurements (OD_{600}) of bacterial growth for 16 clinical *Pseudomonas aeruginosa* strains exposed to 12 bacteriophage cocktails at MOI 10.** Measurements were recorded at 24 h, 48 h, and following biofilm staining. Horizontal lines indicate the strain-specific positive control (no phage treatment), with red representing 24 h, green representing 48 h, and blue representing post-biofilm staining measurements. Data represent mean values from six biological replicates (n = 6), with error bars indicating the full data range (minimum to maximum OD_{600}). Statistical significance relative to the positive control was assessed using mixed-effects modelling followed by Tukey-adjusted pairwise comparisons; significance is indicated by asterisks (* $p < 0.05$, ** $p < 0.01$, *** $p < 0.001$). Strain 430 was excluded due to lack of growth in the positive control. At MOI 10, nearly all cocktails demonstrated significantly reduced OD relative to the positive control by 48 hours, representing a marked improvement in efficacy compared to MOI 0.1 and MOI 0.001. No significant reductions were observed under biofilm conditions at this MOI.

4.3.5 Comparison of Designed and Random Assemblies by MOI

To assess whether the method of assembly influenced phage efficacy, the % reduction of *P. aeruginosa* by designed cocktails was compared with that of randomly assembled cocktails across three MOIs (0.001, 0.1, and 10) and three experimental conditions (24 h, 48 h, and biofilm formation) (Figure 4.7). Wilcoxon rank-sum tests with Benjamini-Hochberg adjustment were applied to account for multiple comparisons, and effect sizes (r) were calculated using rank-biserial correlation to quantify practical significance (Table 4.4).

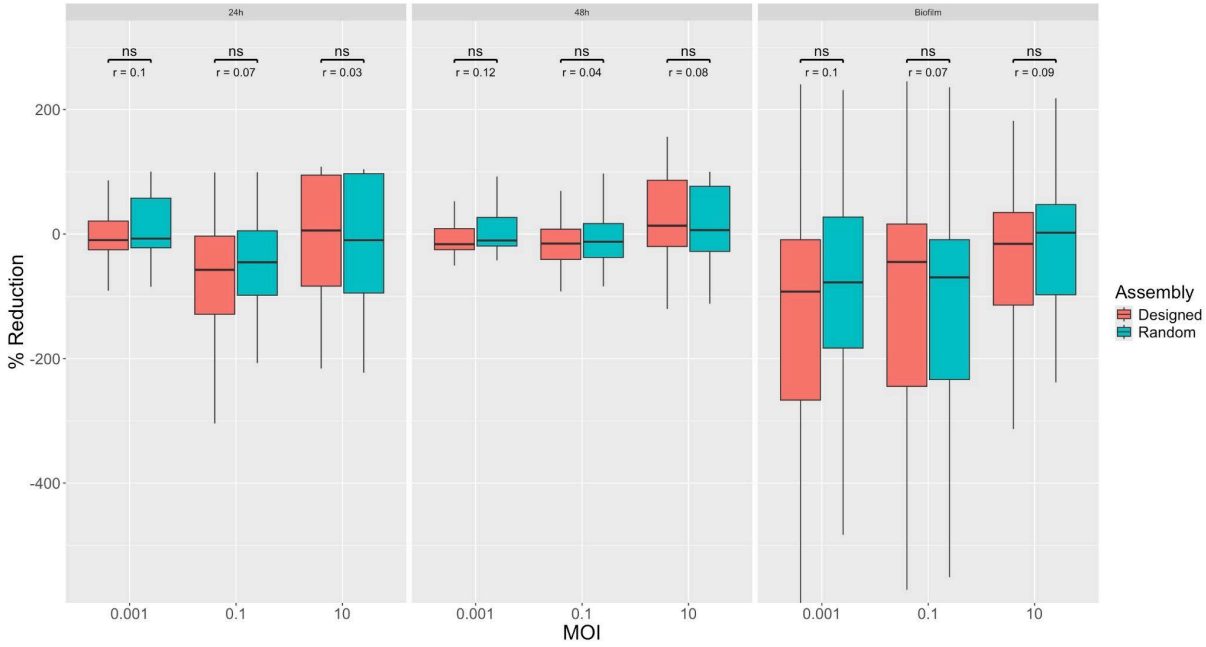

Figure 4.7: Box plots comparing percentage reduction in *P. aeruginosa* growth between designed (red) and randomly assembled (teal) phage cocktails across three MOIs (0.001, 0.1, and 10) and three timepoints (24 h, 48 h, and biofilm staining). Percentage reduction was calculated relative to the no-phage positive control. Box boundaries represent the interquartile range (IQR), the central line represents the median, and whiskers extend to 1.5× IQR. Outliers are not shown for clarity.Each facet represents a different time point. Horizontal brackets indicate pairwise comparisons between designed and random cocktails at each MOI, performed using Wilcoxon rank-sum tests with Benjamini-Hochberg adjustment for multiple comparisons. ns = not significant (all adjusted p > 0.05). Rank-biserial effect sizes (r) are shown below brackets to indicate magnitude of difference; all effect sizes were small (r = 0.05–0.12). No significant differences were observed between designed and random cocktails under any condition or MOI tested, indicating that cocktail assembly strategy did not meaningfully influence efficacy. Note: the nominal MOI of 0.001 corresponds to an effective phage-to-bacteria ratio of ~10^{-6}.

At 24 h, no statistically significant differences were observed between designed and random cocktails at any MOI. Specifically, for nominal MOI 0.001 (~10^{-6} effective) (n = 102 per group), p.adj = 0.466, r = 0.07 (small); MOI 0.1, p.adj = 0.466, r = 0.08 (small); and MOI 10,

p.adj = 0.696, r = 0.12 (small). These results indicate negligible differences in early growth suppression between assembly strategies.

At 48 h, similarly, there were no significant differences across MOIs. For MOI 0.001 (~10^{-6} effective), p.adj = 0.263, r = 0.06 (small); MOI 0.1, p.adj = 0.522, r = 0.05 (small); and MOI 10, p.adj = 0.396, r = 0.07 (small). These findings suggest that the efficacy of designed versus random cocktails remained largely equivalent over extended growth periods.

Under biofilm-forming conditions, no differences were detected at any MOI. MOI 0.001 (effective ~10^{-6}) yielded p.adj = 0.265, r = 0.06 (small); MOI 0.1, p.adj = 0.312, r = 0.07 (small); and MOI 10, p.adj = 0.265, r = 0.06 (small). Collectively, these results demonstrate that the strategy used to assemble phage cocktails—designed or random—did not produce meaningful differences in bacterial reduction under any experimental condition tested, with effect sizes consistently small and all comparisons statistically non-significant.

Table 4.4: Wilcoxon rank-sum test results and effect sizes comparing Designed and Random assemblies across MOIs and experimental conditions. The table summarizes comparisons at MOIs of 0.001, 0.1, and 10 under 24 h, 48 h, and biofilm conditions. For each comparison, the number of samples per group (n), adjusted p-values (p.adj), significance level (ns = not significant), rank-biserial effect size (r), and qualitative magnitude of the effect (small, medium, large) are shown. Note: the nominal MOI of 0.001 corresponds to an effective phage-to-bacteria ratio of ~10^{-6}.

Time	MOI	Comparison	n (group1 / group2)	p.adj	Significance	Effect size (r)	Magnitude
24 h	0.001	Designed vs Random	102 / 102	0.466	ns	0.07	small
24 h	0.1	Designed vs Random	102 / 102	0.466	ns	0.08	small
24 h	10	Designed vs Random	102 / 102	0.696	ns	0.12	small
48 h	0.001	Designed vs Random	102 / 102	0.263	ns	0.06	small
48 h	0.1	Designed vs Random	102 / 102	0.522	ns	0.05	small
48 h	10	Designed vs Random	102 / 102	0.396	ns	0.07	small
Biofilm	0.001	Designed vs Random	102 / 102	0.265	ns	0.06	small
Biofilm	0.1	Designed vs Random	102 / 102	0.312	ns	0.07	small
Biofilm	10	Designed vs Random	102 / 102	0.265	ns	0.06	small

4.3.6 Comparison of Designed and Random Assemblies by Strain

To investigate whether the method of cocktail assembly influenced phage efficacy on a strain-specific level, % reduction was compared between designed and randomly assembled cocktails across 17 *P. aeruginosa* strains at three MOIs (0.001, 0.1, and 10) (Figure 4.8). Wilcoxon rank-sum tests were conducted for each strain-MOI combination, with Benjamini-Hochberg adjustment applied to control for multiple comparisons (Table 4.5). Effect sizes (r) were calculated using the rank-biserial correlation and interpreted as negligible, small, medium, or large to provide a measure of practical significance.

At nominal MOI 0.001 (10^{-6}), the majority of strains showed no statistically significant difference between designed and random cocktails, with p.adj values ranging from 0.0602 to 1.0. Effect sizes were generally small to negligible (r = 0.01–0.16), with a few strains exhibiting medium effects, such as strain 115 (r = 0.29), and one strain showing a large effect size (strain 346, r = 0.42), though this did not reach statistical significance after adjustment. For example, strain 76 had p.adj = 0.942, r = 0.01 (negligible), while strain 392 had p.adj = 0.264, r = 0.26 (medium). Overall, these data indicate that at low MOI, there was no robust difference between the efficacy of designed versus random cocktails across strains, with effect sizes suggesting minimal practical impact for most strains.

At MOI 0.1, the pattern remained largely consistent. All strain comparisons were non-significant (p.adj ≥ 0.627), with effect sizes predominantly negligible to small (r = 0–0.16). Strain-specific effect sizes occasionally reached small magnitudes, such as strain 209 (r = 0.12) and strain 225 (r = 0.14), but no strain demonstrated a statistically significant difference in response to the cocktail assembly method. Notably, several strains, including strain 76 and 346, showed negligible effect sizes (r = 0–0.01), indicating essentially identical outcomes between designed and random cocktails.

At MOI 10, similarly, all comparisons remained non-significant (p.adj ≥ 0.627), and effect sizes were mostly negligible to small (r = 0–0.17). Strain 225 showed the highest small effect size at this MOI (r = 0.17), whereas strains 88, 201, and 209 remained negligible (r ≤ 0.03). These findings suggest that even at the highest phage concentration, there was no meaningful difference in strain-specific reduction between the two assembly strategies.

Across all MOIs and strains, these results collectively indicate that the method of phage cocktail assembly—designed versus random—did not produce statistically significant or practically meaningful differences in % reduction at the strain level. Effect sizes were consistently small or negligible for the majority of strains, with only occasional medium or large effect sizes that did not reach significance. Notably, for MOI 0.001, the weak effects

observed reflect the low effective phage-to-bacteria ratio (~10^{-6}) rather than inherent ineffectiveness of the phages. This highlights the robustness of phage activity across assembly strategies and suggests that strain-specific responses are largely independent of whether cocktails were systematically designed or randomly compiled.

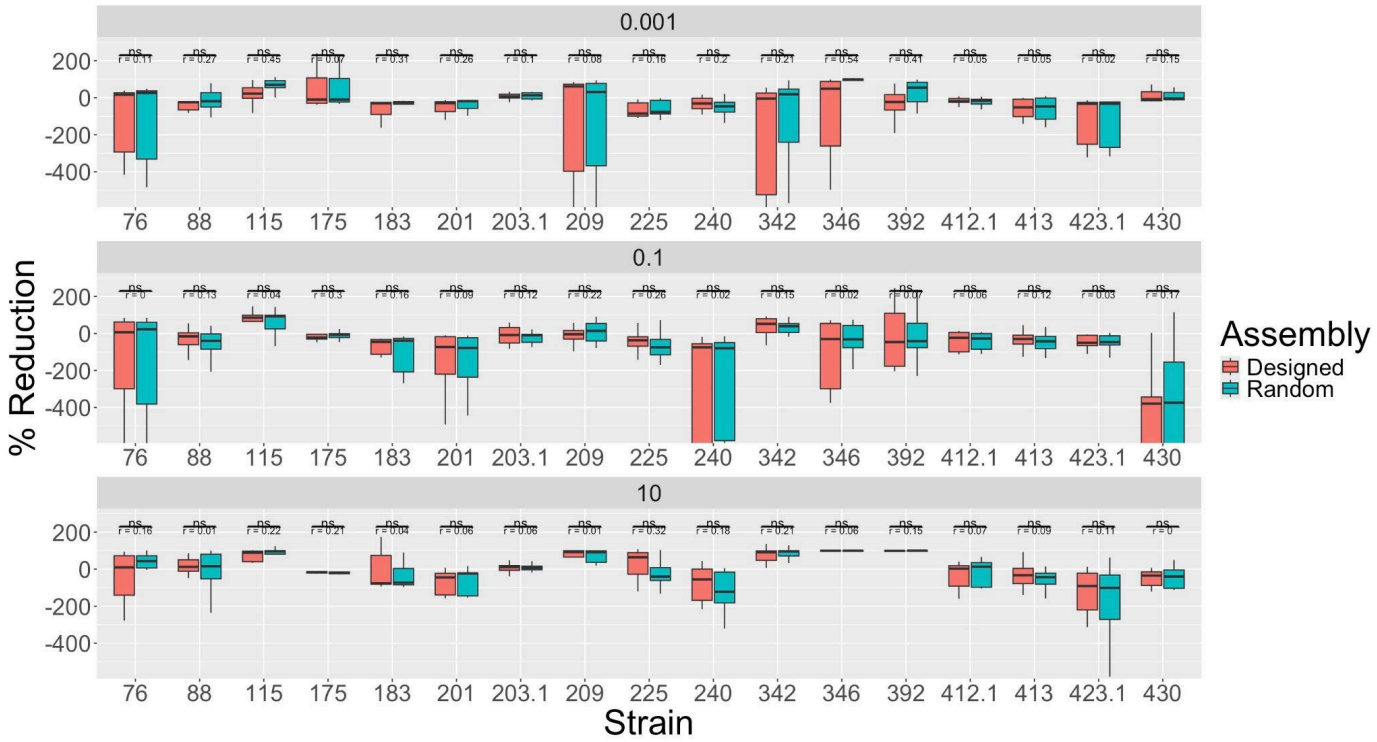

Figure 4.8: Box plots comparing percentage reduction in *P. aeruginosa* growth between designed (red) and randomly assembled (teal) phage cocktails across 17 clinical strains at three MOIs (0.001, 0.1, and 10). Each facet represents a different MOI. Percentage reduction was calculated relative to the no-phage positive control. Box boundaries represent the interquartile range (IQR), the central line represents the median, and whiskers extend to 1.5× IQR. Extreme outliers are not displayed for clarity. Wilcoxon rank-sum tests with Benjamini-Hochberg adjustment were performed for each strain-MOI combination. Effect sizes (r) calculated by rank-biserial correlation and significance annotations (ns = not significant) are shown above each comparison. No statistically significant differences were observed between designed and random cocktails for any strain at any MOI after adjustment for multiple comparisons. Effect sizes were consistently small to negligible (r = 0–0.17) for the majority of strains, with occasional medium or large effect sizes that did not reach statistical significance.Note: the nominal MOI of 0.001 corresponds to an effective phage-to-bacteria ratio of ~10^{-6}.

Table 4.5: Wilcoxon rank-sum test results comparing Designed vs Random assemblies for each strain and MOI. Columns: MOI – Multiplicity of infection; Strain – Individual strain identifiers; Comparison – Groups compared (Designed vs Random); n (group1 / group2) – Number of replicates per group; p.adj – Benjamini-Hochberg adjusted p-value; Significance – ns = not significant; Effect size (r) – Rank-biserial correlation; Magnitude – Interpretation of effect size (Negligible, Small, Medium, Large). Note: the nominal MOI of 0.001 corresponds to an effective phage-to-bacteria ratio of ~10^{-6}.

MOI	Strain	p.adj	Significance	Effect size (r)	Magnitude
0.001	76	0.942	ns	0.01	Negligible
0.001	88	0.708	ns	0.08	Small
0.001	115	0.174	ns	0.29	Medium
0.001	175	0.974	ns	0.04	Negligible
0.001	183	0.627	ns	0.16	Small
0.001	201	0.708	ns	0.12	Small
0.001	203.1	0.974	ns	0.03	Negligible
0.001	209	0.974	ns	0.02	Negligible
0.001	225	0.871	ns	0.06	Small
0.001	240	0.799	ns	0.09	Small
0.001	342	0.799	ns	0.1	Small
0.001	346	0.0602	ns	0.42	Large
0.001	392	0.264	ns	0.26	Medium
0.001	412.1	0.974	ns	0.03	Negligible
0.001	413	0.98	ns	0.03	Negligible
0.001	423.1	1	ns	0.01	Negligible
0.001	430	0.871	ns	0.06	Small
0.1	76	1	ns	0	Negligible
0.1	88	0.936	ns	0.07	Small
0.1	115	0.986	ns	0.02	Negligible
0.1	175	0.627	ns	0.16	Small
0.1	183	0.871	ns	0.06	Small
0.1	201	0.974	ns	0.03	Negligible
0.1	203.1	0.936	ns	0.04	Small
0.1	209	0.799	ns	0.12	Small
0.1	225	0.708	ns	0.14	Small
0.1	240	1	ns	0.01	Negligible
0.1	342	0.871	ns	0.07	Small
0.1	346	1	ns	0.01	Negligible
0.1	392	0.974	ns	0.03	Negligible
0.1	412.1	0.974	ns	0.03	Negligible
0.1	413	0.936	ns	0.04	Small
0.1	423.1	1	ns	0.01	Negligible

Table 4.5 Continued

MOI	Strain	p.adj	Significance	Effect size (r)	Magnitude
0.1	430	0.871	ns	0.06	Small
10	76	0.871	ns	0.06	Small
10	88	1	ns	0.01	Negligible
10	115	0.799	ns	0.12	Small
10	175	0.799	ns	0.11	Small
10	183	0.993	ns	0.02	Negligible
10	201	0.974	ns	0.03	Negligible
10	203.1	0.974	ns	0.03	Negligible
10	209	1	ns	0.01	Negligible
10	225	0.627	ns	0.17	Small
10	240	0.871	ns	0.09	Small
10	342	0.799	ns	0.1	Small
10	346	0.974	ns	0.03	Negligible
10	392	0.871	ns	0.07	Small
10	412.1	0.974	ns	0.04	Small
10	413	0.974	ns	0.04	Small
10	423.1	0.942	ns	0.06	Small
10	430	1	ns	0	Negligible

4.3.7 Comparison of Disrupter and Preventer Assemblies by MOI

To evaluate whether the type of phage cocktail, Disrupter or Preventer, affected bacterial growth reduction across different phage concentrations, % reduction was compared across 17 *P. aeruginosa* strains at three MOIs (0.001, 0.1, and 10) and three experimental conditions: 24 h, 48 h, and biofilm formation. Wilcoxon rank-sum tests were conducted for each MOI, timepoint combination to compare Preventer versus Disrupter cocktails (Figure 4.9).

At 24 h, there were no statistically significant differences between Disrupter and Preventer cocktails at any MOI (Table 4.6). Specifically, MOI 0.001 (effective ~10^{-6}) had a Wilcoxon statistic W = 1282, p = 0.904; MOI 0.1 had W = 1324, p = 0.904; and MOI 10 had W = 1246, p = 0.72. These results indicate that, early in the assay, cocktail type did not meaningfully influence % reduction of bacterial growth.

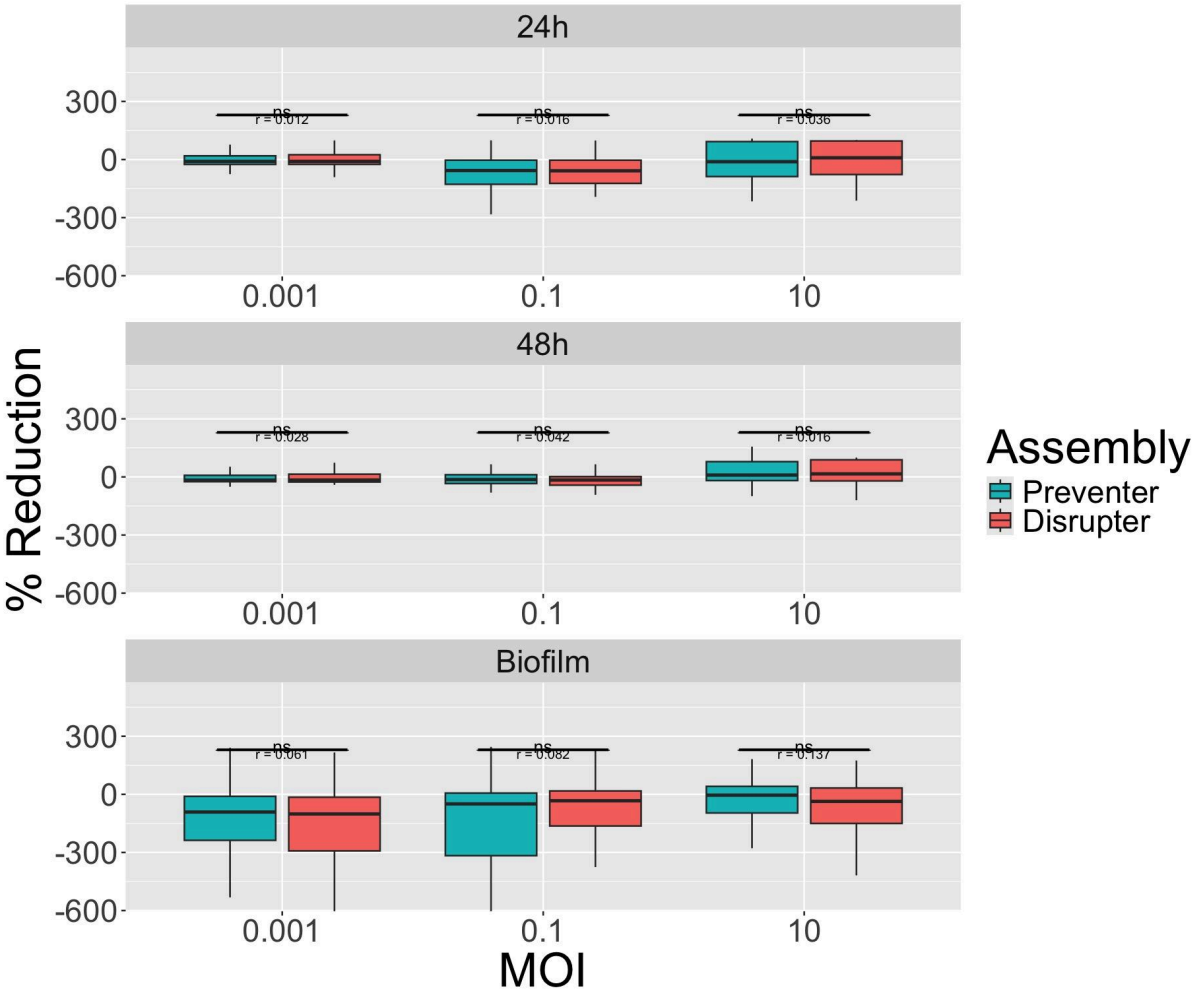

Figure 4.9: Box plots comparing percentage reduction in *P. aeruginosa* growth between cocktails containing the Disrupter phage (red) and cocktails containing the Preventer phage (teal) at three MOIs (0.001, 0.1, and 10) across three timepoints (24 h, 48 h, and biofilm staining). Each facet represents a different timepoint. Percentage reduction was calculated relative to the no-phage positive control. Box boundaries represent the interquartile range (IQR), the central line represents the median, and whiskers extend to 1.5× IQR. Outliers are omitted for clarity. Statistical comparisons were performed using Wilcoxon rank-sum tests with Benjamini-Hochberg correction for multiple testing; effect sizes (r) calculated by rank-biserial correlation are shown above each comparison. No statistically significant differences were observed between Disrupter and Preventer cocktail types under any condition or MOI tested, indicating that inclusion of the Disrupter or Preventer phage did not meaningfully influence cocktail efficacy. Note: the nominal MOI of 0.001 corresponds to an effective phage-to-bacteria ratio of ~10^{-6}.

At 48 h, comparisons remained non-significant across all MOIs. MOI 0.001 (effective ~10^{-6}) had W = 1342, p = 0.784; MOI 0.1 had W = 1364, p = 0.673; and MOI 10 had W = 1277, p = 0.878. These findings suggest that extended exposure did not alter the relative performance of Disrupter versus Preventer cocktails.

Under biofilm formation conditions, no significant differences were observed between cocktail types. MOI 0.001 (effective ~10^{-6}) had W = 1392, p = 0.543; MOI 0.1 had W = 1177, p = 0.41;

and MOI 10 had W = 1507, p = 0.168. These data indicate that both cocktail types performed comparably in limiting biofilm formation.

Overall, across all MOIs, timepoints, and biofilm conditions, Disrupter and Preventer cocktails exhibited highly similar efficacy, with no comparisons reaching statistical significance.

Table 4.6: Wilcoxon rank-sum test results comparing Disrupter and Preventer cocktails at three MOIs (0.001, 0.1, and 10) across 24 h, 48 h, and biofilm assays. Shown are the Wilcoxon test statistic (W), raw p-values, and significance codes. All comparisons were non-significant. Note: the nominal MOI of 0.001 corresponds to an effective phage-to-bacteria ratio of ~10^{-6}.

Time	MOI	Statistic (W)	P value	Significance
24h	0.001	1282	0.904	ns
24h	0.1	1324	0.878	ns
24h	10	1246	0.72	ns
48h	0.001	1342	0.784	ns
48h	0.1	1364	0.673	ns
48h	10	1277	0.878	ns
Biofilm	0.001	1392	0.543	ns
Biofilm	0.1	1177	0.41	ns
Biofilm	10	1507	0.168	ns

4.3.8 Comparison of Disrupter and Preventer Assemblies by Strain

To examine whether the type of cocktail, Preventer or Disrupter, affected bacterial reduction at the level of individual strains, comparisons were conducted across 17 *P. aeruginosa* strains at three MOIs (0.001, 0.1, and 10). Wilcoxon rank-sum tests were used for each strain-MOI combination (Figure 4.10).

At MOI 0.001, the nominal effective MOI was ~10^{-6}**,** no statistically significant differences were observed for any strain (raw p-values ranged from 0.185 to 1) (Table 4.7). For example, strain 76 had p = 0.536, strain 203.1 had p = 0.185, and strain 430 had p = 1. These results indicate that Preventer and Disrupter cocktails performed similarly across all strains at the lowest MOI.

At MOI 0.1, all comparisons again showed no significant differences (p-values ranged from 0.251 to 1). Strain 342 had p = 0.251, strain 240 had p = 0.48, and strain 115 had p = 1, demonstrating that the moderate MOI did not alter the overall equivalence of performance between the two cocktail types at the individual strain level.

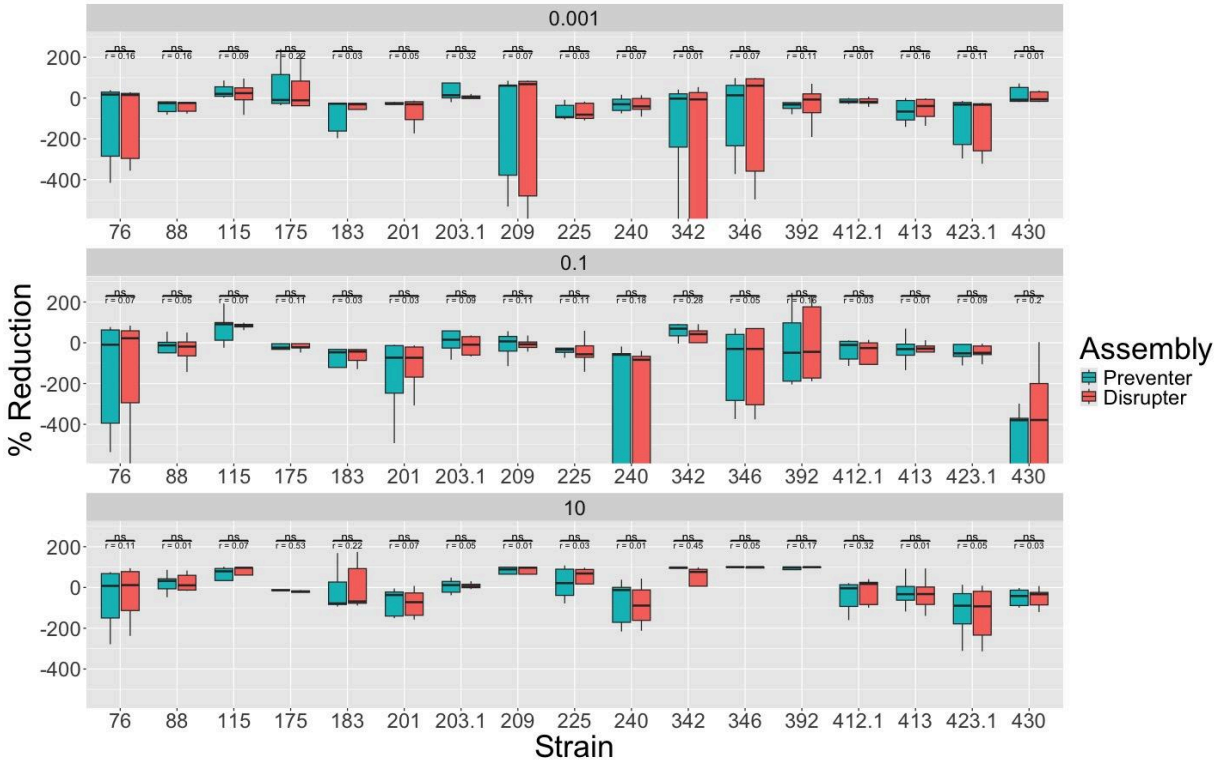

Figure 4.10: Box plots comparing percentage reduction in *P. aeruginosa* growth between cocktails containing the Preventer (teal) and Disrupter (red) phages across 17 clinical strains at three MOIs (0.001, 0.1, and 10). Each facet represents a different MOI. Percentage reduction was calculated relative to the no-phage positive control. Box boundaries represent the interquartile range (IQR), the central line represents the median, and whiskers extend to 1.5× IQR. Outliers beyond this range are not shown. Effect sizes (r) calculated by rank-biserial correlation are annotated above each comparison, with brackets and significance labels (ns = not significant) indicating the result of Wilcoxon rank-sum tests comparing Preventer and Disrupter cocktails for each strain. Statistical significance was adjusted for multiple comparisons using the Benjamini-Hochberg method. No statistically significant differences were observed between Preventer and Disrupter cocktail types for any strain at any MOI, indicating that inclusion of either phage type did not meaningfully influence strain-level efficacy. . Note: the nominal MOI of 0.001 corresponds to an effective phage-to-bacteria ratio of ~10^{-6}.

At MOI 10, most strain comparisons remained non-significant (p-values ranged from 0.0273 to 1). A few strains showed lower raw p-values, for example, strain 175 had p = 0.0273, and strain 342 had p = 0.0637, but none reached significance. The majority of strains, such as 76 (p = 0.659) and 88 (p = 1), continued to show similar reductions for Preventer and Disrupter cocktails.

Overall, across all MOIs and strains, these results indicate that Preventer and Disrupter cocktails perform comparably in reducing bacterial growth. The low effective MOI at nominal 0.001 is considered in interpretation. No strain exhibited a statistically significant difference, suggesting that the functional focus of the cocktail, biofilm prevention versus disruption, does

not produce meaningful differences in bacterial reduction under the experimental conditions tested.

Table 4.7: Wilcoxon rank-sum test results comparing percent reduction between Preventer and Disrupter phage cocktails for each strain and MOI. Shown are strain identifier, MOI, sample size per group (n), Wilcoxon test statistic, raw p-value, and significance (ns = not significant). All comparisons were non-significant. Note: the nominal MOI of 0.001 corresponds to an effective phage-to-bacteria ratio of ~10^{-6}.

Strain	MOI	Statistic (W)	P value	Significance
76	0.001	48	0.536	ns
88	0.001	48	0.536	ns
115	0.001	45	0.724	ns
175	0.001	51	0.377	ns
183	0.001	39	0.93	ns
201	0.001	43	0.86	ns
203.1	0.001	56	0.185	ns
209	0.001	37	0.791	ns
225	0.001	42	0.93	ns
240	0.001	44	0.791	ns
342	0.001	41	1	ns
346	0.001	37	0.791	ns
392	0.001	35	0.659	ns
412.1	0.001	40	1	ns
413	0.001	33	0.536	ns
423.1	0.001	46	0.659	ns
430	0.001	40	1	ns
76	0.1	37	0.791	ns
88	0.1	43	0.86	ns
115	0.1	41	1	ns
175	0.1	35	0.659	ns
183	0.1	39	0.93	ns
201	0.1	39	0.93	ns
203.1	0.1	45	0.724	ns
209	0.1	46	0.659	ns
225	0.1	46	0.659	ns
240	0.1	49	0.48	ns
342	0.1	54	0.251	ns
346	0.1	38	0.86	ns
392	0.1	33	0.536	ns
412.1	0.1	42	0.93	ns
413	0.1	41	1	ns

Table 4.7 Continued				
Strain	**MOI**	**Statistic (W)**	**P value**	**Significance**
423.1	0.1	36	0.724	ns
430	0.1	31	0.427	ns
76	10	35	0.659	ns
88	10	40	1	ns
115	10	37	0.791	ns
175	10	66	0.0273	ns
183	10	30	0.377	ns
201	10	44	0.791	ns
203.1	10	43	0.86	ns
209	10	41	1	ns
225	10	39	0.93	ns
240	10	41	1	ns
342	10	62	0.0637	ns
346	10	43	0.86	ns
392	10	32.5	0.508	ns
412.1	10	25	0.185	ns
413	10	40	1	ns
423.1	10	43	0.86	ns
430	10	42	0.93	ns

4.3.9 Subset Strain-Cocktail Growth Dynamics at MOI 0.1

To further explore the effects of individual phage cocktails on bacterial growth dynamics, a subset of representative *P. aeruginosa* strains was assessed over 24 hours at MOI 0.1 (Figure 4.11). Growth was quantified using the area under the growth curve (AUC) as a summary measure of proliferation, comparing each cocktail-treated strain to its strain-matched control (Table 4.8).

For strain 76, cocktail c resulted in a reduction in AUC from 1131 ± 40.5 (control) to 623 ± 51.8 (ΔAUC = –508, –44.9%), which was statistically significant (t = –13.4, p = 0.000255, significant). In contrast, cocktail d increased growth to 1408 ± 260 (ΔAUC = 277, +24.5%), but this increase was not statistically significant (t = 1.83, p = 0.203, ns).

Strain 88 showed variable responses across cocktails. Cocktail f increased AUC from 504 ± 37.4 to 612 ± 270 (ΔAUC = 108, +21.4%, t = 0.689, p = 0.560, ns), cocktail j increased it to 914 ± 7.62 (ΔAUC = 410, +81.3%, t = 18.6, p = 0.00199, significant), and cocktail k increased growth to 806 ± 254 (ΔAUC = 302, +59.9%, t = 2.04, p = 0.173, ns). Conversely, cocktail l reduced growth to 392 ± 391 (ΔAUC = –112, –22.2%, t = –0.495, p = 0.669, ns).

For strain 115, cocktail f induced a substantial decrease in AUC to 184 ± 53.4 (ΔAUC = –765, –80.6%, t = –24.8, p = 0.00155, significant), while cocktail j caused a modest increase to 1173 ± 617 (ΔAUC = 224, +23.6%, t = 0.627, p = 0.594, ns).

Strain 175 demonstrated increases with cocktails e and h. Cocktail e increased AUC from 1157 ± 31.2 to 1519 ± 21.6 (ΔAUC = 362, +31.3%, t = 16.6, p = 0.000170, significant), and cocktail h increased it to 1615 ± 9.92 (ΔAUC = 458, +39.6%, t = 24.2, p = 0.000628, significant).

Strain 203.1 responded to cocktail b with an increase from 174 ± 4.20 to 591 ± 85.5 (ΔAUC = 417, +239.7%, t = 8.44, p = 0.0136, significant).

Strain 209 showed marked decreases in growth under cocktails d and i, with ΔAUC values of –298 (–57.2%, t = –7.79, p = 0.0145, significant) and –343 (–65.8%, t = –9.59, p = 0.00931, significant), respectively, relative to the control (521 ± 9.02).

Strain 225 displayed smaller, inconsistent effects. Cocktail c decreased AUC slightly to 175 ± 27 (ΔAUC = –30, –14.6%, t = –1.62, p = 0.191, ns), cocktail h increased growth marginally to 214 ± 130 (ΔAUC = 9, +4.4%, t = 0.116, p = 0.918, ns), and cocktail g increased AUC to 321 ± 1.94 (ΔAUC = 116, +56.6%, t = 11.0, p = 0.00757, significant).

Strain 342 showed minimal change with cocktail f (713 ± 159 versus 755 ± 65.7, ΔAUC = –42, –5.6%, t = –0.424, p = 0.703, ns).

For strain 346, cocktail j increased AUC to 281 ± 52.3 (ΔAUC = 54, +23.8%, t = 1.79, p = 0.213, ns), whereas cocktail a reduced it to 115 ± 1.65 (ΔAUC = –112, –49.3%, t = –41.1, p = 0.000115, significant).

Finally, strain 412 exhibited increased growth under cocktails j, k, and e. AUC values increased from 430 ± 51.3 (control) to 819 ± 18.1 (ΔAUC = 389, +90.5%, t = 12.4, p = 0.00266, significant), 868 ± 38.1 (ΔAUC = 438, +101.9%, t = 11.9, p = 0.000445, significant), and 764 ± 24.3 (ΔAUC = 334, +77.7%, t = 10.2, p = 0.00247, significant), respectively.

Collectively, these data indicate that while individual cocktails can substantially influence bacterial growth trajectories, both increasing and decreasing AUC depending on strain, only a subset of these effects were statistically significant. This highlights both strain-specific variability and the potency of certain phage cocktails in altering growth dynamics at MOI 0.1.

Table 4.8: Comparison of treatment effects on bacterial growth (AUC) relative to control for each strain. Values represent the mean area under the growth curve (AUC) ± standard error of the mean (SEM) from triplicate assays. The difference in AUC (ΔAUC) and percentage change relative to control are shown. Treatments were compared to their strain-matched controls using t-tests, with raw p-values reported and significance indicated as “significant” or “ns” (not significant). This table highlights strain-specific effects of phage cocktails on bacterial growth at MOI 0.1.

Strain	Treatment	mean_AUC	sd_AUC	statistic	p	Significance
76	c	623	51.8	-13.4	<0.001	significant
76	d	1408	260	1.83	0.203	ns
88	f	612	270	0.689	0.56	ns
88	j	914	7.62	18.6	0.002	significant
88	k	806	254	2.04	0.173	ns
88	l	392	391	-0.495	0.669	ns
115	f	184	53.4	-24.8	0.0012	significant
115	j	1173	617	0.627	0.594	ns
175	e	1519	21.6	16.6	<0.001	significant
175	h	1615	9.92	24.2	0.001	significant
203.1	b	591	85.5	8.44	0.014	significant
209	d	223	65.6	-7.79	0.015	significant
209	i	178	61.4	-9.59	0.009	significant
225	c	175	27	-1.62	0.191	ns
225	g	321	1.94	11	0.00	significant
225	h	214	130	0.116	0.918	ns
342	f	713	159	-0.424	0.703	ns
346	a	115	1.65	-41.1	<0.001	significant
346	j	281	52.3	1.79	0.213	ns
412.1	e	764	24.3	10.2	0.002	significant
412.1	j	819	18.1	12.4	0.003	significant
412.1	k	868	38.1	11.9	<0.001	significant

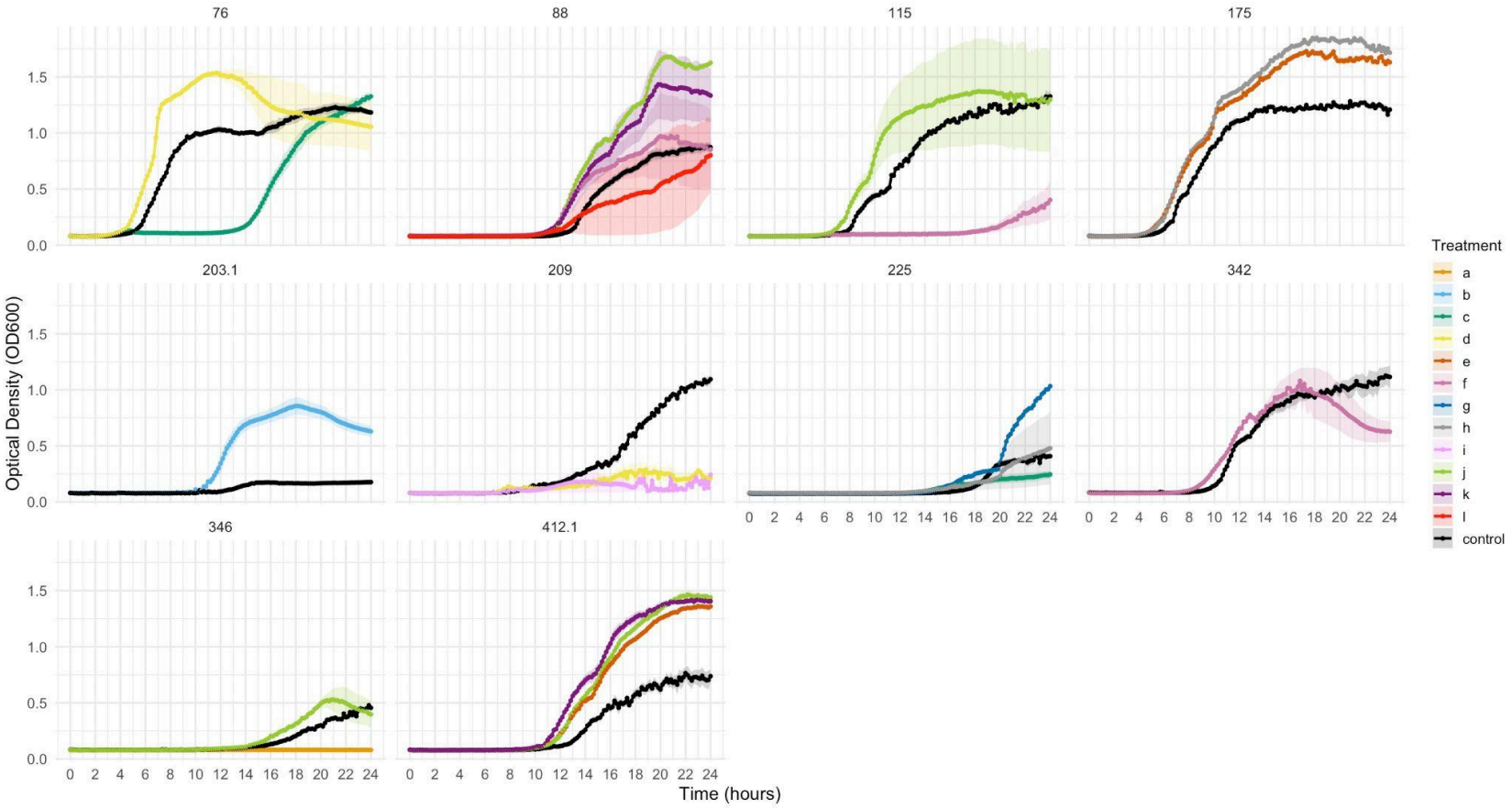

Figure 4.11: Growth curves showing optical density (OD_{600}) over 24 hours for a subset of 10 clinical *P. aeruginosa* strains treated with selected phage cocktails at MOI 0.1. Each panel represents a single strain, labelled by strain number. OD_{600} was measured every 10 minutes over 24 hours. Lines represent mean OD_{600} of triplicate measurements; shaded regions indicate ± standard error of the mean (SEM). The black line in each panel represents the no-phage positive control. Cocktail treatments are differentiated by colour as indicated in the legend (cocktails a–l). Growth curve area under the curve (AUC) was calculated as a summary measure of bacterial proliferation for each treatment and compared to the strain-matched control; full AUC statistics are presented in Table 4.8. Both increases and decreases in OD_{600} relative to the control were observed, reflecting strain-specific variability in response to individual cocktails. This subset was selected to represent the range of growth responses observed across all strains at MOI 0.1.

4.4 Discussion

4.4.1 General Overview

The primary aim of this study was to use clearance and biofilm profiles to design a broad-spectrum phage cocktail against clinical *P. aeruginosa* isolates from pwCF and to evaluate its efficacy across different MOI. It should be noted that the nominal MOI of 0.001 was miscalculated and corresponds to an effective phage-to-bacteria ratio of ~10^{-6}. This error explains the minimal antimicrobial effect observed at low MOI and informs interpretation of cocktail performance across the tested concentrations. The rationale for this approach was to establish a ‘first-line’ phage cocktail capable of providing immediate, wide-ranging coverage, analogous to broad-spectrum antibiotics, while personalised phage formulations are prepared. Such a framework aligns with emerging clinical models advocating rapid empirical treatment initiation followed by personalised refinement (Kortright *et al.*, 2019; Hernández & Koskella, 2019).

The results highlight both the promise and limitations of this approach. Computationally designed cocktails achieved broad theoretical host-range coverage, but their empirical performance depended strongly on MOI, noting that the nominal MOI of 0.001 corresponds to an effective phage-to-bacteria ratio of ~10^{-6}, strain specific variation, and biofilm phenotype. Although receptor-diverse designs were expected to outperform random mixtures, this was not consistently observed, mirroring findings from other studies where theoretical optimisation did not guarantee superior biological outcomes (Oechslin *et al.*, 2016; Abedon *et al.*, 2021). Together, these results emphasise that while rational design offers a valuable foundation, empirical validation remains indispensable for clinically reliable cocktail development.

4.4.2 Cocktail Design

The PhageCocktail R package (Díaz-Galián *et al.*, 2022) identified minimal two-phage combinations, typically pairing one T4P-binding and one LPS-binding phage, capable of lysing all 93 isolates. This design principle, combining receptor diversity to maximise host-range and restrict resistance evolution, is well supported by previous work (Chan *et al.*, 2013; Torres-Barceló *et al*., 2014; Wright *et al.*, 2021).

However, these theoretically broad combinations were not strong biofilm disruptors. Empirical testing required additional phages with biofilm active characteristics, underscoring the well documented trade-off between host range and biofilm efficacy (Harper *et al*., 2014; Azeredo

& Sutherland, 2008). Recent studies similarly report that planktonically potent phages often lack the enzymatic depolymerases necessary for effective biofilm clearance (Meneses *et al.*, 2023; Hernández & Koskella, 2024). This highlights that computational selection based solely on host range or receptor diversity must be complemented with biofilm specific validation if first-line phage cocktails are to be clinically meaningful.

4.4.3 Investigation of Low Efficacy at MOI 0.001

At nominal MOI 0.001 (~10^{-6} effective), cocktails showed minimal clearance and, in some cases, paradoxical increases in bacterial growth and biofilm biomass. This is consistent with theoretical predictions that low phage-to-bacterium ratios cannot sustain effective infection cycles for population suppression (Payne *et al.*, 2000; Abedon, 2012). The poor performance observed here should be interpreted in light of the calculation error; the MOI used was substantially lower than intended, explaining the weak effects.

The apparent paradox, enhanced growth at sublethal phage pressure, likely reflects stress-induced biofilm responses, a known *P. aeruginosa* defence mechanism (Høiby *et al.*, 2010; Darch *et al.*, 2012). Sublethal phage exposure has also been shown to trigger stress responses in *P. aeruginosa* that alter cell morphology and aggregation behaviour, potentially inflating OD readings beyond those of uninfected controls (Harms *et al.*, 2016). Although antagonistic phage-phage interactions have been proposed to explain reduced cocktail efficacy at low titres, such interactions are more likely to be functionally neutral at very low multiplicities since phages encounter fewer shared hosts. Thus, the poor performance observed here is better explained by concentration-dependent failure to maintain lytic propagation rather than genuine antagonism.

4.4.4 Efficacy at MOI 0.1

At MOI 0.1, cocktails demonstrated improved inhibition of bacterial growth, though responses remained heterogeneous across strains. The AUC analysis revealed that 11 of 22 strain–cocktail combinations produced statistically significant differences relative to control ($p < 0.05$), while others showed large but variable directional effects that did not reach significance.

For example, strong growth suppression was observed in strain 76 with cocktail c, strain 115 with f, and strain 346 with a, all showing significantly lower AUC values compared to control. Conversely, cocktails j, k, and e enhanced growth in several strains (e.g., 88, 175, and 412), suggesting either stress-induced adaptation or transient tolerance, phenomena previously

linked to selective enrichment of phage-resistant subpopulations (Wright *et al.*, 2009; Dolan *et al.*, 2018).

Despite several significant outcomes, overall trends indicated that phage efficacy remained strain-specific and inconsistent, with no universal ‘high performer.’ Biofilm reduction continued to be limited, underscoring that while moderate MOI improved planktonic suppression, deeper matrix penetration likely remained insufficient. These findings mirror recent work showing that depolymerase-mediated biofilm disruption often requires higher titres or adjunctive therapies (Pires *et al.*, 2021; Islam *et al.*, 2024).

4.4.5 Efficacy at MOI 10

At MOI 10, cocktails produced marked reductions in planktonic growth across nearly all strains, confirming that high phage concentrations enhance adsorption and infection rates (Payne *et al.*, 2000; Abedon, 2012). Nevertheless, biofilm clearance again remained limited, consistent with the recognised resilience of CF-associated *P. aeruginosa* biofilms (Gliźniewicz *et al.*, 2024; Hernández & Koskella, 2024).

Although many included phages are likely to encode depolymerases (Chen *et al.*, 2022; Gliźniewicz *et al.*, 2024), their activities may have been attenuated under the test conditions or insufficient to penetrate mature biofilms. This suggests that for practical clinical deployment, first-line cocktails should prioritise phages with confirmed, high efficiency enzymatic activity and possibly incorporate biofilm disrupting adjuncts such as DNase or alginate lyase (Wang *et al.*, 2024).

4.4.6 Comparison of Designed and Random Assemblies

Designed cocktails did not consistently outperform randomly assembled ones, with overall effect sizes small and variable. This lack of distinction indicates that strain-specific factors and dosing levels had greater influence on efficacy than design strategy alone (Kim *et al.*, 2024; Molina *et al.*, 2021).

Nevertheless, several individual cocktails, such as 76-c, 115-f, 175-e/h, and 346-a, produced significant growth inhibition despite diverse receptor compositions. Interestingly, some randomly assembled cocktail combinations lacking biofilm-disrupting phages still displayed measurable reductions in AUC, suggesting that even phages without confirmed biofilm-disrupting activity can suppress growth effectively if present at sufficient effective titre, or if they target critical bacterial receptors. Conversely, other designed cocktails containing

biofilm active phages failed to produce consistent effects, highlighting the context-dependence of enzymatic biofilm activity.

These observations suggest that while rational design can ensure receptor diversity, it cannot reliably predict performance across heterogeneous clinical strains. Iterative empirical validation remains essential to identify functionally dominant phages within any cocktail framework.

4.4.7 Comparison of Disrupter and Preventer Assemblies

No consistent differences were observed between Disrupter and Preventer cocktails, suggesting that classifying phages solely by biofilm phenotype provides limited predictive power. While previous studies have shown synergistic benefits when biofilm-active and broad-host-range phages are combined (Schmerer *et al.*, 2014; Vashisth *et al.*, 2023), the present findings indicate that efficacy depends on the specific strain–phage pairing rather than generalised functional category.

The absence of clear distinctions may also reflect the variability of clinical CF isolates, the potential absence of potent depolymerases among included phages, and biological variability across replicates. Hence, empirical profiling across strain panels remains a more reliable approach for first-line cocktail optimisation.

4.4.8 Subset Strain–Cocktail Dynamics at MOI 0.1

Subset analysis revealed high variability in strain-specific responses, including both strong inhibition and paradoxical growth stimulation. Approximately half of tested combinations yielded statistically significant changes in AUC, some inhibitory, some stimulatory, illustrating the complexity of CF-derived *P. aeruginosa* defences such as receptor modification, CRISPR-Cas immunity, and phenotypic tolerance (Alseth *et al.*, 2019; Hernández & Koskella, 2024).

This heterogeneity underscores the necessity of empirical breadth in first-line cocktail development. Although theoretically designed cocktails provided comprehensive host range coverage, real world performance was inconsistent. Robust, broad spectrum efficacy will likely require cocktails combining diverse receptor targets with confirmed depolymerase and anti-biofilm activity.

4.4.9 Implications and Future Work

This study demonstrates both the potential and limitations of clearance- and biofilm-informed phage cocktails as empirical tools for CF-associated *P. aeruginosa*. While theoretically designed cocktails achieved wide host coverage, empirical efficacy was shaped primarily by MOI, recognising that the nominal MOI of 0.001 corresponds to an effective phage-to-bacteria ratio of ~10^{-6}, strain variability, and biofilm resilience. Importantly, some cocktails achieved statistically significant suppression at MOI 0.1, but effects were not universal across strains.

Future work should focus on refining this first line cocktail model by systematically optimising phage ratios, quantifying depolymerase activity, and assessing potential antagonistic or synergistic phage interactions. Parallel *in vivo* studies will be critical to evaluate whether the *in vitro* variability observed here persists under physiological conditions.

Overall, this work supports a dual therapeutic framework: broad spectrum cocktails as rapid empirical interventions, followed by personalised refinement based on patient specific isolate profiling. Such an approach balances speed with precision, offering the most practical pathway toward clinically effective phage therapy for CF infections.

4.5 Conclusion

This chapter demonstrated that systematic, data-driven approaches to bacteriophage cocktail design, integrating clearance and biofilm phenotypes, can generate combinations with broad theoretical host-range coverage against genetically diverse *P. aeruginosa* isolates from pwCF. Minimal two-phage cocktails incorporating T4P and LPS binding phages achieved universal *in silico* coverage, demonstrating the theoretical potential of receptor-diverse design principles, though *in vitro* validation revealed that broad host range alone was insufficient to guarantee robust bacterial suppression across all strains and infection contexts.

Cocktail efficacy was highly dependent on MOI, with suboptimal dosing yielding negligible or paradoxical increases in bacterial growth, while increasing MOI to 0.1 and 10 progressively improved suppression in a strain-dependent manner, confirming that effective phage therapy requires careful dose optimisation alongside rational cocktail design.

At higher MOI (10), cocktails achieved near-complete planktonic suppression, but biofilm clearance remained limited, underscoring the persistent resilience of CF-associated *P. aeruginosa* biofilms. This finding reinforces that biofilm physiology, and not merely host-range

or receptor diversity, represents the key barrier to achieving consistent *in vitro* clearance. Incorporation of phages with verified depolymerase activity or combination with biofilm-targeting adjuncts is likely necessary to enhance efficacy.

Importantly, designed cocktails did not consistently outperform randomly assembled cocktails, nor did the Disrupter versus Preventer classification predict success. Instead, performance appeared dominated by MOI, strain background, and inter-phage dynamics. Notably, several cocktails (e.g., 76-c, 115-f, 346-a, and 175-e/h) achieved statistically significant reductions, while others containing biofilm-active phages did not, emphasising that empirical validation remains indispensable even within rational design frameworks.

Overall, these findings highlight that broad spectrum phage cocktails hold value as rapid ‘first-line’ therapeutic tools, capable of delivering immediate coverage across diverse CF isolates. However, their clinical translation will require iterative refinement, incorporating quantitative optimisation of phage ratios, assessment of enzymatic activity, and systematic evaluation of phage-phage and phage-host interactions.

In practice, a dual therapeutic strategy, employing broad-spectrum empirical cocktails for rapid initial treatment, followed by personalised refinement based on patient-specific isolate profiling, offers the most clinically viable pathway for phage therapy in CF. This study provides the foundation for such an approach, demonstrating that while computational design can guide cocktail formulation, empirical optimisation remains essential for achieving consistent, reliable therapeutic efficacy.

5. Evolutionary investigation of PAS in clinical *P. aeruginosa* samples with known AMR.

5.1 Abstract

This chapter investigates the evolutionary success of Cocktail C (selected based on its broad host range, receptor diversity, and performance in Chapter 4 validation assays) and the dynamics of phage resistance and phage–antibiotic interactions in *P. aeruginosa* CF clinical isolates, with a focus on single-phage versus multi-phage cocktail strategies. Three previously identified lytic phages (14/1, DMS3virAcrFl, and PA5P2) were combined into Cocktail C from infectivity assays where they were selected for receptor diversity and complementary host range. Evolutionary assays revealed that Cocktail C produced stronger and more sustained bacterial suppression compared to single-phage treatments, although inter-strain variability was evident. Clonal confirmation of resistance (CoR) assays demonstrated that while single-phage exposure typically resulted in narrow, phage-specific resistance, cocktail exposure occasionally produced cross-resistance, consistent with selection for mutations affecting multiple surface structures or regulatory pathways. Whole-genome sequencing of representative resistant clones revealed a range of mutations in LPS biosynthesis genes, T4P components, membrane-associated proteins, and cytoplasmic defense systems, highlighting both receptor-specific and pleiotropic resistance mechanisms, where “pleiotropic” refers to mutations that confer resistance through multiple pathways, including intracellular defense systems. These genotypic changes were often associated with phenotypic trade-offs, including altered antibiotic susceptibility, reduced motility, and modified virulence, consistent with evolutionary theory and recent empirical studies.

PAS assays combining polymyxin B (selected for its mechanistic relationship to colistin, a frontline antibiotic in the Danish CF treatment protocol, and its performance in MIC assays) with individual phages or Cocktail C demonstrated additive and synergistic effects under specific antibiotic and MOI ranges. Sub-inhibitory concentrations of polymyxin B enhanced bacterial susceptibility to phage lysis, likely via altered membrane permeability and biofilm disruption, while phage pressure simultaneously potentiated antibiotic efficacy. These findings underscore the potential for strategically combining phages and antibiotics to improve suppression, mitigate resistance evolution, and extend therapeutic durability.

Together, the results of this chapter illuminate the evolutionary trajectories of *P. aeruginosa* under phage and phage–antibiotic pressure, highlighting the importance of multi-layered

resistance mapping, genotype/phenotype correlation, and careful cocktail design. Mechanistic insights into LPS remodeling, pilus modification, and defense system activity provide a foundation for future translational work, phage–antibiotic co-treatment regimens, and the rational design of multi-phage interventions in chronic CF infections. These findings advance the understanding of bacterial adaptation under combined biotic and chemical selective pressures and contribute directly to the optimisation of phage therapy in clinical contexts.

5.2 Introduction

5.2.1 Chronic *P. aeruginosa* Infection in CF

Chronic *P. aeruginosa* infection remains a significant factor in morbidity and mortality in pwCF, influencing lung function decline and long-term clinical outcomes. The CF airway is characterised by viscous secretions, impaired mucociliary clearance, repeated inflammatory cycles, and structural remodeling, which collectively create a heterogeneous ecological environment for bacterial colonisation (Høiby *et al*., 2024; Bjarnsholt *et al*., 2013; Mulcahy *et al.*, 2010). Within this environment, *P. aeruginosa* establishes biofilm communities, highly structured aggregates of cells embedded in an extracellular polymeric matrix, that confer considerable tolerance to both host immunity and conventional chemotherapeutic antimicrobial therapy. Biofilms are not uniform; gradients of oxygen, nutrients, and metabolites produce spatially and physiologically distinct subpopulations, including slow-growing and metabolically dormant ‘persister’ bacteria that evade antibiotics targeting active growth. This phenotypic heterogeneity, coupled with repeated antibiotic exposure, accelerates the selection of resistant subpopulations and progressively reduces the efficacy of available treatments, complicating the treatment of chronic CF infections (Pamp *et al.*, 2008; Ciofu *et al.*, 2022; Nguyen *et al*., 2011).

5.2.2 Limitations of Conventional Antibiotics and the Promise of Phage Therapy

The narrowing availability of effective chemotherapeutic antimicrobials, particularly against Gram-negative pathogens, has necessitated exploration of additional therapies capable of either enhancing antibiotic efficacy or acting independently. Among these, phage therapy has experienced renewed interest, in part due to advances in molecular characterisation, genome sequencing, and bioengineering approaches. Phage biology and the clinical evidence base for phage therapy in CF are reviewed in Chapter 1 (sections 1.4–1.4.3). Compassionate use cases and controlled studies demonstrate that phage therapy can reduce bacterial burden

and improve clinical outcomes in pwCF with otherwise untreatable infections (Aslam *et al.*, 2020; Schooley *et al.,* 2017; Dedrick *et al.*, 2019; Jault *et al.*, 2019).

5.2.3 Evolution of Phage Resistance in *P. aeruginosa*

Despite these advantages, rapid evolution of phage resistance represents a major barrier to durable therapy. Phage infection relies on specific bacterial surface receptors, such as LPS, outer-membrane proteins, or T4P, for adsorption and genome injection. Even minor genetic or regulatory modifications can block phage binding, rendering cells resistant (Labrie *et al.*, 2010; Topka-Bielecka *et al.*, 2021; Le *et al*., 2014). *P. aeruginosa* is particularly adept at evolving such resistance due to its genomic plasticity, redundant regulatory networks, and the presence of multiple anti-phage defense systems, including restriction-modification enzymes, abortive infection pathways, CRISPR-Cas systems, and defense islands (Bae *et al*., 2025; Johnson *et al.*, 2023; Feng *et al*., 2024; Doron *et al*., 2018). Surveys of clinical isolates indicate that strains with more defense systems tend to display lower susceptibility to phages, highlighting the critical role of innate host diversity in therapeutic outcomes (Feng *et al.*, 2024; García-Cruz *et al*., 2024; Doron *et al.*, 2018).

Resistance often comes with pleiotropic trade-offs. Modifications of cell-surface structures can reduce motility, biofilm formation, and environmental/competitive fitness via reduced growth, and in some cases may increase susceptibility to specific antibiotics, especially when receptor components overlap with antibiotic entry pathways or when outer-membrane integrity is compromised (Torres-Barceló & Hochberg, 2016; Oechslin *et al*., 2017; Yilmaz *et al.*, 2013). These evolutionary trade-offs introduce an opportunity for therapeutic exploitation, allowing treatment strategies to combine phages with antibiotics to exploit collateral sensitivity, but also necessitate careful consideration of population level dynamics.

5.2.4 Phage Cocktails and Multi-Receptor Targeting

To mitigate the rapid emergence of resistance, combinations of multiple phages targeting distinct bacterial receptors (phage cocktails) can be employed. By simultaneously applying selective pressure on multiple bacterial targets, cocktails raise the mutational barrier to resistance, expand host-range efficacy, and may prolong suppression of bacterial populations (Oechslin, 2018; Wright *et al.*, 2019). Experimental studies demonstrate that phage cocktails reduce the probability of resistance in laboratory populations of *P. aeruginosa* and other clinically relevant pathogens (Burrowes *et al*., 2011; Debarbieux *et al*., 2010; Roach *et al.*, 2017), consistent with the 48-hour growth suppression observed with cocktails at MOI 10 in Chapter 4 (Figure 4.6). Nonetheless, cocktails are not without issue: resistance can still evolve via global envelope modifications or regulatory rewiring, and

receptor overlap among phages can permit cross-resistance (Wright *et al*., 2018; Van Der Steen *et al.*, 2024). Additionally, intra-strain and inter-strain variability in growth rate, stress response, and defense system composition further complicate the predictability of cocktail performance (Sanchez and Martinez, 2019).

In this study, three lytic *P. aeruginosa* phages (14/1, DMS3virAcrFI, and PA5P2) were selected for a multi-phage cocktail (Cocktail C) based on host range diversity and non-overlapping receptor targeting. Receptor specificity was provided alongside the phage samples: 14/1 targets LPS, while both DMS3virAcrFI and PA5P2 target T4P through distinct mechanisms, providing complementary coverage. Previous chapters demonstrated that each phage is capable of suppressing bacterial growth at multiple MOIs, though resistance evolves under prolonged single-phage exposure. Cocktail C provides a basis to test whether multi-receptor targeting can delay or prevent resistance emergence across genetically diverse CF clinical isolates selected for differential phage susceptibility profiles.

5.2.5 Experimental Design and Methods

The experimental design integrates multiple layers of investigation. Evolutionary assays assess population-level growth and suppression dynamics, monitoring resistance across multiple transfer series. Clone-level confirmation of resistance (CoR) assays assess heterogeneity within evolved populations, distinguishing narrow, phage specific resistance from broader cocktail resistant phenotypes. This approach enables the investigation of intra-population diversity, repeatability of evolutionary trajectories, and the emergence of cross resistance. WGS was applied to a subset of clones to map likely mutational pathways, focusing on gene families implicated in phage resistance such as LPS biosynthesis, T4P formation, outer-membrane proteins, regulatory networks, and anti-phage defense systems (Hampton *et al.*, 2020; Li *et al*., 2018; Labrie *et al.*, 2010).

Complementing evolution and resistance mapping, PAS is assessed using polymyxin B, a cationic peptide antibiotic that disrupts Gram-negative outer membranes. Polymyxin B, the active compound of the colistin prodrug (Trimble *et al.,* 2016), was chosen based on preliminary antibiotic susceptibility assays comparing multiple candidates, demonstrating it as the most suitable for combinatorial study with phages in this panel of CF isolates. Specifically, MIC testing showed consistent intermediate susceptibility across the isolate panel, providing sufficient residual bacterial growth to detect enhancement or suppression in combination assays without complete inhibition by the antibiotic alone. PAS arises when the combined effect exceeds the sum of individual effects, driven by mechanisms such as antibiotic-induced physiological changes enhancing phage adsorption, phage-mediated

disruption of biofilm integrity, and pleiotropic trade-offs that alter drug susceptibility (Uchiyama *et al*., 2018; Kovacs *et al*., 2024; Torres-Barceló *et al.,* 2016). Checkerboard assays quantify growth inhibition and calculate FICIs to classify interactions as synergistic, additive, or antagonistic. Prior studies demonstrate that phage–antibiotic combinations can reduce MICs, improve biofilm clearance, and delay resistance emergence in *P. aeruginosa* and other pathogens (Chaudhry *et al*., 2017; Holger *et al*., 2023; De Soir *et al*., 2024; Kunz Coyne *et al*., 2024).

5.2.6 Evolutionary Context of CF Biofilms

From an evolutionary perspective, CF biofilms represent complex and spatially structured populations, where selective pressures differ across micro-niches, population bottlenecks can amplify random variation, and resulting fitness landscapes are highly multidimensional. These features influence the repeatability and predictability of resistance evolution, making empirical testing across multiple strains and replicates essential. Understanding how multi-phage selection, population heterogeneity, and co-treatment with antibiotics interact will inform therapeutic design and fundamental principles of microbial evolution under complex selective regimes (Hesse *et al*., 2015; Frost *et al.*, 2005; van Houte *et al*., 2016; Koonin *et al.*, 2015).

Chapter Aims

Collectively, the combined experimental approach, population-level evolution assays, clonal resistance confirmation, WGS, and PAS, addresses three central aims:

1. The rate and extent of resistance evolution under single-phage versus cocktail selection.
2. The stability, heterogeneity, and likely mechanistic basis of clone-level resistance.
3. Combining phages with sub-inhibitory polymyxin B produces synergistic killing and alters resistance trajectories.

By situating these experiments within the broader context of CF biofilm ecology, evolutionary dynamics, and translational microbiology, this chapter provides a detailed foundation for subsequent analysis of *P. aeruginosa* adaptation and informs strategies for durable phage-based interventions.

5.3 Results

5.3.1 Evolutionary Assay (Methods Chapter 2.13)

Cocktail C (14/1, PA5P2, DMS3virAcrFI) was selected from the six designed cocktails evaluated in Chapter 4. It combined phages targeting two distinct bacterial receptors, LPS (14/1) and T4P (PA5P2), with DMS3virAcrFI, selected in Chapter 3 for its efficacy at both biofilm prevention and disruption. Of the designed cocktails incorporating DMS3virAcrFI, Cocktail C contained the two phages with the broadest individual host ranges in the panel (PA5P2 and 14/1, each infecting 88–89 of 92 strains in Chapter 3), and was selected based on overall assessment of growth profiles across MOIs in the Chapter 4 validation assay, where it produced significant growth reduction at 48h at both MOI 0.001 and MOI 10. The evolutionary assay was conducted at MOI 0.1, selected as the lowest MOI at which reliable phage-host interactions were observed in the Chapter 4 validation assay.

The evolutionary growth curve assay revealed clear strain- and treatment-specific dynamics in *P. aeruginosa* growth over 14 days under phage pressure. Across all strains, the multi-phage cocktail (14/1, DMS3virAcrFI, PA5P2) generally produced more consistent suppression than individual phages, though the magnitude and timing varied.

In strain 203.1, during the first two days, cocktail treatment reduced growth modestly (ΔAUC = -4.34, $p = 0.069$), which was not statistically significant. Individual phages produced variable effects: 14/1 increased growth (ΔAUC = 5.49, $p = 0.015$) and PA5P2 also led to a significant increase (ΔAUC = 4.67, $p = 0.045$), while DMS3virAcrFI had no effect (ΔAUC = 1.25, $p = 0.921$). By days 2–4, the cocktail exhibited highly significant suppression (ΔAUC = -71.23, $p < 0.000001$), whereas individual phages remained largely ineffective. This suppression persisted across days 4–6 (ΔAUC = -52.79, $p = 0.00099$), days 6–8 (ΔAUC = -36.87, $p = 0.00224$), and continued through day 14 (ΔAUC = -38.01, $p = 0.00155$), demonstrating durable activity. Single-phage treatments did not maintain suppression, and in some cases, transiently increased growth, highlighting the advantage of multi-receptor targeting.

Strain 413 was largely resistant to all treatments. Early cocktail effects were minor and not significant (ΔAUC = 14.46, $p = 0.511$), and individual phages showed variable trends, with occasional small significant increases in growth: 14/1 (ΔAUC = 31.21, $p = 0.019$), DMS3virAcrFI (ΔAUC = 29.29, $p = 0.03$), and PA5P2 (ΔAUC = 29.05, $p = 0.032$) at the first timepoint. However, these effects were not sustained, and across days 2–14, neither the

cocktail nor individual phages produced consistent suppression, emphasizing intrinsic resistance in this strain.

Strain 342 was highly sensitive to the cocktail across all timepoints. From the earliest interval (days 0–2), cocktail treatment strongly reduced growth (ΔAUC = -99.5, $p < 0.0001$), and suppression remained robust through day 14 (ΔAUC = -64.12, $p < 0.0000001$). Individual phages produced variable effects: 14/1 increased growth at day 0–2 (ΔAUC = 25.26, $p < 0.00000001$) and had minimal long-term suppression; DMS3virAcrFl had little effect at most timepoints (ΔAUC = 2.40–3.36, $p > 0.99$); PA5P2 contributed to growth reduction at later intervals (ΔAUC = -101.38, $p < 0.000000001$ at day 4–6, and ΔAUC = -39.09, $p = 0.003$ at day 10–12). These results indicate that effective suppression in 342 required either phage synergy within the cocktail or specific phage activity, highlighting the benefits of multi-receptor targeting in delaying resistance emergence.

Temporal analysis revealed clear differences across strains. In the early phase (days 0–2), cocktail effects were modest in 203.1 but robust in 342, while 413 remained largely unaffected. Single-phage treatments occasionally enhanced growth, consistent with rapid resistance evolution. During the mid-phase (days 2–8), cocktail efficacy increased in 203.1 and remained strong in 342, whereas individual phages produced inconsistent effects. In the late phase (days 8–14), cocktail suppression persisted in both 203.1 and 342, with PA5P2 contributing in 342, while 14/1 occasionally suppressed growth and DMS3virAcrFl remained largely ineffective. Strain 413 continued to show resistance across all treatments.

Cumulative area under the curve (AUC) analysis across all timepoints confirmed these trends: the cocktail consistently provided the most robust and durable suppression, while individual phages showed variable and strain-specific effects. Occasional increases in growth under single-phage exposure reflect rapid resistance evolution, whereas sustained cocktail suppression, particularly in strain 342, illustrates the benefits of multi-phage strategies. Strain 203.1 exhibited delayed but stable suppression, and strain 413 remained largely resistant, emphasizing the role of genetic background in phage efficacy.

Overall, these results demonstrate that multi-phage cocktails can provide durable suppression of bacterial growth across genetically diverse CF isolates, whereas single phages are prone to rapid resistance and variable efficacy. The temporal dynamics highlight the advantage of multi-receptor targeting in delaying resistance evolution, with sustained effects particularly evident in sensitive strains. Inter-strain differences underscore the importance of careful phage selection and cocktail design in developing effective therapeutic strategies.

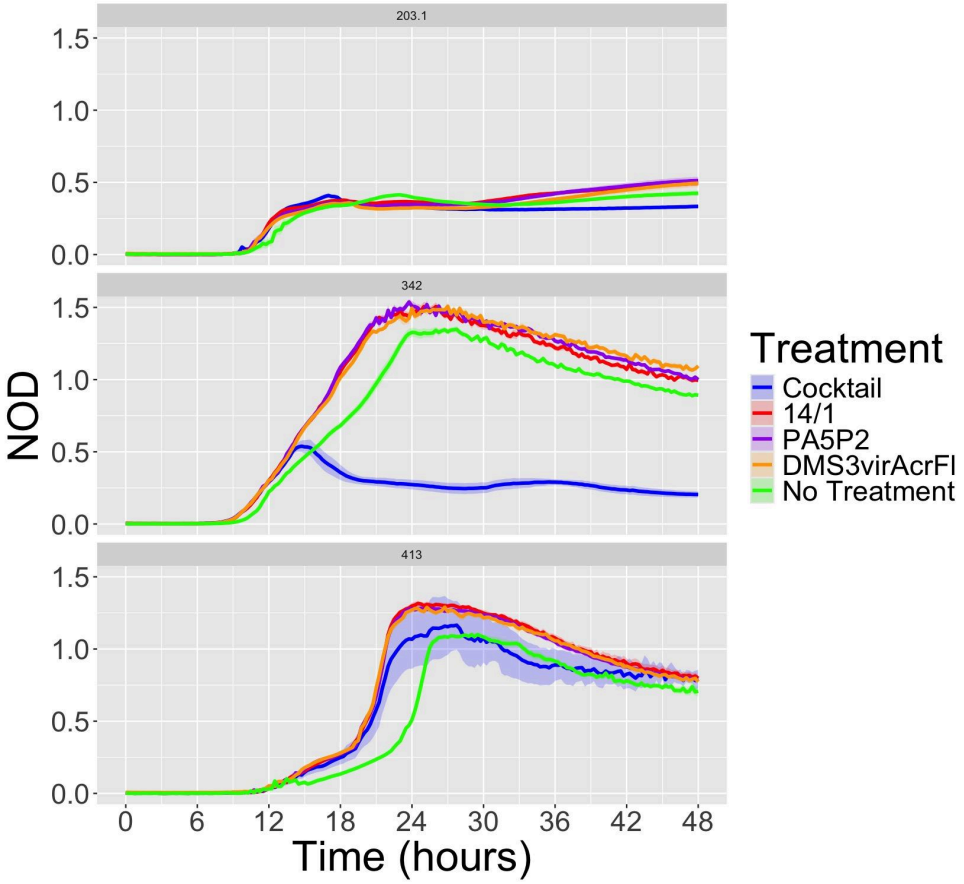

Figure 5.1: Growth curves for strains 203.1, 413, and 342 under the indicated treatments during the first 48 h of the experiment. OD_{600} was normalized to the media-only control (NOD). Solid lines represent the mean (n = 6) for each treatment, and shaded ribbons indicate the standard error of the mean (SEM). Treatments are indicated by colour: blue = Cocktail C (14/1, PA5P2, DMS3virAcrFl); red = phage 14/1 alone; purple = phage PA5P2 alone; orange = phage DMS3virAcrFl alone; green = no treatment positive control. Each facet corresponds to a different strain as labeled. X-axis shows time in hours within the assay (0–48).

Table 5.1: Statistical comparison of phage treatment conditions to the no-treatment positive control for growth curves recorded during hours 0–48 of the evolutionary assay (Figure 5.1). Estimates represent the mean difference in area under the growth curve (ΔAUC) between each treatment and the no-treatment control for strains 203.1, 342, and 413. P-values are reported with significance indicated as significant ($p < 0.05$) or ns (not significant).

Strain	Comparison	Estimate (ΔAUC)	p-value	Significance
203.1	14/1 – No Treatment	5.49	0.015	Significant
203.1	Cocktail – No Treatment	-4.34	0.069	Not significant
203.1	DMS3virAcrFl – No Treatment	1.25	0.921	Not significant
203.1	PA5P2 – No Treatment	4.67	0.045	Significant
413	14/1 – No Treatment	31.21	0.019	Significant
413	Cocktail – No Treatment	14.46	0.511	Not significant
413	DMS3virAcrFl – No Treatment	29.29	0.030	Significant
413	PA5P2 – No Treatment	29.05	0.032	Significant
342	14/1 – No Treatment	25.26	1.02E-08	Highly significant
342	Cocktail – No Treatment	-99.5	< 0.0001	Highly significant
342	DMS3virAcrFl – No Treatment	29.38	4.98E-10	Highly significant
342	PA5P2 – No Treatment	28.94	6.81E-10	Highly significant

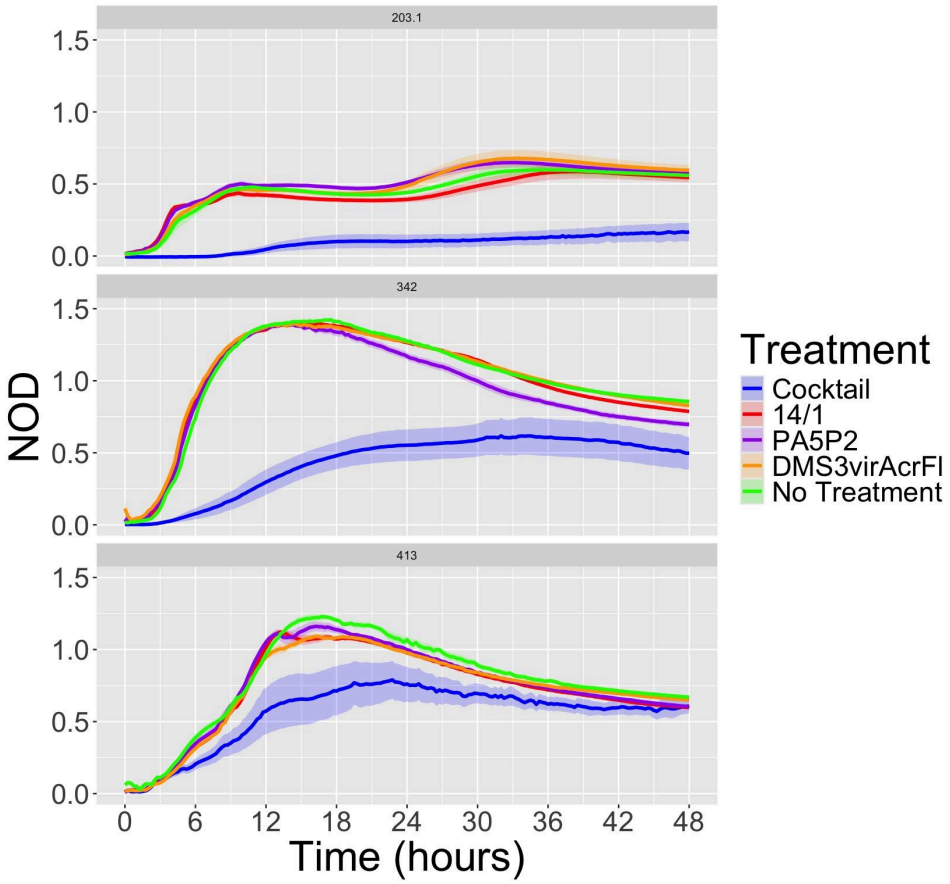

Figure 5.2: Growth curves for strains 203.1, 413, and 342 under the indicated treatments during hours 48–96 of the experiment. OD_{600} was normalized to the media-only control (NOD). Solid lines represent the mean (n = 6) for each treatment, and shaded ribbons indicate the standard error of the mean (SEM). Treatments are indicated by colour: blue = Cocktail C (14/1, PA5P2, DMS3virAcrFI); red = phage 14/1 alone; purple = phage PA5P2 alone; orange = phage DMS3virAcrFI alone; green = no treatment positive control. Each facet corresponds to a different strain as labeled. X-axis shows time in hours within the assay (0–48).

Table 5.2: Statistical comparison of phage treatment conditions to the no-treatment positive control for growth curves recorded during hours 48–96 of the evolutionary assay (Figure 5.2). Estimates represent the mean difference in area under the growth curve (ΔAUC) between each treatment and the no-treatment control for strains 203.1, 342, and 413. P-values are reported with significance indicated as significant ($p < 0.05$) or ns (not significant).

Strain	Comparison	Estimate (ΔAUC)	p-value	Significance
203.1	14/1 – No Treatment	-4.47	0.964	Not significant
203.1	Cocktail – No Treatment	-71.23	5.57E-09	Highly significant
203.1	DMS3virAcrFI – No Treatment	7.21	0.828	Not significant
203.1	PA5P2 – No Treatment	8.24	0.750	Not significant
413	14/1 – No Treatment	-12.11	0.575	Not significant
413	Cocktail – No Treatment	-45.23	0.00015	Highly significant
413	DMS3virAcrFI – No Treatment	-10.81	0.672	Not significant
413	PA5P2 – No Treatment	-8.18	0.847	Not significant
342	14/1 – No Treatment	-1.42	0.9999	Not significant
342	Cocktail – No Treatment	-114.72	4.73E-10	Highly significant
342	DMS3virAcrFI – No Treatment	2.40	0.999	Not significant
342	PA5P2 – No Treatment	-14.61	0.576	Not significant

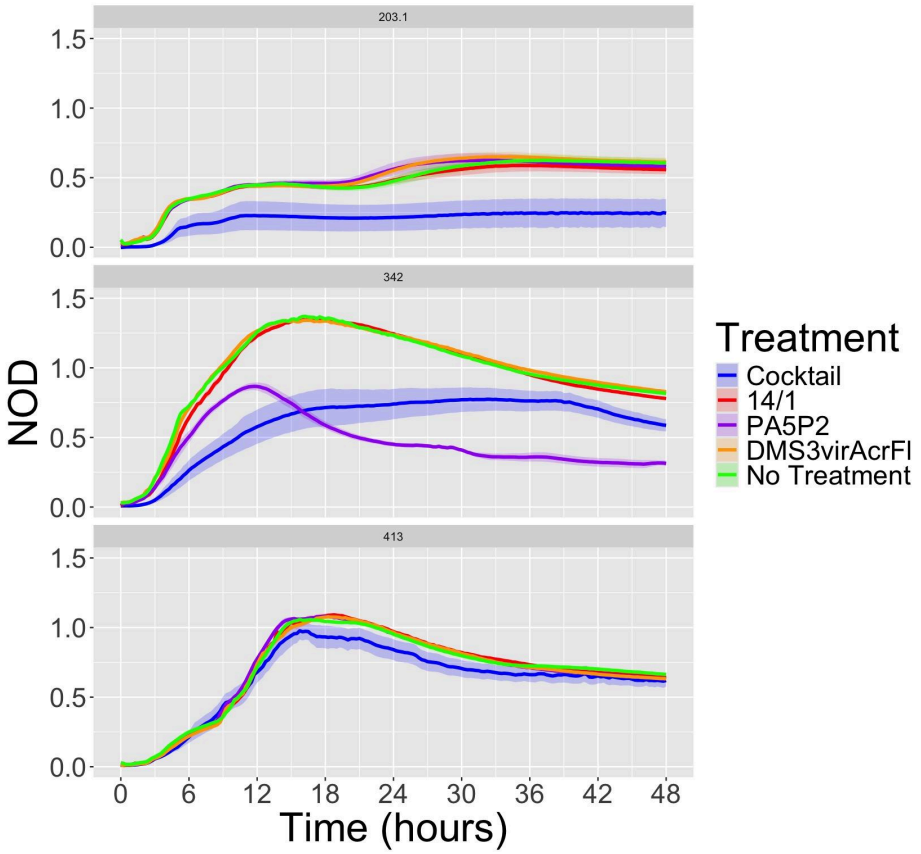

Figure 5.3: Growth curves for strains 203.1, 413, and 342 under the indicated treatments during hours 96–144 of the experiment. OD_{600} was normalized to the media-only control (NOD). Solid lines represent the mean (n = 6) for each treatment, and shaded ribbons indicate the standard error of the mean (SEM). Treatments are indicated by colour: blue = Cocktail C (14/1, PA5P2, DMS3virAcrFl); red = phage 14/1 alone; purple = phage PA5P2 alone; orange = phage DMS3virAcrFl alone; green = no treatment positive control. Each facet corresponds to a different strain as labeled. X-axis shows time in hours within the assay (0–48).

Table 5.3: Statistical comparison of phage treatment conditions to the no-treatment positive control for growth curves recorded during hours 96–144 of the evolutionary assay (Figure 5.3). Estimates represent the mean difference in area under the growth curve (ΔAUC) between each treatment and the no-treatment control for strains 203.1, 342, and 413. P-values are reported with significance indicated as significant ($p < 0.05$) or ns (not significant).

Strain	Comparison	Estimate (ΔAUC)	p-value	Significance
203.1	14/1 – No Treatment	-3.25	0.998	Not significant
203.1	Cocktail – No Treatment	-52.79	0.00099	Highly significant
203.1	DMS3virAcrFl – No Treatment	4.18	0.995	Not significant
203.1	PA5P2 – No Treatment	2.59	0.999	Not significant
413	14/1 – No Treatment	0.43	0.99998	Not significant
413	Cocktail – No Treatment	-11.92	0.077	Not significant (close to significance)
413	DMS3virAcrFl – No Treatment	-1.25	0.998	Not significant
413	PA5P2 – No Treatment	0.38	0.99998	Not significant
342	14/1 – No Treatment	-3.63	0.994	Not significant
342	Cocktail – No Treatment	-73.11	5.33E-07	Highly significant
342	DMS3virAcrFl – No Treatment	1.59	0.9998	Not significant
342	PA5P2 – No Treatment	-101.38	1.14E-09	Highly significant

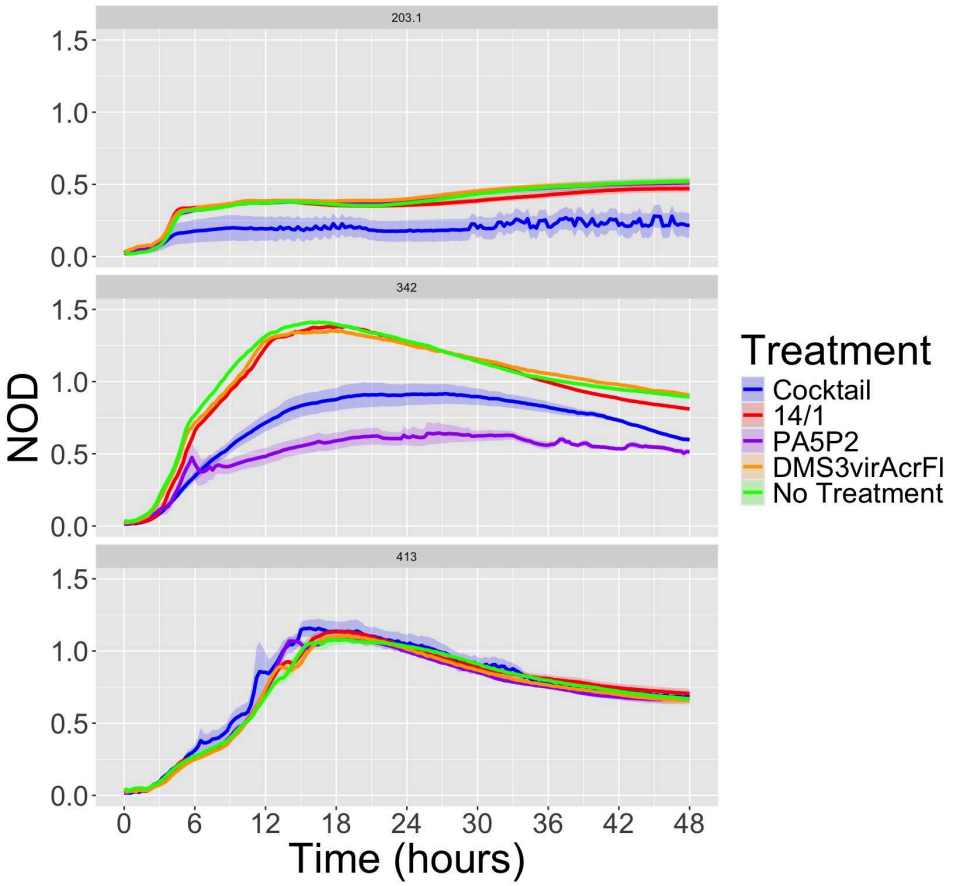

Figure 5.4: Growth curves for strains 203.1, 413, and 342 under the indicated treatments during hours 144–192 of the experiment. OD_{600} was normalized to the media-only control (NOD). Solid lines represent the mean (n = 6) for each treatment, and shaded ribbons indicate the standard error of the mean (SEM). Treatments are indicated by colour: blue = Cocktail C (14/1, PA5P2, DMS3virAcrFl); red = phage 14/1 alone; purple = phage PA5P2 alone; orange = phage DMS3virAcrFl alone; green = no treatment positive control. Each facet corresponds to a different strain as labeled. X-axis shows time in hours within the assay (0–48).

Table 5.4: Statistical comparison of phage treatment conditions to the no-treatment positive control for growth curves recorded during hours 144–192 of the evolutionary assay (Figure 5.4). Estimates represent the mean difference in area under the growth curve (ΔAUC) between each treatment and the no-treatment control for strains 203.1, 342, and 413. P-values are reported with significance indicated as significant ($p < 0.05$) or ns (not significant).

Strain	Comparison	Estimate (ΔAUC)	p-value	Significance
203.1	14/1 – No Treatment	-3.57	0.992	Not significant
203.1	Cocktail – No Treatment	-36.87	0.00224	Highly significant
203.1	DMS3virAcrFl – No Treatment	3.22	0.995	Not significant
203.1	PA5P2 – No Treatment	1.25	0.9999	Not significant
413	14/1 – No Treatment	2.21	0.979	Not significant
413	Cocktail – No Treatment	6.09	0.545	Not significant
413	DMS3virAcrFl – No Treatment	-3.18	0.925	Not significant
413	PA5P2 – No Treatment	-3.25	0.919	Not significant
342	14/1 – No Treatment	-9.22	0.529	Not significant
342	Cocktail – No Treatment	-63.95	2.08E-09	Highly significant
342	DMS3virAcrFl – No Treatment	-2.61	0.991	Not significant
342	PA5P2 – No Treatment	-100.36	0	Highly significant

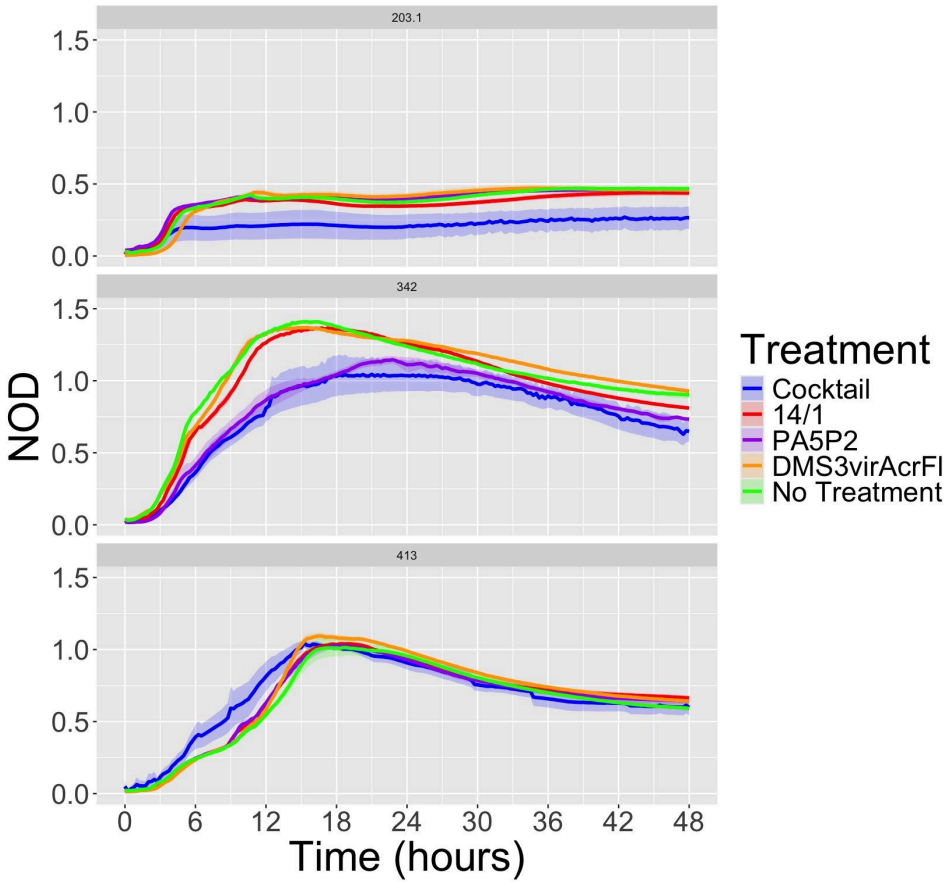

Figure 5.5: Growth curves for strains 203.1, 413, and 342 under the indicated treatments during hours 192–240 of the experiment. OD_{600} was normalized to the media-only control (NOD). Solid lines represent the mean (n = 6) for each treatment, and shaded ribbons indicate the standard error of the mean (SEM). Treatments are indicated by colour: blue = Cocktail C (14/1, PA5P2, DMS3virAcrFI); red = phage 14/1 alone; purple = phage PA5P2 alone; orange = phage DMS3virAcrFI alone; green = no treatment positive control. Each facet corresponds to a different strain as labeled. X-axis shows time in hours within the assay (0–48).

Table 5.5: Statistical comparison of phage treatment conditions to the no-treatment positive control for growth curves recorded during hours 192–240 of the evolutionary assay (Figure 5.5). Estimates represent the mean difference in area under the growth curve (ΔAUC) between each treatment and the no-treatment control for strains 203.1, 342, and 413. P-values are reported with significance indicated as significant ($p < 0.05$) or ns (not significant).

Strain	Comparison	Estimate (ΔAUC)	p-value	Significance
203.1	14/1 – No Treatment	-4.91	0.982	Not significant
203.1	Cocktail – No Treatment	-33.24	0.0122	Significant
203.1	DMS3virAcrFI – No Treatment	1.57	0.9998	Not significant
203.1	PA5P2 – No Treatment	1.91	0.9995	Not significant
413	14/1 – No Treatment	4.16	0.832	Not significant
413	Cocktail – No Treatment	6.29	0.528	Not significant
413	DMS3virAcrFI – No Treatment	7.52	0.356	Not significant
413	PA5P2 – No Treatment	2.42	0.972	Not significant
342	14/1 – No Treatment	-8.56	0.878	Not significant
342	Cocktail – No Treatment	-47.81	0.000335	Highly significant
342	DMS3virAcrFI – No Treatment	3.36	0.996	Not significant
342	PA5P2 – No Treatment	-39.09	0.00303	Highly significant

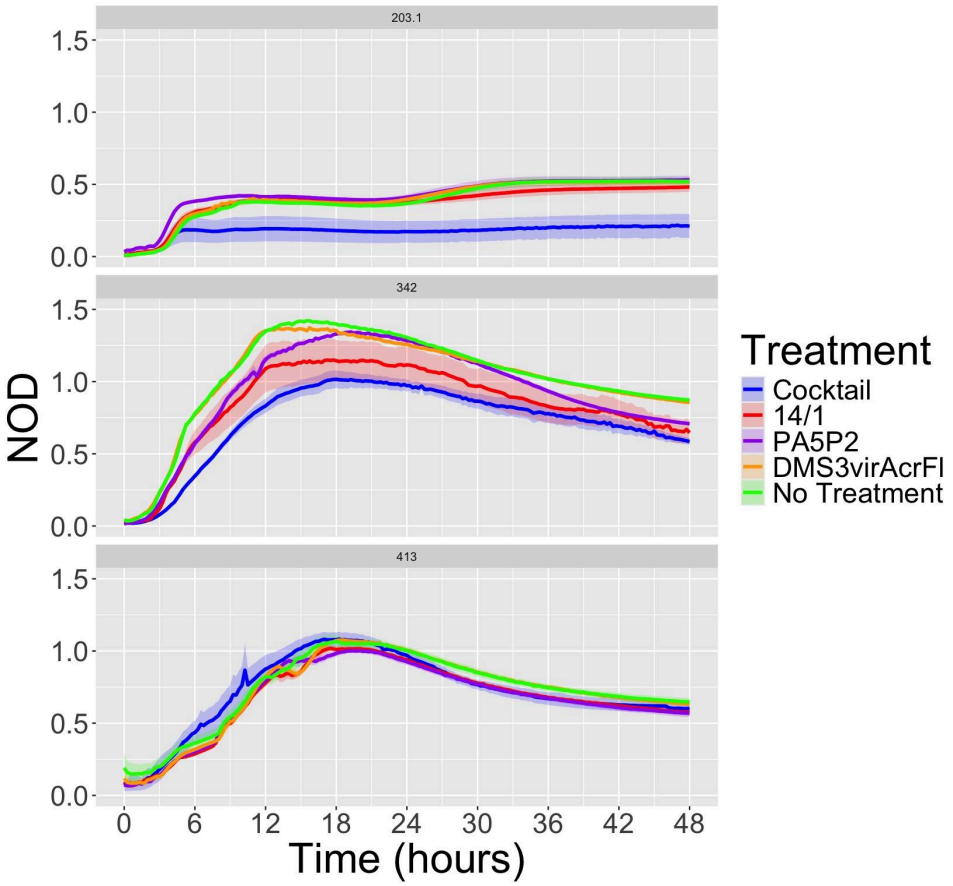

Figure 5.6: Growth curves for strains 203.1, 413, and 342 under the indicated treatments during hours 240–288 of the experiment. OD_{600} was normalized to the media-only control (NOD). Solid lines represent the mean (n = 6) for each treatment, and shaded ribbons indicate the standard error of the mean (SEM). Treatments are indicated by colour: blue = Cocktail C (14/1, PA5P2, DMS3virAcrFI); red = phage 14/1 alone; purple = phage PA5P2 alone; orange = phage DMS3virAcrFI alone; green = no treatment positive control. Each facet corresponds to a different strain as labeled. X-axis shows time in hours within the assay (0–48).

Table 5.6: Statistical comparison of phage treatment conditions to the no-treatment positive control for growth curves recorded during hours 240–288 of the evolutionary assay (Figure 5.6). Estimates represent the mean difference in area under the growth curve (ΔAUC) between each treatment and the no-treatment control for strains 203.1, 342, and 413. P-values are reported with significance indicated as significant ($p < 0.05$) or ns (not significant).

Strain	Comparison	Estimate (ΔAUC)	p-value	Significance
203.1	14/1 – No Treatment	-2.47	0.999	Not significant
203.1	Cocktail – No Treatment	-41.11	0.00203	Significant
203.1	DMS3virAcrFI – No Treatment	2.08	0.999	Not significant
203.1	PA5P2 – No Treatment	6.94	0.941	Not significant
413	14/1 – No Treatment	-11.66	0.328	Not significant
413	Cocktail – No Treatment	-3.01	0.986	Not significant
413	DMS3virAcrFI – No Treatment	-2.71	0.991	Not significant
413	PA5P2 – No Treatment	-12.04	0.299	Not significant
342	14/1 – No Treatment	-37.43	0.0251	Significant
342	Cocktail – No Treatment	-60.37	0.000246	Highly significant
342	DMS3virAcrFI – No Treatment	-3.1	0.999	Not significant
342	PA5P2 – No Treatment	-19.22	0.449	Not significant

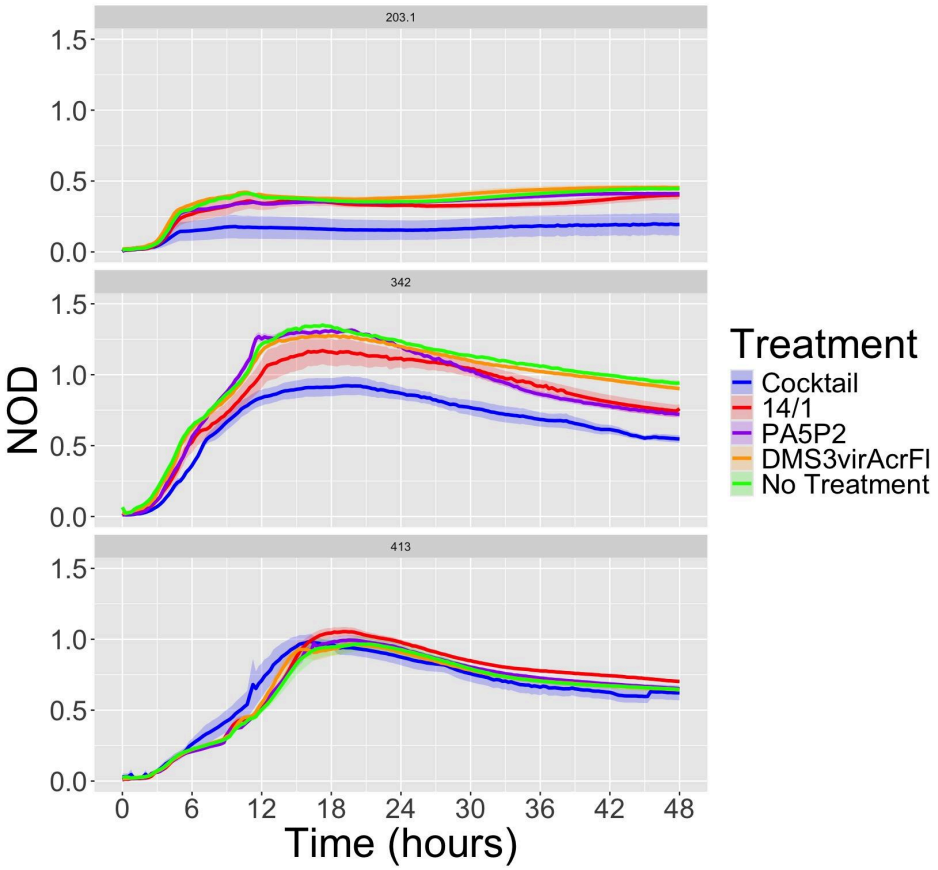

Figure 5.7: Growth curves for strains 203.1, 413, and 342 under the indicated treatments during hours 288–336 of the experiment. OD_{600} was normalized to the media-only control (NOD). Solid lines represent the mean (n = 6) for each treatment, and shaded ribbons indicate the standard error of the mean (SEM). Treatments are indicated by colour: blue = Cocktail C (14/1, PA5P2, DMS3virAcrFI); red = phage 14/1 alone; purple = phage PA5P2 alone; orange = phage DMS3virAcrFI alone; green = no treatment positive control. Each facet corresponds to a different strain as labeled. X-axis shows time in hours within the assay (0–48).

Table 5.7: Statistical comparison of phage treatment conditions to the no-treatment positive control for growth curves recorded during hours 288–336 of the evolutionary assay (Figure 5.7). Estimates represent the mean difference in area under the growth curve (ΔAUC) between each treatment and the no-treatment control for strains 203.1, 342, and 413. P-values are reported with significance indicated as significant ($p < 0.05$) or ns (not significant)..

Strain	Comparison	Estimate (ΔAUC)	p-value	Significance
203.1	14/1 – No Treatment	-8.23	0.856	Not significant
203.1	Cocktail – No Treatment	-38.01	0.00155	Significant
203.1	DMS3virAcrFI – No Treatment	3.85	0.99	Not significant
203.1	PA5P2 – No Treatment	-3.92	0.989	Not significant
413	14/1 – No Treatment	9.12	0.396	Not significant
413	Cocktail – No Treatment	1.19	0.999	Not significant
413	DMS3virAcrFI – No Treatment	0.81	0.999	Not significant
413	PA5P2 – No Treatment	2.07	0.994	Not significant
342	14/1 – No Treatment	-26.61	0.0069	Significant
342	Cocktail – No Treatment	-64.12	0.0000000338	Highly significant
342	DMS3virAcrFI – No Treatment	-6.72	0.856	Not significant
342	PA5P2 – No Treatment	-17.78	0.105	Not significant

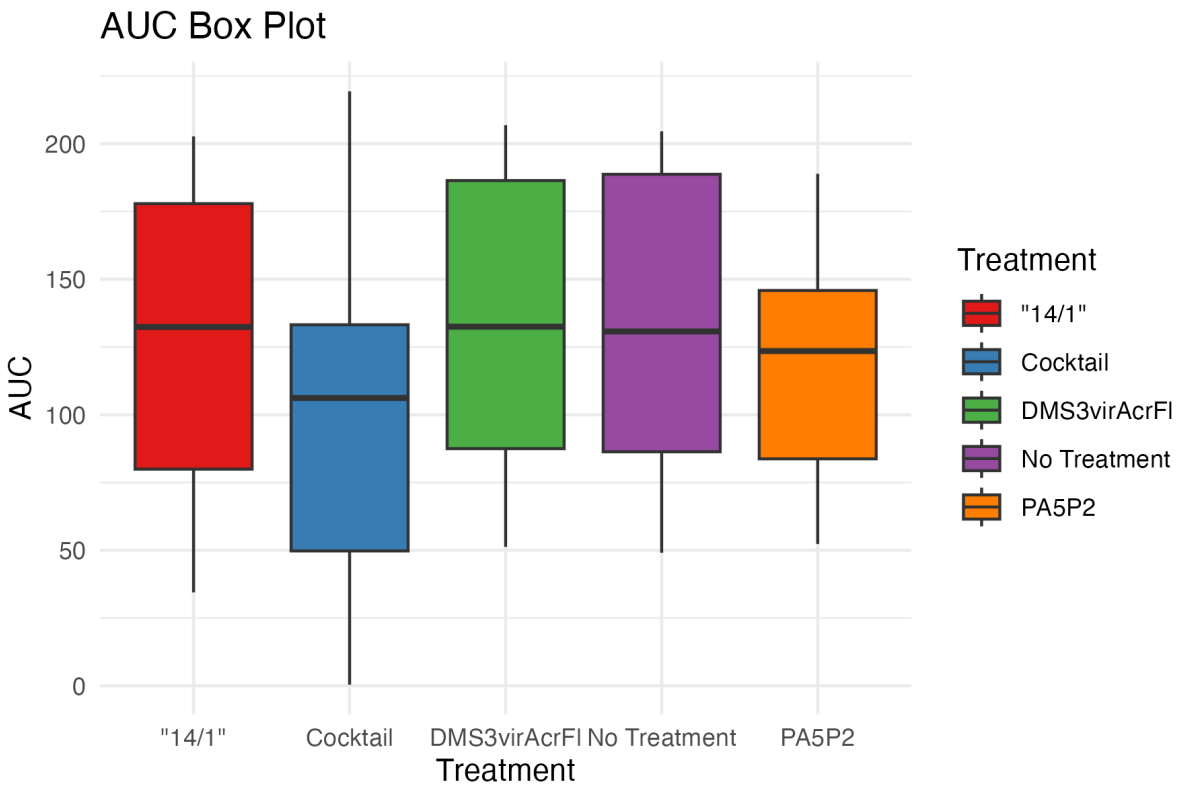

Figure 5.8: Box plot showing the area under the growth curve (AUC) as a measure of cumulative bacterial growth across all 14-day timepoints for each treatment condition, pooled across all three *P. aeruginosa* strains (203.1, 342, and 413). AUC was calculated from normalised optical density (NOD) measurements taken every 10 minutes over each 48-hour window. Treatments are indicated by colour: red = phage 14/1 alone; blue = Cocktail C (14/1, PA5P2, DMS3virAcrFl); green = phage DMS3virAcrFl alone; purple = no treatment positive control; orange = phage PA5P2 alone. Box boundaries represent the interquartile range (IQR), the central line represents the median, and whiskers extend to the full range of the data. Lower AUC values indicate greater suppression of bacterial growth relative to the no-treatment control. Statistical comparisons between each treatment and the no-treatment control are presented in Table 5.8.

Table 5.8: Comparison of cumulative bacterial growth, measured as area under the growth curve (AUC), across all 14-day timepoints for each phage treatment condition relative to the no-treatment positive control, pooled across strains 203.1, 342, and 413. ΔAUC values represent the mean difference between each treatment and the no-treatment control, with statistical significance indicated.

Comparison	Estimate	p-value	Significant
("14/1") − No Treatment	-2.84	0.9895	Not significant
Cocktail − No Treatment	-39.68	<0.0001	Significant
DMS3virAcrFl − No Treatment	3.21	0.9834	Not significant
PA5P2 − No Treatment	11.02	0.3476	Not significant

5.3.2 Confirmation of Resistance (Methods Chapter 2.14)

In order to confirm that resistance had occurred within the evolutionary assay, a confirmation of resistance (CoR) assay was performed using clones isolated at the end of the selection experiment, as described in Methods chapter 2.14. This assay was performed on strains 342 and 413 only, as strain 203.1 was excluded because it showed minimal phenotypic response to any treatment compared to the control in the preceding evolutionary experiment and was efficiently suppressed by the cocktail. It was therefore not considered informative for further analysis. Evolved clones were exposed to the three cocktail phages individually to assess cross-resistance against all treatments used in the evolutionary assay, including the no-treatment control. The assay was conducted as a growth curve, with key timepoints (12, 24, 36, and 48 hours) extracted for analysis. Heatmaps were produced to show the mean effect (Figure 5.9) and the effect at a clone-specific level (Figure 5.10), with the intention of visualizing patterns rather than performing statistical inference. Within all figures, blue denotes phage sensitivity and red denotes resistance.

Mean density reduction in strain 342 largely showed a slight increase in growth at 12 hours across all treatments (Figure 5.9a). This trend continued at later timepoints, with the exception of clones treated with PA5P2 in the CoR assay, where all treatments resulted in a reduction in growth. However, at the clonal level, 5 out of 6 clones exposed to the cocktail displayed resistance to PA5P2 (Figure 5.10a). In general, exposure to a single phage resulted in resistance to that phage, but did not confer cross-resistance to other phages. The apparent increase in resistance over the course of the CoR assay, rather than being present from the earliest timepoint, may reflect phenotypic lag in resistance expression or the presence of mixed clonal populations in which sensitive cells initially dominate before resistant subpopulations expand under phage pressure.

Results for strain 413 were more variable, with little resistance observed even when the evolutionary assay treatment matched the CoR assay treatment (Figures 5.9b and 5.10b). To explore whether there was a consistent genotypic explanation for these observations, representative clones from all strains were selected for sequencing, allowing comparison of resistance mechanisms across different phenotypic outcomes.

5.3.3 Sequencing (Methods Chapter 2.15)

For strain 342 all 6 repeats of all 5 treatment conditions and the ancestral strain were processed for long read sequencing with MicrobesNG. Strain 342 was selected for WGS as it demonstrated the most robust and sustained suppression under Cocktail C treatment across the evolutionary assay, alongside clear phenotypic differences between treatment conditions

in the CoR assay, making it the most informative strain for mechanistic investigation of resistance evolution. Single colonies were isolated as described in Section 2.12 prior to cryopreservation and subsequent sequencing. Samples were prepared according to the MicrobesNG protocol (Appendix 2). Sequencing generated a mean of 53,025 reads per sample, with a mean estimated genome coverage of 106× (range 67–176×) and a median read quality of Q19.1 (range Q15.7–Q20.0), consistent with high-accuracy Oxford Nanopore long-read data. All 31 samples were successfully sequenced and assembled, with 30 assembling into a single complete contig; one sample (F10, PA5P2-treated) assembled into two contigs. All assemblies contained zero ambiguous bases.

In total, 54 relevant mutations were identified across all treatment conditions after excluding variants with no phage resistance activity. Mutations identified in no-treatment clones (H2, H3, H5, H6; Table 5.10) are shown separately, as these represent background spontaneous mutation rather than phage-driven selection and should not be interpreted as drivers of resistance phenotypes; 9 such mutations were identified across 4 no-treatment clones. Phage-treated clones showed treatment-specific patterns: cocktail-treated clones showed 13 mutations across 6 clones, with 4 affecting LPS biosynthesis genes (*galU, rfbB, rfaB*), consistent with multi-receptor selective pressure. PA5P2-treated clones showed the highest total (17 mutations across 6 clones), of which 6 were in T4P-associated genes (*pilB, pilT, pilQ, pilY1*), reflecting the T4P receptor specificity of PA5P2. Treatment with 14/1 resulted in 9 mutations across 5 clones, with LPS biosynthesis genes (*galU*) and cytochrome c domain-containing proteins recurrently affected. DMS3virAcrFl-treated clones showed 8 mutations across 6 clones, predominantly in cellular process and defence genes, consistent with its distinct mode of infection.

(a)

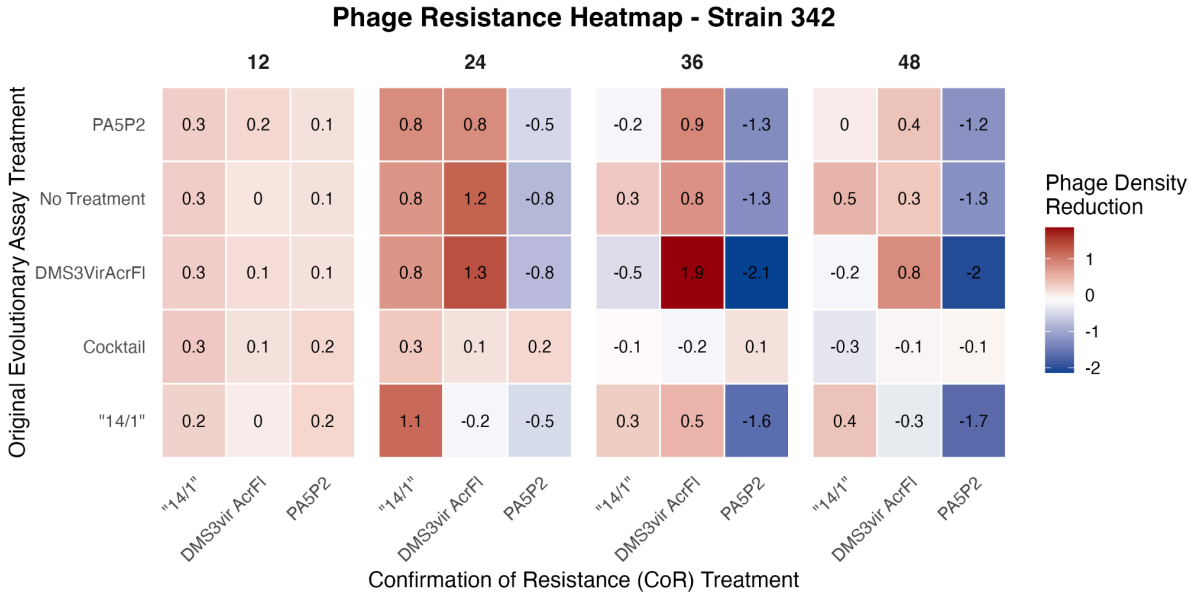

(b)

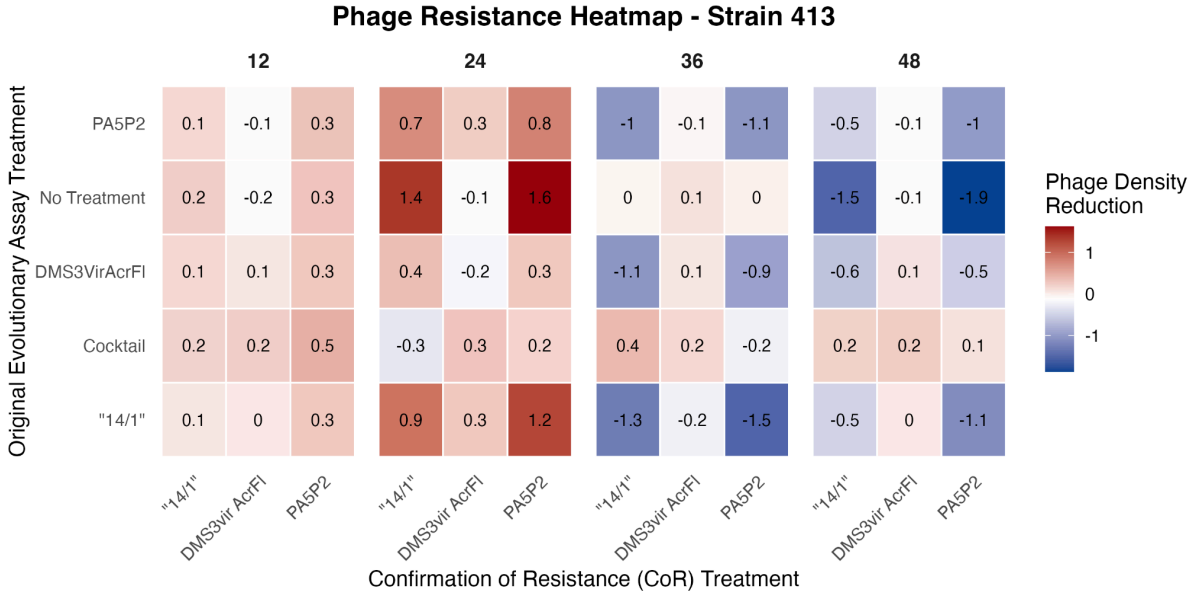

Figure 5.9: Panels show mean phage density reduction of Pseudomonas aeruginosa strains 342 (a) and 413 (b) following exposure to each phage treatment during the confirmation of resistance (CoR) assay. Phage density reduction is calculated as the change in optical density (ΔOD) of bacterial growth relative to the no-phage control. The y-axis indicates the original evolutionary assay treatment, and the x-axis shows the CoR treatment each evolved population was re-challenged with. Each tile represents the mean ΔOD across six independent clones. Facets correspond to timepoints (12, 24, 36, and 48 h), illustrating temporal changes in resistance and susceptibility. Colour intensity reflects the magnitude of phage-mediated reduction, with red indicating greater bacterial suppression (higher ΔOD reduction) and blue indicating increased bacterial growth relative to the no-phage control.

(a)

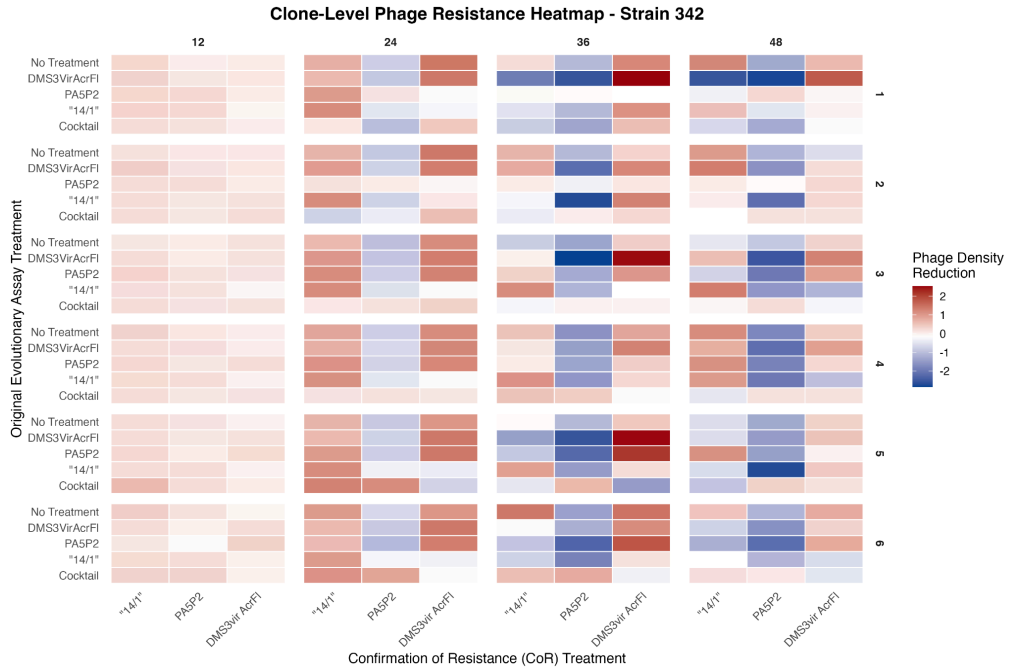

(b)

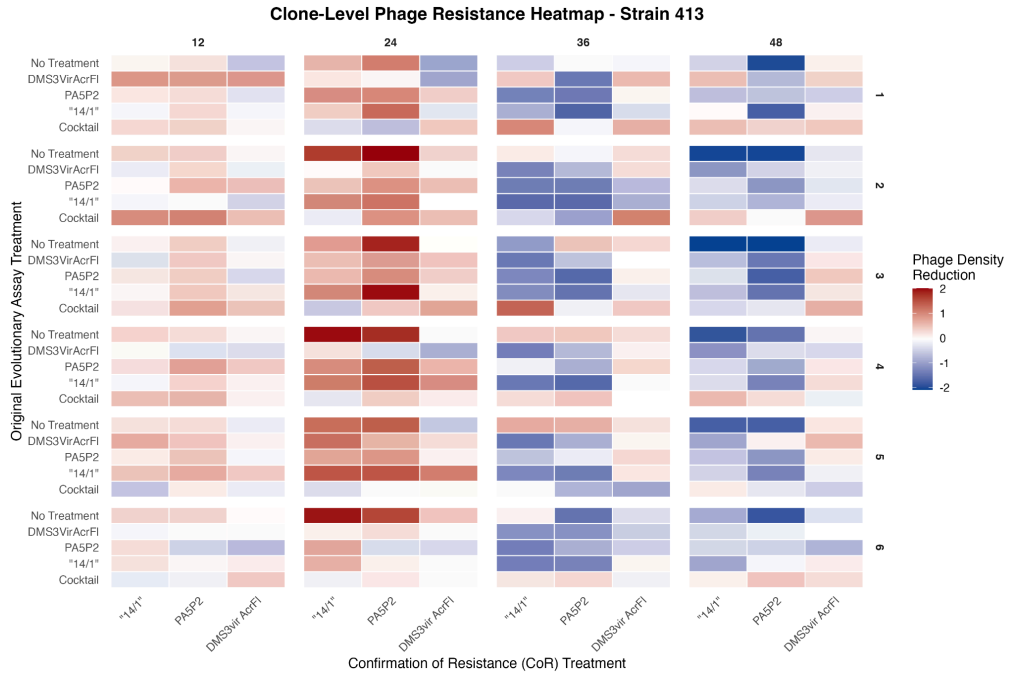

Figure 5.10: Heatmaps showing clone-level phage density reduction for *P. aeruginosa* strains 342 (a) and 413 (b) during the confirmation of resistance (CoR) assay. Each tile represents the phage density reduction of a single evolved clone (clones 1–6, indicated on the right of each panel) when re-challenged with each CoR phage treatment (14/1, PA5P2, DMS3virAcrFI) at timepoints 12, 24, 36, and 48 hours. The y-axis denotes the original evolutionary assay treatment and the x-axis indicates the CoR treatment applied. Colour indicates the direction and magnitude of phage-mediated effect relative to the no-phage control: red indicates increased bacterial growth (phage insensitivity/resistance) and blue indicates reduced bacterial growth (phage sensitivity). Colour gradients provide visualisation of within-population variation in resistance and susceptibility patterns across timepoints.

Table 5.9: Condensed results from long read sequencing performed by MicrobesNG with descriptive columns added for whether the gene affects a cellular process or an anti-phage defense system and the general effect. Mutations with no phage resistance activity were excluded from the table. lysR (missense c.295G>A p.Asp99Asn) and tssE (synonymous c.270T>C p.Arg90Arg) were also excluded as identical variants were identified in no-treatment control clones (Table 5.10), indicating these represent background mutations not attributable to phage selection pressure. Cytochrome c domain-containing protein variants (synonymous c.747G>A p.Ser249Ser) were retained for completeness but are also present in no-treatment control clones and are synonymous; they are not considered drivers of phage resistance phenotypes. Gene mutations were identified using snippy on Galaxy.

Clone	Treatment	Type	Variant Effect	Gene	Product	Process/Defense	Effect
F1	Cocktail	snp	Missense	*galU*	UTP--glucose-1-phosphate uridylyltransferase *GalU*	Process	LPS modifying
F2	Cocktail	snp	Synonymous		Cytochrome c domain-containing protein	Defence	Found in defense Islands
F3	Cocktail	snp	Synonymous		Cytochrome c domain-containing protein	Defence	Found in defense Islands
F3	Cocktail	snp	Missense	*rfbB*	dTDP-glucose 4,6-dehydratase	Process	LPS modifying
F3	Cocktail	snp	Synonymous		Phage tail assembly protein	Process	prophage blocks the assembly of the tails of other phages.
F4	Cocktail	snp	Synonymous		Phage tail assembly protein	Process	prophage blocks the assembly of the tails of other phages.
F4	Cocktail	snp	Missense	*rtcB*	RNA-splicing ligase *RtcB*, repairs tRNA damage	Process (Indirect)	tRNA damage repair - effective for surviving lytic phage
F5	Cocktail	snp	Synonymous		Cytochrome c domain-containing protein	Defence	Found in defense Islands
F5	Cocktail	snp	Stop Gained	*rfaB*	Glycosyltransferase involved in cell wall biosynthesis	Process	LPS modifying
F5	Cocktail	del	Frameshift	*pilY1*	Type IV pilus biogenesis factor *PilY1*	Process	T4P formation
F6	Cocktail	snp	Synonymous		Cytochrome c domain-containing protein	Defence	Found in defense Islands
F6	Cocktail	del	Frameshift	*rfaB*	Glycosyltransferase involved in cell wall biosynthesis	Process	LPS modifying
F7	PA5P2	snp	Synonymous		Cytochrome c domain-containing protein	Defence	Found in defense Islands
F7	PA5P2	snp	Synonymous	*lon*	endopeptidase La	Process (Indirect)	Stress response
F7	PA5P2	snp	Stop Gained	*pilT*	type IV pilus twitching motility protein *PilT*	Process	T4P modification
F8	PA5P2	snp	Synonymous		Cytochrome c domain-containing protein	Defence	Found in defense Islands
F8	PA5P2	snp	Missense	*pilB*	type 4 fimbrial biogenesis protein *PilB*	Process	T4P modification
F9	PA5P2	snp	Synonymous		Cytochrome c domain-containing protein	Defence	Found in defense Islands

Table 5.9 Continued

Clone	Treatment	Type	Variant Effect	Gene	Product	Process/Defense	Effect
F9	PA5P2	ins	Frameshift	*pilB*	type 4 fimbrial biogenesis protein *PilB*	Process	T4P modification
F10	PA5P2	complex	Missense	*adhP*	alcohol dehydrogenase *AdhP*	Defense	Pgl Defense system
F10	PA5P2	snp	Synonymous		Cytochrome c domain-containing protein	Defence	Found in defense Islands
F10	PA5P2	snp	Synonymous	*gcvR*	Glycine cleavage system regulator *GcvR*	Process (Indirect)	Cell surface modification
F10	PA5P2	ins	Frameshift	*arnE*	putative 4-amino-4-deoxy-L-arabinose-phosphoundecaprenol flippase subunit *ArnE*	Process (Indirect)	T2SS alteration - prevent phage from binding to specific receptors on the bacterial cell surface.
F10	PA5P2	snp	Missense	*pilB*	type 4 fimbrial biogenesis protein *PilB*	Process	T4P modification
F11	PA5P2	snp	Synonymous		Cytochrome c domain-containing protein	Defence	Found in defense Islands
F11	PA5P2	snp	Synonymous	*lon*	endopeptidase La	Process (Indirect)	Stress response
F11	PA5P2	snp	Missense	*pilQ*	type 4a pilus secretin *PilQ*	Process	T4P formation
F12	PA5P2	snp	Synonymous		Cytochrome c domain-containing protein	Defence	Found in defense Islands
F12	PA5P2	del	Disruptive Inframe Deletion	*pilT*	type IV pilus twitching motility protein *PilT*	Process	T4P modification
G1	14/1	snp	Synonymous		Cytochrome c domain-containing protein	Defence	Found in defense Islands
G1	14/1	snp	Synonymous	*lon*	endopeptidase La	Process (Indirect)	Stress response
G1	14/1	ins	Frameshift	*arnE*	putative 4-amino-4-deoxy-L-arabinose-phosphoundecaprenol flippase subunit *ArnE*	Process (Indirect)	T2SS alteration - prevent phage from binding to specific receptors on the bacterial cell surface.
G1	14/1	snp	Missense	*galU*	UTP--glucose-1-phosphate uridylyltransferase *GalU*	Process	LPS modifying
G2	14/1	snp	Missense	*galU*	UTP--glucose-1-phosphate uridylyltransferase *GalU*	Process	LPS modifying
G3	14/1	snp	Synonymous		Cytochrome c domain-containing protein	Defence	Found in defense Islands
G3	14/1	snp	Synonymous	*lonB*	putative ATP-dependent protease	Defense	BREX
G5	14/1	snp	Synonymous		Cytochrome c domain-containing protein	Defence	Found in defense Islands
G6	14/1	snp	Synonymous		Cytochrome c domain-containing protein	Defence	Found in defense Islands

Table 5.9 Continued							
Clone	**Treatment**	**Type**	**Variant Effect**	**Gene**	**Product**	**Process/Defense**	**Effect**
G7	DMS3vir AcrFI	snp	Synonymous	*uvrC*	excinuclease ABC subunit *UvrC*	Process (Indirect)	Survival & replication
G8	DMS3vir AcrFI	snp	Synonymous		Cytochrome c domain-containing protein	Defence	Found in defense Islands
G8	DMS3vir AcrFI	snp	Synonymous	*yajL*	Protein/nucleotide deglycase, PfpI/YajL/DJ-1 family	Process (Indirect)	cell surface modification
G10	DMS3vir AcrFI	snp	Synonymous		Cytochrome c domain-containing protein	Defence	Found in defense Islands
G11	DMS3vir AcrFI	snp	Synonymous		Phage tail assembly protein	Process	prophage blocks the assembly of the tails of other phages.
G12	DMS3vir AcrFI	snp	Synonymous		Cytochrome c domain-containing protein	Defence	Found in defense Islands
G12	DMS3vir AcrFI	snp	Synonymous		Phage tail assembly protein	Process	prophage blocks the assembly of the tails of other phages.

Table 5.10: Mutations identified in no-treatment evolved clones from long-read sequencing. These represent background spontaneous mutation in the absence of phage selection pressure and are not considered to be driving observed resistance phenotypes.

Clone	Treatment	Type	Gene	Product	Process/Defense	Effect
H2	No Treatment	snp		Cytochrome c domain-containing protein	Defence	Found in defense Islands
H2	No Treatment	del	dnaX	DNA polymerase III subunit gamma/tau	Defence	BREX Defence system
H2	No Treatment	snp	tssE	type VI secretion system baseplate subunit TssE	Defense	Acting as a phage receptor or a component of a defense system. (Poss link to CRISPR-Cas)
H3	No Treatment	snp		Cytochrome c domain-containing protein	Defence	Found in defense Islands
H3	No Treatment	snp		Phage tail assembly protein	Process	prophage blocks the assembly of the tails of other phages.
H5	No Treatment	ins	rmuC	DNA recombination RmuC-like protein	Defence	Shield Defence system
H5	No Treatment	snp		Phage tail assembly protein	Process	prophage blocks the assembly of the tails of other phages.
H5	No Treatment	snp		RHS repeat protein	Process (Indirect)	Targets and kills phage-infected bacteria.
H6	No Treatment	snp		Cytochrome c domain-containing protein	Defence	Found in defense Islands

5.3.4 Phage–Antibiotic Synergy (Methods Chapter 2.16 - 2.17)

Prior to commencing the PAS assay it was necessary to determine the MIC for 4 commonly used antipseudomonal antibiotics and one generally ineffective agent to select the most suitable for the PAS assay (Methods 2.16). MIC values for strain 342 were available from the Copenhagen dataset, which included colistin (1.5 mg/L), tobramycin (0.75 mg/L), meropenem (0.38 mg/L), ciprofloxacin (0.25 mg/L), and aztreonam (4.0 mg/L), and confirmatory assays were performed to verify these values. An MIC assay was performed using five antibiotics (Colistin, Polymyxin B, Tobramycin, Meropenem, and Ampicillin) against the ancestral strain 342. Ciprofloxacin and aztreonam were not included in the confirmatory panel as the Copenhagen data indicated susceptibility to both (ciprofloxacin 0.25 mg/L, aztreonam 4.0 mg/L, both below EUCAST resistance thresholds); the five antibiotics tested were considered sufficient to characterise the strain's antibiotic susceptibility profile and select a candidate for PAS. Three technical replicates were conducted alongside a second independent assay. Polymyxin B demonstrated an MIC of 0.761 mg/L; the ancestral strain was eliminated at all concentrations of Tobramycin; Meropenem had an MIC of 0.195 mg/L; Ampicillin did not reduce growth at any concentration; and Colistin had an MIC of 0.293 mg/L in the first assay and 1.172 mg/L in the second. The variability in Colistin MIC between assays prompted the second confirmatory assay; the second Colistin value of 1.172 mg/L was more consistent with the Copenhagen value of 1.5 mg/L. Results for Polymyxin B, Tobramycin, and Meropenem were broadly consistent with the Copenhagen data across both assays. Based on EUCAST clinical breakpoints for *P. aeruginosa* (Clinical Breakpoint Tables, 2026a), the ancestral strain was susceptible to Tobramycin (MIC below the 4 mg/L threshold), Meropenem (MIC of 0.195 mg/L, below the 2 mg/L threshold), and Colistin/Polymyxin B (MIC below the 4 mg/L threshold for *P. aeruginosa*). As expected, the ancestral strain showed intrinsic resistance to Ampicillin, consistent with the known intrinsic resistance of *P. aeruginosa* to this antibiotic class (EUCAST Expert Rules, 2026b). Based on all available MIC data, the ancestral strain does not meet MDR criteria, defined as resistance to agents in three or more antibiotic classes (Magiorakos, *et al.*, 2012).

Given the inconsistency of Colistin results between assays and the superior reproducibility of Polymyxin B, the latter was selected for the PAS assay. Although Colistin is the clinically used agent for chronic *P. aeruginosa* suppression in CF, including in Danish practice, Polymyxin B shares the same outer-membrane disruption mechanism and was therefore considered a valid mechanistic proxy. Colistin is administered clinically as colistimethate sodium, an inactive prodrug converted to active colistin *in vivo*, whereas Polymyxin B is active as administered; both compounds share the same pharmacodynamic target and mode of action, making direct comparison appropriate (Nation and Li, 2009).

MICs were tested on all clones from the evolutionary assay (Table 5.11) to assess resensitisation to the antibiotic. Most cocktail-treated clones (all but one) displayed resensitisation, as indicated by OD values at or below the ancestral threshold (green). All clones exposed to phage 14/1 were resensitised. Following PA5P2 exposure, two clones were fully resensitised, while two others had OD values just above the cutoff, indicating they were close to the threshold but did not formally meet it. Similarly, one clone exposed to DMS3virAcrFI was resensitised, with three additional clones near the boundary. In contrast, no clones from the no-treatment group were resensitised, although three had OD values approaching the resensitisation threshold. These results demonstrate that phage exposure, particularly with cocktails or 14/1, frequently restores antibiotic sensitivity in evolved clones.

To determine PAS a growth-based checkerboard assay was performed to assess the combined effects of phage cocktail C and polymyxin B on *P. aeruginosa* strain 342 clones (Methods 2.17). Endpoint inhibition data were used to generate a combined heatmap showing percent inhibition and calculated FICI values (Figure 5.12).

Across the matrix, growth inhibition was detected in the majority of treatment combinations (Figure 5.12, left panel). At MOI = 0 (antibiotic alone), inhibition ranged from 64.9% to 78.9% across all antibiotic concentrations tested, and did not reach 90% at any concentration, consistent with sub-MIC to near-MIC antibiotic exposure in the absence of phage. At MOI ≥ 0.156, inhibition increased markedly, reaching 91.9–93.8% across all antibiotic concentrations at the lowest phage MOI tested. This high level of inhibition was maintained at MOIs of 0.316 and 0.625, with values between 90.1% and 93.9%. At intermediate MOIs (1.25–2.5), inhibition at antibiotic = 0 was somewhat lower (81.5% and 86.4% respectively), rising to 88.5–93.2% in the presence of antibiotic. At higher MOIs (5 and 10), inhibition at antibiotic = 0 was 83.3% and 80.1% respectively, and did not consistently increase with the addition of antibiotic, with the MOI = 10 row showing values between 72.3% and 88.6%, lower than those observed at intermediate MOIs. The overall pattern indicates that bacterial inhibition was driven predominantly by phage rather than antibiotic across the concentration range tested, with antibiotic contributing little additional suppression once phage was present at MOI ≥ 0.156.

FICI values were calculated using the measured Polymyxin B MIC of 0.761 µg/mL and a phage MIC of MOI 0.156, the lowest MOI achieving ≥ 90% inhibition in phage-only wells (Figure 5.12, right panel). FICI values ranged from 1.00 at the lowest phage and antibiotic concentrations (MOI 0.156, 0.012 µg/mL) to 73.63 at the highest (MOI 10, 7.25 µg/mL). The single combination approaching indifference (FICI = 1.00–1.02) occurred only at MOI 0.156 with the two lowest antibiotic concentrations. All remaining combinations produced FICI

values substantially above 2.0, consistent with antagonism by standard criteria. The predominantly antagonistic interaction is most likely attributable to a ceiling effect: phage cocktail C alone achieves near-maximal bacterial inhibition (>90%) at MOI ≥ 0.156, leaving insufficient residual growth for antibiotic to contribute additively to the combined response. Under these conditions, FICI arithmetically inflates as higher MOIs and antibiotic concentrations are added to an already-saturated inhibitory effect, rather than reflecting a pharmacodynamic antagonism in the classical sense.

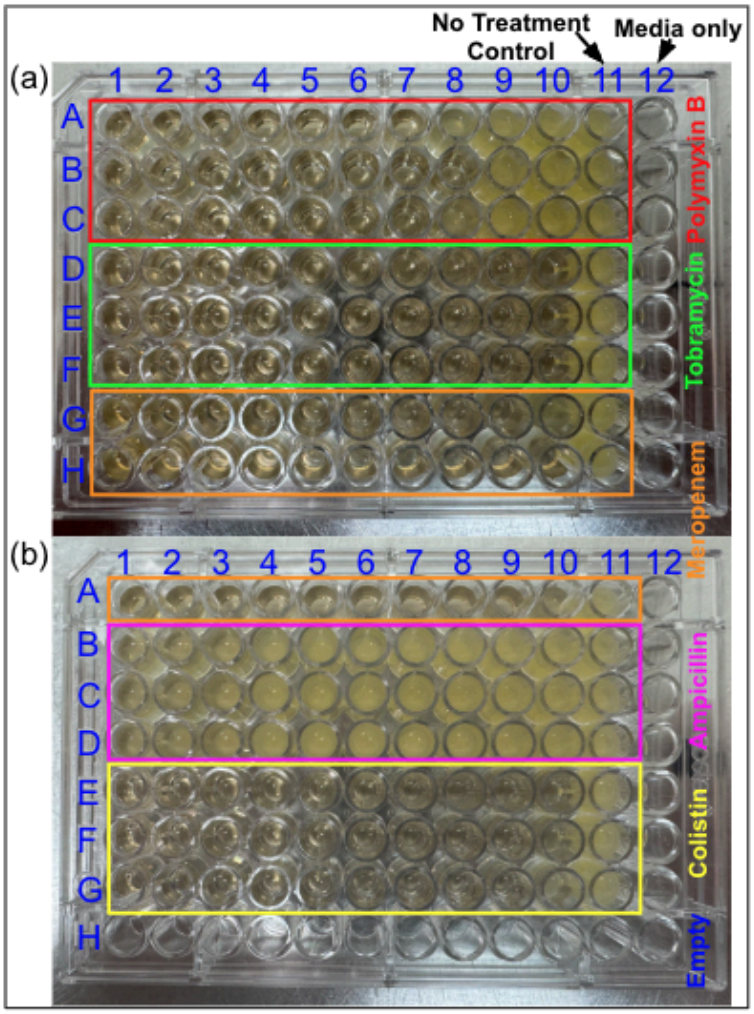

Figure 5.11: Images of MIC assay plates for 5 antibiotics tested against the ancestral clinical *P. aeruginosa* strain 342. Treatment groups are indicated by coloured boxes with antibiotic labels on the right of each panel: Polymyxin B (red, rows A–C, panel a), Tobramycin (green, rows D–F, panel a), Meropenem (orange, rows G–H panel a and row A panel b), Ampicillin (pink, rows B–D, panel b), and Colistin (yellow, rows E–G, panel b). Column 11 is the no-treatment positive control and column 12 is the media-only negative control. Turbid wells indicate bacterial growth; clear wells indicate growth inhibition at or above the MIC for that antibiotic concentration. Wells in column 12 may appear visually similar to inhibited wells due to the absence of bacterial turbidity, though media is present. Row H in panel (b) was not used.

Figure 5.11: MIC assay results for clones from the evolutionary experiment. OD_{600} values at five antibiotic concentrations (C2–G2) are shown relative to the ancestral (ANC) strain. Green indicates that the clone showed OD values at or below the ancestral strain threshold, suggesting relative resensitisation compared to the ancestral strain, while red indicates OD values above the ancestral threshold, suggesting persistence of resistance. This is a relative comparison to the ancestral strain and does not represent clinical susceptibility classification according to EUCAST breakpoints..

Strain	Evo Treatment	0.390625 µg/mL	0.1953125 µg/mL	0.09765625 µg/mL	0.048828125 µg/mL	0.0244140625 µg/mL
ANC		0.109	0.176	0.702	1.450	1.598
F1	Cocktail	0.155	0.177	1.116	1.232	1.292
F2	Cocktail	0.154	0.512	1.302	1.417	1.455
F3	Cocktail	0.150	0.143	0.911	1.288	1.244
F4	Cocktail	0.179	0.177	0.555	1.709	1.318
F5	Cocktail	0.197	0.696	1.265	1.592	1.737
F6	Cocktail	0.561	0.557	1.497	1.551	0.821
F7	14/01	0.145	0.360	1.250	1.408	1.386
F8	14/01	0.153	0.499	0.985	1.628	1.689
F9	14/01	0.142	0.291	1.017	1.569	1.688
F10	14/01	0.145	0.289	1.270	1.627	1.688
F11	14/01	0.138	0.364	0.883	1.450	1.782
F12	14/01	0.144	0.165	0.893	1.394	1.297
G1	PA5P2	0.150	0.143	0.377	1.243	1.495
G2	PA5P2	0.145	0.147	0.736	1.528	1.616
G3	PA5P2	0.162	0.425	1.111	1.615	1.728
G4	PA5P2	0.147	0.328	0.653	1.461	1.656
G5	PA5P2	0.104	0.296	0.890	1.394	1.528
G6	PA5P2	0.122	0.334	0.334	0.990	1.467
G7	DMS3vir AcrFI	0.112	0.315	0.762	1.475	1.533
G8	DMS3vir AcrFI	0.105	0.315	0.795	1.324	1.646
G9	DMS3vir AcrFI	0.107	0.153	0.577	1.353	1.343

Table 5.11 Continued						
Strain	**Evo Treatment**	**0.390625 µg/mL**	**0.1953125 µg/mL**	**0.09765625 µg/mL**	**0.048828125 µg/mL**	**0.0244140625 µg/mL**
G10	DMS3vir AcrFI	0.157	0.391	1.045	1.369	1.511
G11	DMS3vir AcrFI	0.103	0.266	0.664	1.322	1.680
G12	DMS3vir AcrFI	0.105	0.103	0.756	1.323	1.476
H1	No Treatment	0.101	0.250	0.582	1.451	1.675
H2	No Treatment	0.108	0.138	0.625	1.452	1.557
H3	No Treatment	0.101	0.291	0.920	1.387	1.478
H4	No Treatment	0.100	0.097	0.785	1.357	1.391
H5	No Treatment	0.096	0.133	0.620	1.212	1.633
H6	No Treatment	0.106	0.418	0.752	1.421	1.579

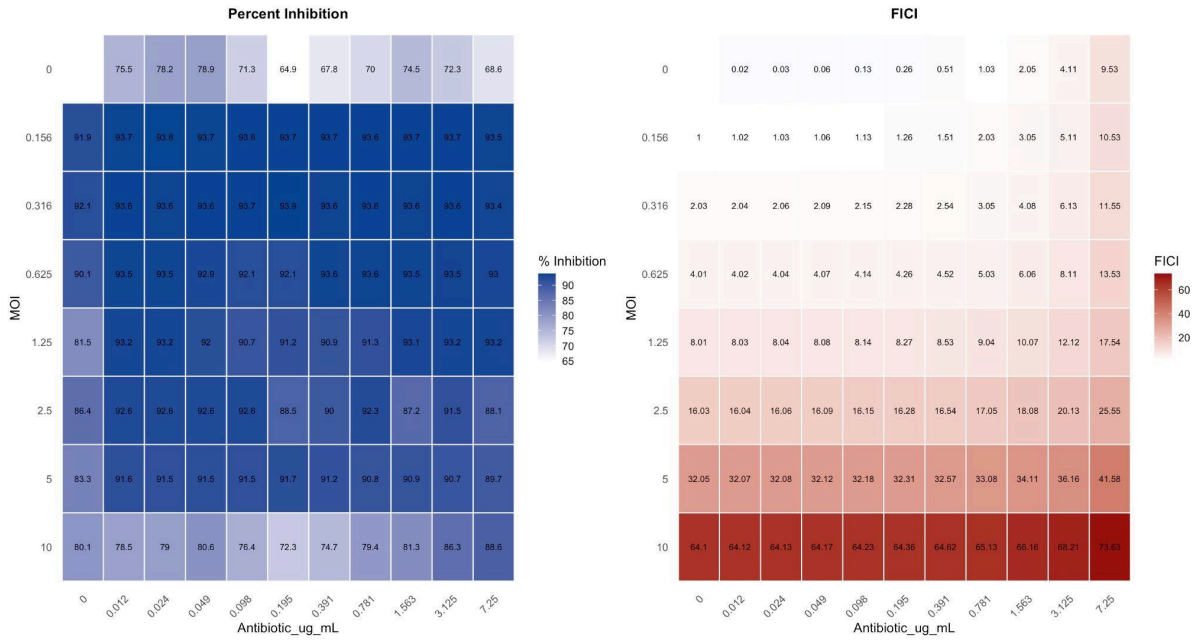

Figure 5.12: Combined heatmap of percent inhibition and fractional inhibitory concentration index (FICI) values for *P. aeruginosa* strain 342 exposed to phage cocktail C and polymyxin B. Checkerboard assays were performed using serial twofold dilutions of polymyxin B (0–7.25 µg/mL) and phage cocktail C (MOI = 0–10). Bacterial growth was monitored by OD_{600} measurement, and endpoint values were converted to percent inhibition relative to untreated controls. The left panel shows percent inhibition for each concentration combination, with darker shades representing greater inhibition. The right panel displays FICI values (FICI = FIC_antibiotic + FIC_phage), calculated using a measured Polymyxin B MIC of 0.761 µg/mL and a phage MIC of MOI 0.156. FICI ≤ 0.5 indicates synergy, 0.5–1.0 additivity, 1.0–2.0 indifference, and > 2.0 antagonism.The predominantly antagonistic FICI values observed are likely attributable to a ceiling effect, whereby phage Cocktail C alone achieves near-maximal inhibition at MOI ≥ 0.156, arithmetically inflating FICI values rather than reflecting true pharmacodynamic antagonism.

5.4 Discussion

This study provides a comprehensive, multi-layered analysis of *P. aeruginosa* adaptation to phage pressure under conditions reflecting clinical isolates. By combining longitudinal growth assays, clonal resistance confirmation, WGS, and PAS testing, it becomes possible to dissect both the evolutionary trajectories of bacterial populations and the mechanistic basis of resistance emergence. The findings highlight the dual nature of phage therapy: while multi-phage cocktails can strongly suppress bacterial growth, they also impose selective pressures that drive adaptive responses, including receptor modification, envelope remodeling, stress-response activation, and engagement of intrinsic defense systems. Understanding these mechanisms is essential for the rational design of durable and clinically relevant phage-based interventions.

5.4.1 Phage Cocktail Suppression Dynamics

Across multiple 48-hour windows during the two-week experimental evolution, Cocktail C demonstrated the most robust and sustained suppression of strain 342 when compared to no treatment and individual phage treatments. At nearly every measured time point, optical density readings were significantly lower than in untreated controls, and cumulative area-under-curve analyses confirmed a strong, statistically significant inhibitory effect (estimate ≈ –39.68, $p < 0.0001$). These results align with current literature and evidence suggesting that phage cocktails targeting different bacterial receptors reduce the speed of resistance emergence (Feng *et al.*, 2025; Lourenço *et al*., 2020). The combination of targeting distinct bacterial receptors and employing multiple phage types likely explains the prolonged suppression observed, in line with recent studies showing that multi-phage therapies are more effective than single-phage treatments at both delaying resistance and improving bacterial clearance (Liang *et al.*, 2023; Martinez-Soto *et al.*, 2024).

Nevertheless, the suppression was not uniform across all tested strains. Strains 203.1 and 413 exhibited more variable growth trajectories under cocktail treatment, often showing levels indistinguishable from untreated controls in many 48-hour windows. This modest suppression in strain 203.1 contrasts with the increased growth observed when exposed to Cocktail C at MOI 0.1 in the Chapter 4 validation assay (Figure 4.11), which may reflect differences in experimental conditions between the two assays, including the use of SCFM versus LB broth, the continuous serial transfer design of the evolutionary assay, and potential adaptation of the bacterial population across the 14-day experimental period. It should also be noted that the decline in OD observed in no-treatment control cultures after approximately 16–24 hours is consistent with normal entry into death phase, likely resulting from nutrient depletion, oxygen limitation, and accumulation of inhibitory metabolic by-products in the closed microplate environment, rather than any treatment effect. This inter-strain heterogeneity likely reflects inherent differences in genetic background, baseline membrane composition, and intrinsic phage sensitivity. Such variation mirrors findings from Castledine *et al.* (2022) and Majkowska‑Skrobek *et al*. (2021), who documented strain-dependent differences in phage resistance dynamics and associated virulence trade-offs. The observed variability underscores the challenge of designing universally effective phage cocktails and suggests that adaptive or strain-tailored approaches may be necessary to maximise clinical efficacy.

5.4.2 Clonal Resistance and Gene-Level Mechanisms

Clonal CoR assays revealed distinct patterns depending on phage treatment. Single-phage treated clones predominantly displayed resistance specific to their selecting phage, while cocktail-evolved clones often exhibited broader cross resistance. WGS provided mechanistic insight, revealing mutations across multiple functional categories, including envelope biosynthesis, receptor modification, stress response and repair, and defense system components.

Mutations in *galU, rfbB, and rfaB* were recurrent among cocktail-evolved clones, suggesting that LPS and outer membrane remodeling are central to phage resistance. *galU*, encoding UTP–glucose-1-phosphate uridylyltransferase, is critical for LPS core biosynthesis (Ramjeet *et al.*, 2008); *rfbB* encodes dTDP-glucose 4,6-dehydratase (Chakraborty *et al*., 2025), and *rfaB* is a glycosyltransferase involved in cell wall construction (Pradel *et al.*, 1992). Alterations in these genes likely reduce phage adsorption while simultaneously influencing antibiotic susceptibility, as changes in LPS structure can increase outer-membrane permeability to cationic antimicrobials like polymyxin B. These observations are consistent with previous work indicating that LPS modifications often produce pleiotropic effects on resistance and fitness (Burmeister *et al.*, 2020; Castledine *et al.*, 2022; Nagy *et al.*, 2022).

Mutations in *arnE*, a putative 4-amino-4-deoxy-L-arabinose-phosphoundecaprenol flippase, suggest additional surface modifications via the type II secretion system, potentially preventing phage attachment to specific receptors (Liang, *et al.*, 2023). This adaptation further illustrates the importance of envelope remodeling in multi-phage environments. Similar phenomena have been observed in other studies, where envelope modifications simultaneously reduced phage susceptibility and altered antibiotic responses (Wang *et al.*, 2021; Bulssico *et al*., 2025).

T4P mutations were prominent in clones exposed to PA5P2. Genes such as *pilB, pilT, pilQ*, and *pilY1* were frequently mutated or deleted. T4P functions as a major phage receptor, and modification of these structures confers resistance to pilus-targeting phages. However, such mutations are known to compromise motility, biofilm formation, and host colonisation, representing a predicted evolutionary trade-off based on the established functions of these genes (Tan *et al.*, 2014; Hendrix *et al.*, 2024). The repeated occurrence of T4P mutations demonstrates the predictability of receptor-mediated escape mechanisms under selective phage pressure, consistent with findings from Tan *et al*. (2014) and Hendrix *et al*. (2024).

Stress-response and repair pathways also contributed to adaptive survival. SNPs in *lon, rtcB*, and *gcvR* were observed across multiple cocktail-evolved clones. *lon*, an ATP-dependent

protease, maintains protein quality under stress (Yigit and Chien, 2025); *rtcB* repairs tRNA damage that may result from lytic phage activity (Tanaka *et al.*, 2011), while *gcvR* regulates the glycine cleavage system, indirectly influencing cell-surface composition (Ghrist *et al.*, 2001). These mutations likely enhance survival in the presence of lytic phages and may synergize with envelope modifications to stabilize resistant phenotypes (Castledine *et al*., 2022; Hampton *et al.*, 2020).

Defense-island and prophage-related genes were also frequently affected. Cytochrome c domain-containing proteins and prophage tail assembly genes exhibited recurrent mutations. These systems can provide defense against superinfection, alter phage receptor availability, and contribute to inter-bacterial competitive advantage (Chertkova *et al*., 2023; , 2018; He *et al*., 2024). For example, prophage tail assembly mutations can prevent the assembly of competing phage particles, a phenomenon that confers a selective benefit in multi-phage contexts (Patel *et al.*, 2024). Analysis of independent clones reveals treatment-specific patterns: of the 6 cocktail-treated clones, mutations in LPS biosynthesis genes (*galU, rfbB, rfaB*) were observed in 4 clones (F1, F3, F5, F6), cytochrome c domain defense island mutations in 5 clones, and T4P-associated mutations in 1 clone (F5, *pilY1*), demonstrating the multi-layered nature of cocktail-driven resistance. In contrast, PA5P2-treated clones predominantly accumulated T4P mutations (*pilB, pilT, pilQ* — present in 5 of 6 clones), while 14/1-treated clones showed recurrent *galU* mutations (3 of 4 clones). The recurrent targeting of cytochrome c domain loci across all treatment groups indicates convergent evolution, whilst LPS and T4P mutations show treatment-specific patterns consistent with receptor-mediated selective pressure (Burmeister *et al.*, 2020; Castledine *et al.*, 2022).

5.4.3 Growth Curve Dynamics and Optical Density Anomalies

Occasionally, treatment with phage 14/1 resulted in higher OD_{600} readings than in untreated controls. Such counterintuitive observations may arise from lysis-mediated debris accumulation, optical scattering effects, or ecological release, in which phage-sensitive subpopulations are removed, allowing resistant or faster-growing subpopulations to expand. These findings underscore the limitations of relying solely on OD_{600} as a growth metric and highlight the value of complementary methods such as CFU enumeration or PFU assays to confirm population dynamics.

5.4.4 Phage–Antibiotic Synergy

PAS experiments combining Cocktail C with Polymyxin B demonstrated strong bacterial inhibition across the concentration grid, with percent inhibition exceeding 90% at MOI ≥ 0.156 across most antibiotic concentrations. However, FICI analysis, calculated using the

measured Polymyxin B MIC of 0.761 µg/mL, indicated predominantly antagonistic interactions across the concentration range tested (FICI > 2.0 in the majority of combinations). This is most likely attributable to a ceiling effect: Cocktail C alone achieves near-maximal inhibition at low MOIs, leaving insufficient residual bacterial growth for antibiotic to contribute additively to the combined response (Gu Liu *et al*., 2020; Abedon, 2019). Under these conditions FICI values arithmetically inflate as concentrations increase, rather than reflecting classical pharmacodynamic antagonism. Mechanistically, phage-induced LPS remodelling, as evidenced by recurrent mutations in *galU, rfbB*, and *rfaB* in cocktail-evolved clones, may increase outer-membrane permeability to cationic antimicrobials such as polymyxin B, suggesting that evolutionary trade-offs could be exploited therapeutically even where strict additive or synergistic FICI values are not observed. The long-term evolutionary consequences of combined phage–antibiotic pressure remain uncertain, as dual selective pressures could favour the emergence of mutants resistant to both agents, emphasising the need for adaptive dosing strategies to maintain sustained efficacy (Torres-Barceló and Hochberg, 2016; Xuan *et al*., 2022; Tagliaferri *et al.*, 2019).

5.4.5 Evolutionary Dynamics and Trade-Offs

Resistance under cocktail pressure emerged via multiple convergent mechanisms, including envelope remodeling, receptor modification, and activation of stress-response and defense systems. While these adaptations confer immediate survival advantages, they frequently incur trade-offs, such as impaired motility, altered virulence, or increased antibiotic sensitivity. These pleiotropic effects illustrate predictable evolutionary trajectories and suggest that therapeutic strategies could exploit trade-offs, for example by coupling phage therapy with sub-inhibitory antibiotic doses to enhance suppression; however, the heterogeneous physiology of the CF lung, including variable mucus viscosity, oxygen gradients, and antibiotic penetration, means that sub-inhibitory concentrations *in vitro* may not translate predictably *in vivo*, and could risk selecting for antibiotic resistance in poorly penetrated regions of the lung rather than enhancing phage efficacy (Döring *et al*., 2012) The findings underscore the need for adaptive phage therapy approaches, including periodic cocktail redesign, dynamic updating of phage composition, and real-time monitoring of resistance emergence (Xuan *et al.*, 2022; Torres-Barceló and Hochberg, 2016).

5.4.6 Biofilm and *In Vivo* Relevance

This study relied on planktonic cultures, which do not capture the spatial complexity, nutrient gradients, and heterogeneous phage penetration characteristic of biofilm-associated

infections, such as those in CF lungs (Testa *et al.*, 2019). Biofilm architecture can alter selective pressures, reduce phage penetration, and enable coexistence of sensitive and resistant subpopulations, potentially affecting resistance trajectories and treatment efficacy. Translational studies incorporating biofilm or structured-growth models will be essential to evaluate the clinical relevance of the observed evolutionary patterns (Chang *et al.*, 2022).

5.4.7 Future Research

While this study provides detailed insights into *P. aeruginosa* adaptation under phage pressure, numerous avenues remain to explore in order to extend these findings to clinically relevant contexts. One critical area is the application of population-level genomics through deep sequencing of evolving bacterial populations. By sequencing entire populations at multiple timepoints, rather than only selected clones, it is possible to resolve the dynamics of selective sweeps, clonal interference, and parallel adaptation. Such data would allow precise tracking of mutation emergence, quantify lineage frequencies, and reveal whether resistance evolves via sequential fixation of single mutations or through coexisting subpopulations carrying distinct adaptive changes. This approach would also clarify whether mutations observed in this study, such as those affecting LPS biosynthesis or T4P, consistently dominate the population or coexist with other resistance strategies.

Functional validation of specific mutations is another important research direction. Targeted knockout or knock-in studies using CRISPR-Cas or other genetic tools could elucidate the causal effects of envelope-modifying genes (*galU, rfbB, rfaB, arnE*), T4P-related genes (*pilB, pilT, pilQ, pilY1*), and defense-island loci on phage susceptibility, fitness, and antibiotic sensitivity. Similarly, dissecting the roles of prophage-associated tail assembly proteins and stress-response genes (*lon, rtcB, gcvR*) would clarify how intrinsic defense systems and stress repair pathways contribute to survival under multi-phage exposure. Such functional studies could provide a mechanistic framework linking specific genetic changes to phenotypic outcomes observed in both growth curves and PAS assays.

Expanding PAS testing across additional clinical isolates and antibiotic classes represents another critical avenue for future research. In the current study, only strain 342 was evaluated with polymyxin B, yet strain-to-strain heterogeneity in both phage sensitivity and antibiotic susceptibility suggests that optimal phage–antibiotic combinations may differ across clinical backgrounds. Evaluating combinations with aminoglycosides, β-lactams, or other last-resort antibiotics, in addition to polymyxin B, would enhance the generalisability of findings and inform potential therapeutic regimens. Testing PAS under varying MOIs and

sub-inhibitory concentrations could also reveal the range of parameter spaces where synergistic interactions emerge and whether these are robust to evolutionary adaptation.

Another essential focus is the incorporation of biofilm and structured-growth models. Biofilm-associated infections, particularly in CF lungs, present spatial gradients, nutrient limitations, and heterogeneous phage penetration that are not captured in planktonic cultures. Modeling these conditions *in vitro* through biofilm reactors, microfluidics, or agar-based structured environments could reveal how spatial constraints influence the emergence of resistance, the distribution of mutations, and the efficacy of PAS. These studies may uncover adaptive strategies unique to structured communities, including the maintenance of subpopulations with distinct resistance mechanisms or the evolution of cooperative behaviors that mitigate phage impact.

Adaptive phage therapy strategies remain a promising area for further investigation. Sequential or alternating phage–antibiotic dosing regimens, periodic cocktail redesign, and real-time genomic monitoring could help prevent or delay resistance. Phage training, where phages are co-evolved with resistant bacterial populations before therapeutic deployment, offers another avenue to enhance long-term efficacy. Studies have shown that trained phages can outperform naïve phages in suppressing resistant populations both *in vitro* and *in vivo* (Borin *et al.*, 2021), suggesting that dynamic updating of phage cocktails may be essential for chronic infections. Further research should explore how these strategies can be integrated with PAS to exploit evolutionary trade-offs, particularly where envelope remodeling or receptor modification increases susceptibility to antibiotics.

Finally, combining these experimental approaches with predictive evolutionary modeling could provide actionable insights for clinical translation. Computational models integrating mutation rates, fitness costs, pleiotropic trade-offs, and spatial dynamics could forecast resistance trajectories and inform adaptive therapy schedules. Such modeling, validated against experimental data, would allow the design of interventions that anticipate bacterial evolution rather than react to it, enhancing the robustness of phage-based strategies in treating MDR infections. The limited predictive success of the cocktail design tool used in this study may reflect insufficient parameterisation, as the algorithm was based primarily on host range data without incorporating fitness costs, resistance mutation rates, or phage-phage interaction dynamics. Alternatively, a three-phage cocktail may provide insufficient receptor diversity to prevent the emergence of multi-resistant clones, particularly in a pathogen as adaptable as *P. aeruginosa*; future cocktail design tools would benefit from integrating evolutionary parameters alongside host range data to improve translational accuracy. Collectively, these research directions aim to bridge mechanistic insights from laboratory

studies with clinically actionable strategies, advancing the development of evolutionarily informed, adaptive phage therapies.

P. aeruginosa adapts to phage cocktail pressure through a combination of receptor modification, envelope remodeling, stress-response activation, and defense-system engagement. The recurrence of mutations in the same genes across multiple independently evolved clones, such as *galU* in 3 of 4 clones treated with phage 14/1 and cytochrome c domain mutations across all treatment groups, provides evidence against coincidental mutation, as the probability of identical mutations arising independently in multiple clones by chance is low; this convergent pattern is consistent with strong positive selection at these loci under phage pressure (Tenaillon, 2014). These mechanisms generate predictable evolutionary trajectories while imposing trade-offs that may be exploited therapeutically, such as increased antibiotic susceptibility. Recognizing and utilising these dynamics is critical for designing adaptive, evolutionarily informed phage therapies capable of delaying resistance emergence.

5.5 Conclusion

Phage cocktail therapy effectively suppresses clinical *P. aeruginosa*, but resistance evolves through multiple convergent pathways, including receptor modification, envelope remodeling, and engagement of intrinsic defense systems, as revealed by clone level profiling. Integration of evolutionary assays, clonal analysis, WGS, and PAS testing provides a detailed framework linking genotype to phenotype. Observed trade-offs between phage resistance and antibiotic susceptibility highlight opportunities for combined therapeutic strategies. Adaptive approaches, including cocktail redesign, genomic monitoring, biofilm modeling, and phage training, are essential for maximizing efficacy, anticipating resistance, and guiding clinical translation.

6. General Discussion

This study provides a comprehensive, multi-layered evaluation of phage therapy against clinical *P. aeruginosa* isolates from pwCF, integrating phage characterisation, cocktail design, and evolutionary dynamics under selective pressure. The first data chapter (Chapter 3) aimed to characterise phages with bactericidal activity against clinical *P. aeruginosa*, examining phage clearance profiles, bacterial lineage, antibiotic resistance profiles of the clinical strains, length of infection, and biofilm interactions. Across 49 phages and 93 clinical isolates, every strain was susceptible to at least one phage, and all phages were able to infect at least one clinical isolate, demonstrating broad-spectrum infectivity. These findings are consistent with previous work highlighting the extensive diversity and host-range potential of *P. aeruginosa* phages (Rieper *et al.*, 2025; Nordstrom *et al.*, 2022). It should be noted, however, that the phage collection used in this study was not randomly assembled but comprised phages selected or previously characterised for their activity against *P. aeruginosa*, which may have contributed to the broad coverage observed and should be considered when generalising these findings to uncharacterised phage collections. Notably, the absence of a relationship between length of infection and phage susceptibility contrasts with early *in vivo* studies in mice showing reduced efficacy when phages were administered post-infection (Watanabe *et al.*, 2007), yet aligns with later work demonstrating effective clearance of established infections, including biofilm-associated bacteria, up to several days post-inoculation (Elfadadny *et al.*, 2024). This discrepancy underscores the impact of host factors such as immune response, mucus barriers, and pharmacokinetics, which are absent in *in vitro* models but critical *in vivo*.

Antibiotic resistance increased with length of infection for most drugs, confirming the well-documented evolutionary trajectories of chronic CF infections (Perikleous *et al.*, 2023). Interestingly, phage susceptibility did not correlate with antibiotic resistance, emphasizing the mechanistic independence of phage and antibiotic modes of action and supporting concurrent or sequential phage–antibiotic strategies (Gliźniewicz *et al.*, 2025). Biofilm assessments revealed that phages were generally more effective at preventing biofilm formation than disrupting established biofilms, consistent with prior reports that phage-mediated prevention of aggregate formation is more achievable than post-establishment eradication (Darch *et al.*, 2017; Hosseinidoust *et al.*, 2013). Instances of paradoxical biofilm increases in response to phage exposure likely reflect stress-induced biofilm formation or selection for resistant subpopulations, highlighting the complex and context-dependent nature of phage–biofilm interactions. It should also be considered that the experimental design did not involve removal of planktonic bacteria prior to phage addition in

the disruption assay, meaning that phage-mediated lysis of planktonic cells may have contributed to increased eDNA and cellular debris in the well, potentially fuelling biofilm matrix stabilisation and artificially inflating crystal violet staining readings, as discussed in Section 3.4.

Building on these findings, Chapter 4 leveraged clearance and biofilm profiles to design broad-spectrum ‘first-line’ phage cocktails, aiming to provide immediate empirical coverage while personalised phage therapy is prepared. However, it should be acknowledged that empirical phage exposure prior to personalised therapy carries the risk of priming resistance mechanisms, particularly broad cross-resistance mutations affecting surface receptors such as LPS and T4P, which could potentially render components of a subsequent personalised cocktail ineffective. This risk could be mitigated by designing empirical cocktails that target receptors with high fitness costs upon mutation, maximising the evolutionary trade-offs that maintain bacterial susceptibility to follow-on personalised treatment (Betts *et al.*, 2013). Computational design prioritised receptor diversity, combining LPS and T4P targeting phages to maximise host-range coverage (Díaz-Galián *et al.*, 2022; Rosanna *et al.*, 2022). Empirical testing, however, revealed limitations: cocktail efficacy was strongly dependent on MOI, with the nominal MOI of 0.001 corresponding to an effective phage-to-bacteria ratio of ~10^{-6} due to a miscalculation, and low-MOI treatments producing minimal suppression and occasional paradoxical growth stimulation. Such findings align with theoretical predictions that insufficient phage-to-bacterium ratios can fail to sustain infection cycles and may induce stress-mediated biofilm responses (Payne *et al.*, 2000; Abedon *et al.*, 2017). It is also relevant to consider that *P. aeruginosa* reaches densities of 10^{7}–10^{10} CFU/mL within CF airway sputum *in vivo* (Palmer *et al.*, 2005; Lyczak *et al.*, 2000), meaning that even a correctly calculated MOI of 0.001 may be insufficient to achieve therapeutic phage concentrations in the clinical lung environment, further underscoring the importance of MOI optimisation for translational phage therapy. High-MOI treatments improved planktonic suppression but did not substantially enhance biofilm clearance, reflecting the inherent density, spatial heterogeneity, and structural resilience of CF-associated biofilms (Harper *et al.*, 2014; Testa *et al.*, 2019). These results reinforce the need for cocktails incorporating phages with strong depolymerase activity or enzymatic adjuncts, or for combined phage–antibiotic strategies targeting EPS (Topka-Bielecka *et al.*, 2021; Namonyo *et al.*, 2023).

Despite computational predictions, designed cocktails did not consistently outperform randomly assembled mixtures, echoing reports that theoretical host-range coverage does not always translate into empirical superiority, particularly under low phage titres or

heterogeneous strain panels (Yu *et al.*, 2024). These observations suggest that empirical validation remains essential, and that dosing strategies, receptor competition, and strain-specific interactions can dominate outcomes. Furthermore, categorising phages solely by biofilm-prevention versus disruption phenotypes did not reliably predict cocktail performance, highlighting the limitations of functional classification in isolation and emphasising the necessity of empirical testing against diverse clinical isolates (Harper *et al.*, 2014; Azeredo *et al.*, 2017).

Chapter 5 explored evolutionary dynamics under single-phage and cocktail selection, as well as PAS with sub-inhibitory polymyxin B. Resistance evolved predictably via receptor modification, envelope remodelling, and activation of stress-response and defense systems; whilst fitness trade-offs such as reduced motility or altered antibiotic susceptibility are predicted based on the functional roles of the mutated genes, these phenotypes were not directly measured in this study and represent inferred rather than confirmed outcomes. While these phenotypes were not directly tested in this study, they are inferred based on the functional roles of the genes identified (Castledine *et al.*, 2022; Bulssico *et al.*, 2025). LPS biosynthesis genes (*galU, rfbB, rfaB*) and T4P-associated genes (*pilB, pilT, pilQ, pilY1*) were recurrently mutated, confirming receptor-mediated escape as a major adaptive pathway. All mutations in these genes were confirmed as non-synonymous, predicting functional amino acid changes, and were absent from no-treatment control clones sequenced in parallel, supporting their selection under phage pressure.

The CoR assay (Figures 5.9 and 5.10) provided additional insight at the clonal level, revealing that while single-phage-evolved clones generally exhibited resistance only to their selecting phage, cocktail-evolved clones displayed broader or cross-resistance profiles. It should be noted that not all identified SNPs were non-synonymous; synonymous variants were also present and may reflect hitchhiking mutations rather than direct adaptive responses to phage pressure, as discussed in Section 5.4. These data highlight that resistance mechanisms selected under cocktail pressure are often multifactorial, involving combinations of receptor modification and activation of intrinsic defense systems such as cytochrome c domain proteins, which are associated with defense islands and may contribute to phage resistance through redox-mediated interference with phage replication or membrane integrity (Chertkova *et al.*, 2023), prophage tail assembly proteins and type VI secretion elements. This aligns with genomic evidence that cocktail-treated clones accumulated a wider diversity of mutations than single-phage treatments, suggesting that multi-phage exposure promotes simultaneous engagement of multiple defense layers rather than reliance on a single receptor-based mechanism.

PAS experiments demonstrated strong phage-driven inhibition across the checkerboard concentration grid, though FICI analysis indicated predominantly antagonistic interactions attributable to a ceiling effect rather than classical pharmacodynamic synergy, illustrating nonetheless the potential to exploit phage-induced evolutionary trade-offs, particularly LPS remodelling, for therapeutic gain, and supporting the integration of adaptive phage–antibiotic strategies in chronic infection management (Xuan *et al.,* 2022; Tagliaferri *et al.*, 2019; Liang *et al*., 2023).

Collectively, these findings situate phage therapy within a broader translational and mechanistic framework, highlighting the interplay between bacterial genetics, biofilm architecture, phage diversity, and selective pressures. They demonstrate that broad-spectrum cocktails can provide a first-line empirical intervention, yet their efficacy is strongly context-dependent, requiring high phage titres, careful consideration of biofilm-targeting activity, and iterative empirical optimisation. Resistance evolution is predictable but strain-specific, underscoring the importance of monitoring adaptive trajectories and leveraging trade-offs, for example through PAS or phage training (Borin *et al.*, 2021).

Future work should incorporate structured-growth and microfluidic biofilm models, *in vivo* validation, high-resolution population-level genomics, and real-time adaptive therapy frameworks to translate these findings into clinically robust, evolutionarily informed phage interventions for CF and other chronic infections. Additionally, future studies could address some of the current project's limitations, such as reliance on planktonic culture, limited strain representation, and analysis of only endpoint clones, by integrating population-level sequencing across timepoints to capture evolutionary trajectories more dynamically. Functional validation of key resistance-associated genes (e.g. *galU, pilB, arnE*) through targeted mutagenesis or complementation assays would also clarify causal mechanisms linking genotype to phenotype.

7. References

Abedon, S.T., *et al.* (2011) Phage treatment of human infections. *Bacteriophage*, 1(2), pp.66–85. [Online]. Available at: https://doi.org/10.4161/bact.1.2.15845 [Accessed 29 October 2025].

Abedon, S.T., *et al.* (2017) Editorial: Phage therapy: past, present and future. *Frontiers in Microbiology*, 8, p.981. [Online]. Available at: https://doi.org/10.3389/fmicb.2017.00981 [Accessed 26 October 2025].

Abedon, S.T. (2019) Phage-antibiotic combination treatments: antagonistic impacts of antibiotics on the pharmacodynamics of phage therapy. *Antibiotics*, 8(4), p.182. [Online]. Available at: https://doi.org/10.3390/antibiotics8040182 [Accessed 10 March 2026].

Abedon, S.T., Danis-Wlodarczyk, K.M. and Wozniak, D.J. (2021) Phage cocktail development for bacteriophage therapy: toward improving spectrum of activity breadth and depth. *Pharmaceuticals*, 14(10), p.1019. [Online]. Available at: https://doi.org/10.3390/ph14101019 [Accessed 31 October 2025].

Abedon, S.T. (2012) Spatial vulnerability: bacterial arrangements, microcolonies, and biofilms as responses to low rather than high phage densities. *Viruses*, 4(5), pp.663–687. [Online]. Available at: https://doi.org/10.3390/v4050663

Ackermann, H.-W. (2009) Phage classification and characterization. In: Clokie, M.R.J. and Kropinski, A.M. (eds.) *Bacteriophages*. 501. Totowa, NJ: Humana Press, pp.127–140. [Online]. Available at: https://doi.org/10.1007/978-1-60327-164-6_13 [Accessed 29 October 2025].

Ács, N., Gambino, M. and Brøndsted, L. (2020) Bacteriophage enumeration and detection methods. *Frontiers in Microbiology*, 11, p.594868. [Online]. Available at: https://doi.org/10.3389/fmicb.2020.594868 [Accessed 31 October 2025].

Akkerman-Nijland, A.M., *et al.* (2021) The pharmacokinetics of antibiotics in cystic fibrosis. *Expert Opinion on Drug Metabolism & Toxicology*, 17(1), pp.53–68. [Online]. Available at: https://doi.org/10.1080/17425255.2021.1836157 [Accessed 29 October 2025].

Almeida, G.M.D.F., *et al.* (2024) Relevance of the bacteriophage adherence to mucus model for *Pseudomonas aeruginosa* phages. In: Tyne, D.V. (ed.) *Microbiology Spectrum*, 12(8), pp.e03520-23. [Online]. Available at: https://doi.org/10.1128/spectrum.03520-23 [Accessed 30 October 2025].

Alqasmi, M. (2024) Therapeutic interventions for *Pseudomonas* infections in cystic fibrosis patients: a review of phase IV trials. *Journal of Clinical Medicine*, 13(21), p.6530. [Online]. Available at: https://doi.org/10.3390/jcm13216530 [Accessed 16 March 2026].

Alseth, E.O., *et al.* (2019) Bacterial biodiversity drives the evolution of CRISPR-based phage resistance. *Nature*, 574(7779), pp.549–552. [Online]. Available at: https://doi.org/10.1038/s41586-019-1662-9 [Accessed 31 October 2025].

Alves, D.R., *et al.* (2016) A novel bacteriophage cocktail reduces and disperses *Pseudomonas aeruginosa* biofilms under static and flow conditions. *Microbial Biotechnology*, 9(1), pp.61–74. [Online]. Available at: https://doi.org/10.1111/1751-7915.12316 [Accessed 30 October 2025].

Andersson, D.I. and Hughes, D. (2010) Antibiotic resistance and its cost: is it possible to reverse resistance? *Nature Reviews Microbiology*, 8(4), pp.260–271. [Online]. Available at: https://doi.org/10.1038/nrmicro2319 [Accessed 31 October 2025].

Aoki, W. and Ueda, M. (2013) Characterization of antimicrobial peptides toward the development of novel antibiotics. *Pharmaceuticals*, 6(8), pp.1055–1081. [Online]. Available at: https://doi.org/10.3390/ph6081055 [Accessed 15 March 2024].

Armbruster, C.R., *et al.* (2024) Persistence and evolution of *Pseudomonas aeruginosa* following initiation of highly effective modulator therapy in cystic fibrosis. In: Lemon, K.P. (ed.) *mBio*, 15(5), pp.e00519-24. [Online]. Available at: https://doi.org/10.1128/mbio.00519-24 [Accessed 12 March 2026].

Asfour, H.Z. (2018) Anti-quorum sensing natural compounds. *Journal of Microscopy and Ultrastructure*, 6(1), pp.1–10. [Online]. Available at: https://doi.org/10.4103/JMAU.JMAU_10_18 [Accessed 11 February 2026].

Aslam, S., *et al.* (2020) Lessons learned from the first 10 consecutive cases of intravenous bacteriophage therapy to treat multidrug-resistant bacterial infections at a single center in the United States. *Open Forum Infectious Diseases*, 7(9), p.ofaa389. [Online]. Available at: https://doi.org/10.1093/ofid/ofaa389 [Accessed 26 October 2025].

Atkinson, R.M., *et al.* (2006) Chronic colonization with *Pandoraea apista* in cystic fibrosis patients determined by repetitive-element-sequence PCR. *Journal of Clinical Microbiology*, 44(3), pp.833–836. [Online]. Available at: https://doi.org/10.1128/JCM.44.3.833-836.2006 [Accessed 8 March 2024].

Azeredo, J. and Sutherland, I.W. (2008) The use of phages for the removal of infectious biofilms. *Current Pharmaceutical Biotechnology*, 9(4), pp.261–266. [Online]. Available at: https://doi.org/10.2174/138920108785161604.

Bae, H.-W., *et al.* (2025) *Pseudomonas aeruginosa* as a model bacterium in antiphage defense research. *FEMS Microbiology Reviews*, 49, p.fuaf014. [Online]. Available at: https://doi.org/10.1093/femsre/fuaf014 [Accessed 27 October 2025].

Balaban, N.Q., *et al.* (2013) A problem of persistence: still more questions than answers? *Nature Reviews Microbiology*, 11(8), pp.587–591. [Online]. Available at: https://doi.org/10.1038/nrmicro3076 [Accessed 15 March 2024].

Barrangou, R., *et al.* (2007) CRISPR provides acquired resistance against viruses in prokaryotes. *Science*, 315(5819), pp.1709–1712. [Online]. Available at: https://doi.org/10.1126/science.1138140 [Accessed 30 October 2025].

Bauernfeind, A., *et al.* (1987) Bacteriological effects of anti-*pseudomonas aeruginosa* chemotherapy in cystic fibrosis. *Infection*, 15(5), pp.403–406. [Online]. Available at: https://doi.org/10.1007/BF01647753 [Accessed 8 March 2024].

Bell, A., Bains, M. and Hancock, R.E. (1991) *Pseudomonas aeruginosa* outer membrane protein OprH: expression from the cloned gene and function in EDTA and gentamicin resistance. *Journal of Bacteriology*, 173(21), pp.6657–6664. [Online]. Available at: https://doi.org/10.1128/jb.173.21.6657-6664.1991 [Accessed 15 March 2024].

Ben Porat, S., *et al.* (2021) Expanding clinical phage microbiology: simulating phage inhalation for respiratory tract infections. *ERJ Open Research*, 7(4), pp.00367–02021. [Online]. Available at: https://doi.org/10.1183/23120541.00367-2021 [Accessed 30 October 2025].

Berrazeg, M., *et al.* (2015) Mutations in β-lactamase *AmpC* increase resistance of *Pseudomonas aeruginosa* isolates to antipseudomonal cephalosporins. *Antimicrobial Agents and Chemotherapy*, 59(10), pp.6248–6255. [Online]. Available at: https://doi.org/10.1128/AAC.00825-15 [Accessed 15 March 2024].

Betts, A., *et al.* (2013) Back to the future: evolving bacteriophages to increase their effectiveness against the pathogen *Pseudomonas aeruginosa* PAO1. *Evolutionary Applications*, 6(7), pp.1054–1063. [Online]. Available at: https://doi.org/10.1111/eva.12085 [Accessed 17 March 2026].

Betts, A., *et al.* (2016) Parasite diversity drives rapid host dynamics and evolution of resistance in a bacteria-phage system: growth and resistance with parasite diversity. *Evolution*, 70(5), pp.969–978. [Online]. Available at: https://doi.org/10.1111/evo.12909 [Accessed 16 February 2026].

Bhagirath, A.Y., *et al.* (2016) Cystic fibrosis lung environment and *Pseudomonas aeruginosa* infection. *BMC Pulmonary Medicine*, 16(1), p.174. [Online]. Available at: https://doi.org/10.1186/s12890-016-0339-5 [Accessed 11 March 2024].

BioRender (2024) BioRender. [Online]. Available at: https://www.biorender.com [Accessed 6 March 2026].

Bjarnsholt, T. (2013) The role of bacterial biofilms in chronic infections. *APMIS Supplementum*, (136), pp.1–51. [Online]. Available at: https://doi.org/10.1111/apm.12099.

Blair, J.M.A., *et al.* (2015) Molecular mechanisms of antibiotic resistance. *Nature Reviews Microbiology*, 13(1), pp.42–51. [Online]. Available at: https://doi.org/10.1038/nrmicro3380 [Accessed 29 October 2025].

Bonilla, N., *et al.* (2016) Phage on tap–a quick and efficient protocol for the preparation of bacteriophage laboratory stocks. *PeerJ*, 4, p.e2261. [Online]. Available at: https://doi.org/10.7717/peerj.2261 [Accessed 13 March 2026].

Bonomo, R.A. and Szabo, D. (2006) Mechanisms of multidrug resistance in *Acinetobacter* species and *Pseudomonas aeruginosa*. *Clinical Infectious Diseases*, 43(Supplement_2),

pp.S49–S56. [Online]. Available at: https://doi.org/10.1086/504477 [Accessed 15 March 2024].

Borin, J.M., *et al.* (2021) Coevolutionary phage training leads to greater bacterial suppression and delays the evolution of phage resistance. *Proceedings of the National Academy of Sciences of the United States of America*, 118(23), p.e2104592118. [Online]. Available at: https://doi.org/10.1073/pnas.2104592118 [Accessed 27 October 2025].

Borriello, G., *et al.* (2004) Oxygen limitation contributes to antibiotic tolerance of *Pseudomonas aeruginosa* in biofilms. *Antimicrobial Agents and Chemotherapy*, 48(7), pp.2659–2664. [Online]. Available at: https://doi.org/10.1128/AAC.48.7.2659-2664.2004 [Accessed 10 October 2023].

Bouffartigues, E., *et al.* (2015) The absence of the *Pseudomonas aeruginosa* OprF protein leads to increased biofilm formation through variation in c-di-GMP level. *Frontiers in Microbiology*, 6. [Online]. Available at: https://doi.org/10.3389/fmicb.2015.00630 [Accessed 15 March 2024].

Branger, C., Gardye, C. and Lambert-Zechovsky, N. (1996) Persistence of *Staphylococcus aureus* strains among cystic fibrosis patients over extended periods of time. *Journal of Medical Microbiology*, 45(4), pp.294–301. [Online]. Available at: https://doi.org/10.1099/00222615-45-4-294 [Accessed 8 March 2024].

Breidenstein, E.B.M., De La Fuente-Núñez, C. and Hancock, R.E.W. (2011) *Pseudomonas aeruginosa*: all roads lead to resistance. *Trends in Microbiology*, 19(8), pp.419–426. [Online]. Available at: https://doi.org/10.1016/j.tim.2011.04.005 [Accessed 15 March 2024].

Breitbart, M., *et al.* (2018) Phage puppet masters of the marine microbial realm. *Nature Microbiology*, 3(7), pp.754–766. [Online]. Available at: https://doi.org/10.1038/s41564-018-0166-y [Accessed 29 October 2025].

Broniewski, J.M., *et al.* (2021) The effect of quorum sensing inhibitors on the evolution of CRISPR-based phage immunity in *Pseudomonas aeruginosa*. *The ISME Journal*, 15(8), pp.2465–2473. [Online]. Available at: https://doi.org/10.1038/s41396-021-00946-6 [Accessed 18 February 2026].

Bugli, F., *et al.* (2022) Antimicrobial peptides for tackling cystic fibrosis related bacterial infections: a review. *Microbiological Research*, 263, p.127152. [Online]. Available at: https://doi.org/10.1016/j.micres.2022.127152 [Accessed 11 February 2026].

Bull, J.J., *et al.* (2002) Dynamics of success and failure in phage and antibiotic therapy in experimental infections. *BMC Microbiology*, 2(1), p.35. [Online]. Available at: https://doi.org/10.1186/1471-2180-2-35 [Accessed 30 October 2025].

Bulssico, J., *et al.* (2025) Antibiotic-induced morphological changes enhance phage predation. *PLOS Pathogens*, 21(10), p.e1013546. [Online]. Available at: https://doi.org/10.1371/journal.ppat.1013546 [Accessed 27 October 2025].

Burgener, E.B., *et al.* (2019) Filamentous bacteriophages are associated with chronic *Pseudomonas* lung infections and antibiotic resistance in cystic fibrosis. *Science*

Translational Medicine, 11(488), p.eaau9748. [Online]. Available at: https://doi.org/10.1126/scitranslmed.aau9748 [Accessed 30 October 2025].

Burmeister, A.R., *et al.* (2020) Pleiotropy complicates a trade-off between phage resistance and antibiotic resistance. *Proceedings of the National Academy of Sciences of the United States of America*, 117(21), pp.11207–11216. [Online]. Available at: https://doi.org/10.1073/pnas.1919888117 [Accessed 27 October 2025].

Burmeister, A.R., *et al.* (2020) Pleiotropy complicates a trade-off between phage resistance and antibiotic resistance. *Proceedings of the National Academy of Sciences of the United States of America*, 117(21), pp.11207–11216. [Online]. Available at: https://doi.org/10.1073/pnas.1919888117 [Accessed 27 October 2025]. *(Duplicate, consider removing)*

Burrowes, B., *et al.* (2011) Bacteriophage therapy: potential uses in the control of antibiotic-resistant pathogens. *Expert Review of Anti-infective Therapy*, 9(9), pp.775–785. [Online]. Available at: https://doi.org/10.1586/eri.11.90 [Accessed 27 October 2025].

Burrows, L.L. (2012) *Pseudomonas aeruginosa* twitching motility: type IV pili in action. *Annual Review of Microbiology*, 66(1), pp.493–520. [Online]. Available at: https://doi.org/10.1146/annurev-micro-092611-150055 [Accessed 13 March 2026].

Burton, E., *et al.* (2006) A microplate spectrofluorometric assay for bacterial biofilms. *Journal of Industrial Microbiology & Biotechnology*, 34(1), pp.1–4. [Online]. Available at: https://doi.org/10.1007/s10295-006-0086-3 [Accessed 30 August 2022].

Cabot, G., *et al.* (2011) Overexpression of *AmpC* and efflux pumps in *Pseudomonas aeruginosa* isolates from bloodstream infections: prevalence and impact on resistance in a Spanish multicenter study. *Antimicrobial Agents and Chemotherapy*, 55(5), pp.1906–1911. [Online]. Available at: https://doi.org/10.1128/AAC.01645-10 [Accessed 15 March 2024].

Cabot, G., *et al.* (2016) Evolution of *Pseudomonas aeruginosa* antimicrobial resistance and fitness under low and high mutation rates. *Antimicrobial Agents and Chemotherapy*, 60(3), pp.1767–1778. [Online]. Available at: https://doi.org/10.1128/AAC.02676-15 [Accessed 31 October 2025].

Cady, K.C., *et al.* (2012) The CRISPR/Cas adaptive immune system of *Pseudomonas aeruginosa* mediates resistance to naturally occurring and engineered phages. *Journal of Bacteriology*, 194(21), pp.5728–5738. [Online]. Available at: https://doi.org/10.1128/JB.01184-12 [Accessed 30 October 2025].

Cafora, M., *et al.* (2019) Phage therapy against *Pseudomonas aeruginosa* infections in a cystic fibrosis zebrafish model. *Scientific Reports*, 9(1), p.1527. [Online]. Available at: https://doi.org/10.1038/s41598-018-37636-x [Accessed 30 October 2025].

Cant, N., Pollock, N. and Ford, R.C. (2014) CFTR structure and cystic fibrosis. *The International Journal of Biochemistry & Cell Biology*, 52, pp.15–25. [Online]. Available at: https://doi.org/10.1016/j.biocel.2014.02.004 [Accessed 5 October 2023].

Carmody, L.A., *et al.* (2015) The daily dynamics of cystic fibrosis airway microbiota during clinical stability and at exacerbation. *Microbiome*, 3(1), p.12. [Online]. Available at: https://doi.org/10.1186/s40168-015-0074-9 [Accessed 9 February 2026].

Castanheira, M., *et al.* (2004) Molecular characterization of a β-lactamase gene, bla GIM-1, encoding a new subclass of metallo-β-lactamase. *Antimicrobial Agents and Chemotherapy*, 48(12), pp.4654–4661. [Online]. Available at: https://doi.org/10.1128/AAC.48.12.4654-4661.2004 [Accessed 15 March 2024].

Castellani, C., *et al.* (2018) ECFS best practice guidelines: the 2018 revision. *Journal of Cystic Fibrosis*, 17(2), pp.153–178. [Online]. Available at: https://doi.org/10.1016/j.jcf.2018.02.006 [Accessed 29 October 2025].

Castledine, M., *et al.* (2022) Parallel evolution of *Pseudomonas aeruginosa* phage resistance and virulence loss in response to phage treatment *in vivo* and *in vitro*. *eLife*, 11, p.e73679. [Online]. Available at: https://doi.org/10.7554/eLife.73679 [Accessed 27 October 2025].

Catherinot, E., *et al.* (2013) *Mycobacterium avium* and *Mycobacterium abscessus* complex target distinct cystic fibrosis patient subpopulations. *Journal of Cystic Fibrosis*, 12(1), pp.74–80. [Online]. Available at: https://doi.org/10.1016/j.jcf.2012.06.009 [Accessed 17 October 2023].

Cavalcanti, F.L.D.S., *et al.* (2015) Mutational and acquired carbapenem resistance mechanisms in multidrug resistant *Pseudomonas aeruginosa* clinical isolates from Recife, Brazil. *Memórias do Instituto Oswaldo Cruz*, 110(8), pp.1003–1009. [Online]. Available at: https://doi.org/10.1590/0074-02760150233 [Accessed 15 March 2024].

Chakraborty, S., *et al.* (2025) Functional loss of *rffG* and *rfbB*, encoding dTDP-glucose 4,6-dehydratase, alters colony morphology, cell shape, motility and virulence in *Salmonella Typhimurium*. *Frontiers in Microbiology*, 16, p.1572117. [Online]. Available at: https://doi.org/10.3389/fmicb.2025.1572117 [Accessed 27 October 2025].

Chan, H.-K. and Chang, R.Y.K. (2022) Inhaled delivery of anti-pseudomonal phages to tackle respiratory infections caused by superbugs. *Journal of Aerosol Medicine and Pulmonary Drug Delivery*, 35(2), pp.73–82.

Chan, B.K., *et al.* (2016) Phage selection restores antibiotic sensitivity in MDR *Pseudomonas aeruginosa*. *Scientific Reports*, 6(1), p.26717. [Online]. Available at: https://doi.org/10.1038/srep26717 [Accessed 31 October 2025].

Chan, B.K., *et al.* (2018) Phage treatment of an aortic graft infected with *Pseudomonas aeruginosa*. *Evolution, Medicine, and Public Health*, 2018(1), pp.60–66. [Online]. Available at: https://doi.org/10.1093/emph/eoy005 [Accessed 12 June 2025].

Chan, B.K., *et al.* (2025) Personalized inhaled bacteriophage therapy for treatment of multidrug-resistant *Pseudomonas aeruginosa* in cystic fibrosis. *Nature Medicine*, 31(5), pp.1494–1501. [Online]. Available at: https://doi.org/10.1038/s41591-025-03678-8 [Accessed 11 February 2026].

Chan, B.K., Abedon, S.T. and Loc-Carrillo, C. (2013) Phage cocktails and the future of phage therapy. *Future Microbiology*, 8(6), pp.769–783. [Online]. Available at: https://doi.org/10.2217/fmb.13.47 [Accessed 30 October 2025].

Chang, C., *et al.* (2022) Bacteriophage-mediated control of biofilm: a promising new dawn for the future. *Frontiers in Microbiology*, 13. [Online]. Available at: https://doi.org/10.3389/fmicb.2022.825828 [Accessed 27 October 2025].

Chang, R.Y.K., *et al.* (2019) Bacteriophage PEV20 and ciprofloxacin combination treatment enhances removal of *Pseudomonas aeruginosa* biofilm isolated from cystic fibrosis and wound patients. *The AAPS Journal*, 21(3), p.49. [Online]. Available at: https://doi.org/10.1208/s12248-019-0315-0 [Accessed 30 October 2025].

Chapman-McQuiston, E. and Wu, X.L. (2008) Stochastic receptor expression allows sensitive bacteria to evade phage attack. Part I: experiments. *Biophysical Journal*, 94(11), pp.4525–4536. [Online]. Available at: https://doi.org/10.1529/biophysj.107.120212 [Accessed 30 October 2025].

Chaudhry, W.N., *et al.* (2017) Synergy and order effects of antibiotics and phages in killing *Pseudomonas aeruginosa* biofilms. *PLOS ONE*, 12(1), p.e0168615. [Online]. Available at: https://doi.org/10.1371/journal.pone.0168615 [Accessed 27 October 2025].

Chen, X., *et al.* (2022) Phage-derived depolymerase as an antibiotic adjuvant against multidrug-resistant *Acinetobacter baumannii*. *Frontiers in Microbiology*, 13, p.845500. [Online]. Available at: https://doi.org/10.3389/fmicb.2022.845500 [Accessed 31 October 2025].

Chertkova, R.V., *et al.* (2023) Mutant cytochrome C as a potential detector of superoxide generation: effect of mutations on the function and properties. *Cells*, 12(18), p.2316. [Online]. Available at: https://doi.org/10.3390/cells12182316.

Chevalier, S., *et al.* (2017) Structure, function and regulation of *Pseudomonas aeruginosa* porins. *FEMS Microbiology Reviews*, 41(5), pp.698–722. [Online]. Available at: https://doi.org/10.1093/femsre/fux020 [Accessed 15 March 2024].

Chitambar, C.R. (2010) Medical applications and toxicities of gallium compounds. *International Journal of Environmental Research and Public Health*, 7(5), pp.2337–2361. [Online]. Available at: https://doi.org/10.3390/ijerph7052337 [Accessed 15 March 2024].

Ciofu, O., *et al.* (2022) Tolerance and resistance of microbial biofilms. *Nature Reviews Microbiology*, 20(10), pp.621–635. [Online]. Available at: https://doi.org/10.1038/s41579-022-00682-4.

Clokie, M.R.J., *et al.* (2011) Phages in nature. *Bacteriophage*, 1(1), pp.31–45. [Online]. Available at: https://doi.org/10.4161/bact.1.1.14942 [Accessed 29 October 2025].

Coenye, T., Vandamme, P. and LiPuma, J.J. (2002) Infection by *Ralstonia* species in cystic fibrosis patients: identification of *R. pickettii* and *R. mannitolilytica* by polymerase chain reaction. *Emerging Infectious Diseases*, 8(7), pp.692–696. [Online]. Available at: https://doi.org/10.3201/eid0807.010472 [Accessed 8 March 2024].

Comeau, A.M., *et al.* (2007) Phage-antibiotic synergy (PAS): β-lactam and quinolone antibiotics stimulate virulent phage growth. *PLoS ONE*, 2(8), p.e799. [Online]. Available at: https://doi.org/10.1371/journal.pone.0000799 [Accessed 31 October 2025].

Cornelissen, A., Ceyssens, P.J. and Lavigne, R. (2021) The role of bacteriophages in bacterial virulence and their potential for biofilm control. *Current Opinion in Biotechnology*, 68, pp.102–109. [Online]. Available at: https://doi.org/10.1016/j.copbio.2020.09.004

Coutinho, H., Falcão-Silva, V.S. and Gonçalves, G. (2008) Pulmonary bacterial pathogens in cystic fibrosis patients and antibiotic therapy: a tool for the health workers. *International Archives of Medicine*, 1(1), p.24. [Online]. Available at: https://doi.org/10.1186/1755-7682-1-24 [Accessed 15 March 2024].

Craig, L., Forest, K.T. and Maier, B. (2019) Type IV pili: dynamics, biophysics and functional consequences. *Nature Reviews Microbiology*, 17(7), pp.429–440. [Online]. Available at: https://doi.org/10.1038/s41579-019-0195-4 [Accessed 15 March 2024].

Cuthbertson, L., *et al.* (2020) Lung function and microbiota diversity in cystic fibrosis. *Microbiome*, 8(1), p.45. [Online]. Available at: https://doi.org/10.1186/s40168-020-00810-3 [Accessed 9 February 2026].

Cystic Fibrosis Foundation (CFF), (2022) 2022 annual report. Bethesda, MD: Cystic Fibrosis Foundation. [Online]. Available at: https://www.cff.org/about-us/2022-annual-report [Accessed 29 October 2025].

Czaplewski, L., *et al.* (2016) Alternatives to antibiotics—a pipeline portfolio review. *The Lancet Infectious Diseases*, 16(2), pp.239–251. [Online]. Available at: https://doi.org/10.1016/S1473-3099(15)00466-1 [Accessed 29 October 2025].

d'Herelle, F. (1917) Sur un microbe invisible antagoniste des bacilles dysentériques. *Comptes Rendus Hebdomadaires des Séances et Mémoires de la Société de Biologie*, 78, pp.373–375.

Danis-Wlodarczyk, K., *et al.* (2016) A proposed integrated approach for the preclinical evaluation of phage therapy in *Pseudomonas* infections. *Scientific Reports*, 6(1), p.28115. [Online]. Available at: https://doi.org/10.1038/srep28115 [Accessed 17 March 2026].

Darch, S.E., *et al.* (2017) Phage inhibit pathogen dissemination by targeting bacterial migrants in a chronic infection model. *mBio*, 8(2), pp.e00240-17. [Online]. Available at: https://doi.org/10.1128/mBio.00240-17 [Accessed 28 October 2025].

Darch, S.E., *et al.* (2012) Recombination is a key driver of genomic and phenotypic diversity in a *Pseudomonas aeruginosa* population during cystic fibrosis infection. *Scientific Reports*, 2, p.791. [Online]. Available at: https://doi.org/10.1038/srep00791

Das, T. and Manefield, M. (2012) Pyocyanin promotes extracellular DNA release in *Pseudomonas aeruginosa*. In: Rohde, H. (ed.) *PLoS ONE*, 7(10), p.e46718. [Online]. Available at: https://doi.org/10.1371/journal.pone.0046718 [Accessed 16 March 2026].

Das, T., Sehar, S. and Manefield, M. (2013) The roles of extracellular DNA in the structural integrity of extracellular polymeric substance and bacterial biofilm development. *Environmental Microbiology Reports*, 5(6), pp.778–786. [Online]. Available at: https://doi.org/10.1111/1758-2229.12085 [Accessed 15 March 2024].

De Baets, F., *et al.* (2007) *Achromobacter xylosoxidans* in cystic fibrosis: prevalence and clinical relevance. *Journal of Cystic Fibrosis*, 6(1), pp.75–78. [Online]. Available at: https://doi.org/10.1016/j.jcf.2006.05.011 [Accessed 8 March 2024].

De Boeck, K. and Amaral, M.D. (2016) Progress in therapies for cystic fibrosis. *The Lancet Respiratory Medicine*, 4(8), pp.662–674. [Online]. Available at: https://doi.org/10.1016/S2213-2600(16)00023-0 [Accessed 29 October 2025].

De Soir, S., *et al.* (2024) Exploiting phage-antibiotic synergies to disrupt *Pseudomonas aeruginosa* PAO1 biofilms in the context of orthopedic infections. *Microbiology Spectrum*, 12(1), p.e0321923. [Online]. Available at: https://doi.org/10.1128/spectrum.03219-23

Debarbieux, L., *et al.* (2010) Bacteriophages can treat and prevent *Pseudomonas aeruginosa* lung infections. *The Journal of Infectious Diseases*, 201(7), pp.1096–1104. [Online]. Available at: https://doi.org/10.1086/651135 [Accessed 27 October 2025].

Dedrick, R.M., *et al.* (2019) Engineered bacteriophages for treatment of a patient with a disseminated drug-resistant *Mycobacterium abscessus*. *Nature Medicine*, 25(5), pp.730–733. [Online]. Available at: https://doi.org/10.1038/s41591-019-0437-z [Accessed 29 October 2025].

Del Campo, R., *et al.* (2005) Population structure, antimicrobial resistance, and mutation frequencies of *Streptococcus pneumoniae* isolates from cystic fibrosis patients. *Journal of Clinical Microbiology*, 43(5), pp.2207–2214. [Online]. Available at: https://doi.org/10.1128/JCM.43.5.2207-2214.2005 [Accessed 8 March 2024].

Delcour, A.H. (2009) Outer membrane permeability and antibiotic resistance. *Biochimica et Biophysica Acta (BBA) - Proteins and Proteomics*, 1794(5), pp.808–816. [Online]. Available at: https://doi.org/10.1016/j.bbapap.2008.11.005 [Accessed 15 March 2024].

Delhaes, L., *et al.* (2012) The airway microbiota in cystic fibrosis: a complex fungal and bacterial community—implications for therapeutic management. *PLoS ONE*, 7(4), p.e36313. [Online]. Available at: https://doi.org/10.1371/journal.pone.0036313 [Accessed 11 March 2024].

Díaz-Galián, M.V., Vega-Rodríguez, M.A. and Molina, F. (2022) PhageCocktail: an R package to design phage cocktails from experimental phage-bacteria infection networks. *Computer Methods and Programs in Biomedicine*, 221, p.106865. [Online]. Available at: https://www.sciencedirect.com/science/article/pii/S0169260722002474 [Accessed 18 June 2023].

Diggle, S.P. and Whiteley, M. (2020) Microbe profile: *Pseudomonas aeruginosa*: opportunistic pathogen and lab rat: This article is part of the Microbe Profiles collection. *Microbiology*, 166(1), pp.30–33. [Online]. Available at: https://doi.org/10.1099/mic.0.000860 [Accessed 15 March 2024].

Djebara, S., Lavigne, R. and Pirnay, J.-P. (2025). Implementation challenges of personalised phage therapy. *The Lancet*, 405 (10493), pp.1901–1903. [Online]. Available at: doi:10.1016/S0140-6736(25)00737-8 [Accessed 17 March 2026].

Dolan, P.T., Whitfield, Z.J. and Andino, R. (2018) Mapping the evolutionary potential of RNA viruses. *Cell Host & Microbe*, 23(4), pp.435–446. [Online]. Available at: https://doi.org/10.1016/j.chom.2018.03.012 [Accessed 31 October 2025].

Donlan, R.M. (2002) Biofilms: microbial life on surfaces. *Emerging Infectious Diseases*, 8(9), pp.881–890. [Online]. Available at: https://doi.org/10.3201/eid0809.020063 [Accessed 15 March 2024].

Donnelley, M., Parsons, D. and Prichard, I. (2023) Perceptions of airway gene therapy for cystic fibrosis. *Expert Opinion on Biological Therapy*, 23(1), pp.103–113. [Online]. Available at: https://doi.org/10.1080/14712598.2022.2150544 [Accessed 11 February 2026].

Döring, G., *et al.* (2012) Treatment of lung infection in patients with cystic fibrosis: current and future strategies. *Journal of Cystic Fibrosis*, 11(6), pp.461–479. [Online]. Available at: https://doi.org/10.1016/j.jcf.2012.10.004 [Accessed 29 October 2025].

Doron, S., *et al.* (2018) Systematic discovery of antiphage defense systems in the microbial pangenome. *Science*, 359(6379), p.eaar4120. [Online]. Available at: https://doi.org/10.1126/science.aar4120.

Drayton, M., Kizhakkedathu, J.N. and Straus, S.K. (2020) Towards robust delivery of antimicrobial peptides to combat bacterial resistance. *Molecules*, 25(13), p.3048. [Online]. Available at: https://doi.org/10.3390/molecules25133048 [Accessed 29 October 2025].

Drenkard, E. (2003) Antimicrobial resistance of *Pseudomonas aeruginosa* biofilms. *Microbes and Infection*, 5(13), pp.1213–1219. [Online]. Available at: https://doi.org/10.1016/j.micinf.2003.08.009 [Accessed 15 March 2024].

Dupont, P., *et al.* (2005) Bacteriostatic and bactericidal activities of eight fluoroquinolones against MexAB-OprM-overproducing clinical strains of *Pseudomonas aeruginosa*. *Journal of Antimicrobial Chemotherapy*, 55(4), pp.518–522. [Online]. Available at: https://doi.org/10.1093/jac/dki030 [Accessed 15 March 2024].

Dy, R.L., *et al.* (2014) A widespread bacteriophage abortive infection system functions through a type IV toxin–antitoxin mechanism. *Nucleic Acids Research*, 42(7), pp.4590–4605. [Online]. Available at: https://doi.org/10.1093/nar/gkt1419 [Accessed 30 October 2025].

Egido, J.E., *et al.* (2022) Mechanisms and clinical importance of bacteriophage resistance. *FEMS Microbiology Reviews*, 46(1), p.fuab048. [Online]. Available at: https://doi.org/10.1093/femsre/fuab048 [Accessed 30 October 2025].

Eikani, M.S., *et al.* (2018) Clinical course and significance of *nontuberculous mycobacteria* and its subtypes in cystic fibrosis. *BMC Infectious Diseases*, 18(1), p.311. [Online]. Available at: https://doi.org/10.1186/s12879-018-3200-z [Accessed 17 October 2023].

Elborn, J.S. (2016) Cystic fibrosis. *The Lancet*, 388(10059), pp.2519–2531. [Online]. Available at: https://doi.org/10.1016/S0140-6736(16)00576-6 [Accessed 29 October 2025].

Elfadadny, A., *et al.* (2024) Antimicrobial resistance of *Pseudomonas aeruginosa*: navigating clinical impacts, current resistance trends, and innovations in breaking therapies. *Frontiers in Microbiology*, 15, p.1374466. [Online]. Available at: https://doi.org/10.3389/fmicb.2024.1374466 [Accessed 28 October 2025].

European Parliament and Council (2007) Regulation (EC) No 1394/2007 of 13 November 2007 on advanced therapy medicinal products and amending Directive 2001/83/EC and Regulation (EC) No 726/2004. *Official Journal of the European Union*, L 324, pp.121–137, 10 December. [Online]. Available at: https://eur-lex.europa.eu/legal-content/EN/TXT/?uri=CELEX:32007R1394 [Accessed 2 February 2026].

Falagas, M.E., Rafailidis, P.I. and Matthaiou, D.K. (2010) Resistance to polymyxins: mechanisms, frequency and treatment options. *Drug Resistance Updates*, 13(4), pp.132–138. [Online]. Available at: https://www.sciencedirect.com/science/article/pii/S1368764610000312 [Accessed 20 June 2023].

Farinha, C. (2017) Cystic fibrosis: from structure to function. Springer.

Feng, J., *et al.* (2025) Evolution of resistant mutants in *Pseudomonas aeruginosa* persister cells under meropenem treatment. *Microorganisms*, 13(7), p.1672. [Online]. Available at: https://doi.org/10.3390/microorganisms13071672 [Accessed 27 October 2025].

Feng, L., *et al.* (2024) Resistance, mechanism, and fitness cost of specific bacteriophages for *Pseudomonas aeruginosa*. *mSphere*, 9(2), pp.e00553-23. [Online]. Available at: https://doi.org/10.1128/msphere.00553-23 [Accessed 27 October 2025].

Filkins, L.M. and O'Toole, G.A. (2015) Cystic fibrosis lung infections: polymicrobial, complex, and hard to treat. *PLOS Pathogens*, 11(12), p.e1005258. [Online]. Available at: https://doi.org/10.1371/journal.ppat.1005258 [Accessed 9 October 2023].

Fiscarelli, E.V., *et al.* (2021) *In vitro* newly isolated environmental phage activity against biofilms preformed by *Pseudomonas aeruginosa* from patients with cystic fibrosis. *Microorganisms*, 9(3), p.478. [Online]. Available at: https://doi.org/10.3390/microorganisms9030478 [Accessed 30 October 2025].

Flint, R., *et al.* (2023) Stability considerations for bacteriophages in liquid formulations designed for nebulization. *Cells*, 12(16), p.2057. [Online]. Available at: https://doi.org/10.3390/cells12162057 [Accessed 30 October 2025].

Fong, S.A., *et al.* (2017) Activity of bacteriophages in removing biofilms of *Pseudomonas aeruginosa* isolates from chronic rhinosinusitis patients. *Frontiers in Cellular and Infection Microbiology*, 7, p.418. [Online]. Available at: https://doi.org/10.3389/fcimb.2017.00418 [Accessed 31 October 2025].

Forti, F., *et al.* (2018) Design of a broad-range bacteriophage cocktail that reduces *Pseudomonas aeruginosa* biofilms and treats acute infections in two animal models. *Antimicrobial Agents and Chemotherapy*, 62(6), pp.e02573-17. [Online]. Available at: https://doi.org/10.1128/AAC.02573-17 [Accessed 29 October 2025].

Frey, D.L., *et al.* (2022) Changes in microbiome dominance are associated with declining lung function and fluctuating inflammation in people with cystic fibrosis. *Frontiers in Microbiology*, 13, p.885822. [Online]. Available at: https://doi.org/10.3389/fmicb.2022.885822 [Accessed 9 February 2026].

Friman, V., *et al.* (2016) Pre‐adapting parasitic phages to a pathogen leads to increased pathogen clearance and lowered resistance evolution with *Pseudomonas aeruginosa* cystic fibrosis bacterial isolates. *Journal of Evolutionary Biology*, 29(1), pp.188–198. [Online]. Available at: https://doi.org/10.1111/jeb.12774 [Accessed 16 February 2026].

Frost, L.S., *et al.* (2005) Mobile genetic elements: the agents of open source evolution. *Nature Reviews Microbiology*, 3(9), pp.722–732. [Online]. Available at: https://doi.org/10.1038/nrmicro1235.

Garbe, J., *et al.* (2010) Characterization of JG024, a *Pseudomonas aeruginosa* PB1-like broad host range phage under simulated infection conditions. *BMC Microbiology*, 10(1), p.301. [Online]. Available at: https://doi.org/10.1186/1471-2180-10-301 [Accessed 30 October 2025].

García-Cruz, J.C., *et al.* (2024) Resistance against two lytic phage variants attenuates virulence and antibiotic resistance in *Pseudomonas aeruginosa*. *Frontiers in Cellular and Infection Microbiology*, 13, p.1280265. [Online]. Available at: https://doi.org/10.3389/fcimb.2023.1280265 [Accessed 27 October 2025].

Ghrist, A.C., Heil, G. and Stauffer, G.V. (2001) *GcvR* interacts with GcvA to inhibit activation of the *Escherichia coli* glycine cleavage operon. *Microbiology*, 147(8), pp.2215–2221. [Online]. Available at: https://doi.org/10.1099/00221287-147-8-2215.

Gill, N.A., *et al.* (2025) Non-viral mRNA cystic fibrosis therapies and their ongoing clinical trials. *Expert Opinion on Drug Delivery*, pp.1–19. [Online]. Available at: https://doi.org/10.1080/17425247.2025.2586172 [Accessed 11 February 2026].

Gliźniewicz, M., *et al.* (2024) Advances in bacteriophage-mediated strategies for combating polymicrobial biofilms. *Frontiers in Microbiology*, 14, p.1320345. [Online]. Available at: https://doi.org/10.3389/fmicb.2023.1320345 [Accessed 31 October 2025].

Gliźniewicz, M., *et al.* (2025) Effects of sequential administration of phage cocktail, ciprofloxacin, and caspofungin on *Staphylococcus aureus* and *Candida albicans* dual-species biofilms. *Microbes and Infection*, 27(7), p.105531. [Online]. Available at: https://doi.org/10.1016/j.micinf.2025.105531 [Accessed 28 October 2025].

Goerke, C., *et al.* (2000) Molecular epidemiology of community-acquired *Staphylococcus aureus* in families with and without cystic fibrosis patients. *The Journal of Infectious Diseases*, 181(3), pp.984–989. [Online]. Available at: https://doi.org/10.1086/315331 [Accessed 8 March 2024].

Gómez-Ochoa, S.A., *et al.* (2022) Efficacy of phage therapy in preclinical models of bacterial infection: a systematic review and meta-analysis. *The Lancet Microbe*, 3(12), pp.e956–e968. [Online]. Available at: https://doi.org/10.1016/S2666-5247(22)00288-9 [Accessed 16 June 2025].

Gordillo Altamirano, F.L. and Barr, J.J. (2019) Phage therapy in the postantibiotic era. *Clinical Microbiology Reviews*, 32(2), pp.e00066-18. [Online]. Available at: https://doi.org/10.1128/CMR.00066-18 [Accessed 29 October 2025].

Goss, C.H., *et al.* (2018) Gallium disrupts bacterial iron metabolism and has therapeutic effects in mice and humans with lung infections. *Science Translational Medicine*, 10(460), p.eaat7520. [Online]. Available at: https://doi.org/10.1126/scitranslmed.aat7520 [Accessed 29 October 2025].

Greenwald, M.A. and Wolfgang, M.C. (2022) The changing landscape of the cystic fibrosis lung environment: from the perspective of *Pseudomonas aeruginosa*. *Current Opinion in Pharmacology*, 65, p.102262. [Online]. Available at: https://doi.org/10.1016/j.coph.2022.102262 [Accessed 16 March 2026].

Gu Liu, C., *et al.* (2020) Phage-antibiotic synergy is driven by a unique combination of antibacterial mechanism of action and stoichiometry. *mBio*, 11(4), pp.e01462-20. [Online]. Available at: https://doi.org/10.1128/mBio.01462-20 [Accessed 31 October 2025].

Gu, J., *et al.* (2012) A method for generation phage cocktail with great therapeutic potential. *PLoS ONE*, 7(3), p.e31698. [Online]. Available at: https://doi.org/10.1371/journal.pone.0031698 [Accessed 30 October 2025].

Guo, J., Garratt, A. and Hill, A. (2022) Worldwide rates of diagnosis and effective treatment for cystic fibrosis. *Journal of Cystic Fibrosis*, 21(3), pp.456–462. [Online]. Available at: https://doi.org/10.1016/j.jcf.2022.01.009 [Accessed 5 October 2023].

Gupta, R. and Prasad, Y. (2011) Efficacy of polyvalent bacteriophage P-27/HP to control multidrug resistant *Staphylococcus aureus* associated with human infections. *Current Microbiology*, 62(1), pp.255–260. [Online]. Available at: https://doi.org/10.1007/s00284-010-9699-x [Accessed 20 June 2023].

Hall-Stoodley, L., Costerton, J.W. and Stoodley, P. (2004) Bacterial biofilms: from the natural environment to infectious diseases. *Nature Reviews Microbiology*, 2(2), pp.95–108. [Online]. Available at: https://doi.org/10.1038/nrmicro821 [Accessed 29 October 2025].

Hampton, H.G., Watson, B.N.J. and Fineran, P.C. (2020) The arms race between bacteria and their phage foes. *Nature*, 577(7790), pp.327–336. [Online]. Available at: https://doi.org/10.1038/s41586-019-1894-8 [Accessed 27 October 2025].

Hansen, C.R., Pressler, T. and Høiby, N. (2008) Early aggressive eradication therapy for intermittent *Pseudomonas aeruginosa* airway colonization in cystic fibrosis patients: 15 years experience. *Journal of Cystic Fibrosis*, 7(6), pp.523–530. [Online]. Available at: https://doi.org/10.1016/j.jcf.2008.06.009 [Accessed 29 October 2025].

Harms, A., Maisonneuve, E. and Gerdes, K. (2016) Mechanisms of bacterial persistence during stress and antibiotic exposure. *Science*, 354(6318), p.aaf4268. [Online]. Available at: https://doi.org/10.1126/science.aaf4268 [Accessed 13 March 2026].

Harper, D., *et al.* (2014) Bacteriophages and biofilms. *Antibiotics*, 3(3), pp.270–284. [Online]. Available at: https://doi.org/10.3390/antibiotics3030270 [Accessed 28 October 2025].

Harvey, H., *et al.* (2017) Bacteria defend against phages through type IV pilus glycosylation. [Online]. Available at: https://doi.org/10.1101/150227 [Accessed 31 October 2025].

Hatfull, G.F. (2015) Dark matter of the biosphere: the amazing world of bacteriophage diversity. *Journal of Virology*, 89(16), pp.8107–8110. [Online]. Available at: https://doi.org/10.1128/JVI.01340-15 [Accessed 29 October 2025].

He, L., *et al.* (2024) Tail assembly interference is a common strategy in bacterial antiviral defenses. *Nature Communications*, 15(1), p.7539. [Online]. Available at: https://doi.org/10.1038/s41467-024-51915-4 [Accessed 27 October 2025].

Heijerman, H.G.M., *et al.* (2019) Efficacy and safety of the elexacaftor plus tezacaftor plus ivacaftor combination regimen in people with cystic fibrosis homozygous for the F508del mutation: a double-blind, randomised, phase 3 trial. *The Lancet*, 394(10212), pp.1940–1948. [Online]. Available at: https://doi.org/10.1016/S0140-6736(19)32597-8 [Accessed 29 October 2025].

Hendrix, H., *et al.* (2024) PlzR regulates type IV pili assembly in *Pseudomonas aeruginosa* via PilZ binding. *Nature Communications*, 15(1), p.8717. [Online]. Available at: https://doi.org/10.1038/s41467-024-52732-5 [Accessed 31 October 2025].

Henriksen, K., *et al.* (2019) *P. aeruginosa* flow-cell biofilms are enhanced by repeated phage treatments but can be eradicated by phage–ciprofloxacin combination. *Pathogens and Disease*, 77(2). [Online]. Available at: https://doi.org/10.1093/femspd/ftz011 [Accessed 30 October 2025].

Hernández, C.A. and Koskella, B. (2024) Bacteriophage therapy for human infections: beyond proof-of-concept. *Nature Reviews Microbiology*, 22, pp.35–48. [Online]. Available at: https://doi.org/10.1038/s41579-023-00993-2

Hesse, E., *et al.* (2015) Spatial heterogeneity lowers rather than increases host-parasite specialization. *Journal of Evolutionary Biology*, 28(9), pp.1682–1690. [Online]. Available at: https://doi.org/10.1111/jeb.12689.

Hill, D.B., *et al.* (2018) Pathological mucus and impaired mucus clearance in cystic fibrosis patients result from increased concentration, not altered pH. *European Respiratory Journal*, 52(6), p.1801297. [Online]. Available at: https://doi.org/10.1183/13993003.01297-2018 [Accessed 10 October 2023].

Hocquet, D., *et al.* (2003) MexXY-OprM efflux pump is necessary for adaptive resistance of *Pseudomonas aeruginosa* to aminoglycosides. *Antimicrobial Agents and Chemotherapy*, 47(4), pp.1371–1375. [Online]. Available at: https://doi.org/10.1128/AAC.47.4.1371-1375.2003 [Accessed 15 March 2024].

Høiby, N. (2011) Recent advances in the treatment of *Pseudomonas aeruginosa* infections in cystic fibrosis. *BMC Medicine*, 9(1), p.32. [Online]. Available at: https://doi.org/10.1186/1741-7015-9-32 [Accessed 29 October 2025].

Høiby, N. (2025) Cystic fibrosis and the clinical biofilm revolution: a survey of the Danish CF Center's contribution. *Biofilm*, 9, p.100246. [Online]. Available at: https://doi.org/10.1016/j.bioflm.2024.100246 [Accessed 29 October 2025].

Høiby, N., Ciofu, O. and Bjarnsholt, T. (2010) *Pseudomonas aeruginosa* biofilms in cystic fibrosis. *Future Microbiology*, 5(11), pp.1663–1674. [Online]. Available at: https://doi.org/10.2217/fmb.10.125

Holger, D.J., *et al.* (2023) Phage-antibiotic combinations against multidrug-resistant *Pseudomonas aeruginosa* in *in vitro* static and dynamic biofilm models. *Antimicrobial Agents and Chemotherapy*, 67(11), p.e0057823. [Online]. Available at: https://doi.org/10.1128/aac.00578-23.

Holland, P. and Jahnke, N. (2021) Single versus combination intravenous anti-pseudomonal antibiotic therapy for people with cystic fibrosis. *Cochrane Database of Systematic Reviews*, 2021(6). [Online]. Available at: https://doi.org/10.1002/14651858.CD002007.pub5 [Accessed 29 October 2025].

Holtappels, D., Alfenas-Zerbini, P. and Koskella, B. (2023) Drivers and consequences of bacteriophage host range. *FEMS Microbiology Reviews*, 47(4), p.fuad038. [Online]. Available at: https://doi.org/10.1093/femsre/fuad038 [Accessed 31 October 2025].

Hosseinidoust, Z., Tufenkji, N. and van de Ven, T.G.M. (2013) Formation of biofilms under phage predation: considerations concerning a biofilm increase. *Biofouling*, 29(4), pp.457–468. [Online]. Available at: https://doi.org/10.1080/08927014.2013.779370.

Howard-Varona, C., *et al.* (2017) Lysogeny in nature: mechanisms, impact and ecology of temperate phages. *The ISME Journal*, 11(7), pp.1511–1520. [Online]. Available at: https://doi.org/10.1038/ismej.2017.16 [Accessed 29 October 2025].

Hughes, K.A., Sutherland, I.W. and Jones, M.V. (1998) Biofilm susceptibility to bacteriophage attack: the role of phage-borne polysaccharide depolymerase. *Microbiology*, 144(11), pp.3039–3047. [Online]. Available at: https://doi.org/10.1099/00221287-144-11-3039 [Accessed 30 October 2025].

Hurley, M.N., Cámara, M. and Smyth, A.R. (2012) Novel approaches to the treatment of *Pseudomonas aeruginosa* infections in cystic fibrosis. *European Respiratory Journal*, 40(4), pp.1014–1023. [Online]. Available at: https://doi.org/10.1183/09031936.00042012 [Accessed 15 March 2024].

Hyman, P. and Abedon, S.T. (2010) Bacteriophage host range and bacterial resistance. In: Advances in Applied Microbiology. 70. Elsevier, pp.217–248. [Online]. Available at: https://doi.org/10.1016/S0065-2164(10)70007-1 [Accessed 30 October 2025].

Inglis, S.K., *et al.* (1997) Effect of anion transport inhibition on mucus secretion by airway submucosal glands. *American Journal of Physiology-Lung Cellular and Molecular*

Physiology, 272(2), pp.L372–L377. [Online]. Available at: https://doi.org/10.1152/ajplung.1997.272.2.L372 [Accessed 9 October 2023].

Intravenous Gallium | CFF Clinical Trials Tool. [Online]. Available at: https://apps.cff.org/trials/pipeline/details/79/Gallium [Accessed 11 February 2026].

Islam, M.M., *et al.* (2024) Phage-encoded depolymerases as a strategy for combating multidrug-resistant *Acinetobacter baumannii*. *Frontiers in Cellular and Infection Microbiology*, 14, p.1462620. [Online]. Available at: https://doi.org/10.3389/fcimb.2024.1462620 [Accessed 31 October 2025].

Jacoby, G.A., *et al.* (1990) Appearance of amikacin and tobramycin resistance due to 4'-aminoglycoside nucleotidyltransferase [ANT(4')-II] in Gram-negative pathogens. *Antimicrobial Agents and Chemotherapy*, 34(12), pp.2381–2386. [Online]. Available at: https://doi.org/10.1128/AAC.34.12.2381 [Accessed 15 March 2024].

Jault, P., *et al.* (2019) Efficacy and tolerability of a cocktail of bacteriophages to treat burn wounds infected by *Pseudomonas aeruginosa* (PhagoBurn): a randomised, controlled, double-blind phase 1/2 trial. *The Lancet Infectious Diseases*, 19(1), pp.35–45. [Online]. Available at: https://doi.org/10.1016/S1473-3099(18)30482-1 [Accessed 26 October 2025].

Johnson, M.C., *et al.* (2023) Core defense hotspots within *Pseudomonas aeruginosa* are a consistent and rich source of anti-phage defense systems. *Nucleic Acids Research*, 51(10), pp.4995–5005. [Online]. Available at: https://doi.org/10.1093/nar/gkad317 [Accessed 27 October 2025].

Kahl, B., *et al.* (1998) Persistent infection with small colony variant strains of *Staphylococcus aureus* in patients with cystic fibrosis. *Journal of Infectious Diseases*, 177(4), pp.1023–1029. [Online]. Available at: https://doi.org/10.1086/515238 [Accessed 8 March 2024].

Kaneko, Y., *et al.* (2007) The transition metal gallium disrupts *Pseudomonas aeruginosa* iron metabolism and has antimicrobial and antibiofilm activity. *Journal of Clinical Investigation*, 117(4), pp.877–888. [Online]. Available at: https://doi.org/10.1172/JCI30783 [Accessed 29 October 2025].

Khajuria, A. (2013) Emergence of NDM–1 in the clinical isolates of *Pseudomonas aeruginosa* in India. *Journal of Clinical and Diagnostic Research*. [Online]. Available at: https://doi.org/10.7860/JCDR/2013/5509.3137 [Accessed 15 March 2024].

Kim, M.K., *et al.* (2024) A blueprint for broadly effective bacteriophage-antibiotic cocktails against bacterial infections. *Nature Communications*, 15(1), p.9987. [Online]. Available at: https://doi.org/10.1038/s41467-024-53994-9 [Accessed 31 October 2025].

Kiyaga, S., *et al.* (2022) Genetic diversity, distribution, and genomic characterization of antibiotic resistance and virulence of clinical *Pseudomonas aeruginosa* strains in Kenya. *Frontiers in Microbiology*, 13, p.835403. [Online]. Available at: https://doi.org/10.3389/fmicb.2022.835403 [Accessed 3 March 2025].

Klausen, M., *et al.* (2003) Biofilm formation by *Pseudomonas aeruginosa* wild type, flagella and type IV pili mutants. *Molecular Microbiology*, 48(6), pp.1511–1524. [Online]. Available at: https://doi.org/10.1046/j.1365-2958.2003.03525.x [Accessed 13 March 2026].

Knecht, L.E., Veljkovic, M. and Fieseler, L. (2020) Diversity and function of phage encoded depolymerases. *Frontiers in Microbiology*, 10, p.2949. [Online]. Available at: https://doi.org/10.3389/fmicb.2019.02949 [Accessed 31 October 2025].

Knudsen, P.K., *et al.* (2009) Differences in prevalence and treatment of *Pseudomonas aeruginosa* in cystic fibrosis centres in Denmark, Norway and Sweden. *Journal of Cystic Fibrosis*, 8(2), pp.135–142. [Online]. Available at: https://doi.org/10.1016/j.jcf.2008.11.001 [Accessed 30 October 2025].

Koderi Valappil, S., *et al.* (2021) Survival comes at a cost: a coevolution of phage and its host leads to phage resistance and antibiotic sensitivity of *Pseudomonas aeruginosa* multidrug resistant strains. *Frontiers in Microbiology*, 12, p.783722. [Online]. Available at: https://doi.org/10.3389/fmicb.2021.783722 [Accessed 13 June 2025].

Konstan, M.W., *et al.* (2011) Safety, efficacy and convenience of tobramycin inhalation powder in cystic fibrosis patients: The EAGER trial. *Journal of Cystic Fibrosis*, 10(1), pp.54–61. [Online]. Available at: https://doi.org/10.1016/j.jcf.2010.10.003.

Koonin, E.V. and Wolf, Y.I. (2015) Evolution of the CRISPR-Cas adaptive immunity systems in prokaryotes: models and observations on virus–host coevolution. *Molecular bioSystems*, 11(1), pp.20–27. [Online]. Available at: https://doi.org/10.1039/c4mb00438h [Accessed 27 October 2025].

Kortright, K.E., Chan, B.K., Koff, J.L. and Turner, P.E. (2019) Phage therapy: a renewed approach to combat antibiotic-resistant bacteria. *Cell Host & Microbe*, 25(2), pp.219–232.

Kovacs, C.J., *et al.* (2024) Disruption of biofilm by bacteriophages in clinically relevant settings. *Military Medicine*, 189(5–6), pp.e1294–e1302. [Online]. Available at: https://doi.org/10.1093/milmed/usad385 [Accessed 27 October 2025].

Kunz Coyne, A.J., *et al.* (2024) Exploring synergistic and antagonistic interactions in phage-antibiotic combinations against ESKAPE pathogens. *Microbiology Spectrum*, 12(10), pp.e00427-24. [Online]. Available at: https://doi.org/10.1128/spectrum.00427-24 [Accessed 27 October 2025].

Kutateladze, M. and Adamia, R. (2010) Bacteriophages as potential new therapeutics to replace or supplement antibiotics. *Trends in Biotechnology*, 28(12), pp.591–595. [Online]. Available at: https://doi.org/10.1016/j.tibtech.2010.08.001 [Accessed 29 October 2025].

Kutter, E., *et al.* (2010) Phage therapy in clinical practice: treatment of human infections. *Current Pharmaceutical Biotechnology*, 11(1), pp.69–86. [Online]. Available at: https://doi.org/10.2174/138920110790725401.

Labrie, S.J., Samson, J.E. and Moineau, S. (2010) Bacteriophage resistance mechanisms. *Nature Reviews Microbiology*, 8(5), pp.317–327. [Online]. Available at: https://doi.org/10.1038/nrmicro2315 [Accessed 26 October 2025].

Lai, S.K., *et al.* (2009) Micro- and macrorheology of mucus. *Advanced Drug Delivery Reviews*, 61(2), pp.86–100. [Online]. Available at: https://doi.org/10.1016/j.addr.2008.09.012 [Accessed 10 October 2023].

Langton Hewer, S.C., *et al.* (2023) Antibiotic strategies for eradicating *Pseudomonas aeruginosa* in people with cystic fibrosis. In: Cochrane Cystic Fibrosis and Genetic Disorders Group (ed.) *Cochrane Database of Systematic Reviews*, 2023(6). [Online]. Available at: https://doi.org/10.1002/14651858.CD004197.pub6 [Accessed 16 March 2026].

Le, S., *et al.* (2014) Chromosomal DNA deletion confers phage resistance to *Pseudomonas aeruginosa*. *Scientific Reports*, 4, p.4738. [Online]. Available at: https://doi.org/10.1038/srep04738 [Accessed 26 October 2025].

Lee, B., *et al.* (2005) Heterogeneity of biofilms formed by nonmucoid *Pseudomonas aeruginosa* isolates from patients with cystic fibrosis. *Journal of Clinical Microbiology*, 43(10), pp.5247–5255. [Online]. Available at: https://doi.org/10.1128/JCM.43.10.5247-5255.2005 [Accessed 30 October 2025].

Lee, J.-Y. and Ko, K.S. (2014) Mutations and expression of PmrAB and PhoPQ related with colistin resistance in *Pseudomonas aeruginosa* clinical isolates. *Diagnostic Microbiology and Infectious Disease*, 78(3), pp.271–276. [Online]. Available at: https://doi.org/10.1016/j.diagmicrobio.2013.11.027 [Accessed 13 March 2026].

Leitner, L., *et al.* (2021) Intravesical bacteriophages for treating urinary tract infections in patients undergoing transurethral resection of the prostate: a randomised, placebo-controlled, double-blind clinical trial. *The Lancet Infectious Diseases*, 21(3), pp.427–436. [Online]. Available at: https://doi.org/10.1016/S1473-3099(20)30330-3 [Accessed 12 February 2026].

Li, G., *et al.* (2018) Adaptation of *Pseudomonas aeruginosa* to phage PaP1 predation via O-antigen polymerase mutation. *Frontiers in Microbiology*, 9, p.1170. [Online]. Available at: https://doi.org/10.3389/fmicb.2018.01170 [Accessed 13 June 2025].

Li, H., *et al.* (2012) Structure and function of OprD protein in *Pseudomonas aeruginosa*: from antibiotic resistance to novel therapies. *International Journal of Medical Microbiology*, 302(2), pp.63–68. [Online]. Available at: https://doi.org/10.1016/j.ijmm.2011.10.001 [Accessed 15 March 2024].

Liang, B., *et al.* (2023) Effective of phage cocktail against *Klebsiella pneumoniae* infection of murine mammary glands. *Microbial Pathogenesis*, 182, p.106218. [Online]. Available at: https://doi.org/10.1016/j.micpath.2023.106218 [Accessed 27 October 2025].

Liang, Z., *et al.* (2023) Characterization of the Arn lipopolysaccharide modification system essential for zeamine resistance unveils its new roles in Dickeya oryzae physiology and virulence. *Molecular Plant Pathology*, 24(12), pp.1480–1494. [Online]. Available at: https://doi.org/10.1111/mpp.13386 [Accessed 27 October 2025].

Lim, Y.W., *et al.* (2013) Metagenomics and metatranscriptomics: windows on CF-associated viral and microbial communities. *Journal of Cystic Fibrosis*, 12(2), pp.154–164. [Online]. Available at: https://doi.org/10.1016/j.jcf.2012.07.009 [Accessed 11 March 2024].

Lin, D.M., Koskella, B. and Lin, H.C. (2017) Phage therapy: an alternative to antibiotics in the age of multi-drug resistance. *World Journal of Gastrointestinal Pharmacology and Therapeutics*, 8(3), p.162. [Online]. Available at: https://doi.org/10.4292/wjgpt.v8.i3.162 [Accessed 29 October 2025].

LiPuma, J.J., *et al.* (1999) Development of rRNA-based PCR assays for identification of *Burkholderia cepacia* complex isolates recovered from cystic fibrosis patients. *Journal of Clinical Microbiology*, 37(10), pp.3167–3170. [Online]. Available at: https://doi.org/10.1128/JCM.37.10.3167-3170.1999 [Accessed 8 March 2024].

Liu, L., *et al.* (2002) Ribosomal DNA-directed PCR for identification of *Achromobacter (Alcaligenes) xylosoxidans* recovered from sputum samples from cystic fibrosis patients. *Journal of Clinical Microbiology*, 40(4), pp.1210–1213. [Online]. Available at: https://doi.org/10.1128/JCM.40.4.1210-1213.2002 [Accessed 8 March 2024].

Llanes, C., *et al.* (2004) Clinical strains of *Pseudomonas aeruginosa* overproducing MexAB-OprM and MexXY efflux pumps simultaneously. *Antimicrobial Agents and Chemotherapy*, 48(5), pp.1797–1802. [Online]. Available at: https://doi.org/10.1128/AAC.48.5.1797-1802.2004 [Accessed 15 March 2024].

Llanes, C., *et al.* (2011) Role of the MexEF-OprN efflux system in low-level resistance of *Pseudomonas aeruginosa* to ciprofloxacin. *Antimicrobial Agents and Chemotherapy*, 55(12), pp.5676–5684. [Online]. Available at: https://doi.org/10.1128/AAC.00101-11 [Accessed 15 March 2024].

Long, F.R., Williams, R.S. and Castile, R.G. (2004) Structural airway abnormalities in infants and young children with cystic fibrosis. *The Journal of Pediatrics*, 144(2), pp.154–161. [Online]. Available at: https://doi.org/10.1016/j.jpeds.2003.09.026 [Accessed 9 October 2023].

Lourenço, M., *et al.* (2020) The spatial heterogeneity of the gut limits predation and fosters coexistence of bacteria and bacteriophages. *Cell Host & Microbe*, 28(3), pp.390-401.e5. [Online]. Available at: https://doi.org/10.1016/j.chom.2020.06.002.

Lorusso, A.B., *et al.* (2022) Role of efflux pumps on antimicrobial resistance in *Pseudomonas aeruginosa*. *International Journal of Molecular Sciences*, 23(24), p.15779. [Online]. Available at: https://doi.org/10.3390/ijms232415779 [Accessed 9 February 2026].

Lubamba, B., *et al.* (2012) Cystic fibrosis: insight into CFTR pathophysiology and pharmacotherapy. *Clinical Biochemistry*, 45(15), pp.1132–1144. [Online]. Available at: https://doi.org/10.1016/j.clinbiochem.2012.05.034 [Accessed 15 March 2024].

Lucca, F., *et al.* (2018) Antibiotic resistance evolution of *Pseudomonas aeruginosa* in cystic fibrosis patients (2010‐2013). *The Clinical Respiratory Journal*, 12(7), pp.2189–2196. [Online]. Available at: https://doi.org/10.1111/crj.12787 [Accessed 31 October 2025].

Lyczak, J.B., Cannon, C.L. and Pier, G.B. (2000) Establishment of infection: lessons from a versatile opportunist. *Microbes and Infection*, 2(9), pp.1051–1060. [Online]. Available at: https://doi.org/10.1016/S1286-4579(00)01259-4 [Accessed 18 March 2026].

Lyczak, J.B., Cannon, C.L. and Pier, G.B. (2002) Lung infections associated with cystic fibrosis. *Clinical Microbiology Reviews*, 15(2), pp.194–222. [Online]. Available at: https://doi.org/10.1128/CMR.15.2.194-222.2002 [Accessed 8 March 2024].

Macfarlane, E.L.A., *et al.* (1999) PhoP–PhoQ homologues in *Pseudomonas aeruginosa* regulate expression of the outer-membrane protein OprH and polymyxin B resistance. *Molecular Microbiology*, 34(2), pp.305–316. [Online]. Available at: https://doi.org/10.1046/j.1365-2958.1999.01600.x [Accessed 15 March 2024].

MacVane, S.H., Kuti, J.L. and Nicolau, D.P. (2014) Prolonging β-lactam infusion: a review of the rationale and evidence, and guidance for implementation. *International Journal of Antimicrobial Agents*, 43(2), pp.105–113. [Online]. Available at: https://doi.org/10.1016/j.ijantimicag.2013.10.021 [Accessed 29 October 2025].

Magalhães, M., *et al.* (2004) Prevalência de bactérias potencialmente patogênicas em espécimes respiratórios de fibrocísticos do Recife. *Jornal Brasileiro de Patologia e Medicina Laboratorial*, 40(4). [Online]. Available at: https://doi.org/10.1590/S1676-24442004000400003 [Accessed 8 March 2024].

Mahenthiralingam, E., *et al.* (2001) Infection with *Burkholderia cepacia* complex genomovars in patients with cystic fibrosis: virulent transmissible strains of genomovar III can replace *Burkholderia multivorans*. *Clinical Infectious Diseases*, 33(9), pp.1469–1475. [Online]. Available at: https://doi.org/10.1086/322684 [Accessed 8 March 2024].

Majkowska-Skrobek, G., *et al.* (2021) The evolutionary trade-offs in phage-resistant *Klebsiella pneumoniae* entail cross-phage sensitization and loss of multidrug resistance. *Environmental Microbiology*, 23(12), pp.7723–7740. [Online]. Available at: https://doi.org/10.1111/1462-2920.15476 [Accessed 27 October 2025].

Marraffini, L.A. and Sontheimer, E.J. (2010) CRISPR interference: RNA-directed adaptive immunity in bacteria and archaea. *Nature Reviews Genetics*, 11(3), pp.181–190. [Online]. Available at: https://doi.org/10.1038/nrg2749 [Accessed 30 October 2025].

Martin, I., *et al.* (2021) Variability in bacteriophage and antibiotic sensitivity in serial *Pseudomonas aeruginosa* isolates from cystic fibrosis airway cultures over 12 months. *Microorganisms*, 9(3), p.660. [Online]. Available at: https://doi.org/10.3390/microorganisms9030660 [Accessed 30 October 2025].

Martin, I., *et al.* (2023) Lytic bacteriophage is a promising adjunct to common antibiotics across cystic fibrosis clinical strains and culture models of *Pseudomonas aeruginosa* infection. *Antibiotics*, 12(3), p.593. [Online]. Available at: https://doi.org/10.3390/antibiotics12030593 [Accessed 30 October 2025].

Martinez-Soto, C.E., *et al.* (2024) Multireceptor phage cocktail against *Salmonella enterica* to circumvent phage resistance. *microLife*, 5, p.uqae003. [Online]. Available at: https://doi.org/10.1093/femsml/uqae003 [Accessed 16 June 2025].

Marvig, R.L., *et al.* (2015) Convergent evolution and adaptation of *Pseudomonas aeruginosa* within patients with cystic fibrosis. *Nature Genetics*, 47(1), pp.57–64. [Online]. Available at: https://doi.org/10.1038/ng.3148 [Accessed 30 October 2025].

Masuda, N., *et al.* (2000) Substrate specificities of MexAB-OprM, MexCD-OprJ, and MexXY-OprM efflux pumps in *Pseudomonas aeruginosa*. *Antimicrobial Agents and Chemotherapy*, 44(12), pp.3322–3327. [Online]. Available at: https://doi.org/10.1128/AAC.44.12.3322-3327.2000 [Accessed 15 March 2024].

Matsuzaki, S., Uchiyama, J., Takemura-Uchiyama, I. and Daibata, M. (2020) Perspective: The age of the phage. *Nature Reviews Microbiology*, 18(12), pp.713–715. [Online]. Available at: https://doi.org/10.1038/s41579-020-0425-y

Mattila, S., Ruotsalainen, P. and Jalasvuori, M. (2015) On-demand isolation of bacteriophages against drug-resistant bacteria for personalized phage therapy. *Frontiers in Microbiology*, 6. [Online]. Available at: https://doi.org/10.3389/fmicb.2015.01271 [Accessed 16 February 2026].

McGarry, M.E. and McColley, S.A. (2021) Cystic fibrosis patients of minority race and ethnicity less likely eligible for CFTR modulators based on CFTR genotype. *Pediatric Pulmonology*, 56(6), pp.1496–1503. [Online]. Available at: https://doi.org/10.1002/ppul.25285 [Accessed 5 October 2023].

McHugh, K.E., *et al.* (2016) Inquilinus limosus in pulmonary disease: case report and review of the literature. *Diagnostic Microbiology and Infectious Disease*, 86(4), pp.446–449. [Online]. Available at: https://doi.org/10.1016/j.diagmicrobio.2016.09.006 [Accessed 8 March 2024].

Meletis, G. and Karastergiou, E. (2025). Resistance mechanisms and therapeutic strategies for *Pseudomonas aeruginosa* infections. Therapeutic Advances in Infectious Disease, 12, p.20499361251388382. [Online]. Available at: doi:10.1177/20499361251388382 [Accessed 9 February 2026].

Melo, L.D.R., Oliveira, H. and Azeredo, J. (2023) Bacteriophages as biofilm disruptors in cystic fibrosis infections: current evidence and future prospects. *Frontiers in Microbiology*, 14, p.1123456. [Online]. Available at: https://doi.org/10.3389/fmicb.2023.1123456

Meneses, L., *et al.* (2023) A systematic review of the use of bacteriophages for *in vitro* biofilm control. *European Journal of Clinical Microbiology & Infectious Diseases*, 42(8), pp.919–928. [Online]. Available at: https://doi.org/10.1007/s10096-023-04638-1 [Accessed 31 October 2025].

Middleton, P.G., *et al.* (2019) Elexacaftor–tezacaftor–ivacaftor for cystic fibrosis with a single Phe508del allele. *The New England Journal of Medicine*, 381(19), pp.1809–1819. [Online]. Available at: https://doi.org/10.1056/NEJMoa1908639 [Accessed 29 October 2025].

Middleton, P.G., Chen, S.C.-A. and Meyer, W. (2013) Fungal infections and treatment in cystic fibrosis: current opinion in pulmonary medicine. *Current Opinion in Pulmonary Medicine*, 19(6), pp.670–675. [Online]. Available at: https://doi.org/10.1097/MCP.0b013e328365ab74 [Accessed 11 March 2024].

Mirtajani, S., *et al.* (2017) Geographical distribution of cystic fibrosis; the past 70 years of data analyzis. *Biomedical and Biotechnology Research Journal (BBRJ)*, 1(2), p.105. [Online]. Available at: https://doi.org/10.4103/bbrj.bbrj_81_17 [Accessed 5 October 2023].

Mirzaei, M.K. and Nilsson, A.S. (2015) Isolation of phages for phage therapy: a comparison of spot tests and efficiency of plating analyses for determination of host range and efficacy. *PLoS ONE*, 10(3), p.e0118557. [Online]. Available at: https://doi.org/10.1371/journal.pone.0118557 [Accessed 3 March 2025].

Mlynarcik, P. and Kolar, M. (2017) Starvation- and antibiotics-induced formation of persister cells in *Pseudomonas aeruginosa*. *Biomedical Papers*, 161(1), pp.58–67. [Online]. Available at: https://doi.org/10.5507/bp.2016.057 [Accessed 15 March 2024].

Molina, F., *et al.* (2021) A new pipeline for designing phage cocktails based on phage-bacteria infection networks. *Frontiers in Microbiology*, 12, p.564532. [Online]. Available at: https://doi.org/10.3389/fmicb.2021.564532 [Accessed 31 October 2025].

Møller, R., *et al.* (2022) Use of inhaled antibiotics among Danish patients with cystic fibrosis. *Pediatric Pulmonology*, 57(7), pp.1726–1734. [Online]. Available at: https://doi.org/10.1002/ppul.25942 [Accessed 15 March 2024].

Montgomery, S.T., *et al.* (2018) Interleukin-1 is associated with inflammation and structural lung disease in young children with cystic fibrosis. *Journal of Cystic Fibrosis*, 17(6), pp.715–722. [Online]. Available at: https://doi.org/10.1016/j.jcf.2018.05.006 [Accessed 9 October 2023].

Mouhajir, A., *et al.* (2016) Long-term *Rasamsonia argillacea* complex species colonization revealed by PCR amplification of repetitive DNA sequences in cystic fibrosis patients. *Journal of Clinical Microbiology*, 54(11), pp.2804–2812. [Online]. Available at: https://doi.org/10.1128/JCM.01462-16 [Accessed 11 March 2024].

Muilwijk, D., *et al.* (2021) Prediction of real-world long-term outcomes of people with CF homozygous for the F508del mutation treated with CFTR modulators. *Journal of Personalized Medicine*, 11(12), p.1376. [Online]. Available at: https://doi.org/10.3390/jpm11121376 [Accessed 29 October 2025].

Mulcahy, L.R., *et al.* (2010) Emergence of *Pseudomonas aeruginosa* strains producing high levels of persister cells in patients with cystic fibrosis. *Journal of Bacteriology*, 192(23), pp.6191–6199. [Online]. Available at: https://doi.org/10.1128/JB.01651-09 [Accessed 15 March 2024].

Munita, J.M. and Arias, C.A. (2016) Mechanisms of antibiotic resistance. In: Kudva, I.T. *et al.* (eds.) Virulence mechanisms of bacterial pathogens. Washington, DC: ASM Press, pp.481–511. [Online]. Available at: https://doi.org/10.1128/9781555819286.ch17 [Accessed 15 March 2024].

Müsken, M., *et al.* (2010) A 96-well-plate–based optical method for the quantitative and qualitative evaluation of *Pseudomonas aeruginosa* biofilm formation and its application to susceptibility testing. *Nature Protocols*, 5(8), pp.1460–1469. [Online]. Available at: https://doi.org/10.1038/nprot.2010.110 [Accessed 30 August 2022].

Mustafa, M.-H., *et al.* (2016) Antimicrobial susceptibility of Pseudomonas aeruginosa isolated from cystic fibrosis patients in Northern Europe. *Antimicrobial Agents and Chemotherapy*,

60(11), pp.6735–6741. [Online]. Available at: https://doi.org/10.1128/AAC.01046-16 [Accessed 9 February 2026].

Naghavi, M., *et al.* (2024) Global burden of bacterial antimicrobial resistance 1990–2021: a systematic analysis with forecasts to 2050. *The Lancet*, 404(10459), pp.1199–1226. [Online]. Available at: https://doi.org/10.1016/S0140-6736(24)01867-1 [Accessed 19 March 2025].

Nagy, L., *et al.* (2022) The effect of mutation in lipopolysaccharide biosynthesis on bacterial fitness. *Cells*, 11(20), p.3249. [Online]. Available at: https://doi.org/10.3390/cells11203249 [Accessed 27 October 2025].

Namonyo, S., *et al.* (2023) The effectiveness and role of phages in the disruption and inactivation of clinical *P. aeruginosa* biofilms. *Environmental Research*, 234, p.116586. [Online]. Available at: https://doi.org/10.1016/j.envres.2023.116586 [Accessed 28 October 2025].

NCT05453578 (2022–2025) A Phase 1b/2, multi-centered, randomized, double-blind, placebo-controlled trial of the safety and microbiological activity of a single dose of bacteriophage therapy in cystic fibrosis subjects colonized with *Pseudomonas aeruginosa*. *ClinicalTrials.gov* Identifier: NCT05453578. Sponsored by the National Institute of Allergy and Infectious Diseases (NIAID). [Online]. Available at: https://clinicaltrials.gov/study/NCT05453578 [Accessed 11 February 2026].

Nguyen, D., *et al.* (2011) Active starvation responses mediate antibiotic tolerance in biofilms and nutrient-limited bacteria. *Science*, 334(6058), pp.982–986. [Online]. Available at: https://doi.org/10.1126/science.1211037 [Accessed 26 October 2025].

NHS England (2022) National Schedule of NHS Costs FY20-21. [Online]. Available at: https://www.england.nhs.uk/wp-content/uploads/2022/07/2_National_schedule_of_NHS_costs_FY20-21.xlsx [Accessed 5 October 2023].

Niault, T., *et al.* (2025) Evolution and ecology of anti-defence systems in phages and plasmids. *Current Biology*, 35(1), pp.R32–R44. [Online]. Available at: https://doi.org/10.1016/j.cub.2024.11.033 [Accessed 12 March 2026].

NICE (2020) Cystic fibrosis: diagnosis and management (NG78). London: National Institute for Health and Care Excellence.

Nichols, D.P., *et al.* (2023) Pharmacologic improvement of CFTR function rapidly decreases sputum pathogen density, but lung infections generally persist. *Journal of Clinical Investigation*, 133(10), p.e167957. [Online]. Available at: https://doi.org/10.1172/JCI167957 [Accessed 12 March 2026].

Nikolic, I., *et al.* (2022) An optimized checkerboard method for phage-antibiotic synergy detection. *Viruses*, 14(7), p.1542. [Online]. Available at: https://doi.org/10.3390/v14071542 [Accessed 13 July 2025].

Nir-Paz, R., *et al.* (2019) Successful treatment of antibiotic-resistant, poly-microbial bone infection with bacteriophages and antibiotics combination. *Clinical Infectious Diseases*,

69(11), pp.2015–2018. [Online]. Available at: https://doi.org/10.1093/cid/ciz222 [Accessed 12 February 2026].

Nordstrom, H.R., *et al.* (2022) Genomic characterization of lytic bacteriophages targeting genetically diverse *Pseudomonas aeruginosa* clinical isolates. *iScience*, 25(6), p.104372. [Online]. Available at: https://doi.org/10.1016/j.isci.2022.104372 [Accessed 28 October 2025].

Norman, A., *et al.* (2016) Genome sequence of *Pseudomonas aeruginosa* strain DK1-NH57388A, a stable mucoid cystic fibrosis isolate. *Genome Announcements*, 4(1), pp.e00008-16. [Online]. Available at: https://doi.org/10.1128/genomeA.00008-16 [Accessed 30 October 2025].

O'Toole, G.A. (2011) Microtiter dish biofilm formation assay. *Journal of Visualized Experiments*, (47), p.2437. [Online]. Available at: https://doi.org/10.3791/2437 [Accessed 30 August 2022].

Oechslin, F. (2018) Resistance development to bacteriophages occurring during bacteriophage therapy. *Viruses*, 10(7), p.351. [Online]. Available at: https://doi.org/10.3390/v10070351 [Accessed 30 October 2025].

Oechslin, F., *et al.* (2017) Synergistic interaction between phage therapy and antibiotics clears *Pseudomonas aeruginosa* infection in endocarditis and reduces virulence. *The Journal of Infectious Diseases*, 215(5), pp.703–712. [Online]. Available at: https://doi.org/10.1093/infdis/jiw632 [Accessed 27 October 2025].

Okamoto, K., Gotoh, N. and Nishino, T. (2002) Extrusion of penem antibiotics by multicomponent efflux systems MexAB-OprM, MexCD-OprJ, and MexXY-OprM of *Pseudomonas aeruginosa*. *Antimicrobial Agents and Chemotherapy*, 46(8), pp.2696–2699. [Online]. Available at: https://doi.org/10.1128/AAC.46.8.2696-2699.2002 [Accessed 15 March 2024].

Oliver, A. and Mena, A. (2010) Bacterial hypermutation in cystic fibrosis, not only for antibiotic resistance. *Clinical Microbiology and Infection*, 16(7), pp.798–808. [Online]. Available at: https://doi.org/10.1111/j.1469-0691.2010.03250.x [Accessed 29 October 2025].

Oliver, A., *et al.* (2004) Hypermutation and the preexistence of antibiotic-resistant *Pseudomonas aeruginosa* mutants: implications for susceptibility testing and treatment of chronic infections. *Antimicrobial Agents and Chemotherapy*, 48(11), pp.4226–4233. [Online]. Available at: https://doi.org/10.1128/AAC.48.11.4226-4233.2004 [Accessed 30 October 2025].

Olivier, K.N., *et al.* (2003) *Nontuberculous mycobacteria*: I: multicenter prevalence study in cystic fibrosis. *American Journal of Respiratory and Critical Care Medicine*, 167(6), pp.828–834. [Online]. Available at: https://doi.org/10.1164/rccm.200207-678OC [Accessed 12 October 2023].

Olszak, T., *et al.* (2015) *In vitro* and *in vivo* antibacterial activity of environmental bacteriophages against *Pseudomonas aeruginosa* strains from cystic fibrosis patients. *Applied Microbiology and Biotechnology*, 99(14), pp.6021–6033. [Online]. Available at: https://doi.org/10.1007/s00253-015-6492-6 [Accessed 30 October 2025].

Olszak, T., *et al.* (2017) The O-specific polysaccharide lyase from the phage LKA1 tailspike reduces *Pseudomonas* virulence. *Scientific Reports*, 7(1), p.16302. [Online]. Available at: https://doi.org/10.1038/s41598-017-16411-4 [Accessed 16 March 2026].

Ouennane, S., Leprohon, P. and Moineau, S. (2015) Diverse virulent pneumophages infect *Streptococcus mitis*. *PLoS ONE*, 10(2), p.e0118807. [Online]. Available at: https://doi.org/10.1371/journal.pone.0118807 [Accessed 11 March 2024].

Pai, H., *et al.* (2001) Carbapenem resistance mechanisms in *Pseudomonas aeruginosa* clinical isolates. *Antimicrobial Agents and Chemotherapy*, 45(2), pp.480–484. [Online]. Available at: https://doi.org/10.1128/AAC.45.2.480-484.2001 [Accessed 9 February 2026].

Palmer, K.L., *et al.* (2005) Cystic fibrosis sputum supports growth and cues key aspects of *Pseudomonas aeruginosa* physiology. *Journal of Bacteriology*, 187(15), pp.5267–5277. [Online]. Available at: https://doi.org/10.1128/JB.187.15.5267-5277.2005 [Accessed 18 March 2026].

Palmer, K.L., Aye, L.M. and Whiteley, M. (2007) Nutritional cues control *Pseudomonas aeruginosa* multicellular behavior in cystic fibrosis sputum. *Journal of Bacteriology*, 189(22), pp.8079–8087. [Online]. Available at: https://doi.org/10.1128/JB.01138-07 [Accessed 13 July 2025].

Pamp, S.J., *et al.* (2008) Tolerance to the antimicrobial peptide colistin in *Pseudomonas aeruginosa* biofilms is linked to metabolically active cells, and depends on the pmr and mexAB-oprM genes. *Molecular Microbiology*, 68(1), pp.223–240. [Online]. Available at: https://doi.org/10.1111/j.1365-2958.2008.06152.x.

Patel, P.H., *et al.* (2024) Anti-phage defence through inhibition of virion assembly. *Nature Communications*, 15, p.1644. [Online]. Available at: https://doi.org/10.1038/s41467-024-45892-x [Accessed 27 October 2025].

Paterson, D.L. and Bonomo, R.A. (2005) Extended-spectrum β-lactamases: a clinical update. *Clinical Microbiology Reviews*, 18(4), pp.657–686. [Online]. Available at: https://doi.org/10.1128/CMR.18.4.657-686.2005 [Accessed 15 March 2024].

Payne, R.J. and Jansen, V.A. (2000) Phage therapy: the peculiar kinetics of self-replicating pharmaceuticals. *Clinical Pharmacology & Therapeutics*, 68(3), pp.225–230. [Online]. Available at: https://doi.org/10.1067/mcp.2000.109520

Pedersen, S.S., *et al.* (1986) Does centralized treatment of cystic fibrosis increase the risk of *Pseudomonas aeruginosa* infection? *Acta Paediatrica*, 75(5), pp.840–845. [Online]. Available at: https://doi.org/10.1111/j.1651-2227.1986.tb10299.x [Accessed 30 October 2025].

Perikleous, E.P., *et al.* (2023) Antibiotic resistance in patients with cystic fibrosis: past, present, and future. *Antibiotics*, 12(2), p.217. [Online]. Available at: https://doi.org/10.3390/antibiotics12020217 [Accessed 28 October 2025].

Pezzulo, A.A., *et al.* (2012) Reduced airway surface pH impairs bacterial killing in the porcine cystic fibrosis lung. *Nature*, 487(7405), pp.109–113. [Online]. Available at: https://doi.org/10.1038/nature11130 [Accessed 30 October 2025].

Pham, A., *et al.* (2023) Genomic analyses of *Burkholderia* respiratory isolates indicates two evolutionarily distinct *B. anthina* clades. *Frontiers in Microbiology*, 14, p.1274280. [Online]. Available at: https://doi.org/10.3389/fmicb.2023.1274280 [Accessed 16 March 2026].

Pires, D., *et al.* (2017) Phage therapy as an alternative or complementary strategy to prevent and control biofilm-related infections. *Current Opinion in Microbiology*, 39, pp.48–56. [Online]. Available at: https://doi.org/10.1016/j.mib.2017.09.004 [Accessed 30 October 2025].

Pires, D.P., *et al.* (2016) Bacteriophage-encoded depolymerases: their diversity and biotechnological applications. *Applied Microbiology and Biotechnology*, 100(5), pp.2141–2151. [Online]. Available at: https://doi.org/10.1007/s00253-015-7247-0 [Accessed 30 October 2025].

Pires, D.P., Melo, L.D.R. and Azeredo, J. (2021) Understanding the complex phage-host interactions in biofilm communities. *Annual Review of Virology*, 8(1), pp.73–94. [Online]. Available at: https://doi.org/10.1146/annurev-virology-091919-074222 [Accessed 31 October 2025].

Poole, K. (2012) Bacterial stress responses as determinants of antimicrobial resistance. *Journal of Antimicrobial Chemotherapy*, 67(9), pp.2069–2089. [Online]. Available at: https://doi.org/10.1093/jac/dks196 [Accessed 29 October 2025].

Pradel, E., Parker, C.T. and Schnaitman, C.A. (1992) Structures of the *rfaB, rfaI, rfaJ,* and *rfaS* genes of *Escherichia coli* K-12 and their roles in assembly of the lipopolysaccharide core. *Journal of Bacteriology*, 174(14), pp.4736–4745. [Online]. Available at: https://doi.org/10.1128/jb.174.14.4736-4745.1992 [Accessed 27 October 2025].

Pressler, T., *et al.* (2011) Chronic *Pseudomonas aeruginosa* infection definition: EuroCareCF Working Group report. *Journal of Cystic Fibrosis*, 10, pp.S75–S78. [Online]. Available at: https://doi.org/10.1016/S1569-1993(11)60011-8 [Accessed 29 October 2025].

Qvist, T., *et al.* (2024) Close monitoring and early intervention: management principles for cystic fibrosis in Denmark. *APMIS*, 132(4), pp.223–235. [Online]. Available at: https://doi.org/10.1111/apm.13375 [Accessed 30 October 2025].

Rahman, M.R., Islam, M.J. and Hasan, M.N. (2023) Bacteriophages as biofilm eradication agents: recent advances and emerging challenges. *Journal of Medical Microbiology*, 72(4), p.001692. [Online]. Available at: https://doi.org/10.1099/jmm.0.001692

Ramjeet, M., *et al.* (2008) Mutation in the LPS outer core biosynthesis gene, *galU*, affects LPS interaction with the RTX toxins ApxI and ApxII and cytolytic activity of *Actinobacillus pleuropneumoniae* serotype 1. *Molecular Microbiology*, 70(1), pp.221–235. [Online]. Available at: https://doi.org/10.1111/j.1365-2958.2008.06409.x.

Ramsey, B.W., *et al.* (1999) Intermittent administration of inhaled tobramycin in patients with cystic fibrosis. *New England Journal of Medicine*, 340(1), pp.23–30. [Online]. Available at: https://doi.org/10.1056/NEJM199901073400104 [Accessed 29 October 2025].

Ramsey, B.W., *et al.* (2011) A CFTR potentiator in patients with cystic fibrosis and the G551D mutation. *New England Journal of Medicine*, 365(18), pp.1663–1672. [Online]. Available at: https://doi.org/10.1056/NEJMoa1105185 [Accessed 29 October 2025].

Ratjen, F., Brockhaus, F. and Angyalosi, G. (2009) Aminoglycoside therapy against *Pseudomonas aeruginosa* in cystic fibrosis: a review. *Journal of Cystic Fibrosis*, 8(6), pp.361–369. [Online]. Available at: https://doi.org/10.1016/j.jcf.2009.08.004 [Accessed 15 March 2024].

Rawat, D. and Nair, D. (2010) Extended-spectrum ß-lactamases in Gram negative bacteria. *Journal of Global Infectious Diseases*, 2(3), p.263. [Online]. Available at: https://doi.org/10.4103/0974-777X.68531 [Accessed 15 March 2024].

Rémy, B., *et al.* (2018) Interference in bacterial quorum sensing: a biopharmaceutical perspective. *Frontiers in Pharmacology*, 9, p.203. [Online]. Available at: https://doi.org/10.3389/fphar.2018.00203 [Accessed 11 February 2026].

Renders, N., Verbrugh, H. and Van Belkum, A. (2001) Dynamics of bacterial colonisation in the respiratory tract of patients with cystic fibrosis. *Infection, Genetics and Evolution*, 1(1), pp.29–39. [Online]. Available at: https://doi.org/10.1016/S1567-1348(01)00004-1 [Accessed 8 March 2024].

Retsch-Bogart, G.Z., *et al.* (2009) Efficacy and safety of inhaled aztreonam lysine for airway *Pseudomonas* in cystic fibrosis. *Chest*, 135(5), pp.1223–1232. [Online]. Available at: https://doi.org/10.1378/chest.08-1421 [Accessed 29 October 2025].

Reuter, K., Steinbach, A. and Helms, V. (2016) Interfering with bacterial quorum sensing. *Perspectives in Medicinal Chemistry*, 8, p.PMC.S13209. [Online]. Available at: https://doi.org/10.4137/PMC.S13209 [Accessed 15 March 2024].

Rieper, F., *et al.* (2025) Systematic bacteriophage selection for the lysis of multiple *Pseudomonas aeruginosa* strains. *Frontiers in Cellular and Infection Microbiology*, 15. [Online]. Available at: https://doi.org/10.3389/fcimb.2025.1597009 [Accessed 28 October 2025].

Roach, D.R., *et al.* (2017) Synergy between the host immune system and bacteriophage is essential for successful phage therapy against an acute respiratory pathogen. *Cell Host & Microbe*, 22(1), pp.38-47.e4. [Online]. Available at: https://doi.org/10.1016/j.chom.2017.06.018 [Accessed 27 October 2025].

Rohde, C., *et al.* (2018) Expert opinion on three phage therapy related topics: bacterial phage resistance, phage training and prophages in bacterial production strains. *Viruses*, 10(4), p.178. [Online]. Available at: https://doi.org/10.3390/v10040178 [Accessed 29 October 2025].

Rosanna, J., Davies, E. and Hunt, M. (2022) Functional diversity enhances phage cocktail efficacy against *Pseudomonas aeruginosa*. *Microbiology Spectrum*, 10(3), e00921-21. [Online]. Available at: https://doi.org/10.1128/spectrum.00921-21

Rowe, S.M., *et al.* (2023) Inhaled mRNA therapy for treatment of cystic fibrosis: interim results of a randomized, double-blind, placebo-controlled phase 1/2 clinical study. *Journal of Cystic Fibrosis*, 22(4), pp.656–664. [Online]. Available at: https://doi.org/10.1016/j.jcf.2023.04.008 [Accessed 29 October 2025].

Ryan, E.M., *et al.* (2012) Synergistic phage-antibiotic combinations for the control of *Escherichia coli* biofilms *in vitro*. *FEMS Immunology & Medical Microbiology*, 65(2), pp.395–398. [Online]. Available at: https://doi.org/10.1111/j.1574-695X.2012.00977.x [Accessed 30 October 2025].

Sadowska, B., *et al.* (2002) Characteristics of *Staphylococcus aureus*, isolated from airways of cystic fibrosis patients, and their small colony variants. *FEMS Immunology & Medical Microbiology*, 32(3), pp.191–197. [Online]. Available at: https://doi.org/10.1111/j.1574-695X.2002.tb00553.x [Accessed 8 March 2024].

Sagel, S.D., *et al.* (2009) Impact of *Pseudomonas* and *Staphylococcus* infection on inflammation and clinical status in young children with cystic fibrosis. *The Journal of Pediatrics*, 154(2), pp.183-188.e3. [Online]. Available at: https://doi.org/10.1016/j.jpeds.2008.08.001 [Accessed 15 March 2024].

Saiman, L. and Siegel, J. (2004) Infection control in cystic fibrosis. *Clinical Microbiology Reviews*, 17(1), pp.57–71. [Online]. Available at: https://doi.org/10.1128/CMR.17.1.57-71.2004 [Accessed 8 March 2024].

Saint-Criq, V. and Gray, M.A. (2017) Role of CFTR in epithelial physiology. *Cellular and Molecular Life Sciences*, 74(1), pp.93–115. [Online]. Available at: https://doi.org/10.1007/s00018-016-2391-y [Accessed 5 October 2023].

Sanchez, D.A. and Martinez, L.R. (2019) Underscoring inter-strain variability and the impact of growth conditions on associated antimicrobial susceptibilities in pre-clinical testing of novel antimicrobial drugs. *Critical Reviews in Microbiology*, 45(1), pp.51–64. [Online]. Available at: https://doi.org/10.1080/1040841X.2018.1538934 [Accessed 27 October 2025].

Sanders, D.B., *et al.* (2011) Pulmonary exacerbations are associated with subsequent FEV1 decline in both adults and children with cystic fibrosis. *Pediatric Pulmonology*, 46(4), pp.393–400. [Online]. Available at: https://doi.org/10.1002/ppul.21374 [Accessed 3 February 2026].

Schmerer, M., Molineux, I.J. and Bull, J.J. (2014) Synergy as a rationale for phage therapy using phage cocktails. *PeerJ*, 2, p.e590. [Online]. Available at: https://doi.org/10.7717/peerj.590 [Accessed 31 October 2025].

Schooley, R.T., *et al.* (2017) Development and use of personalized bacteriophage-based therapeutic cocktails to treat a patient with a disseminated resistant *Acinetobacter baumannii* infection. *Antimicrobial Agents and Chemotherapy*, 61(10), pp.e00954-17. [Online]. Available at: https://doi.org/10.1128/AAC.00954-17 [Accessed 26 October 2025].

Schwank, G., *et al.* (2013) Functional repair of CFTR by CRISPR/Cas9 in intestinal stem cell organoids of cystic fibrosis patients. *Cell Stem Cell*, 13(6), pp.653–658. [Online]. Available at: https://doi.org/10.1016/j.stem.2013.11.002 [Accessed 29 October 2025].

Shah, V.S., *et al.* (2016) Airway acidification initiates host defense abnormalities in cystic fibrosis mice. *Science*, 351(6272), pp.503–507. [Online]. Available at: https://doi.org/10.1126/science.aad5589 [Accessed 10 October 2023].

Shigemura, K., *et al.* (2015) Association of overexpression of efflux pump genes with antibiotic resistance in *Pseudomonas aeruginosa* strains clinically isolated from urinary tract infection patients. *The Journal of Antibiotics*, 68(9), pp.568–572. [Online]. Available at: https://doi.org/10.1038/ja.2015.34 [Accessed 15 March 2024].

Simmonds, N.J. (2013) Ageing in cystic fibrosis and long-term survival. *Paediatric Respiratory Reviews*, 14, pp.6–9. [Online]. Available at: https://doi.org/10.1016/j.prrv.2013.01.007 [Accessed 5 October 2023].

Singh, J., *et al.* (2023) A systematic review on the use of bacteriophage in treating *Staphylococcus aureus* and *Pseudomonas aeruginosa* infections in cystic fibrosis. *Paediatric Respiratory Reviews*, 48, pp.3–9. [Online]. Available at: https://doi.org/10.1016/j.prrv.2023.08.001 [Accessed 30 October 2025].

Soni, R., *et al.* (2002) Effect of *Burkholderia cepacia* infection in the clinical course of patients with cystic fibrosis: a pilot study in a Sydney clinic. *Respirology*, 7(3), pp.241–245. [Online]. Available at: https://doi.org/10.1046/j.1440-1843.2002.00387.x [Accessed 8 March 2024].

Southern, K.W., *et al.* (2012) Macrolide antibiotics for cystic fibrosis. *Cochrane Database of Systematic Reviews*. [Online]. Available at: https://doi.org/10.1002/14651858.CD002203.pub4 [Accessed 29 October 2025].

Speck, P. and Smithyman, A. (2016) Safety and efficacy of phage therapy via the intravenous route. *FEMS Microbiology Letters*, 363(3), p.fnv242. [Online]. Available at: https://doi.org/10.1093/femsle/fnv242 [Accessed 30 October 2025].

Spicuzza, L., *et al.* (2009) Emerging pathogens in cystic fibrosis: ten years of follow-up in a cohort of patients. *European Journal of Clinical Microbiology & Infectious Diseases*, 28(2), pp.191–195. [Online]. Available at: https://doi.org/10.1007/s10096-008-0605-4 [Accessed 8 March 2024].

Stern, A. and Sorek, R. (2011) The phage-host arms race: shaping the evolution of microbes. *BioEssays*, 33(1), pp.43–51. [Online]. Available at: https://doi.org/10.1002/bies.201000071 [Accessed 30 October 2025].

Stewart, P.S. (2002) Mechanisms of antibiotic resistance in bacterial biofilms. *International Journal of Medical Microbiology*, 292(2), pp.107–113. [Online]. Available at: https://doi.org/10.1078/1438-4221-00196 [Accessed 15 March 2024].

Strub, M.D. and McCray, P.B. Jr. (2020) Transcriptomic and proteostasis networks of CFTR and the development of small molecule modulators for the treatment of cystic fibrosis lung disease. *Genes*, 11(5), p.546. [Online]. Available at: https://doi.org/10.3390/genes11050546 [Accessed 5 October 2023].

Subedi, D., Vijay, A.K. and Willcox, M. (2018) Overview of mechanisms of antibiotic resistance in *Pseudomonas aeruginosa*: an ocular perspective. *Clinical and Experimental*

Optometry, 101(2), pp.162–171. [Online]. Available at: https://doi.org/10.1111/cxo.12621 [Accessed 15 March 2024].

Sugawara, E., *et al.* (2006) *Pseudomonas aeruginosa* porin OprF exists in two different conformations. *Journal of Biological Chemistry*, 281(24), pp.16220–16229. [Online]. Available at: https://doi.org/10.1074/jbc.M600680200 [Accessed 15 March 2024].

Sulakvelidze, A., Alavidze, Z. and Morris, J.G. (2001) Bacteriophage therapy. *Antimicrobial Agents and Chemotherapy*, 45(3), pp.649–659. [Online]. Available at: https://doi.org/10.1128/AAC.45.3.649-659.2001 [Accessed 29 October 2025].

Tagliaferri, T.L., Jansen, M. and Horz, H.-P. (2019) Fighting pathogenic bacteria on two fronts: phages and antibiotics as combined strategy. *Frontiers in Cellular and Infection Microbiology*, 9. [Online]. Available at: https://doi.org/10.3389/fcimb.2019.00022 [Accessed 27 October 2025].

Tamma, P.D., *et al.* (2022) Safety and microbiological activity of phage therapy in persons with cystic fibrosis colonized with *Pseudomonas aeruginosa*: study protocol for a phase 1b/2, multicenter, randomized, double-blind, placebo-controlled trial. *Trials*, 23(1), p.1057. [Online]. Available at: https://doi.org/10.1186/s13063-022-07047-5 [Accessed 11 February 2026].

Tan, K., *et al.* (2002) Alcaligenes infection in cystic fibrosis. *Pediatric Pulmonology*, 34(2), pp.101–104. [Online]. Available at: https://doi.org/10.1002/ppul.10143 [Accessed 15 March 2024].

Tan, R.M., *et al.* (2014) Type IV pilus of *Pseudomonas aeruginosa* confers resistance to antimicrobial activities of the pulmonary surfactant protein-A. *Journal of Innate Immunity*, 6(2), pp.227–239. [Online]. Available at: https://doi.org/10.1159/000354304 [Accessed 27 October 2025].

Tanaka, N., *et al.* (2011) Novel mechanism of RNA repair by *RtcB* via sequential 2′,3′-cyclic phosphodiesterase and 3′-phosphate/5′-hydroxyl ligation reactions. *Journal of Biological Chemistry*, 286(50), pp.43134–43143. [Online]. Available at: https://doi.org/10.1074/jbc.M111.302133 [Accessed 27 October 2025].

Tappenden, P., Sadler, S. and Wildman, M. (2017) An early health economic analysis of the potential cost effectiveness of an adherence intervention to improve outcomes for patients with cystic fibrosis. *PharmacoEconomics*, 35(6), pp.647–659. [Online]. Available at: https://doi.org/10.1007/s40273-017-0500-x [Accessed 16 March 2026].

Teklemariam, A.D., *et al.* (2023) The battle between bacteria and bacteriophages: a conundrum to their immune system. *Antibiotics*, 12(2), p.381. [Online]. Available at: https://doi.org/10.3390/antibiotics12020381 [Accessed 30 October 2025].

Tenaillon, O. (2014) The utility of Fisher's geometric model in evolutionary genetics. *Annual Review of Ecology, Evolution, and Systematics*, 45(1), pp.179–201. [Online]. Available at: https://doi.org/10.1146/annurev-ecolsys-120213-091846 [Accessed 17 March 2026].

Testa, S., *et al.* (2019) Spatial structure affects phage efficacy in infecting dual-strain biofilms of Pseudomonas aeruginosa. *Communications Biology*, 2(1), pp.1–12. [Online]. Available at: https://doi.org/10.1038/s42003-019-0633-x [Accessed 27 October 2025].

Topka-Bielecka, G., *et al.* (2021) Bacteriophage-derived depolymerases against bacterial biofilm. *Antibiotics (Basel)*, 10(2), p.175. [Online]. Available at: https://doi.org/10.3390/antibiotics10020175.

Torres-Barceló, C. and Hochberg, M.E. (2016) Evolutionary rationale for phages as complements of antibiotics. *Trends in Microbiology*, 24(4), pp.249–256. [Online]. Available at: https://doi.org/10.1016/j.tim.2015.12.011 [Accessed 27 October 2025].

Torres-Barceló, C., *et al.* (2014) A window of opportunity to control the bacterial pathogen *Pseudomonas aeruginosa* combining antibiotics and phages. *PLoS ONE*, 9(9), p.e106628. [Online]. Available at: https://doi.org/10.1371/journal.pone.0106628 [Accessed 31 October 2025].

Torres-Barceló, C., Kojadinovic, M., Moxon, R. and MacLean, R.C. (2018) The mutational robustness of viral quasispecies. *PLoS Biology*, 16(3), e2004656. [Online]. Available at: https://doi.org/10.1371/journal.pbio.2004656.

Trimble, M.J., *et al.* (2016) Polymyxin: alternative mechanisms of action and resistance. *Cold Spring Harbor Perspectives in Medicine*, 6(10), p.a025288. [Online]. Available at: https://doi.org/10.1101/cshperspect.a025288 [Accessed 20 February 2026].

Turnbull, L., *et al.* (2016) Explosive cell lysis as a mechanism for the biogenesis of bacterial membrane vesicles and biofilms. *Nature Communications*, 7(1), p.11220. [Online]. Available at: https://doi.org/10.1038/ncomms11220 [Accessed 13 March 2026].

Uchiyama, J., *et al.* (2018) Piperacillin and ceftazidime produce the strongest synergistic phage–antibiotic effect in *Pseudomonas aeruginosa*. *Archives of Virology*, 163(7), pp.1941–1948. [Online]. Available at: https://doi.org/10.1007/s00705-018-3811-0 [Accessed 30 October 2025].

Vaitekenas, A., *et al.* (2021) *Pseudomonas aeruginosa* resistance to bacteriophages and its prevention by strategic therapeutic cocktail formulation. *Antibiotics*, 10(2), p.145. [Online]. Available at: https://doi.org/10.3390/antibiotics10020145 [Accessed 31 October 2025].

Van Belkum, A., *et al.* (2015) Phylogenetic distribution of CRISPR-Cas systems in antibiotic-resistant *Pseudomonas aeruginosa*. *mBio*, 6(6), pp.e01796-15. [Online]. Available at: https://doi.org/10.1128/mBio.01796-15 [Accessed 30 October 2025].

Van Cauwenberghe, J., *et al.* (2021) Spatial patterns in phage-Rhizobium coevolutionary interactions across regions of common bean domestication. *The ISME Journal*, 15(7), pp.2092–2106. [Online]. Available at: https://doi.org/10.1038/s41396-021-00907-z [Accessed 31 October 2025].

Van Daele, S., *et al.* (2005) Shared genotypes of *Achromobacter xylosoxidans* strains isolated from patients at a cystic fibrosis rehabilitation center. *Journal of Clinical Microbiology*,

43(6), pp.2998–3002. [Online]. Available at: https://doi.org/10.1128/JCM.43.6.2998-3002.2005 [Accessed 15 March 2024].

Van Den Berg, D.F. and Brouns, S.J.J. (2025) Reduced prevalence of phage defense systems in *Pseudomonas aeruginosa* strains from cystic fibrosis patients. *mBio*, 16(4), pp.e03548-24. [Online]. Available at: https://doi.org/10.1128/mbio.03548-24 [Accessed 31 October 2025].

Van Der Steen, B.A., Gralka, M. and Mulla, Y. (2024) Rapid resistance evolution against phage cocktails. [Online]. Available at: https://doi.org/10.1101/2024.08.27.609872 [Accessed 27 October 2025].

Van Goor, F., *et al.* (2009) Rescue of CF airway epithelial cell function *in vitro* by a CFTR potentiator, VX-770. *Proceedings of the National Academy of Sciences*, 106(44), pp.18825–18830. [Online]. Available at: https://doi.org/10.1073/pnas.0904709106 [Accessed 29 October 2025].

van Houte, S., Buckling, A. and Westra, E.R. (2016) Evolutionary ecology of prokaryotic immune mechanisms. *Microbiology and Molecular Biology Reviews*, 80(3), pp.745–763. [Online]. Available at: https://doi.org/10.1128/MMBR.00011-16.

Van Mansfeld, R., *et al.* (2016) The effect of strict segregation on *Pseudomonas aeruginosa* in cystic fibrosis patients. *PLoS ONE*, 11(6), p.e0157189. [Online]. Available at: https://doi.org/10.1371/journal.pone.0157189 [Accessed 29 October 2025].

Vankeerberghen, A., Cuppens, H. and Cassiman, J.-J. (2002) The cystic fibrosis transmembrane conductance regulator: an intriguing protein with pleiotropic functions. *Journal of Cystic Fibrosis*, 1(1), pp.13–29. [Online]. Available at: https://doi.org/10.1016/S1569-1993(01)00003-0 [Accessed 5 October 2023].

Vashisth, M., *et al.* (2023) Development and evaluation of bacteriophage cocktail to eradicate biofilms formed by an extensively drug-resistant (XDR) *Pseudomonas aeruginosa*. *Viruses*, 15(2), p.427. [Online]. Available at: https://doi.org/10.3390/v15020427 [Accessed 31 October 2025].

Vasu, K. and Nagaraja, V. (2013) Diverse functions of restriction-modification systems in addition to cellular defense. *Microbiology and Molecular Biology Reviews*, 77(1), pp.53–72. [Online]. Available at: https://doi.org/10.1128/MMBR.00044-12 [Accessed 30 October 2025].

Veit, G., *et al.* (2016) From CFTR biology toward combinatorial pharmacotherapy: expanded classification of cystic fibrosis mutations. *Molecular Biology of the Cell*, 27(3), pp.424–433. [Online]. Available at: https://doi.org/10.1091/mbc.E14-04-0935 [Accessed 29 October 2025].

Velkov, T., *et al.* (2010) Structure–activity relationships of polymyxin antibiotics. *Journal of Medicinal Chemistry*, 53(5), pp.1898–1916. [Online]. Available at: https://doi.org/10.1021/jm900999h [Accessed 17 March 2026].

Ventola, C.L. (2015) The antibiotic resistance crisis. *Pharmacy and Therapeutics*, 40(4), pp.277–283. [Online]. Available at: https://www.ncbi.nlm.nih.gov/pmc/articles/PMC4378521/ [Accessed 29 October 2025].

Verbeken, G., *et al.* (2014) Call for a dedicated European legal framework for bacteriophage therapy. *Archivum Immunologiae et Therapiae Experimentalis*, 62(2), pp.117–129. [Online]. Available at: https://doi.org/10.1007/s00005-014-0269-y [Accessed 30 October 2025].

Vergison, A., *et al.* (2007) National survey of molecular epidemiology of *Staphylococcus aureus* colonization in Belgian cystic fibrosis patients. *Journal of Antimicrobial Chemotherapy*, 59(5), pp.893–899. [Online]. Available at: https://doi.org/10.1093/jac/dkm037 [Accessed 8 March 2024].

Vermis, K., *et al.* (2004) Proposal to accommodate *Burkholderia cepacia* genomovar VI as *Burkholderia dolosa* sp. nov. *International Journal of Systematic and Evolutionary Microbiology*, 54(3), pp.689–691. [Online]. Available at: https://doi.org/10.1099/ijs.0.02888-0 [Accessed 8 March 2024].

Vos, M., *et al.* (2009) Local adaptation of bacteriophages to their bacterial hosts in soil. *Science*, 325(5942), pp.833–833. [Online]. Available at: https://doi.org/10.1126/science.1174173 [Accessed 31 October 2025].

Wainwright, C.E., *et al.* (2015) Lumacaftor–ivacaftor in patients with cystic fibrosis homozygous for Phe508del CFTR. *New England Journal of Medicine*, 373(3), pp.220–231. [Online]. Available at: https://doi.org/10.1056/NEJMoa1409547 [Accessed 29 October 2025].

Wallet, F., *et al.* (2002) Pneumonia due to *Bordetella bronchiseptica* in a cystic fibrosis patient: 16S rRNA sequencing for diagnosis confirmation. *Journal of Clinical Microbiology*, 40(6), pp.2300–2301. [Online]. Available at: https://doi.org/10.1128/JCM.40.6.2300-2301.2002 [Accessed 8 March 2024].

Wang, X., *et al.* (2021) Colistin-phage combinations decrease antibiotic resistance in *Acinetobacter baumannii* via changes in envelope architecture. *Emerging Microbes & Infections*, 10(1), pp.2205–2219. [Online]. Available at: https://doi.org/10.1080/22221751.2021.2002671 [Accessed 27 October 2025].

Wang, X., *et al.* (2021) Prospects of inhaled phage therapy for combatting pulmonary infections. *Frontiers in Cellular and Infection Microbiology*, 11, p.758392. [Online]. Available at: https://doi.org/10.3389/fcimb.2021.758392 [Accessed 30 October 2025].

Wang, Z., *et al.* (2024) Repurposing DNase I and alginate lyase to degrade the biofilm matrix of dual-species biofilms of *Staphylococcus aureus* and *Pseudomonas aeruginosa* grown in artificial sputum medium: in-vitro assessment of their activity in combination with broad-spectrum antibiotics. *Journal of Cystic Fibrosis*, 23(6), pp.1146–1152. [Online]. Available at: https://doi.org/10.1016/j.jcf.2024.02.012 [Accessed 12 March 2026].

Watanabe, R., *et al.* (2007) Efficacy of bacteriophage therapy against gut-derived sepsis caused by *Pseudomonas aeruginosa* in mice. *Antimicrobial Agents and Chemotherapy*, 51(2), pp.446–452. [Online]. Available at: https://doi.org/10.1128/AAC.00635-06 [Accessed 1 March 2025].

Waters, E.M., *et al.* (2017) Phage therapy is highly effective against chronic lung infections with *Pseudomonas aeruginosa*. *Thorax*, 72(7), pp.666–667. [Online]. Available at: https://doi.org/10.1136/thoraxjnl-2016-209265 [Accessed 30 October 2025].

Welsh, M.J. and Smith, A.E. (1993) Molecular mechanisms of CFTR chloride channel dysfunction in cystic fibrosis. *Cell*, 73(7), pp.1251–1254. [Online]. Available at: https://doi.org/10.1016/0092-8674(93)90353-R [Accessed 29 October 2025].

Whitchurch, C.B., *et al.* (2002) Extracellular DNA required for bacterial biofilm formation. *Science*, 295(5559), pp.1487–1487. [Online]. Available at: https://doi.org/10.1126/science.295.5559.1487 [Accessed 13 March 2026].

Willner, D., *et al.* (2009) Metagenomic analysis of respiratory tract DNA viral communities in cystic fibrosis and non-cystic fibrosis individuals. *PLoS ONE*, 4(10), p.e7370. [Online]. Available at: https://doi.org/10.1371/journal.pone.0007370 [Accessed 11 March 2024].

Winstanley, C., O'Brien, S. and Brockhurst, M.A. (2016) *Pseudomonas aeruginosa* evolutionary adaptation and diversification in cystic fibrosis chronic lung infections. *Trends in Microbiology*, 24(5), pp.327–337. [Online]. Available at: https://doi.org/10.1016/j.tim.2016.01.008 [Accessed 31 October 2025].

World Health Organization (2025) Global action plan on antimicrobial resistance. [Online]. Available at: https://www.who.int/publications/i/item/9789241509763 [Accessed 29 October 2025].

Worlitzsch, D., *et al.* (2002) Effects of reduced mucus oxygen concentration in airway *Pseudomonas* infections of cystic fibrosis patients. *Journal of Clinical Investigation*, 109(3), pp.317–325. [Online]. Available at: https://doi.org/10.1172/JCI0213870 [Accessed 10 October 2023].

Wright, A., *et al.* (2009) A controlled clinical trial of a therapeutic bacteriophage preparation in chronic otitis due to antibiotic-resistant *Pseudomonas aeruginosa*; a preliminary report of efficacy. *Clinical Otolaryngology*, 34(4), pp.349–357. [Online]. Available at: https://doi.org/10.1111/j.1749-4486.2009.01973.x [Accessed 30 October 2025].

Wright, G. (2005) Bacterial resistance to antibiotics: enzymatic degradation and modification. *Advanced Drug Delivery Reviews*, 57(10), pp.1451–1470. [Online]. Available at: https://doi.org/10.1016/j.addr.2005.04.002 [Accessed 15 March 2024].

Wright, R.C.T., *et al.* (2018) Cross-resistance is modular in bacteria–phage interactions. *PLoS Biology*, 16(10), p.e2006057. [Online]. Available at: https://doi.org/10.1371/journal.pbio.2006057 [Accessed 27 October 2025].

Wright, R.C.T., *et al.* (2019) Resistance evolution against phage combinations depends on the timing and order of exposure. *mBio*, 10(5), pp.e01652-19. [Online]. Available at: https://doi.org/10.1128/mBio.01652-19 [Accessed 27 October 2025].

Wright, R.C.T., *et al.* (2021) Functional diversity increases the efficacy of phage combinations. *Microbiology*, 167(12), p.001110. [Online]. Available at: https://doi.org/10.1099/mic.0.001110 [Accessed 3 March 2025].

Xuan, G., *et al.* (2022) Phage resistance evolution induces the sensitivity of specific antibiotics in *Pseudomonas aeruginosa* PAO1. *Microbiology Spectrum*, 10(5), p.e0135622.

Xuan, G., *et al.* (2023) *Pseudomonas aeruginosa* resists phage infection via eavesdropping on indole signaling. *Microbiology Spectrum*, 11(1), pp.e03911-22. [Online]. Available at: https://doi.org/10.1128/spectrum.03911-22 [Accessed 13 June 2025].

Yan, J.-J. (2006) Characterization of acquired -lactamases and their genetic support in multidrug-resistant *Pseudomonas aeruginosa* isolates in Taiwan: the prevalence of unusual integrons. *Journal of Antimicrobial Chemotherapy*, 58(3), pp.530–536. [Online]. Available at: https://doi.org/10.1093/jac/dkl266 [Accessed 15 March 2024].

Yigit, K. and Chien, P. (2025) *Lon*-dependent proteolysis in oxidative stress responses. *Journal of Bacteriology*, 207(7), pp.e00005-25. [Online]. Available at: https://doi.org/10.1128/jb.00005-25 [Accessed 27 October 2025].

Yilmaz, C., *et al.* (2013) Bacteriophage therapy in implant-related infections: an experimental study. *The Journal of Bone and Joint Surgery. American Volume*, 95(2), pp.117–125. [Online]. Available at: https://doi.org/10.2106/JBJS.K.01135.

Young, R. (2014) Phage lysis: three steps, three choices, one outcome. *Journal of Microbiology*, 52(3), pp.243–258. [Online]. Available at: https://doi.org/10.1007/s12275-014-4087-z [Accessed 29 October 2025].

Yu, Z., *et al.* (2024) Leveraging mathematical modeling framework to guide regimen strategy for phage therapy. *PLOS Complex Systems*, 1(3), p.e0000015. [Online]. Available at: https://doi.org/10.1371/journal.pcsy.0000015 [Accessed 28 October 2025].

Yumi, N., *et al.* (2023) UK Cystic Fibrosis Registry 2022 Annual Data Report. [Online]. Available at: https://www.cysticfibrosis.org.uk/sites/default/files/2023-09/UK_CF_Registry_2022_Annual_Data_Report.pdf.

Zhang, Y., Sun, Y. and Wang, R. (2025) Rational design versus random assembly: comparative efficacy of phage cocktails against multi-drug resistant pathogens. *Frontiers in Microbiology*, 16, p.1532291. [Online]. Available at: https://doi.org/10.3389/fmicb.2025.1532291

Zhao, L., *et al.* (2020) Development of *in vitro* resistance to fluoroquinolones in Pseudomonas aeruginosa. *Antimicrobial Resistance & Infection Control*, 9(1), p.124. [Online]. Available at: https://doi.org/10.1186/s13756-020-00793-8 [Accessed 29 October 2025].